Faculty of Science and Engineering
Department of Civil Engineering

Performance, Evaluation, and Enhancement of Hydrated Cement Treated Crushed Rock Base (HCTCRB) as a Road Base Material for Western Australian Roads

Suphat Chummuneerat

This thesis is presented for the Degree of
Doctor of Philosophy
of
Curtin University

March 2014

DECLARATION

To the best of my knowledge and belief this thesis contains no material previously published by any other person except where due acknowledgment has been made.

This thesis contains no material which has been accepted for the award of any other degree or diploma in any university.

Signature: Suphat Chummuneerat

Date: March 31, 2014

LIST OF PUBLICATION

The following publications have resulted from the works carried out for this degree.

Journal Papers

1. Chummuneerat, S., Jitsangiam, P., and Nikraz, H., (under review). Fatigue Characteristics of Cement-Treated Base for Western Australian Roads. *Journal of Materials in Civil Engineering*, (submitted February 2014).

2. Jitsangiam, P., Chummuneerat, S., Jotisankasa, A., Nusit, K., and Nikraz, H., (under review). A New Mechanistic Framework for Evaluation of Cyclic Behaviour of Unsaturated Unbound Granular Materials with respect to Australian Pavement Conditions. *Canadian Geotechnical Journal,* (submitted November 2013).

3. Jitsangiam, P., Chummuneerat, S., Phenrat, T., and Nikraz, H., (in-press). Characteristics and Performance of Cement Modified–Basecourse Material in Western Australia. *Journal of Materials in Civil Engineering*, (accepted August 2013).

4. Jitsangiam, P., Chummuneera,t S., and Nikraz, H., (2013). Engineering Characteristics of Cement Modified Basecourse Material for Western Australian Pavements. *Australian Journal of Civil Engineering*, Vol. 11, No. 1, pp. 13-21.

Conference Papers

1. Chummuneerat, S., Jitsangiam, P., Nikraz, H., (2013). Shrinkage Behaviour of Cement Modified Basecourse Materials for Western Australian Pavements. *The 2013 International Public Works Conference*, Darwin, Australia, 11st-15th August.

2. Chummuneerat, S., Jitsangiam, P., Nikraz, H., (2013). Fatigue Characteristics of Cement Treated Base for Western Australian Roads. *The 2nd International Conference on Engineering and Applied Science*, Tokyo, Japan, 15th- 17th March.

3. Chummuneerat, S., Jitsangiam, P., Nikraz, H., (2012). Mechanical Behaviour of a Cement Treated Basecourse Material in Western Australia. *The 25th ARRB Conference*, Perth, Australia, 23rd- 26th September.

4. Chummuneerat, S., Jitsangiam, P., Nikraz, H., (2012). Mechanical characteristics of Hydrated Cement Treated Crushed Rock Base for Western Australian Road Base. *The 2nd International Conference on Transportation Geotechnics (IS-Hokkaido 2012)*, Sapporo, Japan, 10th-12th September.

5. Chummuneerat, S., Jitsangiam, P., Nikraz, H., (2012). Performance of Hydrated Cement Treated Crushed Rock Base as a Road Base Material in Western Australia. *The 11st Australia New Zealand Conference on Geomechanics*, Melbourne, Australia, 15th-18th July.

6. Chummuneerat, S., Jitsangiam, P., Nikraz, H., (2012). Performances of Hydrated Cement Treated Crushed Rock Base for Western Australian Roads. *International Symposium on Heavy Duty Asphalt Pavements and Bridge Deck Pavements (ISAP 2012)*, Nanjing, China, 23rd-25th May.

7. Chummuneerat, S., Jitsangiam, P., Nikraz, H., (2012). Resilient Modulus of Hydrated Cement Treated Crushed Rock Base (HCTCRB) for Road Base Material in Western Australia. *The International Conference on Highway Engineering 2012*, Bangkok, Thailand, 18th-20th April.

8. Chummuneerat, S., Jitsangiam, P., Nikraz, H. (2011). Characteristics of Hydrated Cement Treated Crushed Rock Base (HCTCRB) for Western Australian Roads. *The 7th International Conference on Road and Airfield Pavement Technology (ICPT)*, Bangkok, Thailand, 3rd-5th August.

PERFORMANCE, EVALUATION, AND ENHANCEMENT OF HYDRATED CEMENT TREATED CRUSHED ROCK BASE (HCTCRB) AS A ROAD BASE MATERIAL FOR WESTERN AUSTRALIAN ROADS

ABSTRACT

Hydrated Cement Treated Crushed Rock Base (HCTCRB) is produced by mixing 2% Portland cement (by mass) with standard crushed rock base (CRB) at an optimum moisture condition. The unique production process for HCTCRB is different from that of common cement-treated base (CTB) in that a re-mixing process is performed after the hydration of the cement. This technique aims to improve the engineering characteristics of unbound granular materials for road bases, without them becoming fully cemented (bound) materials. HCTCRB has been designed to be stronger and less susceptible to moisture than conventional unbound base materials, whilst still possessing unbound material characteristics. This study was set up to evaluate the basic geotechnical and mechanical properties of HCTCRB by using a sophisticated laboratory test program that covered significant factors affecting HCTCRB performance during its manufacture and construction processes. The performance of HCTCRB in terms of resilient modulus (MR) and permanent deformation (PD) were evaluated throughout repeated load triaxial (RLT) tests. The results of this study show that differences in material hydration periods affect the performance of HCTCRB. However, a consistent performance trend over various hydration periods was not evident. The moisture content of samples significantly influenced the performance of HCTCRB. Higher amounts of added water during compaction generally caused a decrease in PD and MR performance even after dryback, in comparison with the samples compacted without the added water. This indicates that HCTCRB is still susceptible to moisture, thus the amount of added water for compaction must be carefully controlled for HCTCRB to be put to effective use in the field. Finally, the stress dependency models for the resilient modulus derived from the test results were proposed. These were then used for the mechanistic empirical pavement analysis and design. Along with HCTCRB characterisation, this study initiated a framework which incorporated the soil suction effect into the resilient response of unbound granular materials such as CRB without the need for real matric suction measurement. Another multi-strain flexural fatigue test was also

introduced with a view to reducing the testing time and the number of test specimens, as is the case with conventional fatigue tests for CTB.

ACKNOWLEDGEMENT

I would like to acknowledge the Australian Research Council (ARC) and Main Roads Western Australia (MRWA) for financial support, under the ARC Linkage Scheme (LP100100734), to conduct this PhD research at the Department of Civil Engineering, Curtin University.

I would like to express my genuine and sincere gratitude to my supervisor, Dr. Peerapong Jitsangiam, and my co-supervisor, Professor Hamid Nikraz for their encouragement, expert guidance, constructive comments and support throughout the course of this study. I gratefully acknowledge their encouragement to publish the findings of this research in journal and conference papers. Without their help, this work would not be possible. Above all and the most needed, they provided me unflinching encouragement and support in various ways.

I greatly appreciate Dr. Komsun Siripun, Mark Whittaker and Darren Isaac for their guidance and support for conducting the laboratory works at the Geomechanics laboratory, Curtin University. Thanks are extended towards Paul Tubbs and his colleagues for supplying the quarry material for use throughout this study.

I would like to extend my thanks to administrative staffs and secretary at the School of Civil and Mechanical Engineering for their support in administrative matters.

I also wish to thank Komsun Siripun, Korakod Nusit and Behzad Ghadimi for their help in modelling, analysis and design of pavements.

Finally, a special note of thanks must go to my parents, grandparents and all of my family members in Thailand. Their unconditional love and an invaluable source of inspiration continuously support me during my study in Australia

TABLE OF CONTENTS

LIST OF FIGURES

LIST OF TABLES

CHAPTER 1
INTRODUCTION

1.1 Background

Flexible pavement structures in roads in Western Australia (WA) typically consist of four layers of asphalt wearing surface, an unbound granular basecourse, a subbase of crushed limestone, and a subgrade consisting of Perth sand. Pavement structures are predominantly designed around the concept of a thin bituminous surface pavement. An asphalt surface thickness of approximately 30mm - 40 mm is usually overlaid on an unbound granular basecourse layer. Accordingly, traffic loads on the relatively thin road surface result in significantly high stress levels on the basecourse layer. Thus, the pavement base layer must be of sufficient strength and appropriate thickness to efficiently withstand traffic loads and transfer stresses from the pavement surface to the underlying layers. Crushed rock base (CRB) is the traditional basecourse material used in WA. CRB is a conventional unbound granular material that does not have the capability to withstand the increased loads and growth of today's traffic. Its weakness is due to granular disintegration from the heavy, numerous and frequent loads applied to the thin asphalt pavement system in WA. Moreover, CRB is moisture-sensitive, a property which accelerates pavement deterioration. Higher quality aggregates are therefore required for the basecourse layer of a pavement due to the above reasons, and due to its proximity to the road surface. These requirements have led to attempts to improve basecourse material in WA.

In North America, cement-modified soil (CMS) is described as a soil that has been treated with a relatively small amount of cement in order to improve its engineering properties, thereby making it suitable for construction purposes. This soil stabilisation technique is employed in WA, using a typical local basecourse material (CRB). A hydration process is also involved in the process, the outcome of which eventuates in a unique basecourse material used only in WA called "Hydrated Cement Treated Crushed Rock Base" (HCTCRB). The general definition of HCTCRB is that it is a manufactured road base material made by blending standard CRB with 2% cement (General Purpose Portland cement) by mass of dry CRB, at the

optimum moisture content obtained by the test method WA 133.1 (Main Roads Western Australia 2012b). The material is mixed and then stockpiled for a hydration period. A more accurate definition of the hydration period cannot yet be provided, as changes are continually being made, based on research and ongoing testing, in order to tackle problems that have been encountered to date. As illustrated in Figure 1.1, HCTCRB does not have the nature of a modified or stabilised cement-treated base. After a hydration period, the HCTCRB is re-treated in order to maintain the properties of the unbound material (by breaking the cementitious bonds generated during the hydration time and the re-mixing processes before compaction). HCTCRB has been implemented, and is being developed, to overcome the disadvantages of conventional CRB and the fatigue deterioration problems in fully cemented treated crushed rock base. HCTCRB is expected to provide a higher shear strength and a lower moisture sensitivity than CRB, while avoiding the significant tensile strength and bound characteristics that lead to fatigue and cracking problems in cement-treated basecourse.

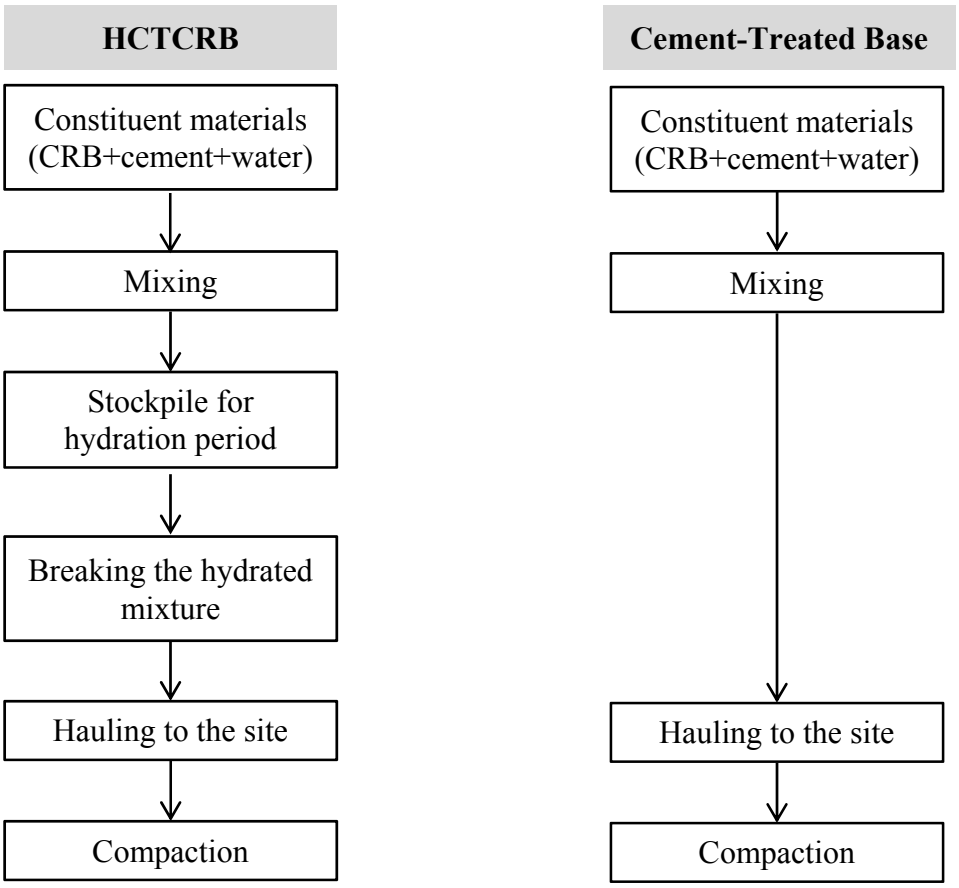

Figure 1.1: Comparison of the production procedure between HCTCRB and common cement-treated base

HCTCRB has been widely used as a basecourse material in WA since its introduction into road construction in 1977. It has also been trusted as a sufficient (relatively high) modulus material (about 800 MPa – 1,000 MPa) for use in heavy traffic pavements such as freeways. However, in the last ten years, there has been significant premature damage on some highways and roads in WA constructed with HCTCRB basecourse. This has led to a demand for more consistency in HCTCRB itself and for more effective use of HCTCRB in WA pavements. Experience in the use of HCTCRB has been gained over time. However, pavement analysis and design in WA relies predominantly on empirical design, which is based mainly on experience from actual construction, along with simple tests on pavement materials. Consequently, a clear explanation for the premature damage occurring under present conditions is difficult to obtain and assess due to empirical design, and the complexities of intrinsic cement stabilisation along with the manufacturing processes. This study aims to discover whether factors involved in the manufacture of HCTCRB, and in road design, or construction , such as cement content, hydration period, cement type, water addition, mixing processes, compaction processes, and curing time and methods, are partly involved in leading to such damage. Accordingly, an understanding of the material characteristics of HCTCRB, in accordance with a pavement mechanistic approach, is strongly advised to maximise the effectiveness of using this material.

1.2 Objectives and scope

The broad purpose of this investigation is to present a method whereby successful and reliable use of HCTCRB in manufacturing and construction may be achieved. In order to reach this goal, uncertainties encountered during construction and post-construction, and any associated instability attributed to the raw materials or manufacturing process must be eliminated. The project aims to achieve improved HCTCRB analysis and design procedures, which would result in cost-effective and highly reliable use of HCTCRB. To achieve these objectives, the research objectives are to:

1) Evaluate the basic geotechnical and mechanical properties of HCTCRB through fundamental and sophisticated laboratory testing.

2) Examine the factors influencing the production and construction of HCTCRB, e.g., mix-proportion, hydration periods and moisture content, to understand how these factors affect the performance of HCTCRB.
3) Characterise HCTCRB and develop the material modulus model with respect to the mechanistic-empirical pavement analysis and design principles.
4) Implement a material modulus model into multi-layered finite element modelling to perform structural analysis of a typical flexible pavement structure in WA.
5) Establish suitable guidelines and practical tools for using HCTCRB.

In addition to a major work on characterisation of HCTCRB which is the specific type of cement stabilisation used only in Western Australia, characterisation of a common cement-treated base is also important to gain an understanding of a common cement-treated base material as a reference to HCTCRB. Moreover, the characteristic of an unbound granular material which is a parent material of a cement-treated base material also relevant to be further investigated into the effect of matric suction to its overall performance. Thus this research also additionally aims to:

6) Characterise the significant properties of a common cement-treated base (CTB), relating to shrinkage and fatigue characteristics.
7) Evaluate the matric suction effect on the resilient properties of unbound granular pavement materials through the repeated load triaxial tests.

1.3 Significance

This study is scientifically significant as it provides a most comprehensive and complete investigation of HCTCRB. It is based on sophisticated tests and scientific characterisation, and implements mathematical models and finite element procedures.

A mechanistic approach will be introduced which will characterise, design, and analyse the use of HCTCRB. It aims to resolve the ongoing problems encountered in the design and construction of HCTCRB pavements, as they are encountered in WA.

The end result aims to provide an increased degree of confidence in national implementation.

The current use of HCTCRB in WA pavements cannot fully embrace mechanistic-empirical design principles. This is due to its being developed during the empirical design period, along with the fact that it is has not yet been characterised in terms of following the mechanistic approach. In addition, there is some doubt about its consistency in manufacturing such as material proportion and hydration time, and its construction practice such as compaction, curing and dryback. These factors lead to uncertainty regarding the best utilisation of this material.

Of key significance in the project is the generation of proper guidelines for the manufacturing process, its use, and the analysis and design of HCTCRB based on the mechanistic-empirical approach. The results of this work should then specifically yield:

- a more streamlined and competent manufacturing process, and more effective use of HCTCRB based on comprehensive characterisation;
- an understanding of the behaviour of HCTCRB under repetitive load conditions based on mechanistic characterisation. This should not only determine the proper capacity of HCTCRB but would also contribute to a more complete understanding of how to fit the material into a new analysis and design approach;
- a specific material modulus model for HCTCRB for specific use in mechanistic-empirical design.

1.4 Methodology

Figure 1.2 shows the project methodology overview which consists of the study of the basic properties of the material, its mechanical characterisation and the results analysis. Following this, two final outcomes will be produced for the guidelines; the use of HCTCRB and a thickness design for HCTCRB pavements.

HCTCRB is unique to WA pavements, and its basic soil properties and mechanical performance will be investigated in order to explore how the suggested stabilisation

technique modifies the material. The modifications are seen in terms of the differences between HCTCRB and traditional basecourse materials such as CRB and cement-treated base.

A series of material characterisations of HCTCRB was made through repeated load triaxial (RLT) tests to investigate the many factors involved in HCTCRB performance. HCTCRB samples made with various amounts of cement and water were tested to evaluate their performance in terms of strength and resilient response. Factors during production and construction which could affect performance, such as hydration period, curing time, and dryback were also taken into account.

The extensive laboratory data and the results analysis delivered two major findings;

1) Effects of various factors on the material's performance
   The test results were subjected to quantitative evaluation to identify an optimum mix of HCTCRB. All test results and analytical results from the project were collected and modified for practical use in order to propose a suitable guidelines practical tools for using HCTCRB; the final objective of the study.

2) The material model under repetitive loading of HCTCRB
   The material model of HCTCRB for implementation in mechanistic-empirical (M-E) pavement design and analysis was developed. The multi-layer pavement structures were then analysed using the finite element method which yielded stresses and strains under given loadings and pavement configurations. Determination of the stress-strain distribution, together with the M-E design criteria and transfer function ultimately obtained the allowable amount of traffic and the thickness design charts for HCTCRB pavements.

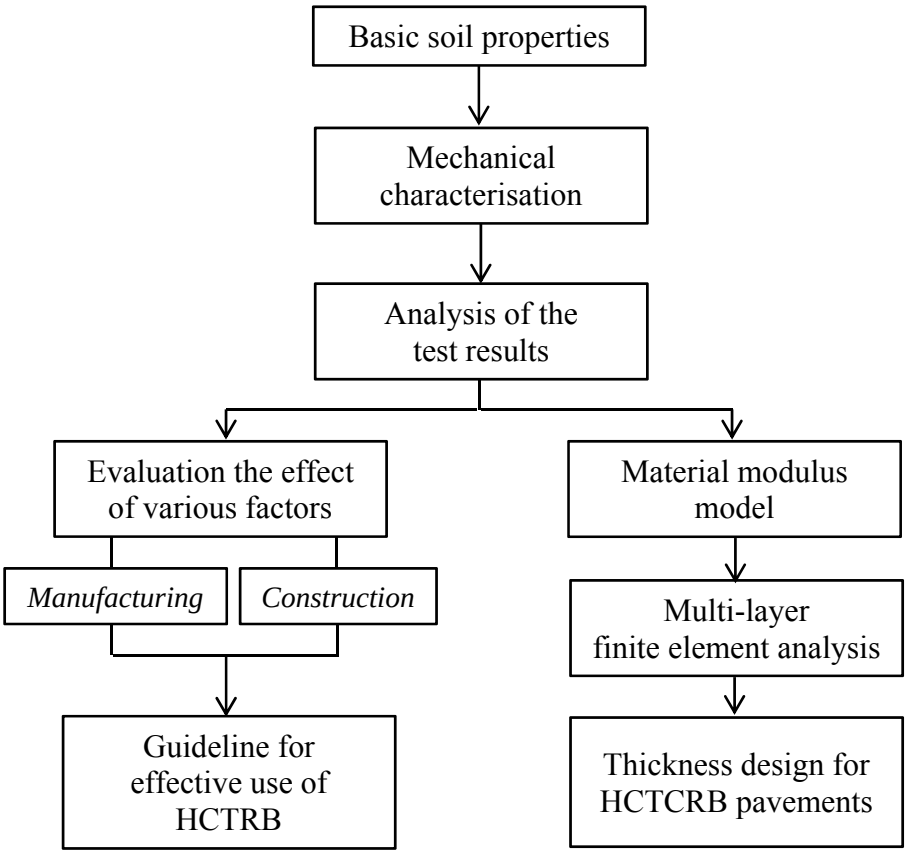

Figure 1.2: Diagram for the research methodology of this study

1.5 Thesis organisation

This dissertation comprises eight chapters. Chapter 1 gives an overview of the thesis, including the organisation of the work itself, the research background, problem statement, objectives and scope, and significance and methodology. Chapter 2 provides an overview of basecourse materials, with a focus on the classification of pavement materials in Australia, material characterisation methods and factors affecting the properties of the materials. A typical basecourse material and the stabilisation technique for use in WA road pavements are also presented in Chapter 2. The significant properties of a common cement-treated base (CTB) such as shrinkage and fatigue characteristics were investigated in this study and detailed in Chapter 3. Then Chapter 4 explains the manufacturing and construction process of HCTCRB along with the determination of the basic geotechnical properties of HCTCRB. The results of the mechanical characterisation of HCTCRB, primarily conducted through repeated load triaxial tests, are reported upon in Chapter 5. The

concept of unsaturated soils has also been adapted for use in this research. A proposed method for assessing the effect of matric suction on the characterisation of the pavement materials was developed and is described in Chapter 6. Chapter 7 presents the implementation of the repeated load triaxial test results into the structural analysis and design for road pavements. The thesis concludes in Chapter 8 by providing the major findings of the investigation, and it makes recommendations for further research.

CHAPTER 2
PAVEMENT MATERIALS OVERVIEW

This chapter provides an overview of pavement materials, with an emphasis on the basecourse materials used in flexible pavements. The classification of pavement materials according to Austroads standards is introduced and this is followed with a presentation of the range of basecourse materials used in Western Australia (WA). The material behaviour of pavement under moving traffic loads is then described, along with some of the laboratory test methods used to simulate stresses and material responses under field conditions. Various factors affecting the behaviour of the material under load repetitions are described. The chapter finishes with a review of material response modelling in terms of the resilient modulus and permanent deformation derived from laboratory tests.

2.1 Flexible pavement structure and pavement materials

Pavement structure is a made up of multiple layers of compacted materials which are designed and constructed over the design formation (cut or fill) of existing subgrade. The pavement acts as a structural component to prevent the failure of the existing subgrade and to provide good ride quality. Each layer of pavement must be of a specific thickness and strength which is sufficient to carry the stresses from the overlying layer. These stresses are then distributed at a level that is low enough for the underlying layer to absorb. Layers of pavement must also be of satisfactory durability in order to withstand environmental conditions such as moisture and temperature changes. Pavement structure consists of two types; rigid and flexible. This study focuses only on flexible pavements as rigid pavements are rarely constructed in WA (Payne 2012).

Flexible pavements usually consist of an asphalt wearing surface, basecourse and subbase. They may also include selected materials over the subgrade, as shown in Figure 2.1. The wearing surface primarily provides comfortable ride quality and includes aspects such as smoothness, skid-resistance, dust-suppression and surface drainage. It can also serve as partial structural resistance if it is thick enough, i.e., more than 50 mm (Austroads 2005). The basecourse layer is a major load-carrying component in pavements, due to its proximity to the surface. This is particularly the

case with thin asphalt (less than 50 mm) and sprayed seal pavements (Austroads 2005). The subbase is made up of a lesser quality material than that of the base layer due to its function of sustaining lower stresses. The subbase is also a load-carrying layer; it supports the basecourse layer and transfers stresses that are low enough for the subgrade or selected material to withstand. Selected materials are superior quality materials in comparison with subgrade but have lesser quality than that of subbase. Selected materials may be used as an additional layer placing between subbase and subgrade if the local or natural subgrade is weak, or in case of heavy-duty pavements.

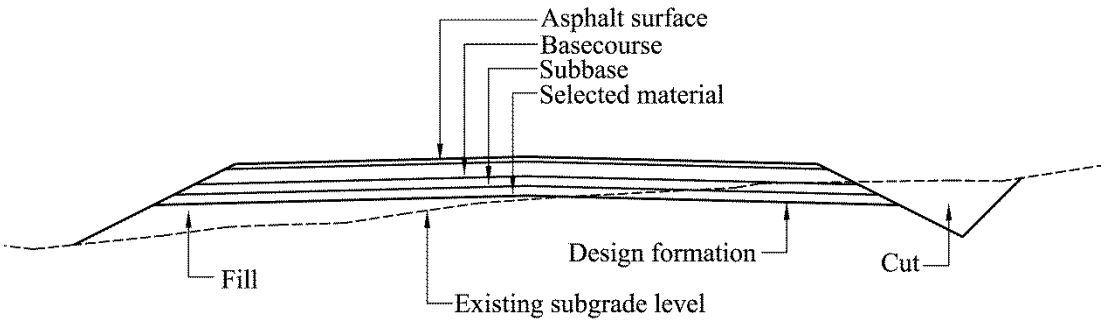

Figure 2.1: Typical flexible pavement structure

Austroads (2005) categorised pavement materials into five types based on their behaviour under traffic loading:

- unbound granular material
- modified granular material
- cemented material or bound stabilised materials
- asphalt
- concrete

Asphalt and concrete are usually used for the surface layer of flexible pavement and rigid pavement respectively. The basecourse layer is usually designed and constructed with either unbound granular materials, modified granular materials, or cemented materials. The main features and differences between the three materials used for the basecourse layer are summarised as follows:

1) Unbound granular materials

   Unbound granular materials are made up of crushed rock or gravel. The materials are able to resist traffic loads through the shear strength of the interlocking particles. There is no significant tensile strength in these materials. The distress modes of the material are rutting and shoving.

2) Modified granular materials

   Modified granular material is stabilised by adding a small amount of stabilising binder such as bitumen, cement or pozzolanic material to the original granular materials. The performance of the material is thus improved with regard to aspects such as shear strength, plasticity, and moisture susceptibility. However, the improvement of tensile strength is not one of the purposes of stabilisation, as producing a bound material must be avoided. The 28-day unconfined compressive strength (UCS) values of these materials range from 0.7 MPa to 1.5 MPa. The distress modes of the materials are similar to the granular materials.

3) Cemented materials or bound stabilised materials

   A single type of stabilising binder or a combination is added to granular materials in order to gain significant tensile strength i.e., to produce the bound layer. This is the main difference between cemented materials and modified granular materials. Cracking of cemented materials is due to shrinkage and fatigue; these being the main distress modes of the cemented material.

Table 2.1 summarises the strength criteria for basecourse material classification and their major characteristics.

Table 2.1: Basecourse material categories and characteristics

Material	Strength criteria (Austroads 2002)	Strength criteria (Austroads 2006b)	Characteristics (Austroads 2010c)
Granular	N/A	40%< CBR[1] <+100%	Development of shear strength through particle interlock. No significant tensile strength.
Modified	UCS[2] < 1 MPa	0.7MPa < UCS[2] < 1.5MPa	Development of shear strength through particle interlock. No significant tensile strength.
Bound	Lightly bound: 1 MPa < UCS[2] < 4 MPa Heavily bound: UCS[2] >4 MPa	UCS[2] > 1.5MPa	Development of shear strength through particle interlock and chemical bonding. Significant tensile strength.

Note:
1. Four day soaked CBR.
2. UCS determined from test specimens stabilised with GP cement and prepared using Standard compactive effort, normal curing for a minimum 28 days and 4 hour soak conditioning.

2.2 Basecourse materials in Western Australia (WA)

Western Australia has a total road network of approximately 149,000 km. Around 18,000 km is made up of State roads, managed by Main Roads Western Australia (MRWA). A total of 139 local governments are responsible for about 131,000 km of local road network (Main Roads Western Australia 2011d). The basecourse layer plays an important role in WA's pavements, as most pavements usually have only a sprayed seal or thin asphalt surface (30 mm - 40 mm) for covering. A wide range of materials have been used for the basecourse, including naturally occurring materials such as natural gravel and ferricrete. Other materials include quarry materials such as crushed rock base (CRB) and stabilised materials. In this study, a performance evaluation of various basecourse materials was undertaken in both the field and laboratory and the results compared.

In 1975, MRWA examined the performance of stabilised limestone by comparing cement stabiliser to bitumen stabiliser, the common stabiliser applied in WA.

Samples were prepared with variations in binder content ranging from 1% - 6%. A 2% cement sample provided superior compression and tensile strength to that of a 3% bitumen sample (the typical amount of bitumen for basecourse treatment adopted in WA). The results of these experimental works led MRWA to undertake constructed pavement trials in 1977 on Leach Highway (within the Perth metropolitan area) using 1% and 2% bitumen, and 2% cement for the limestone basecourse. The California bearing ratio (CBR) values of the cement-treated section were double those of the two sections of stabilised bitumen. Assessment of these pavements in 1980, using Accelerated Loading Facility tests, ascertained that the best performance was given by the cement-treated section in the pavement trial. However, there were concerns about the risk of cracking and the lack of comprehensive fatigue failure criteria.

Enhancement of standard CRB, according to MRWA specifications for pavement construction, became more popular in the 1990s. However, the pavement failure of Kwinana Freeway (between South Street, and Forrest/Yangebup Road in Perth) in 1992, due to the moisture susceptibility of CRB, led to recurring investigations into the cement stabilisation technique. Test results suggested that small amounts of cement (0.5%, 1%, 2%, and 3%) could improve the resilient modulus and the permanent deformation of CRB, along with reducing sensitivity to moisture damage. However, even the addition of only 1% cement caused the treated CRB to behave as a bound material. This conclusion was based solely on the criterion that the UCS of test samples exceeded 1.0 MPa. The key finding of this investigation revealed that if a hydrated mix of CRB and 2% cement was disturbed after the hydration period, the material showed increased strength, reduced permanent deformation and moisture susceptibility, while still behaving as an unbound material (Yeo and Nikraz 2011). This technique contributed to the development of a unique basecourse material used in WA, called *Hydrated Cement Treated Crushed Rock Base (HCTCRB)*.

In 1996, pavement trials were undertaken on Reid Highway (within the section between West Swan Road and Bennett Brook Bridge in Caversham, north-east of Perth). The test sections were designed for 35 million equivalent single axle loads (ESALs) on a designed subgrade CBR of 12%. Different varieties of basecourse materials with varying thicknesses were constructed using CRB, HCTCRB, bitumen-

stabilised limestone, cement-stabilised CRB, and cement-stabilised limestone. In 2003 and 2009 the basecourse performance was monitored in terms of deflection and curvature of the test sections by using a falling weight deflectometer (FWD), and the Benkleman Beam. Curvature is defined as the value of D_0 - $D_{200,}$ which describes the shape of the deflection bowl, indicating the relative deflection and strength of the basecourse. D_0 represents the deflection under the centre of the load plate, and D_{200} is the deflection at a 200 mm distance from the centre. A large deflection bowl usually indicates a larger curvature. It also implies a relatively higher deflection which is the result of weaker strength test materials. HCTCRB pavement with 2% cement provided the best performance in terms of reliably sufficient stiffness, with no drying shrinkage cracking. The 1% cement HCTCRB, and 0.75% cement-treated base initially provided the most promising performance, but then returned the same performance as CRB. This phenomenon demonstrated that the improvement of material with a small amount of cement (lower than 2%) is not permanent. CRB pavement when dried back to approximately 50% – 60% OMC was found to be suitable for light to moderate traffic conditions. Stabilised limestone pavements were deemed inappropriate for heavy traffic conditions due to producing the least effective performance (Butkus 2004; Harris and Lockwood 2009).

Other pavement test sections were built in 2009 on Kwinana Freeway between Paganoni Road and Stock Road in the City of Rockingham, Perth (Rehman 2012). As in 2011, the deflection and curvature values of HCTCRB pavement were lower than that of CRB, bitumen-stabilised limestone and ferricrete sections, and higher than those of full-depth asphalt and crushed recycled concrete base pavements. Performance monitoring has been ongoing and will be reported upon periodically.

According to Main Roads Western Australia (2010a), cemented material is only permitted in pavement construction as a working platform below the design formation. It must then be overlaid with an unbound granular material. It is also prohibited to place cemented material in a position underlying pavement surfaces; this prevents reflective cracking. However, Adamson (2012) stated that cement stabilisation with naturally occurring materials such as lateritic and ferricrete gravels, is often used as a process in rural roads to save the cost of hauling the materials. MRWA also adopted cement to stabilise failed sections of major highways in the

Perth metropolitan area. For example, in 2011, a failed section of Great Eastern Highway was stabilised with 1.5% low-heat cement (Adamson 2012). Unsuccessful uses of cement stabilisation have still been reported (Keeley 2004). These were due to improper design and construction such as incorrect use of mechanistic design, inappropriate type and amounts of stabiliser, and insufficient mixing, compaction and dryback (Adamson 2012).

2.3 Material behaviour under traffic loading and laboratory simulation

The understanding of the behaviour and responses of pavement materials under repeated traffic loading is essential for the analysis and design of pavements. Stress and strain are the most significant responses that researchers and engineers have obtained from the materials. Since the various behaviours of the materials in the field are well understood, simulation can be carried out in the laboratory to evaluate the materials' responses and establish a response model for further analysis and design of pavements.

The cubic element in Figure 2.2a presents two types of stresses, i.e., normal stress and shear stress, on three global axes (x, y and z) on any element of pavement material. Stresses in the element can be represented without shear stresses by the resulting principal stresses perpendicular to the plane of the three principal axes, i.e., 1) major principal axis, 2) intermediate principal axis and, 3) minor principal axis, on the rotated element, as shown in Figure 2.2b. Strains in the element are also attributed to points on similar axes.

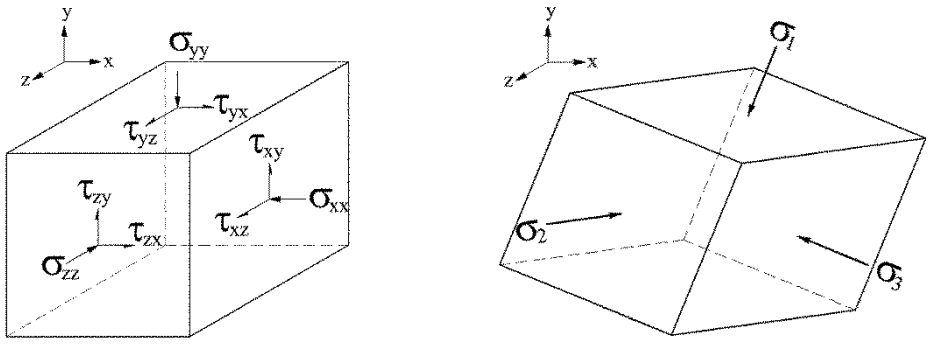

(a) (b)

Figure 2.2: Stresses in a cubic element (a) no rotation (b) principal axes rotation

Figure 2.3 demonstrates stresses occurring in an element of granular materials along a longitudinal profile, thus only a two-dimensional view is presented (x and y - minor and major principal axes). At rest, the materials experience stresses due to their selfweight or an overburdening caused by pressure. When an approaching vehicle subjects the pavement to a moving wheel load, the vertical and horizontal stresses in an element go up to reach a peak when the load is vertically above an element. Both stresses then decrease when the load moves further away from the element. The principal axes of the element rotate with the position of the wheel load, as shown in Figure 2.3a. If there is no rotation of an element, there will be shear stress (see Figure 2.3b). Shear stress in an element increases to reach a peak point and it then starts decreasing and goes down to zero when the load is directly above the element. There is a reversal of shear stress once the wheel load leaves the element. Figure 2.3c shows the variation in stress magnitudes with the changing position of a moving wheel load.

The materials also deform when subjected to moving loads. Deformation of the materials also presents as strain, which is a ratio of a change in dimension from the original dimension. As a moving load moves toward an element, the induced strain in the element also increases and it then reaches a peak when the element is directly under the load. Consequently, induced strain reduces as the load moves away. However, the strain in an element does not fully recover, even when the influence of the load disappears. Thus strain in an element comprises a recoverable part and an unrecoverable part, and these are usually called the resilient strain and the permanent strain, respectively. Figure 2.4 presents a simple figure of the vertical strain in relation to the location of a moving load and the stress applied to an element. Permanent strain accumulates and increases due to the number of load repetitions and this factor is important in evaluating the long-term performance and failure of pavements (e.g., rutting). Resilient strain is an index of load resistance capability (Lekarp et al. 2000b). It is used for the calculation of the resilient modulus which is a significant input for pavement analysis and design.

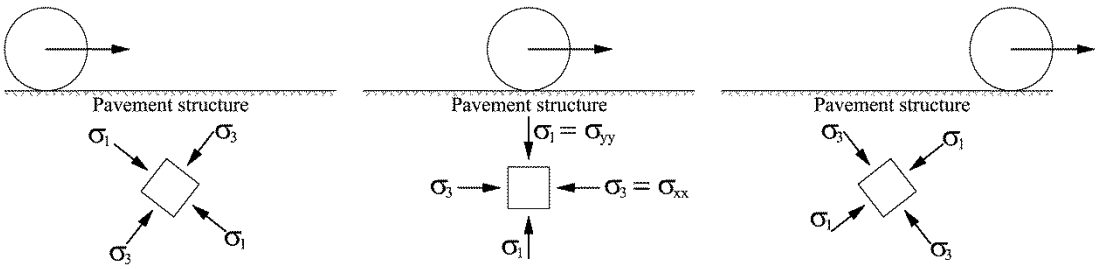

(a) Principal stress rotation

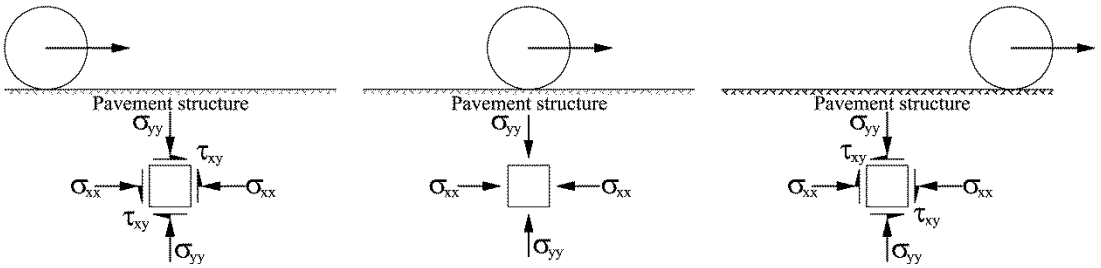

(b) Shear stress reversal

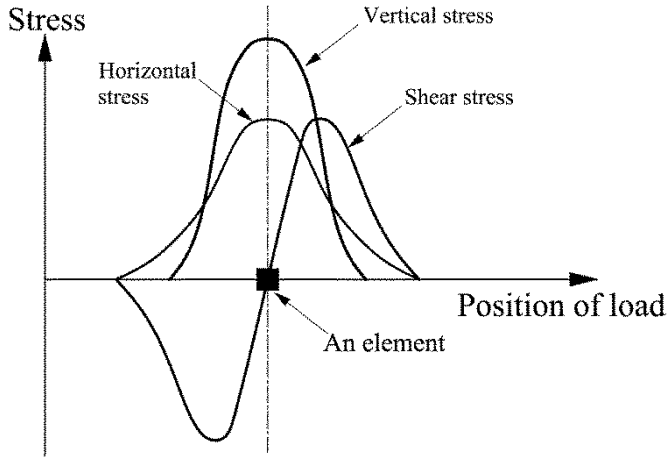

(c) Variation of stresses according to the position of the wheel load

Figure 2.3: Stresses on an element of pavement under a moving wheel load (Boyce 1976; Brown 1996; Lekarp et al. 2000a)

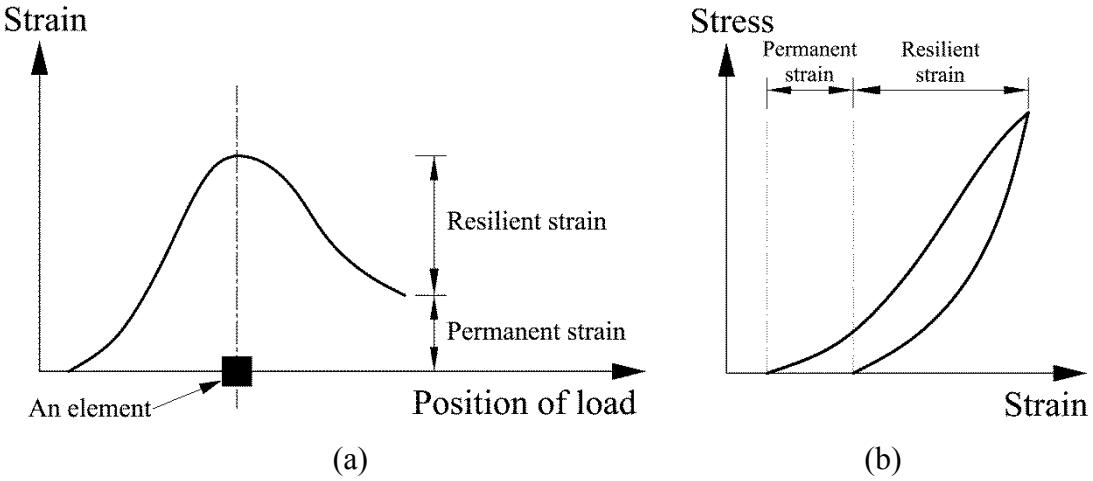

Figure 2.4: Strain in an element due to the cycle of a moving load

The simulation of stresses and strains occurring in pavement structure due to moving traffic loading has been attempted with various laboratory tests. These include the hollow cylinder triaxial test, the repeated load triaxial test, the k-mould, the fastcell and the springbox test. A brief description, along with the advantages and drawbacks of each of these tests is explained below.

2.3.1 Hollow cylinder triaxial test

The hollow cylinder triaxial (HCT) test can closely simulate the stresses in granular material subjected to moving loads. This is particularly the case for the simulation of shear stress or principal stress rotation. The test applies vertical, horizontal and shear stresses to a hollow cylinder specimen, as displayed in Figure 2.5. Vertical stress (axial stress) represents a major principal stress (σ_1). The intermediate (σ_2) and minor (σ_3) principal stress in a horizontal direction are equal, as the test specimen is cylindrical. Horizontal stresses (or confining stresses or confining pressure) apply to both the inner and outer surfaces of the cylinder wall. The magnitude of stress for the inner surface can be differentiated from that on the outer surface. Shear stresses on horizontal and vertical planes of the cylinder wall are applied to the specimen by torsion which is generated through rotation of the top platen attached to the specimen.

The test specimen has a wall thickness of 28 mm (Arnold 2004). The ratio of external diameter to wall thickness is equal to 10:1 and the height to diameter ratio is 2:1. The wall thickness limits the maximum size of the test material to less than 4.75

mm (Steven 2005), which is applicable to fine-grained soil or sand only. With regard to pavement materials, e.g., basecourse material with a maximum size of 19 mm, a much larger specimen triaxial cell and loading apparatus is required (see Figure 2.6). Figure 2.6 shows a diagram of the large HCT apparatus from the Department of Civil Engineering, Curtin University. This large HCT set is used for cylinder specimens of 300 mm by 600 mm with a 150 mm-thick wall which makes it applicable for aggregates with a maximum size of 30 mm. Due to the complexity of the test equipment and the operation, along with the limitation of aggregate size, the HCT test is not particularly suitable for the routine characterisation of pavement materials.

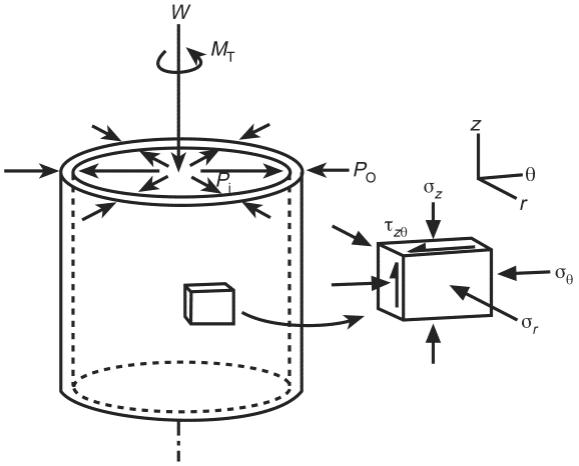

Figure 2.5: Stresses on a sample in the hollow cylinder triaxial test (after Brown 1996)

Figure 2.6: Large hollow cylinder triaxial apparatus at Curtin University

2.3.2 Repeated load triaxial test

The repeated load triaxial (RLT) test has been adapted from the static triaxial test which is usually used to characterise the shear strength of soils. The RLT test applies stresses to a solid cylindrical specimen along three normal principal axes (see Figure 2.7). The intermediate and minor principal stresses are constant and equal while vertical stress is cyclical. A major drawback of the test is its inability to simulate the principal axes rotation and shear stress reversal. However, Chan (1990) stated that resilient strains were not affected by principal stress rotation (Adu-Osei 2000). More sophisticated RLT test apparatus is able to apply variable confining pressure (VCP) in addition to cyclic vertical stresses. However, it is still unable to produce principal stress rotation.

A specimen for the RLT test usually has a height to diameter ratio of 2:1. Most available RLT apparatus is appropriate for use with specimens of 100 mm - 150 mm in diameter, allowing a test aggregate containing a maximum particle size of 30 mm. The large HCT test set shown in Figure 2.6 is usable for the RLT test with a solid specimen of 300 mm in diameter and 600 mm in height which is applicable for a maximum aggregate size of 60 mm.

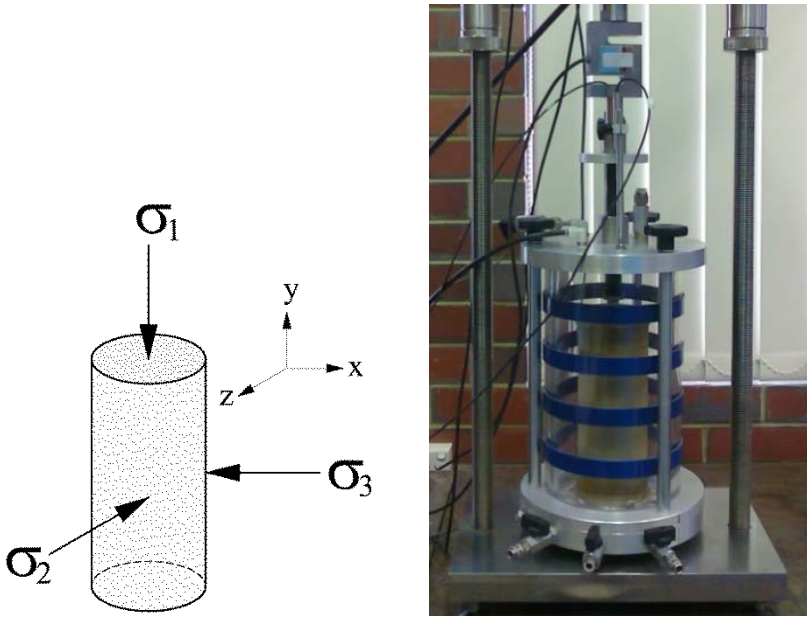

Figure 2.7: Stresses on a cylindrical sample in the RLT test

2.3.3 FastCell test

The FastCell test was designed by Seyhan and Tutumluer (1998) at the University of Illinois in order to study material responses under various cyclical vertical stresses and radial (confining) stresses. Seyhan and Tutumluer (1998) have described various features of this apparatus. These two types of stresses can be independently cycled during the course of the test, in both compression and tension modes. The test apparatus has the ability to create a radial pulse which is higher in a radial direction than in a vertical direction. Thus a material's anisotropy can be evaluated by separately applying the deviator stress in a vertical direction and then in a radial direction. Moreover, this test is capable of principal stress rotation which is achieved by independently applying different magnitudes of vertical and radial cyclic stresses. The range of principal stress rotation is not limited to 0° or 90° with respect to the horizontal plane.

Figure 2.8 shows a test apparatus and a solid cylindrical specimen, 150-mm in diameter and 150-mm in height. On-specimen displacements, in vertical and radial directions, are measured by four linear variable displacement transducers (LVDTs) contacted around the specimen. Vertical axial force and displacement are also monitored by external instruments. Pore pressures in undrained and/or cyclic loading are measured by a transducer installed at the bottom of the apparatus.

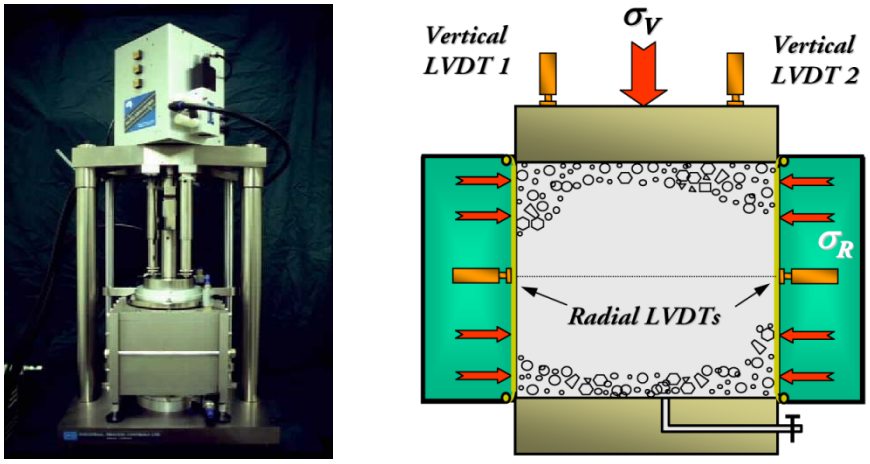

(a) (b)

Figure 2.8: FastCell test (a) Test equipment (b) Schematic diagram of the test (Seyhan and Tutumluer 1998)

2.3.4 K-mould test

The K-mould test was developed in South Africa after being adapted from a concept by Professor Handy of Iowa State University (Semmelink 1991). The K-mould (see Figure 2.9 and Figure 2.10) consists of 8 rigid wall segments forming an inner-core with an inside diameter of 152.4 mm, radial bearings, disc springs and an external mould housing. Each segment connects to radial bearings and disc springs which are supported by the outer mould housing. The inner-core can either be fixed to prevent horizontal deformation of a test specimen, or it can be allowed to move radially. Once a vertical stress is applied to a specimen, the confining stress can then be determined from a known spring-stiffness and measured radial strain.

This test is capable of providing the resilient modulus, Poisson's ratio and shear strength parameters of a test material from a single test. The confining stress in this test is a result of axial deformation which is similar to the material's behaviour in the field. However, the radial stiffness of materials may be stress-dependent rather than fixed, as is the case with spring-stiffness.

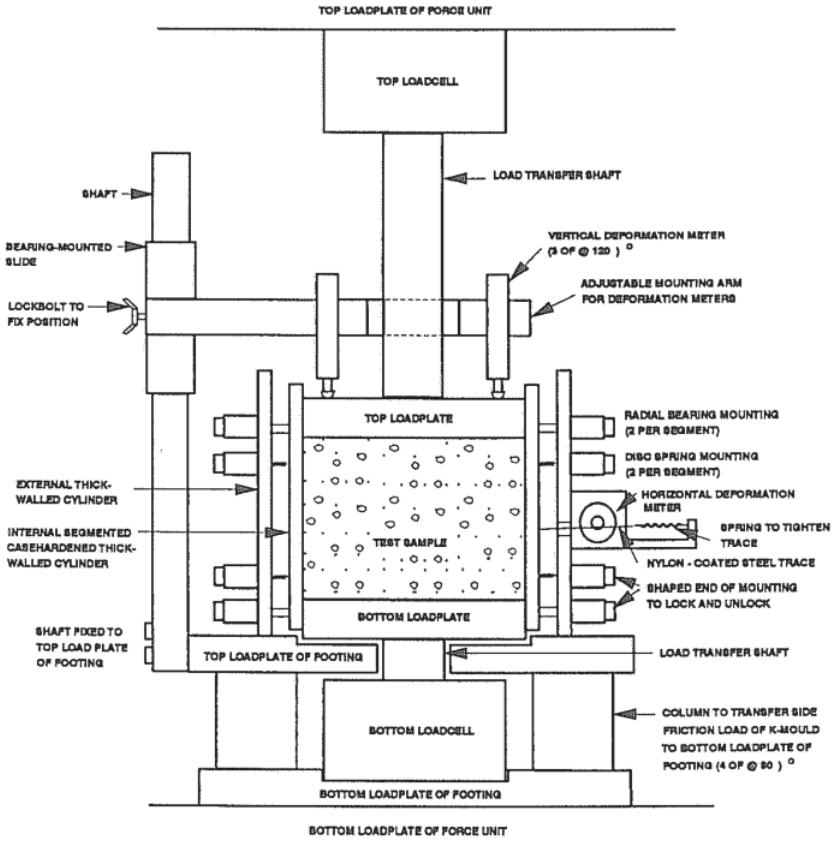

Figure 2.9: Schematic diagram for K-mould test setup (Semmelink 1991)

Figure 2.10: K-mould apparatus (Dynatest)

2.3.5 Springbox test

The concept of the Springbox test (Edwards 2007) is similar to the K-mould test in that a vertical load is applied to a test specimen and a horizontal stress (or confining stress) is then induced due to vertical deformation and spring stiffness. However, the test specimen is a 170 mm cube and it is allowed to move in only one direction along a pair of spring-supported sides while the other two sides are fixed, as shown in Figure 2.11 and Figure 2.12. The application of this test is limited as it was designed for use with the Nottingham asphalt tester loading frame.

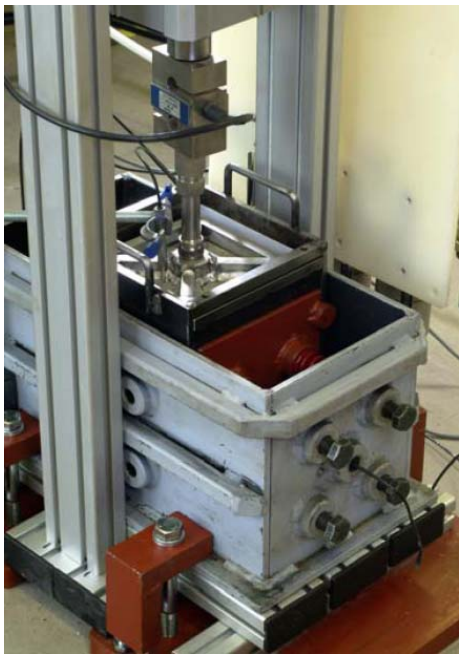

Figure 2.11: Springbox test (Edwards 2007)

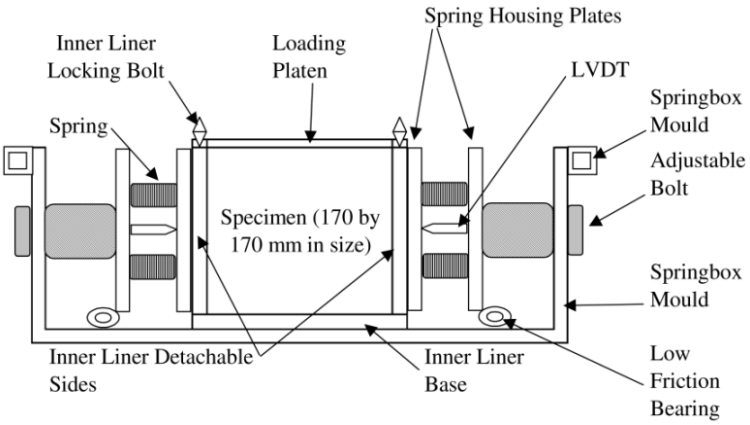

Figure 2.12: Schematic diagram of the springbox - longitudinal section (Edwards 2007)

Despite the fact that the RLT test has limitations with regard to simulating the rotation of the principal stresses, it is more favourable than some other tests due to the number of supporting previous studies undertaken (e.g., National Cooperative Highway Research Program 2008), various corresponding models for performance evaluation (e.g., Lekarp et al. 2000a, b) and the availability of easy-use testing equipment. Various features of applied stresses can be defined, such as magnitude, frequency and the number of loading cycles, and strains (axial, radial and volumetric) can be accurately measured. A number of standard test protocols for RLT are available. Some selected protocols, i.e., in the US, Europe, Australia, New Zealand and South Africa, are summarised and compared in section 2.4.

The National Cooperative Highway Research Program (NCHRP) synthesis 382 report (National Cooperative Highway Research Program 2008) summarised the abundant research on the resilient modulus of subgrade soils and aggregate materials that has been conducted in the US since 1986. NCHRP 1-37A (National Cooperative Highway Research Program 2004b), which provided a mechanistic-empirical pavement design guide (MEPDG), also recommended characterisation of the resilient modulus by RLT tests. In Australia, the pavement design guide (Austroads 2010c) mentions the RLT tests for the determination of the design modulus. Since 2003, when Austroads commenced the development of performance-based specifications, the RLT test has been recommended for determining material performance parameters such as shear strength, resilient modulus and pavement layer deformation (Austroads 2003). Voung et al. (Austroads 2007b) have evaluated and

compared the performance of various granular materials from New South Wales, Victoria and South Australia through the RLT tests. Jameson et al. (Austroads 2010a) also assessed the rutting of granular materials using RLT tests, along with the accelerated loading facility. Gonzalez et al. (Austroads 2012a) conducted RLT tests for the development of a finite element response model. As the adoption of recycled materials increases, the properties of some recycled materials have also been examined with RLT tests (e.g., Arulrajah et al. 2012; Gabr and Cameron 2012; Azam and Cameron 2013), with a view to further use of such materials in pavements.

2.4 Repeated load triaxial test protocols

A repeated load triaxial (RLT) test involves measuring the resilient and permanent strains of test samples after a number of loading repetitions in order to evaluate the resilient modulus (M_R) and permanent deformation (PD) of granular materials. Applied stresses in the RLT test usually consist of applying a constant confining pressure to the test specimen along with the application of cyclic vertical stress (deviator stress). Stresses in an element under moving traffic loads are complicated, thus various test protocols specify different sets of applied stresses to cover the range of deviator stress, confining stress, mean stress and ratio of deviator stress to confining stress.

The resilient modulus (M_R) is the ratio of deviatoric stress (σ_d) to the resilient strain (ε_r), as shown in Eq 2.1. The resilient modulus test executes a large number of stress stages by varying the ranges of deviator stress and confining stress applied to the same specimen. Each stage of the resilient modulus test usually applies 50 – 200 cycles of deviator stress before continuing on to the next stage. Conversely, permanent deformation tests generally keep a constant confining pressure throughout the test and apply a few different levels of deviator stress to a specimen. The number of loading cycles per stage in the permanent deformation test is usually given in terms of cycles of ten-thousand. The accumulated deformation is evaluated after a large number of load repetitions have been carried out. Thus permanent deformation tests are more time-consuming as they must cover a wider range of stress ratios and conditions of samples e.g., moisture and density. The tests also require a number of

test specimens, as once the specimen has completed the deformation test and experienced some amount of deformation it is not reliable for use in further tests.

$$M_R = \frac{\sigma_d}{\varepsilon_r} \tag{2.1}$$

where M_R = resilient modulus, σ_d = axial deviator stress and ε_r = axial resilient strain

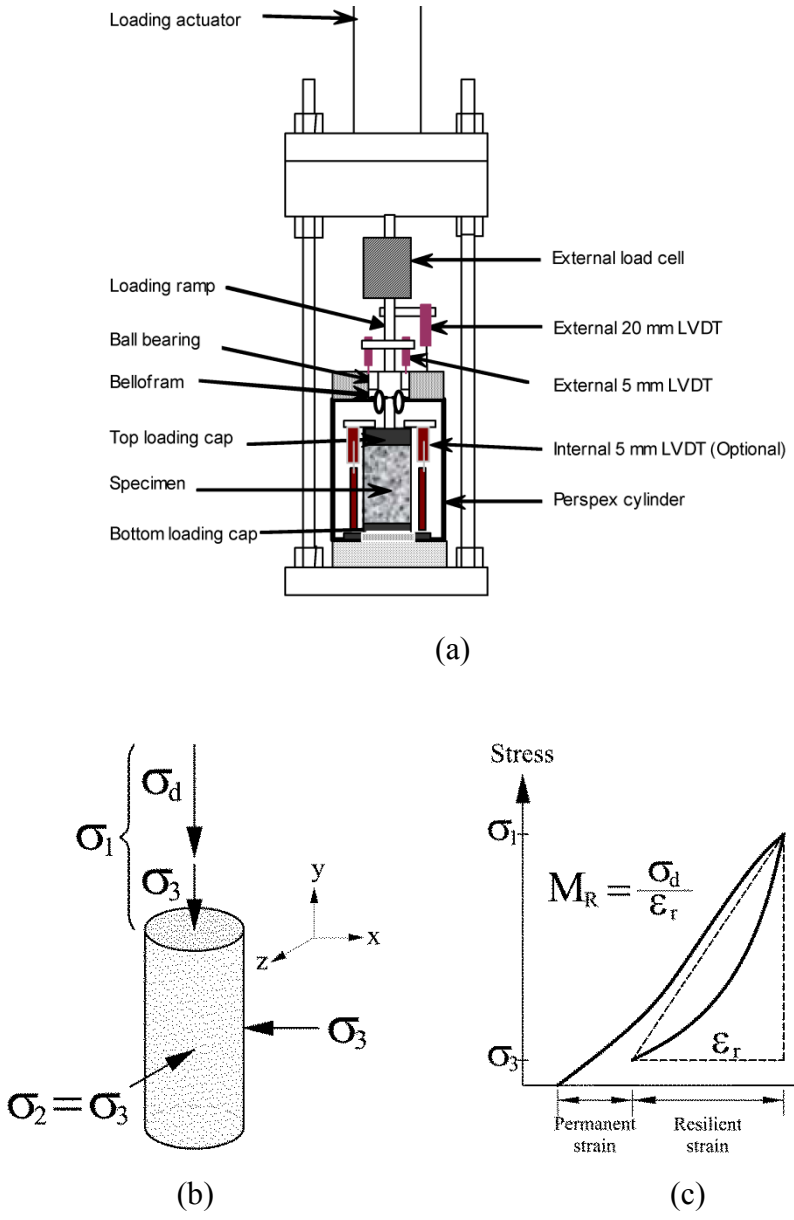

Figure 2.13: (a) Schematic diagram of RLT apparatus (Austroads 2007a) (b) Applied stresses on a sample (c) Definition of M_R

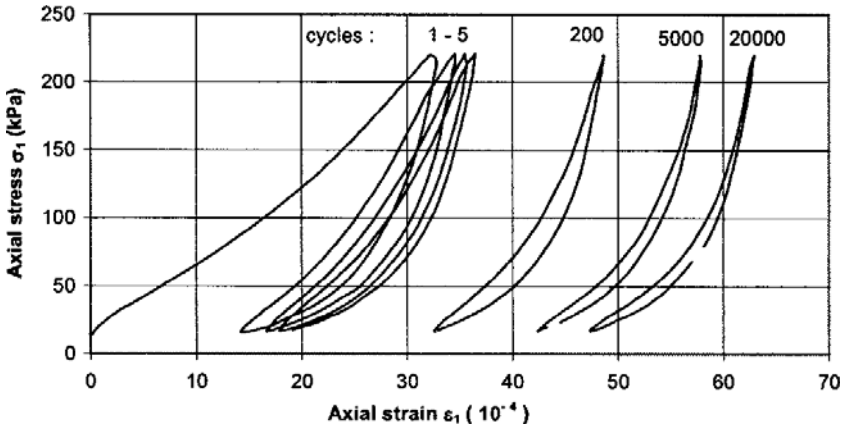

Figure 2.14: Stress-strain at large number of load repetitions (Chazallon et al. 2006)

The current test methods for M_R in the US, recommended by NCHRP 1-37A (National Cooperative Highway Research Program 2004b), are AASHTO T307-99 (AASHTO 2003) and the NCHRP 1-28A method (National Cooperative Highway Research Program 2004a). Both protocols evolved from the previous standard tests that were developed chronologically, i.e., AASHTO T 274-82, AASHTO T 292-91, AASHTO T 294-92 and AASHTO P46-94 (National Cooperative Highway Research Program 2008). Christopher et al. (2006) stated that there is no ASTM or AASHTO standard for permanent deformation tests. However, the permanent deformation obtained from 1000 conditioning cycles of an M_R test according to AASHTO T 307-99 is often used (Christopher et al. 2006).

The standard RLT test methods in Australia cover both M_R and PD tests. Austroads (1992) recommended selected stress regime for RLT test analysed from the triaxial test results of granular materials which covered wide range of applied stresses and finite element analysis of representative pavement structures (Austroads 2008d). The standard test method AS 1289.6.8.1 (Standards Australia 1995) was first issued in 1995 (superseded but still currently used in South Australia). Following this, Vuong and Brimble (2000) developed RLT test method APRG 00/33 to improve sample preparation, equipment specifications and loading regimes from the previous test method. The representative stress regime resulted from the finite element analysis of sprayed seal surface on granular pavements with various base thicknesses and basecourse material types subjected to standard axle load (Vuong and Arnold 2006). Eventually, Austroads (2007a) established the current standard test method

AG:PT/T053, based on Vuong and Brimble (2000), for greater uniformity of national performance-based specifications. Based on finite element analyses, a set of deviator stress of 450 kPa and confining stress of 50 kPa is expected to be a typical in-service conditions under an axle load of 40 kN on each single wheel (Vuong and Arnold 2006). This standard test method suggests 66 stress stages including this expected in-service stress for resilient modulus test to cover ranges of deviator stress, stress ratio and mean stress in order to examine the elastic condition and stress dependency of the test materials. For the permanent deformation test, only three stress conditions which include in-service condition, underloading and overloading, are specified.

Australian Road Research Board (1991) summarised the vertical loading shape, loading time and unloading time to standardise of the RLT test protocol. The vertical load waveform was suggested as a rectangle with load ramp as there was little influence of load waveforms on the RLT test results. Duske and Pender (1998) found there was insignificant different resilient modulus values resulted from haversine and square loading waveforms. The effect of loading frequency is also insignificant e.g., Kalcheff and Hicks (1973) found no difference in resilient properties of unbound granular materials when the loading frequency varied from 10 rpm to 80 rpm (0.167 to 1.33 Hz). Hence, the specified loading time was relied on the apparatus capability to produce the vertical load. Loading time between 0.3 seconds to 1.0 seconds was allowed for pneumatic system equipment. However, if available, closed loop systems which capable of applying shorter load as 0.1 seconds can be used to closely simulate the in-situ condition. Unloading time was suggested to be a minimum of 2.0 seconds allowing the test sample to fully recover during the test.

Table 2.2 illustrates the main features of various M_R test protocols including material and sample preparation, instrumentation and stress conditions. Applied stresses for permanent deformation tests are summarised in Table 2.3.

Table 2.2: Comparison of RLT test protocols for resilient modulus
(Vuong and Arnold 2006; Anochie-Boateng et al. 2009; Austroads 2010a)

Testing details	Austroads (2007) AG:PT/T053	Transit New Zealand T/15*	EN 13286-7 (2004)
Material	Max. aggregate size 19 mm – discard oversize	Max. aggregate size in the range of 37.5 mm	Max. aggregate size < 0.2 sample diameter
Specimen preparation	Standard proctor (5 lifts) or modified proctor (8 lifts)	Vibrating compaction test method (5 lifts)	Vibrating compaction (1 layer) Vibratory hammer (6-7 lifts)
Specimen size (height: diameter ratio, diameter)	H:D = 2:1, 100 mm diameter and 200 mm height	H:D = 2:1, 150 mm diameter and 300 mm height	H:D = 2:1, 160 x 320 mm, Diameter > 5 times of max. aggregate size
Response measurement	External or internal load cell, 2 external LVDTs, optional internal LVDTs	N.A.	Internal load cell 3 axials LVDTs measuring centre 100 mm of sample at 120˚, attached to membrane
Load type	Trapezoidal pulse of 3 s period with 1s load ,and rise and fall of 3 s	sinusoidal/haversine loading at 4 to 5 Hz	Axial load frequency 0.2-10Hz
Conditioning	1000 cycles, 50 kPa for σ_3 and 100 kPa for σ_d	N.A.	20000 cycles, 70 kPa for σ_3 and 200-340 kPa for σ_d
Confining pressure	constant	constant	Variable and constant (vacuum option)
Test sequence	50-200 cycles at 66 stress stages; 20- 150 kPa for σ_3, 100-600 for σ_d	50000 cycles at 6 stages ; 41.7 kPa – 140 kPa for σ_3, 90 kPa - 420 kPa for σ_d	100 cycles at 29 stress stages; 20- 150 kPa for σ_3, either 30-475 kPa or 20-300 for σ_d

* Transit New Zealand has now changed to New Zealand Transport Agency

Table 2.2: Comparison of RLT test protocols for resilient modulus (continued)

Testing details	AASHTO T307-99	NCHRP 1-28A (2004)	CSIR transportek (2002)
Material	1. less than 70% passing 2 mm sieve and less than 20% passing 0.075 sieve, PI < 10% 2. all others	1. Max. size > 9.5; 25.4 scalped 2. Max. size < 9.5; less than 10% passing 0.075 sieve 3. Max size < 9.5; more than 10% passing 0.075 sieve 4. Thin wall undisturbed	No details – Borrow pit or test pit max. aggregate size 37.5 mm
Specimen preparation	1. Vibratory hammer (6 lifts) 2. Static (5 lifts) or pneumatic kneading (5 lifts)	Type 1: Impact Proctor / vibratory hammer (or rotary) Type 2: vibratory Type 3: impact/ kneading	Vibratory table 3-lifts in split mould
Specimen size (height: diameter ratio, diameter)	H:D = 2:1, diameter 150 mm or 70 mm for subgrade; min dia. 5 times max. aggregate size (base/ subbase)	H:D = 2:1, 70 mm dia. (fine-grained); 100-150 mm dia. (coarse-grained)	H:D 2, 150mm dia. x 300-305 mm high
Response measurement	External load cell, 2 external LVDTs	Internal load cell, 2 internal LVDTs	Load cell on sample full length
Load type	Haversine, load for 0.1 s load and rest for 0.9 s (hydraulic); or rest for 0.9 to 3 s (pneumatic)	Haversine, 0.1 s load and 0.9 s rest (base/subbase); 0.2 load and 0.8 s rest (subgrade)	Haversine, 0.2 s load and 0.8 s rest period
Conditioning	500-1000 cycles, 103.4 kPa for σ_3 and 103.4 kPa for σ_d	1000 cycles, 27.6-103.5 kPa for σ_3 and 50.8-227.7 kPa for σ_d	500-1000 cycles, 200 kPa for σ_3 and 45% of σ_d at failure
Confining pressure	Constant	Constant	Constant
Test sequence	20.7- 138 kPa for σ_3 and 20.7- 286 kPa for $\sigma_{d;}$ 100 cycles at 15 stress stages	20.7- 138 kPa for σ_3 and 20.7- 993kPa for $\sigma_{d;}$ 100 cycles for each stress stage; 30 stress stages for Type 1, 20 stress stages for Type 2, and 16 stress stages for Type 3	20 - 200 kPa for σ_3 and 0.08 - 0.81of failure stress for $\sigma_{d;}$ 100 cycles at 14 stress stages

Table 2.2: Comparison of RLT test protocols for resilient modulus (continued)

Testing details	University of Illinois (1998)	University of Stellenbosch (2007)	Nottingham University
Material	Unbound aggregate and subgrade soils max. aggregate size 25 mm	Unbound and bound granular materials. Max size 19 mm duplicate specimens	Max. aggregate size in the range of 20–40 mm
Specimen preparation	Standard pneumatic concrete vibratory compactor 3 lifts I split mould	Not specified	Vibrating compaction test method (BS 1377-4: 1990)
Specimen size (height: diameter ratio, diameter)	H:D = 2:1, 50 mm dia. for subgrade soils; 150 mm dia. for base / subbase	H:D 2, 150mm dia. x 300 mm high	H:D 2, 150mm dia. x 300 mm high
Response measurement	Internal load cell, 2 external LVDTs	Load cell on specimen LVDTs over middle third	Internal load cell and on-sample strain measured at sample mid-half using studs embedded in the specimen at two opposite locations
Load type	Haversine, 0.1 s load and 0.9 s rest period	Haversine, 0.5 s load and 0.5 s rest period	Sinusoidal pulse at 5 Hz
Conditioning	1000 cycles, 103.4 kPa for σ_3 and 310.5 kPa for σ_d	5000 cycles, 200 kPa for σ_3 and 20 kPa for σ_d	N.A.
Confining pressure	Constant	Constant	Constant
Test sequence	34.5 - 207 kPa for σ_3 and 69 - 414 kPa for $\sigma_{d;}$ 100 cycles at 8 stress stages	20 - 200 kPa for σ_3 (coarse), 20 - 140 kPa for σ_3 (fine), and 0.1 - 0.9 of failure stress for $\sigma_{d;}$ 100 cycles at 15 stress stages	50-300 kPa for mean normal stress, 50 - 700 kPa for σ_d 50000 cycles of at 21stages using 3 specimens, viz. 7 stages per specimen

Table 2.3: Comparison of RLT test protocols for permanent deformation (Vuong and Arnold 2006; Austroads 2010a)

Testing details	Stress condition	No. of loading cycles
Austroads AG:PT/T053 (2007)	3 stages on one specimen with constant σ_3 of 50 kPa and increasing σ_d being selected based on function of the material in the pavement (350, 450 and 550 kPa for base, 250, 350 and 450 kPa for upper subbase and 150, 250 and 350 kPa for lower sub-base)	10,000 cycles per stage
Australian Standards AS1289.6.8.1(1995)	Single stage with σ_d of 460 kPa and constant σ_3 of 196 kPa	50,000 cycles per stage
Transit New Zealand* M/22 (2000)	Single stage with σ_d of 425 kPa and constant σ_3 of 125 kPa	50,000 cycles per stage
Transit New Zealand* T/15 (2007)	6 stages on one specimen with constant σ_3 of 41.7 kPa – 140 kPa and σ_d of 90 kPa - 420 kPa	50,000 cycles per stage
Nottingham University	21 stages using 3 specimens, viz. 7 stages per specimen with constant mean stresses and increasing shear stresses	50,000 cycles per stage

* Transit New Zealand has now changed to New Zealand Transport Agency

2.5 Factors affecting material responses under repetitive loadings

Responses of granular materials are usually measured in terms of resilient modulus and permanent strain. The two responses of these materials are influenced by their individual material properties and external excitation, i.e., applied stresses. Characteristics of stresses cover the magnitude of the deviator stress, the confining stress, the stress ratio of deviator stress to confining stress, stress history, and principal stresses rotation along with the number of load repetitions and the duration, frequency and sequence of applied stresses. The material properties include moisture content, density, particle size distribution, fines content, maximum aggregate size, and aggregate shape and surface (Lekarp et al. 2000a, b). Material characteristics are important for the establishment of pavement material specifications, while the effects

of stress conditions are useful for setting up the loading regimes in laboratory test protocols.

2.5.1 Effects of stress characteristics

Permanent strain decreases with increasing confining stress (Lekarp et al. 2000b; Uthus 2007), but it increases with higher deviator stress and the stress ratio of deviator stress to confining stress (Lekarp et al. 2000b). Permanent strain also increases with the occurrence of principal stresses rotation or shear stresses; this effect is more pronounced with higher magnitude ratios of shear stresses to normal stresses and vice versa (Chan 1990). If the material experiences gradual densification due to a past stress history, there appears to be a reduction in the proportion of permanent strain to resilient strain during subsequent loading cycles. However, the effect of stress history is the reverse if previous stress dilated the material (Lekarp et al. 2000b).

The increments in permanent strain from the number of loading cycles depends on the deviator stress magnitude which can be explained by the shakedown concept as shown in Figure 2.15 (Arnold 2004). The shakedown concept classifies the long-term incremental rate of permanent strain as: range A - the plastic shakedown, range B - the plastic creep, and range C – the incremental collapse. Due to the low stress magnitude in range A, the permanent strain rate is high during the initial compaction period. Subsequently, the permanent strain rate decreases with an increase in load cycles until there is no further permanent strain. Thus strain becomes entirely resilient. In range B, the moderate stress magnitude applied to the materials also results in a high permanent strain rate during the initial compaction period. Consequently, the incremental rate decreases and becomes constant with the increase in load cycles. The permanent strain rate increases with the increase in load cycles, i.e., failure is likely when the material is subjected to high stress magnitudes in the C range (Arnold 2004).

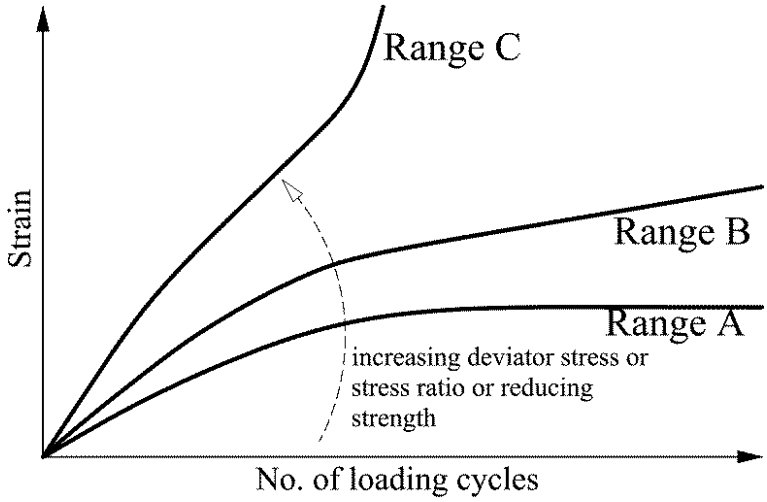

Figure 2.15: Schematic diagram of permanent strain increment with number of loading cycles (Arnold 2004)

The resilient modulus increases considerably with confining pressure and bulk stress, and is less pronounced with deviator stress (Lekarp et al. 2000a; Uthus 2007). Uthus (2007) also found that the influence of confining stress seems to be 3-5 times that of the deviatoric stress. Chan (1990) concluded that resilient strains were not affected by principal stresses rotation (Adu-Osei 2000). The stress history and number of load cycles affect the resilient properties as a consequence of material densification and particle rearrangement (Uthus 2007). Hicks (1970) found that the resilient response became stable after approximately 100 cycles at the same stress level. The effect of the stress history can be avoided by applying a preconditioning stage (approximately 1,000 loading cycles) to a test specimen prior to the RLT tests (Allen 1973), and by avoiding the application of high stress ratios during the tests (Boyce 1976). Several studies (Seed et al. 1965; Morgan 1966; Hicks 1970; Allen 1973; Boyce et al. 1976; Thom and Brown 1987) found that the duration, frequency and sequence of stresses do not significantly affect the resilient properties of granular materials. However, the resilient modulus can be reduced at high load frequencies if the materials approach saturation point (Lekarp et al. 2000a).

2.5.2 Effects of material properties

The presence of moisture influences the performance of materials, and therefore pore water pressure, effective stress and lubrication have an effect on the materials. With an adequate amount of water, a higher density is achieved and this has a positive influence on the strength and stiffness of the unbound granular material. As the moisture content increases and approaches the saturation condition, it results in a noticeable reduction of the resilient modulus and deformation resistance. This is probably a consequence of the pore water pressure that is generated, and this brings a reduction in effective stress while water lubricates the material particles (Lekarp et al. 2000a, b). An increase in the density of a granular material generally improves the shear strength, resilient modulus and resistance to permanent strain. It can be explained as the number of particle contacts per particle increasing greatly with increased density and then decreasing the average contact stress of a certain load (Kolisoja 1997).

Gradation indirectly influences material performance as it has an impact upon the density, particle contacts, moisture condition and drainage of the materials. Fine particles can fill the void space in the material skeleton to increase its density. However the particles can block the drainage of water, which results in an increase in pore water pressure. During load transfer, an excess amount of fines may displace the coarse particles which are the major components. The coarse particle contacts then decrease which reduces the load carrying capacity and resistance to deformation. Uthus (2007) found that increasing the fines content at equal dry densities resulted in a decrease in the resilient modulus and resistance to permanent deformation. Maximum aggregate size influences the material performance as an effect of the amount of particle contacts. At the same fines content and gradation, an increase in maximum aggregate size was found to increase the resilient modulus and decrease the total deformation due to the lesser number of particle contacts (Kolisoja 1997). Crushed, angular materials provided a higher resilient modulus and a lower permanent deformation than that of uncrushed, rounded or sub-rounded grains at the same density as a result of a higher angle of internal friction in angular materials (Allen 1973; Uthus 2007).

From a construction point of view, pavement specifications usually require the basic properties of materials to meet requirements of gradation, maximum aggregate size, density and moisture content. These factors have an interrelated effect on material performance in the field. Well-graded material, compacted with the optimum amount of water achieves a higher density than poorly-graded material. It is expected that this well-graded material would perform more effectively in terms of strength and resistance to deformation. As the gradation and density of materials can be controlled, it is the moisture condition of the pavement materials that must be carefully attended to. All pavement specifications throughout Australia require pavement materials to be dried back prior to the construction of the upper layer (Midgley 2009). A given amount of water must be added to pavement material in order to achieve a specific density during compaction. The material must then be allowed to dry out until it reaches a particular moisture content level. The main purpose of dryback is to maximise pavement service life along with to allow satisfactory penetration of the primer binder into the pavement surface (Australian Road Research Board 2003). Despite this, there are few specific explanations of how the dryback process actually affects the material's performance. However, enhanced pavement performance from the drying out of pavement basecourse was proven in Queensland in 1996 with pavement trials using an Accelerated Loading Facility. This investigation indicated that the drying back of pavements can maximise service life. In this study, it was found that in the long-term, dried back pavement material tends to remain drier and stronger than pavement material which has not been dried back (Australian Road Research Board 2003).

Khoury et al. (2009) studied the resilient modulus of subgrade soils with respect to moisture content after compaction. An example of their experimental results is shown in Figure 2.16, where soil samples were compacted at optimum moisture content (OMC), below OMC and above OMC. Subsequently, all samples were subjected to drying and/or wetting and the M_R values of the test samples were then measured. There was a tendency for the resilient moduli of subgrade soils to increase with respect to sample drying and vice versa.

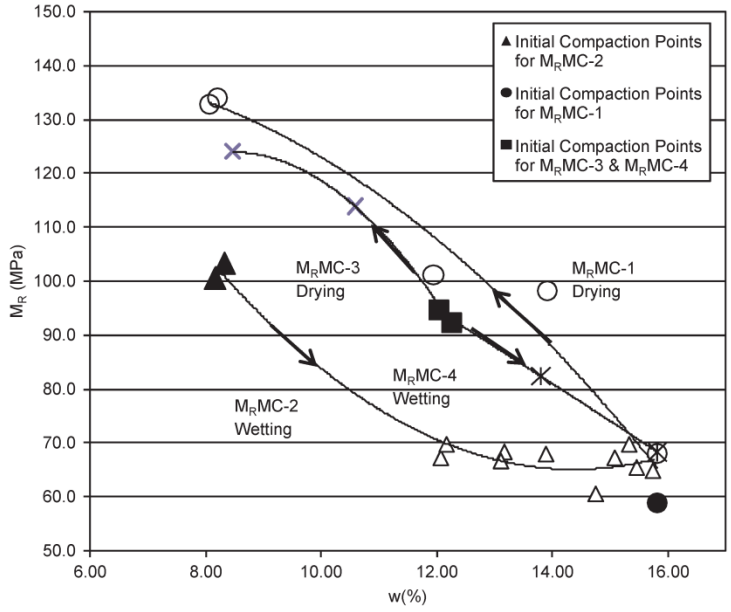

Figure 2.16 Variation of M_R with drying and wetting of a soil sample (Khoury et al. 2009)

2.6 Modelling of materials responses under repetitive loadings

2.6.1 Resilient modulus models

The stress-dependent formulation for the resilient modulus has been widely used despite the fact that it is also influenced by material properties. Several researchers have proposed different stress components for input into the resilient modulus model based on their experimental data and various constitutive equations for determining the resilient modulus of granular materials have been proposed. Hicks and Monismith (1971) introduced the k-θ model where the resilient modulus was related solely to bulk stress, (Eq. 2.2). Uzan (1985) considered the M_R affected by bulk and deviator stresses, as shown in Eq. 2.3. Furthermore, the universal model (Eq. 2.4) proposed by Witczak and Uzan (1988) replaced the deviator stress in the Uzan model with octahedral shear stress in order for the model to be suitable for 3D analysis. However, these two equations resulted in parallel model parameters since octahedral shear stress is a multiple of deviator stress for cylindrical triaxial tests. Nataatmadja and Parkin (1989) examined the earlier models and found the best fit for M_R was as a function of deviator and bulk stresses, as seen in Eq. 2.6. Austroads (2010c) recommended the modified universal model (Eq. 2.5), which is identical to the

design guide of NCHRP project 1-37A (National Cooperative Highway Research Program 2004b) for the characterisation of granular materials. NCHRP project 1-28 Barksdale et al. (1997) suggested that the M_R depends on deviator and confining stresses, as can be seen in Eq. 2.7. Andrei et al. (2004) reported the modification of Eq. 2.7 which became Eq. 2.8 to validate $\sigma_3 = 0$ or $\sigma_d = 0$. All of the abovementioned equations are summarised in Table 2.4.

Guo and Emery (2011) highlighted the importance of resilient strain in the modelling of the resilient modulus, as seen in Eq. 2.10, which was initiated by integration of the NCHRP 1-37A model with the resilient strain. Previously, the UTEP model (Feliberti et al. 1992), as shown in Eq. 2.9, was used where the resilient strain term was combined with the bulk stress model.

Table 2.4: Resilient modulus model with respect to applied stresses

Eq.	Model	Authors
2.2	$M_R = k_1 \theta^{k_2}$	Hick and Monismith (1971)
2.3	$M_R = k_1 p_a \left(\frac{\theta}{p_a}\right)^{k_2} \left(\frac{\sigma_d}{p_a}\right)^{k_3}$	Uzan (1985)
2.4	$M_R = k_1 p_a \left(\frac{\theta}{p_a}\right)^{k_2} \left(\frac{\tau_{oct}}{p_a}\right)^{k_3}$	Witczak and Uzan (1988)
2.5	$M_R = k_1 p_a \left(\frac{\theta}{p_a}\right)^{k_2} \left(\frac{\tau_{oct}}{p_a}+1\right)^{k_3}$	Austroads (2010c); NCHRP 1-37A (2004)
2.6	$M_R = \left(\frac{\theta}{\sigma_1}\right)\left(k_1 + k_2\sigma_d\right)$	Nataatmadja & Parkin (1989)
2.7	$M_R = k_1 p_a \left(\frac{\sigma_3}{p_a}\right)^{k_2} \left(\frac{\sigma_d}{p_a}\right)^{k_3}$	NCHRP 1-28 (Barksdale et al. 1997)
2.8	$M_R = k_1 p_a \, k_2^{\left(\frac{\sigma_3}{p_a}\right)} \, k_3^{\left(\frac{\sigma d}{p_a}\right)}$	Andrei et al. (2004)

M_R = resilient modulus in MPa; pa = atmospheric pressure (100 kPa); θ = Bulk stress in kPa (first invariance of stress) = $(\sigma_1 + 2\sigma_3)$; τ_{oct} = octahedral shear stress in kPa = $\frac{\sqrt{2}}{3}\sigma_d$ for cylindrical specimens in triaxial tests; σ_1 = major principal stress in kPa; σ_3 = minor principal stress or confining pressure in kPa; σ_d = deviator stress in kPa = σ_1- σ_3; and k_1, k_2 and k_3= regression constant.

Table 2.5: Resilient modulus model with respect to applied stresses and resilient strain

Eq.	Model	Authors
2.9	$M_R = k_1 p_a \left(\frac{\theta}{p_a}\right)^{k_2} \varepsilon_r^{k_3}$	UTEP model (Feliberti et al. 1992).
2.10	$M_R = k_1 p_a \left(\frac{\theta}{p_a}\right)^{k_2} \left(\frac{\tau_{oct}}{p_a}+1\right)^{k_3} \left(\frac{1}{1+\frac{\varepsilon_r}{k_4}}\right)$	Guo and Emery (2011)
ε_r = resilient axial strain		

In addition to the stress-dependent model, resilient models that incorporate moisture, density and temperature conditions of materials in can be found in Appendix DD-2 of the NCHRP 1-37A report (National Cooperative Highway Research Program 2000), for example, the models proposed by Rada and Witczak (1981), Jin et al. (1994). Rada and Witczak (1981) developed a model that takes into account a degree of saturation and density ratio on top of bulk stress (see Eq. 2.11). Jin et al. (1994) integrated temperature, density and moisture conditions into their model; water content and density were used instead of degree of saturation and density ratio respectively, as shown in Eq 2.12. In both equations, a regression constant of bulk stress is similar to k_2, while the combination of other constants is equivalent to k_1 in the bulk stress model (Eq. 2.2). A relationship between $M_{R,}$ at any moisture condition, to the saturated condition is expressed in Eq. 2.13. Eventually, the unified universal model was combined with Eq. 2.13, leading to Eq. 2.14 which is the final model recommended for implementation into the AASHTO mechanistic-empirical pavement design guide (MEPDG). Later, Attia and Abdelrahman (2010) revised Eq. 2.14 by replacing saturation terms with moisture content terms, and obtained Eq. 2.15.

Table 2.6: Resilient modulus model with respect to applied stresses and material conditions

Eq.	Model	Authors
2.11	$\log \mathrm{M_R} = \mathrm{C_1} + \mathrm{C_2}\,\mathrm{S} + C_3 D_R + C_4 \log\theta$	Rada & Witczak (1981)
2.12	$\log \mathrm{M_R} = \mathrm{C_1} + \mathrm{C_2}\,\mathrm{W_c} + C_3 T + C_4 \gamma_d + C_5 \log\theta$	Jin et al. (1994)
2.13	$\log \frac{\mathrm{M_R}}{\mathrm{M_{Ropt}}} = a + \frac{b-a}{1+\exp[\beta + k_s (S - S_{opt})]}$	NCHRP 1-37A
2.14	$\mathrm{M_R} = 10^{\left[a+\frac{b-a}{1+\exp[\beta+k_s(S-S_{opt})]}\right]} \mathrm{k_1 p_a} \left(\frac{\theta}{\mathrm{p_a}}\right)^{\mathrm{k_2}} \left(\frac{\tau_{\mathrm{oct}}}{\mathrm{p_a}}+1\right)^{\mathrm{k_3}}$	NCHRP 1-37A
2.15	$\mathrm{M_R} = 10^{\left[a+\frac{b-a}{1+\exp[\beta+k_w(W-W_{opt})]}\right]} \mathrm{k_1 p_a} \left(\frac{\theta}{\mathrm{p_a}}\right)^{\mathrm{k_2}} \left(\frac{\tau_{\mathrm{oct}}}{\mathrm{p_a}}+1\right)^{\mathrm{k_3}}$	Attia & Abdelrahman (2010)

$\mathrm{M_{Ropt}}$ = resilient modulus at maximum dry density and optimum moisture content; S = degree of saturation at a specific point, (%); Sopt = degree of saturation at maximum dry density and optimum moisture content, (%);W = water content at a specific point, (%); Wopt = water content at maximum dry density and optimum moisture content, (%);$\mathrm{C_1}$, $\mathrm{C_2}$, $\mathrm{C_3}$, $\mathrm{C_4}$ and $\mathrm{C_5}$ = regression constant; $\mathrm{k_S}$, $\mathrm{k_w}$ = regression material constant in the semi-log space; a = minimum of log(MR/MRopt); b = maximum of log(MR/MRopt); β = location parameter obtained as a function of a and b by imposing the condition of a zero intercept and $\beta - \ln\left(\frac{b}{a}\right)$

2.6.2 Permanent strain models

There are a number of different relationships for predicting permanent strain in granular materials. These are generally based on the effect of two components, being the number of loading cycles and the applied stresses. These two components are either separated (see Table 2.7 and Table 2.8) or integrated (see Table 2.9) for permanent strain models. The number of loading cycles results in a gradual accumulation of the rate of permanent strain, while the stress-based relationships show the outcome of the amount of permanent strain after a certain number of load cycles. Another previous model related to resilient strain, is that of Veverka (1979), as shown in Eq.2.16. Bodin et al. (Austroads 2013a) also categorised many previously proposed relationships based on the shakedown concept, i.e., Ranges A, B and C. The models based on applied stress suggested that stabilisation and failure of

permanent strain are governed by on levels of stresses (Lekarp et al. 2000b). Several authors developed prediction models on an empirical basis, to fit their experimental results. Thus these may not apply to other materials (Austroads 2013a).

Christopher et al. (2006) stated that the NCHRP 1-37A design guide characterises the permanent strain of basecourse, subbase and subgrade materials based on the findings of Tseng and Lytton (1989) as shown in Eq 2.21. Bodin et al. (Austroads 2013a) selected two relationships from each of number of loading cycle-based models and applied stresses-based models which then delivered four combined equations, as shown in Table 2.10. These four relationships were evaluated with a wheel-tracker and accelerated loading facility (ALF) test results. Further work is required in order to improve the modelling approach, as at this stage the predicted models underestimate the permanent deformations in the tested pavements.

Table 2.7: Permanent strain model with respect to number of loading cycles

Eq.	Model	Constants	Author(s)	Shakedown range[2]
2.16	$\varepsilon_p = a\varepsilon_r N^b$	a, b	[1]Veverka 1979	B
2.17	$\varepsilon_p = a + b\log N$	a, b	[1]Barksdale 1972	B
2.18	$\frac{\varepsilon_p}{N} = \frac{A}{N^b}$	A, b	[1]Khedr 1985	B
2.19	$\varepsilon_p^* = \frac{A\sqrt{N}}{\sqrt{N} + D}$	A, D	[1]Paute et al. 1988	A
2.20	$\varepsilon_p = \varepsilon_0 e^{-\left(\frac{\rho}{N}\right)^\beta}$	ε_0, ρ and β	Tseng and Lytton 1989	A
2.21	$\varepsilon_p = aN^b$	a, b	[1]Sweere 1990	B
2.22	$\varepsilon_p^* = A\left(1 - \left(\frac{N}{100}\right)^{-B}\right)$	A, B	[2]Hornych et al. 1993; [1]Paute et al. 1996	A
2.23	$\varepsilon_p = (cN + a)(1 - e^{-bN})$	a, b and c	[1]Wolff and Visser 1994	A and B
2.24	$\varepsilon_p = A\left(\frac{N}{1000}\right)^B + C\left(e^{\frac{DN}{1000}} - 1\right)$	A, B, C and D	Huurman 1997	A, B and C
2.25	$\varepsilon_p = dN + \frac{cN}{\left(1 + \left(\frac{cN}{a}\right)^b\right)^{\frac{1}{b}}}$ $\varepsilon_p = dN + a\left(1 - e^{-bN}\right)$	a, b, c and d	[2]Theyse 2007	A and B
2.26	$\varepsilon_p = aN^b + (mN + c)\left(1 - e^{-dN}\right)$	a, b, c, d and m	[2]Perez and Gallego2010	A, B and C
2.27	$\varepsilon_p = a + bN - ce^{-dN}$	a, b, c and d	Cerni et al. 2012	A and B

ε_p = permanent axial strain; ε_p^* = permanent axial strain after first 100 cycles; ε_r = resilient axial strain; e = natural logarithm

[1] referred to Lekarp et al. (2000b);

[2] referred to Austroads (2013a)

Table 2.8: Permanent strain model with respect to applied stresses

Eq.	Model	Constants	Author(s)
2.28	$\varepsilon_p = \dfrac{q / a\sigma_3^b}{1 - \left[\dfrac{(R_f q)/2(C\cos\phi + \sigma_3 \sin\phi)}{(1-\sin\phi)}\right]}$	a	[1]Barksdale 1972
2.29	$\varepsilon_p = a\dfrac{q}{\sigma_3}$	a	[3]Hyde 1974
2.30	$\varepsilon_p = K\left(\dfrac{q_{\max}}{\sigma_3}\right)^{\alpha}$	K and α	[3]Shenton 1974
2.31	$\varepsilon_{Sp} = fn(N)\left(\dfrac{\sqrt{2/3}.q}{\sqrt{3}.p}\right)^{2.8}_{\max}$	$fn(N)$	[1]Pappin 1979
2.32	$\varepsilon_p = \varepsilon_{0.95S}\ln(1-q/S)^{-0.15} + \left(\dfrac{a(q/S)}{1-b(q/S)}\right)\ln(N)$	a and b	[1]Lentz and Baladi 1981
2.33	$\varepsilon_p(N_{ref}) = a\left(\dfrac{L}{p_a}\right)\left(\dfrac{q}{p}\right)^b_{\max}$	a and b	[1]Lekarp and Dawson 1998
2.35	$\varepsilon_p = e^a e^{bp}(e^{cq} - 1)$	a, b and c	Arnold 2004

ε_p = permanent axial strain; ε_{Sp} = permanent shear strain; $\varepsilon_{0.95S}$ = axial strain at 95% of static strength; $\varepsilon_p(N_{ref})$ = permanent axial strain after number of cycles N_{ref}; q = deviator stress; p = mean stress; p_a = atmospheric pressure; σ_3 = confining stress; R_f = ratio of the applied stress q to deviator stress at failure; L = length of stress path = $\sqrt{p^2 + q^2}$; S = static strength; C = cohesion; ϕ = angle of internal friction; e = natural logarithm

[1] referred to Lekarp et al. (2000b);

[2] referred to Austroads (2013a);

[3] referred to Gidel et al. (2001)

Table 2.9: Permanent strain model with respect to combination of number of loading cycles and applied stresses

Eq.	Model	Constants	Author(s)
2.34	$\varepsilon_p = AN^{\alpha}\left(\frac{\sigma_z}{p_a}\right)^{\beta}$	A, α and β	[1]Ullditz 1993
2.35	$\varepsilon_p = \frac{\frac{q}{(p+p^*)}}{b\left(m-\frac{q}{(p+p^*)}\right)}\left(1-\left(\frac{N}{100}\right)^{-B}\right)$	B and b	[2]Paute et al. 1996
2.35	$\varepsilon_p = AN^{\alpha}\left(\frac{p}{p_a}\right)^{\beta}$	A, α and β	[1]Puppala and Mohammad 1999
2.36	$\varepsilon_p = A\left(1-\left(\frac{N}{100}\right)^{-B}\right)\left(\frac{L_{\max}}{p_a}\right)\frac{1}{\left(m+\frac{s}{p_{\max}}-\frac{q_{\max}}{p_{\max}}\right)}$	A and B	Gidel et al. 2001
2.37	$\varepsilon_p = k_1 N^{k_2}(\theta/p_0)^{k_3}(\tau_{oct}/p_0)^{k_4}$	k_1, k_2, k_3 and k_4	Puppala et al. 2009

ε_p = permanent axial strain; q = deviator stress; σ_z = vertical effective stress p = mean stress; p* = stress parameter defined by intersection of static failure line and p-axis in p-q space; θ = bulk stress; τ_{oct} = octahedral shear stress; p_a = atmospheric pressure; L = length of stress path = $\sqrt{p^2+q^2}$; m and s are shear stress envelope in q = mp+s

[1] referred to Puppala et al. (1999);

[2] referred to Lekarp et al. (2000b)

Table 2.10: Combination of permanent strain models (Austroads 2013a)

Eq.	Model	Combination
2.38	$\varepsilon_p = AN^B \left(\frac{L}{p_a}\right)\left(\frac{q}{p}\right)^b_{\max}$	Sweere – Lekarp
2.39	$\varepsilon_p = AN^B \left(\frac{L_{\max}}{p_a}\right)\frac{1}{\left(m + \frac{s}{p_{\max}} - \frac{q_{\max}}{p_{\max}}\right)}$	Sweere – Gidel
2.40	$\varepsilon_p = A\left(1 - \left(\frac{N}{N_0}\right)^{-B}\right)\left(\frac{L}{p_a}\right)\left(\frac{q}{p}\right)^b_{\max}$	Hornych – Lekarp
2.41	$\varepsilon_p = A\left(1 - \left(\frac{N}{N_0}\right)^{-B}\right)\left(\frac{L_{\max}}{p_a}\right)\frac{1}{\left(m + \frac{s}{p_{\max}} - \frac{q_{\max}}{p_{\max}}\right)}$	Hornych – Gidel

CHAPTER 3
CHARACTERISTICS OF CEMENT-TREATED BASE

Cement-stabilised material has been in use for some time in pavements in many countries including the United States, United Kingdom, China, South Africa and South Korea (Cho et al. 2006; Molenaar et al. 2011). In Australia, cement-treated base (CTB) has been reliably used in pavement in the eastern states (Department of Planning Transport and Infrastructure 2011; Roads Corporation 2011; Department of Transport and Mainroads 2012; Roads and Maritime Services 2013). Its use is backed by research that is applicable to local conditions (Austroads 2008a, c, b, 2010b, 2012b). However, its utilisation in Western Australian pavements is limited due to a lack of locally-focused research, and past incidences of cracking in the cement-stabilised material. This chapter presents the significant characteristics of cement-stabilised material (unconfined compressive strength, shrinkage and flexural fatigue) which is produced from Western Australian crushed rock base. The study aims to acquire and develop further knowledge of the characteristics of cement-treated base, known as CTB. The eventual aim is to produce an improved CTB mix design, thereby restoring confidence in the material so that it may be used successfully in structural designs and the construction of pavements in Western Australia.

3.1 General Background

Cement-treated base (CTB) is a mixture of natural or manufactured aggregate, or soil or gravel blended with a prescribed amount of Portland cement and water. It can be classified as either a cemented material or a bound stabilised material (Austroads 2005). In new pavement construction, CTB can be mixed at the manufacturing plant, or for the rehabilitation of existing pavement it may be mixed in-situ. CTB must be thoroughly mixed with the appropriate amount of cement and water in order to achieve workability and maximum density. After compaction, CTB must be cured effectively for hydration to reach an acceptable level and to allow the optimum hydration reaction to take place.

The purpose of CTB is to improve the engineering properties of the parent materials used in road pavements. These improved properties would include greater strength, increased resistance to rutting and a reduction in susceptibility to moisture. The engineering properties of CTB mixtures are dependent on the individual constituent materials properties (i.e., aggregate material and cement type properties), curing conditions, and age.

The load-carrying capacity of a base also depends on the strength and thickness of the base layer. Thicknesses for CTB are less than those required for unstabilised granular bases carrying the same amount of traffic. This is due to CTB having the capacity to distribute loads across a wider area and the ability to transfer lower stresses to the underlying layer. Theoretically, a thin-strong base can sustain the equivalent load of a thick-weak base. However, a thick-weak base is preferable as a thin-strong base is more brittle and therefore more likely to crack (Garber et al. 2011).

Despite its advantages, CTB can deteriorate in the early stages following construction. This deterioration takes the form of shrinkage-cracking, erosion (lightly-bound CTB), and fatigue-cracking (bound CTB) which is a long-term form of deterioration (Kodikara 2006).

3.2 Reflection cracking in flexible pavements and countermeasures

Reflection cracking in asphalt surfaces propagates upwards from the base layer. The appearances of crack patterns on the surface are similar to the cracks in the base layer below (van-Blerk and Scullion 1995; Halsted 2010). This cracking can accelerate the deterioration of the pavement by allowing moisture to penetrate down through the pavement structure. Cracking in the CTB layer occurs when the induced tensile stresses in the layer, caused by fatigue or shrinkage, exceed its tensile strength. Fatigue-cracking is one of the major distress modes in CTB pavements; it is associated with the stiffness degradation of the material under repetitive loading from traffic. Cracks from fatigue failure generally originate at the bottom of the CTB layer and spread throughout the asphalt surface (Little et al. 1995; Goerge 2002). Shrinkage strains can constrain and cause stresses in the CTB layer as a consequence

of the friction from the underlying layer constraining the movement of the base layer (Cauley and Kennedy 1972).

Little et al. (1995) stated that fatigue-cracking can be prevented by adequate pavement design. However, most failures in CTB are caused by shrinkage or thermal-cracking in the layer, or by a combination of these two effects occurring from traffic- induced stresses. Shrinkage of cement-treated material mainly consists of drying shrinkage and autogenous shrinkage. Drying shrinkage is a result of water from the mixture evaporating into the atmosphere. Autogenous shrinkage is not related to the moisture that is lost to the environment; it is caused by the water consumption of the CTB when undergoing a hydration reaction, known as self-desiccation (Dunlop et al. 1975; Zhang et al. 2012).

Many studies have suggested methods for the prevention of shrinkage cracking in cement-treated materials. These include changing the mix ratio of the material, using shrinkage-reducing additives and employing tighter construction controls. Goerge (2002) suggested the use of fly ash with an appropriate curing time in order to reduce shrinkage cracking in CTB. Cho et al. (2006) developed an appropriate mix for CTB use in South Korea, with an evaluation of UCS for 5% and 7% cement CTB initial samples. The test results showed a 7-day UCS of 4.5 MPa and 8.5 MPa of 5% and 7% cement samples respectively. Consequently, 7% cement content was used throughout a series of experimental works to achieve the minimum strength specification (4.9 MPa for the 7-day UCS). A mixture with 25% fly ash reduced shrinkage by approximately half. A mixture containing 25% fly ash with 10% expansive additive was found to be the optimal mix for low-shrinkage CTB.

A micro-cracking technique was proposed by Scullion (2002) to reduce reflective cracking in a soil-cement base in Texas. The technique suggests that the soil cement base be moist-cured for 24–48 hours. This is followed by passing a 12 ton steel vibratory roller over the base for 2–4 passes, or until the average base stiffness reduces by 40%. This should then induces micro-cracking and prevents the considerable transverse cracking which would otherwise occur. The base layer is then further moist-cured for 48 hours.

Chen et al. (2008) identified premature failure in the road frontage of US Highway 290 in Texas, USA after only two months of construction. Poor performance of both the asphalt and CTB, as well as a lack of bond between the asphalt–CTB and two layers of CTB contributed to the failure. Segregation of CTB during placement was also attributed to the pavement distress.

Most specifications in the USA (Goerge 2002; United States Department of Transport 2003). Australia (Austroads 2013b), the UK, China, South Africa (Molenaar et al. 2011) and South Korea (Cho et al. 2006), require a minimum unconfined compressive strength (UCS) in the CTB that is used for pavements. Table 3.1 summarises the minimum UCS values of cemented bound materials required by state road authorities in Australia.

Table 3.1: Minimum UCS requirements of cemented materials from road authorities in Australia (Austroads 2013b)

Road authority	7-day UCS	28-day UCS	Test density
Roads and Maritime Services (RMS), New South Wales	GP cement: 4 MPa Slow setting[1]: 3 MPa	-	100% standard MDD
Roads Corporation (VicRoads) , Victoria	GP cement: 5 MPa GB cement: 3.5 MPa Supplementary cementitious blends: 3 MPa	-	100% modified MDD
Department of Transport and Main Roads, Queensland (Queensland TMR) [2]	Category 1: 3 MPa Category 2: 2 MPa	-	unsoaked, 100% standard MDD,
Department of Planning, Transport, and Infrastructure (DPTI), South Australia	-	GB cement: 4 MPa	96% modified MDD

Note:

1. 3 MPa limit applies provided at least 1 MPa strength gain between 7 and 28 days.
2. The minimum 7-day UCS shown is based on a cementitious blend of 75% cement and 25% fly ash. Where another combination of stabilising agent is to be used, the minimum 7-day UCS is to be determined through laboratory testing to ensure a one year UCS equivalent to the 75/25 cement/fly ash blend.

However, the maximum UCS should also be limited, so the material becomes neither too weak nor too stiff, thus minimising the propensity to failure. Based on a number of studies in the field and laboratory, the Portland cement Association (PCA) suggests a maximum 7-day UCS of 2.1 MPa (300 psi) for fine-grained soils and 3.1 MPa (450 psi) for course-grained soils, to limit the crack-width in CTB (Goerge 2002).

Chen, Hong, et al. (2011) studied the causes of transverse cracks at 9–15 m intervals along 9.6 km of State Highway 24 in Texas. They found that an excessive amount of cement (3%) was used in the construction where 1.5% was the given or conventional value. An excess of cement causes an overly-stiff CTB. A cement content of 1.5% was sufficient for the CTB to gain 2.07 MPa over the 7-day UCS. Moreover, the CTB was compacted at almost 2% above its optimum moisture content (OMC). These two factors led to excessive shrinkage of the CTB and consequent failure of the pavement. Subsequently, Chen, Chang, et al. (2011) proposed a threshold of base moduli ranging from 1,033 MPa – 3,445 MPa for stabilised bases.

Other methods to reduce shrinkage include: (a) reducing the clay content in the treated soil, (b) providing a stress relief layer between the CTB and the asphalt surface, such as an unbound granular material, (c) the use of a bituminous surface treatment and (d) the application of a geotextile fabric (Halsted 2010).

Austroads (2010c) also suggested various measures to minimise cracking in cemented materials and consequential reflection cracking in asphalt surface, covering pavement configuration, materials constituent and construction practice. For thick asphalt surface placed directly above the bound layer, the asphalt thickness must be sufficiently designed through the Austroads's mechanistic approach (Austroads 2010c). For thin bituminous surface, it is recommended to configure an unbound granular basecourse layer between thin asphalt and cemented layer. Application of strain alleviating membrane interlayers or geotextile layer above cemented layer is another option for thin asphalt surface pavements. In term of cemented material mixture, shrinkage in bound materials can be reduced by minimising the cementitious binder content or using slow-setting binders. The fine particles passing the 75 μm sieve and the plasticity index of the sourced materials should be limited to

a maximum of 20% and 20 respectively, to reduce the activation between fines and cement. In construction stage, the bound layer should be covered with a bituminous coat soon after finish compaction to prevent rapid drying. Then allow cracking in the bound layer occurs before surfacing.

The department for main roads in Western Australia (Main Roads Western Australia 2010a) applies some similar concepts for cement stabilisation in order to avoid reflection cracking in pavement. Cement-stabilised material is only permitted for use in the construction of the road working platform under the pavement structure. It must then be overlaid with an unbound granular material. Moreover, any reduction in the thickness of the unbound granular layer is not permitted when using it in conjunction with cement- stabilised material in order to prevent the tendency towards cracking in pavements. A maximum UCS limit (1.0 MPa and 1.5 MPa for 7-day UCS and 28-day UCS respectively) is also specified for the stabilised material to act as a modified material and to avoid it becoming a bound material.

3.3 Previous studies on shrinkage of CTB

The shrinkage of cement-treated crushed rock base in Western Australia has previously been examined in terms of linear shrinkage and nitrogen adsorption (Yeo 2011). The results showed that swelling was evident in material with low cement content (1% - 3%), whereas CTB with 4% - 5% cement content experienced shrinkage. It should be pointed out that only fine particles passing through a 0.425 mm sieve were sampled for these tests. Thus the bulk shrinkage characteristics of the samples may differ from CTB made with fine to medium-grain aggregate.

Beam specimens were used in the shrinkage evaluation of the laboratory compacted specimens reviewed in the following literature. The correlation between CTB cracking in the field and CTB shrinkage in the laboratory was evaluated by Smith (1974) and (Cho et al. 2006). Smith (1974) studied the shrinkage of CTB at 11 sites in California, USA. Test samples were prepared with the same cement content, moisture content and relative density as those at the sites. It was found that the number of cracks that occurred in the field related to the experimental shrinkage values, as shown in Figure 3.1. It was also found that the shrinkage property

differences in CTB samples were insignificant for the samples prepared by employing the following scenarios: Portland cement type I and II, cement content varying from 2.5% to 6%, density from 90% -100 % maximum dry density (MDD) and moisture content ranging from 2% below the optimum moisture content (OMC) to 2% above the OMC.

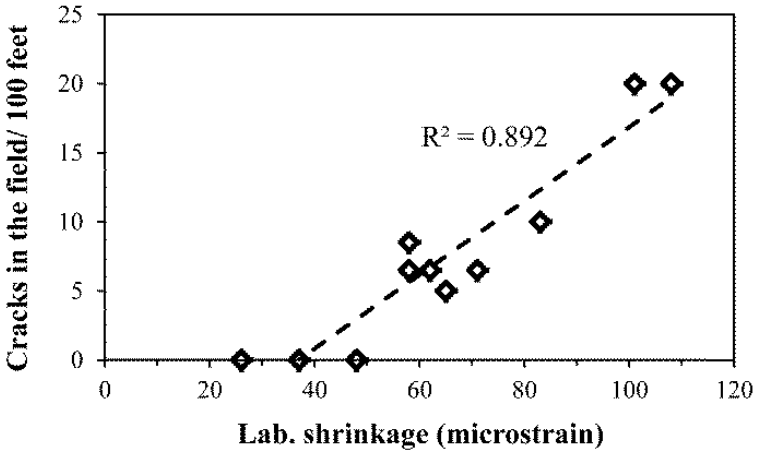

Figure 3.1: Comparison of laboratory shrinkage samples with number of cracks in the field samples (Smith 1974)

Cho et al. (2006) also evaluated the shrinkage properties of CTB samples in the laboratory and compared them with field-trial samples. Three types of samples were examined i.e., normal CTB (7% cement), CTB with 25% fly ash replacement and CTB with 25% fly ash replacement and 10% expansive additive. As illustrated in Figure 3.2, the normal CTB underwent the highest shrinkage in the laboratory and showed the highest number of cracks in the field at 7 weeks. The sample containing 25% fly ash with 10% additive exhibited no cracks in the field, even though it showed higher shrinkage characteristics than the 25% fly ash (with no additive) sample. It was assumed this sample was subjected to a higher compressive strength than the 25% fly ash with 10% additive sample.

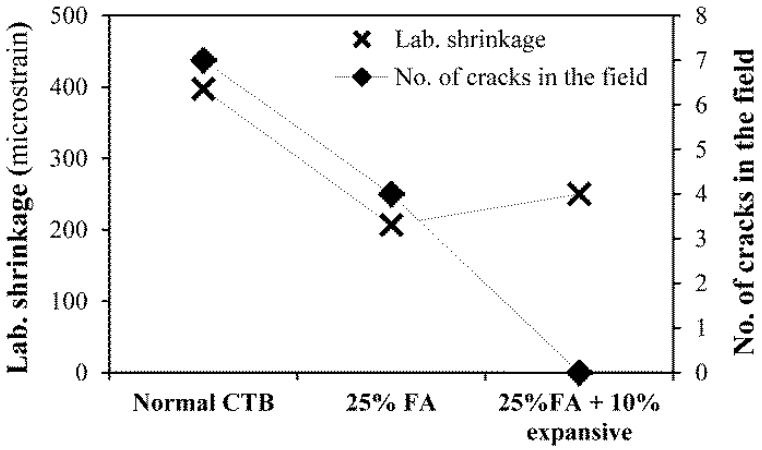

Figure 3.2: Comparison of laboratory shrinkage samples with number of cracks in the field samples (Cho et al. 2006)

The effects of plasticity on the parent materials and the effects of cement content on the shrinkage of CTB were also examined. The results revealed that the higher plasticity of the original aggregate eventually resulted in higher shrinkage with the same cement content (Goerge 1968; van-Blerk and Scullion 1995; Chakrabarti and Kodikara 2005). Adaska and Luhr (2004) reported that in the investigation by Goerge (1968), the shrinkage of CTB made by non-plastic aggregate, increased with the addition of extra amounts of cement ranging from 0% to 10%. However, the shrinkage of plastic aggregate CTB declined when the cement content was increased from 0% to 3% and then rose when cement content was increased up to 10%.

van-Blerk and Scullion (1995) found that the shrinkage of CTB was greatly reduced when a higher quality aggregate base was used, i.e., one with no plasticity. Shrinkage properties were compared between CTB made with non-plastic limestone and CTB made with the same type of limestone blended with clay fines. The latter material contained 21% higher fine particles passing through a sieve size of 0.425 mm and it had a plasticity index (PI) of 7.4. However, it could not be concluded that the trends in shrinkage accorded with an increase or a decrease in cement content varying from 2%, to 4% and 6 % for both types of CTB.

Chakrabarti and Kodikara (2005) investigated the shrinkage behaviour of CTB samples made with General Purpose Portland cement (GP cement) and crushed basaltic rock (CBSR). The shrinkage in CTB increased when the cement content was increased from 2% to 4% for normal CSBR (PI 3%). However, the increase in

shrinkage from the addition of 2% - 4 % cement could not be found in CTB made with CBSR and 6% fines (PI 14 %). CBSR mixed with 15% fines (PI 24%) provided the highest shrinkage result amongst these three types of samples and showed a reduction in shrinkage with an additional cement content of 2% to 4%.

Scullion et al. (2005) conducted a performance evaluation in Texas of three marginal materials which were stabilised with Portland cement type I. The shrinkage of river gravel was reduced with an increase in cement content from 1.5% to 4.5%. However, the shrinkage of recycled concrete aggregate and low-quality limestone initially reduced when the cement content was increased from 1.5% to 3%, but shrinkage increased with the addition of cement up to 4% content.

3.4 Fatigue relationship of CTB

Fatigue life or fatigue failure is where a number of repeated loading cycle reduces the flexural stiffness of the material to 50% of its initial stiffness (Abojaradeh et al. 2003; Austroads 2006a). The initial stiffness is defined at number 50 in the loading cycle (Abojaradeh et al. 2003; Austroads 2006a). The fatigue relationship is the correlation between fatigue life and applied stress or strain. The experimental data for fatigue life against tensile strain/stress induced in the test samples can be obtained via a number of fatigue tests conducted at different magnitudes of applied strain or stress. Fatigue tests can be carried out in two modes, so-called “controlled strain” and “controlled stress”. In the controlled-strain mode, strain is maintained by reducing the applied load during the test, while the stress is kept constant and the strain is increased during the controlled stress test.

The simplest form of the fatigue relationship is shown in Eq. 3.1 (Austroads 2008a).

$$N = \left(\frac{k_1}{\varepsilon}\right)^{k_2} or \left(\frac{k_3}{\sigma}\right)^{k_4} \tag{3.1}$$

where N = fatigue life or loading cycle to failure, ε = tensile strain at the bottom of the specimen, σ = applied tensile stress, and k_1-k_4 are the regression parameters.

The fatigue relationship is adopted for the structural analysis and design of flexible pavements. The tensile strain at the bottom of the CTB layer is converted to a number of standard axle load repetitions and then compared with the designed number of standard axle repetitions. If pavement thicknesses are well designed, and strains in pavement caused by repetitive loadings are low enough, fatigue-cracking is not a problem (Souliman et al. 2012).

Austroads (2010c) recommends the fatigue relationship of cemented materials for the structural analysis and design of cemented pavements be as expressed in Eq. 3.2. The parameter, k_2 in Eq. 3.1 is also called the strain-damage exponent, which in Eq. 3.2 is equal to 12.

$$N = RF\left(\frac{\left(\frac{113000}{E^{0.804}}\right)+191}{\mu\varepsilon}\right)^{12} \tag{3.2}$$

where N = the allowable number of standard axle load repetitions, με = the tensile microstrains at the bottom of the CTB layer, E = the cemented material modulus (MPa), and RF = the reliability factor for the fatigue life of cemented materials.

Gonzalez et al. (Austroads 2010b) developed fatigue relationships for cement-treated materials containing 3% and 5% cement. The strain damage exponents from this investigation varied widely from 14 to 36, with an average value of 22.

The fatigue relationship of CTB under strain-control has been evaluated in the eastern states of Australia and adopted throughout Australia. Based on the lack of information on cement-stabilised materials in WA, the research presented here has been undertaken in order to understand the fatigue behaviour of CTB, and to allow further analysis and more advanced design of CTB pavements. Controlled-strain testing relates to thin (less than 100 mm) asphalt surface pavements where the elastic recovery property of the material is the key measure of its fatigue life (Baburamani

1999; Artamendi and Khalid 2004). Strain-control tests were performed in this study as the pavement in Western Australia consists of thin bituminous pavement.

3.5 Materials

This investigation aims to evaluate the characteristics of CTB in terms of unconfined compressive strength, shrinkage and flexural fatigue. These properties are important for the mix design and structural design of CTB. The characterisation of CTB produced from local standard CRB, under laboratory controlled conditions, was undertaken with reference to the standard test methods of MRWA, Australian Standards and Austroads. The details of the materials, testing protocols and corresponding results are explained in the subsequent sections.

General Purpose Portland cement (GP), according to AS 3972 (Standards Australia 1997), was used as a stabiliser. Standard crushed rock base (CRB), with a maximum size of 19 mm, was collected from a local quarry in Perth. The basic properties of CRB were checked for conformity to MRWA standard (Main Roads Western Australia 2010b). The PI of CRB was 4.8%. CRB samples were dried in an oven at 105 C for 24 hours and then passed through a sieve of the standard size for (Main Roads Western Australia 2010b). Dry particles retained on each sieve were then stored in sealed plastic containers. As the ratio of specimen size to maximum aggregate size should be not less than 5:1, the maximum size of CRB used throughout all tests was 13.2 mm. To maintain identical gradation for all samples, the CRB samples retained on each standard sieve were blended according to the proportions specified for particle size distribution by the standard (Main Roads Western Australia 2010b), as shown in Figure 3.3 . CRB particles greater than 13.2 mm were replaced with CRB which had passed through a 13.2 mm sieve and was then retained on a 9.7 mm sieve.

The moisture-dry density relationships of CRB-cement mixtures were determined in terms of modified proctors, in accordance with test method WA 133.1 (Main Roads Western Australia 2012b), as shown in Figure 3.4 and Table 3.2. There was a slight reduction (3.7%) in optimum moisture content (OMC), and an insignificant increase (approximately 0.6%) in maximum dry density (MDD), where the cement content

was increased from 2% to 6%. It should be noted that there were significant differences in the water-cement ratio (w/c) between these five mixtures.

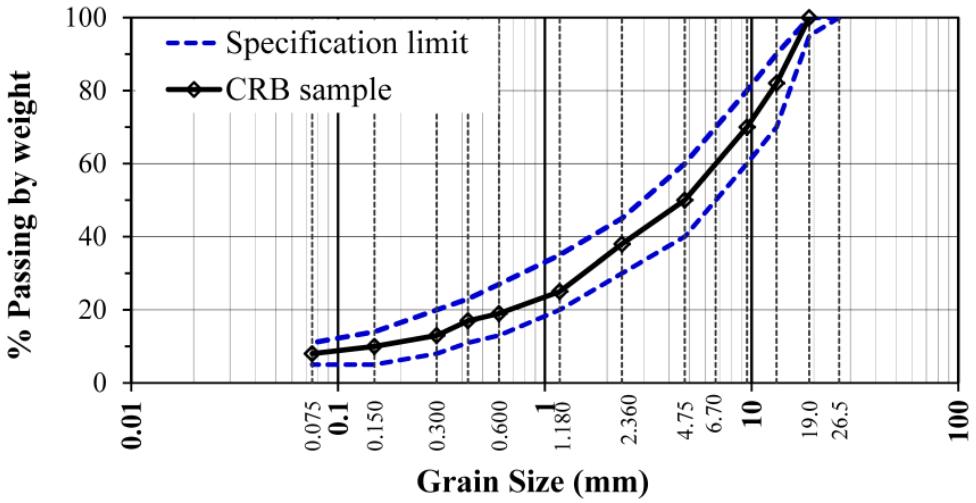

Figure 3.3: Particle size distribution of CRB used in this study

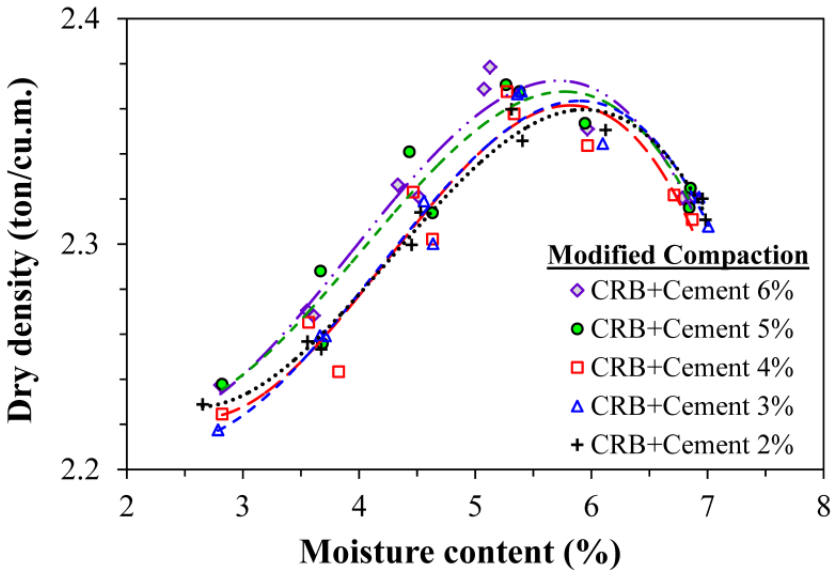

Figure 3.4: Moisture - dry density relationships for CRB and cement mixtures by modified proctor

Table 3.2: OMC and MDD from modified compaction for CRB-cement mixes

Cement content	OMC (%)	MDD (ton/m^3)	Water- cement ratio (w/c)
2%	5.94	2.360	3.03
3 %	5.90	2.364	2.02
4 %	5.82	2.361	1.51
5 %	5.77	2.368	1.21
6 %	5.72	2.373	1.01

3.6 Unconfined compressive strength (UCS) test

The UCS test is a commonly used laboratory test; it provides a basic indicator of the strength of compacted samples and is used for quality control in construction in the field. The UCS tests for CTB were performed according to standard test method WA 143.1 (Main Roads Western Australia 2012c). The test specimens, of 105 mm in diameter and 115.5 in height, were compacted by modified compaction into five equal layers. All samples were then extruded from their moulds and cured for 7 days. Prior to setting up the test, all samples were soaked in water for 4 hours. The 7-day UCS values for all CTB samples are presented in Figure 3.5 and Figure 3.6. As the cement content was increased from 2% to 6 %, the UCS rose from 3.8 MPa to 11.8 MPa and the compressive modulus improved from 160 MPa to 480 MPa. All test samples may be defined as "bound" material, i.e., the UCS is more than 1.0 MPa at the 7-day UCS point (Main Roads Western Australia 2010b).

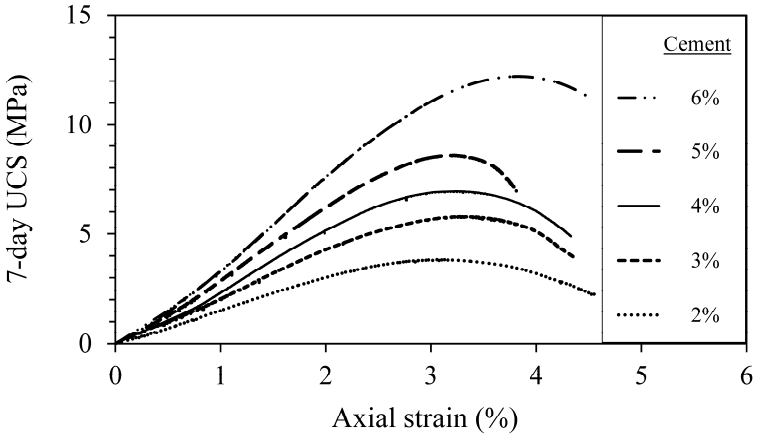

Figure 3.5: 7-day soaked UCS test results for CTB with range of cement content

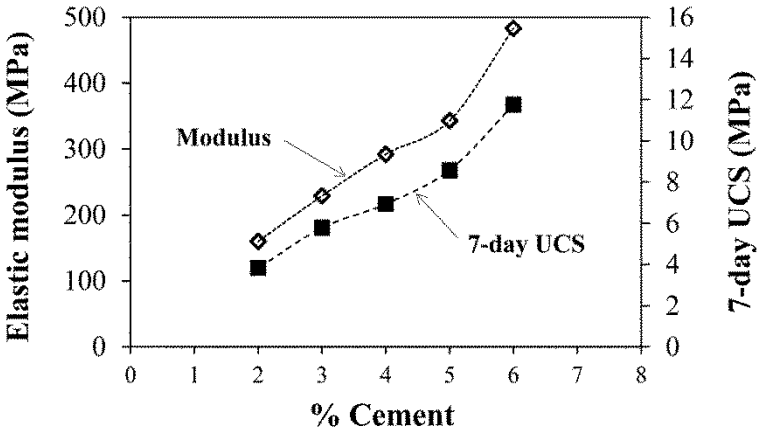

Figure 3.6: Modulus and UCS of CTB samples with range of cement content

3.7 Shrinkage test

The amount of shrinkage depends on cement content, aggregate type, fines content, water content, degree of compaction and curing (van-Blerk and Scullion 1995). In this investigation, shrinkage in CTB samples with variations in cement content from 2% - 6% was examined, while the other aforementioned factors were kept constant. The test protocol to examine the shrinkage of CTB was adapted from the standard shrinkage test for concrete, AS 1012.13 (Standards Australia 1992). Shrinkage test specimens were prepared in moulds of 75 x 75 x 280 mm. Two steel studs were inserted at 1.5 mm into both central ends of the mould and embedded in the specimen. The aim was to facilitate the measurement of changes in length while the samples were subjected to controlled environmental conditions. The gauge length between the two steel studs embedded in the specimen was 250 mm. A predetermined amount of CTB prepared at its OMC was then compacted to achieve 95% MDD. Once compaction was completed, each specimen was cured in a mould for 24 hours to gain sufficient strength for handling. If the inserted studs swayed after unmoulding, the studs were then carefully cemented by the same mixture. Then, sample curing was continued for a further six days at a controlled temperature of 23 °C and 90% relative humidity (RH). Thus each specimen was cured totally for 7 days to ensure that steel studs embedded firmly in each beam specimen. At the end of 7-day curing, the initial length of each test specimen was measured using a horizontal comparator with an accuracy of 0.001 mm as demonstrated in Figure 3.8. Azam and Cameron (2013) also measured the initial length of test samples after 7 days of curing. The specimens were then dried by exposing all surfaces to a controlled environment at a controlled temperature of 23 °C and 50% RH. Consequently, length changes in all specimens were checked periodically.

The average shrinkage values for all CTB samples, measured up to 120 days of drying, are presented in Figure 3.9. The rates of shrinkage for all samples were rapid in the first few days of drying. After 21 days of drying, samples with 4%, 5% and 6% cement content had undergone approximately 80% of their shrinkage values at the end-of-test. At 21 days, the shrinkage of the 2% and 3% samples reached 91% and 85% of their end-of-test values. The shrinkage of all specimens insignificantly increased after 90 days of drying. The shrinkage of CTB decreased as the cement

content was increased from 2% to 4%. Shrinkage then increased with cement content up to 6%. The 4% cement sample provided the lowest shrinkage value at the end-of-test of 380 microstrains (με). The 2% and 6% cement samples exhibited the highest degree of shrinkage of about 440 με. The shrinkage for the 3% and 5% cement samples measured close to 425 με and 410 με, respectively. There was an approximate difference of 17% between the maximum and minimum shrinkage amongst these 5 types of specimens.

Figure 3.10 depicts the investigations' shrinkage test results after 21 days of drying for CTB with various ranges of cement content. The amount of shrinkage and tendency towards shrinkage, in relation to cement content, varied from material to material. For any particular material, a greater degree of shrinkage can be found in samples with higher plasticity and fine particles at the same cement content. The evaporation of excess water, which is not needed for hydration, also increases shrinkage (Wu 2011). Chakrabarti and Kodikara (2005) concluded that the dissimilar shrinkage behaviours of the test materials found in their study depended on the different amounts of shrinkage which were contributed by hydration and loss of water from the fine pores.

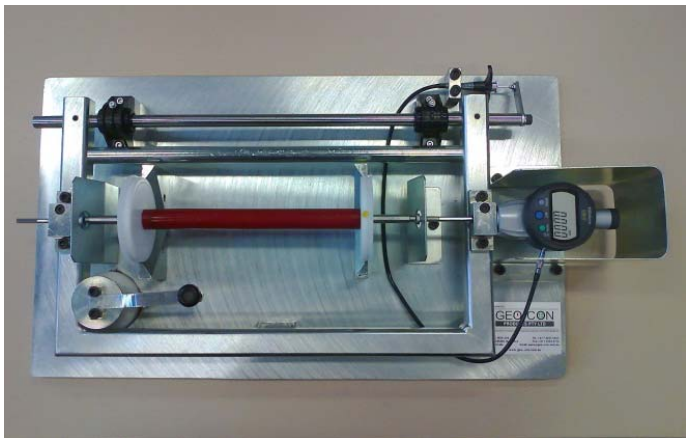

Figure 3.7: Zero setting by reference bar

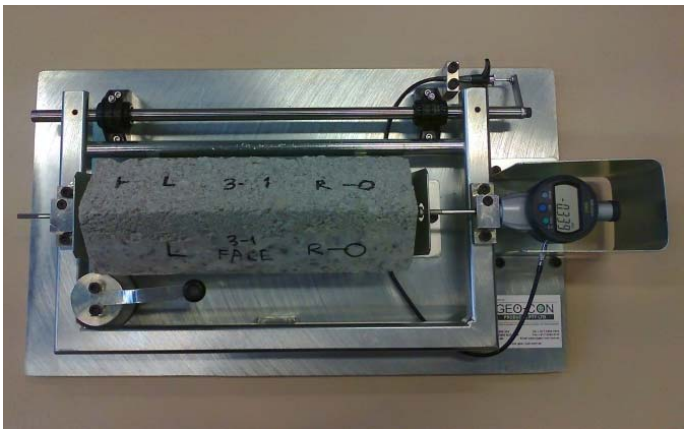

Figure 3.8: Length measurements using a horizontal comparator

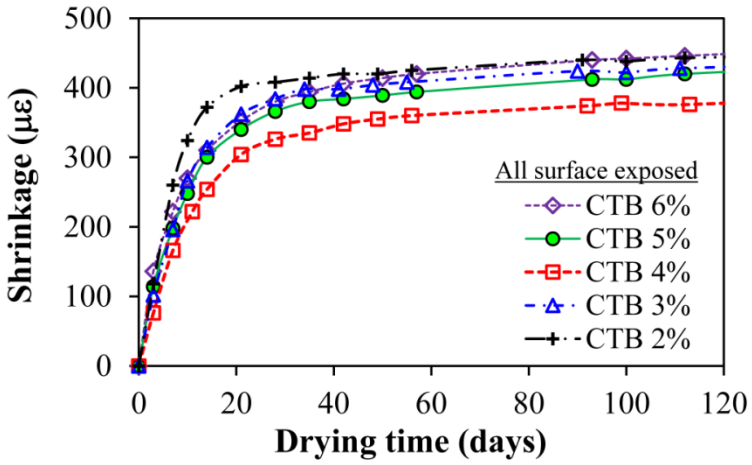

Figure 3.9: Shrinkage test results for CTB with cement content 2% - 6%

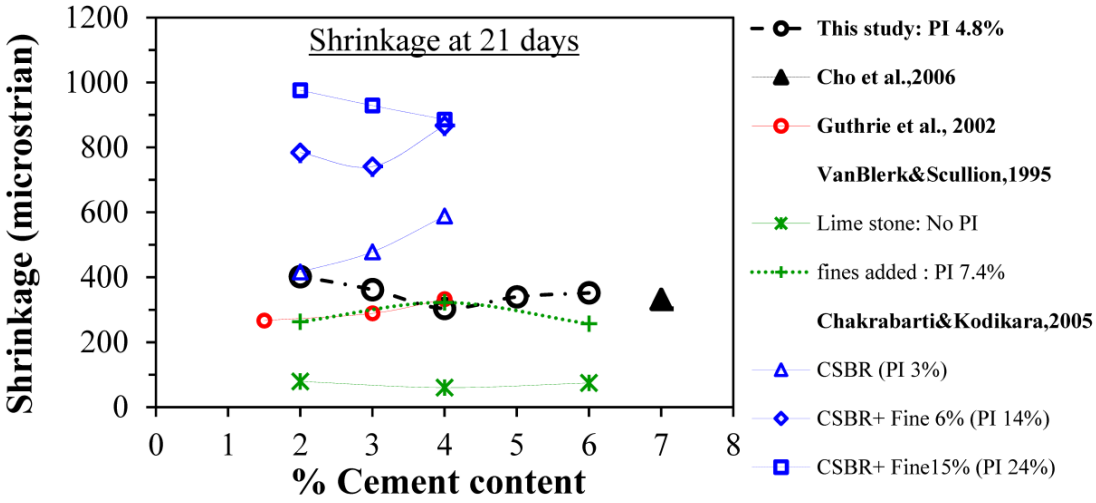

Figure 3.10: Shrinkage test results after 21 days of drying CTB samples containing a range of cement contents

Since cement content and w/c were the only variables in the samples in this study, shrinkage may have been due to the amount of water lost from both hydration and evaporation. It was assumed that the high shrinkage in the higher cement content CTB i.e., 5% and 6%, was dominated by self-desiccation or loss of water during hydration. For the low CTB cement content (2%-3%) which resulted in high w/c, smaller amounts of water were required for hydration than existed in the excess water in the samples. In this instance, shrinkage was predominantly due to drying shrinkage.

Figure 3.11 summarises the relationship between 7-day UCS measures and 21-day shrinkage with cement content at the optimum cement content of 4%. Figure 3.12 illustrates the relationship between the shrinkage and the UCS of CTB used in this study, and marginal materials studied by Scullion et al. (2005) . The shrinkage results for all marginal materials were very sensitive to the amount of cement and UCS. Utilisation of standard aggregate as a parent material for CTB reduces its sensitivity in this regard.

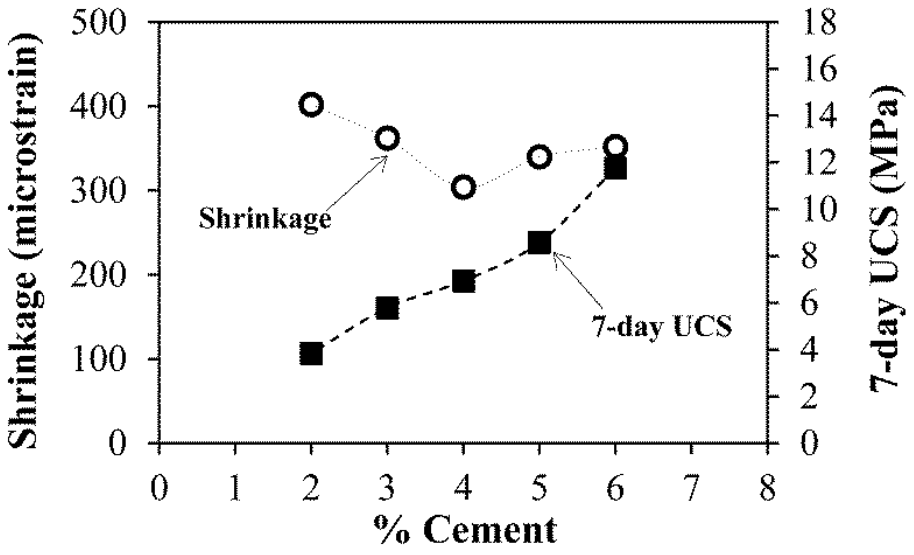

Figure 3.11: Shrinkage at 21 days of drying and 7-day UCS for CTB with cement content 2% - 6%

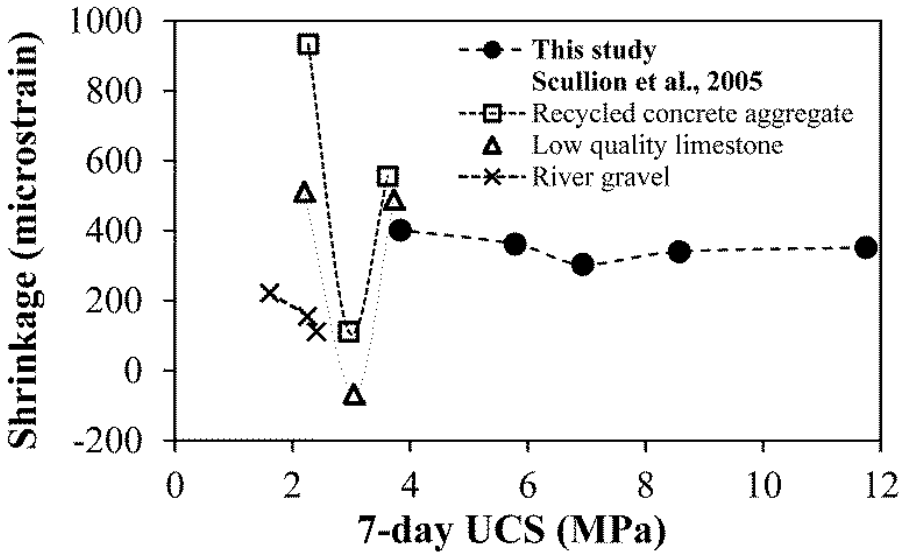

Figure 3.12: Relationship between shrinkage and UCS for cement-treated materials

3.8 Flexural fatigue tests

Flexural fatigue tests were performed on 3% and 5% cement samples. The prismatic beams used for the tests were cut from compacted slabs. CTB slabs, with dimensions of 400 x 300 mm^2 and a thickness of 75mm were made by mixing CRB and cement at 100% OMC. These were then compacted to achieve 95% MDD using a roller compactor (see Figure 3.13a). Each CTB slab was cured for at least 7 days in order to gain sufficient strength before it was cut. Four prismatic beams, 400 mm long, 63.5 mm wide and 50 mm thick, were then cut from each compacted slab, as shown in Figure 3.13b and Figure 3.13c. After adding cement and water to the CRB, all specimens were cured at 25°C for 28 days prior to setting up the test.

Flexural fatigue tests, following the Austroads standard test method, AG:PT/T233 (Austroads 2006a), were adapted for use with CTB samples. Continuous haversine loading, with a loading frequency of 10 Hz was applied until the flexural stiffness of the sample was either reduced to 50% of the initial flexural stiffness or it reached up to one million loading cycles (taking approximately 28 hours). These test limiting conditions are specified in the standard test method. The fatigue tests in this study were conducted under strain-control mode at a controlled temperature of 25 °C. In strain-control mode, the deformation of a beam is measured and the applied load is adjusted to maintain a constant strain throughout the test. The beam fatigue apparatus

is shown in Figure 3.14. The apparatus is usually used for four-point fatigue testing of beam specimens subjected to repeated flexural bending. The specimen is restrained by four clamps, with two outside clamps as beam supports and two points of loading applied via the two central clamps. The deflection of the specimen is measured at the mid-span and bottom of the specimen.

(a)

(b)

(c)

Figure 3.13: Manufacturing of beam specimens (a) a roller compactor used for making CTB slabs (b) a cutting machine (c) four beams were cut from each compacted slab

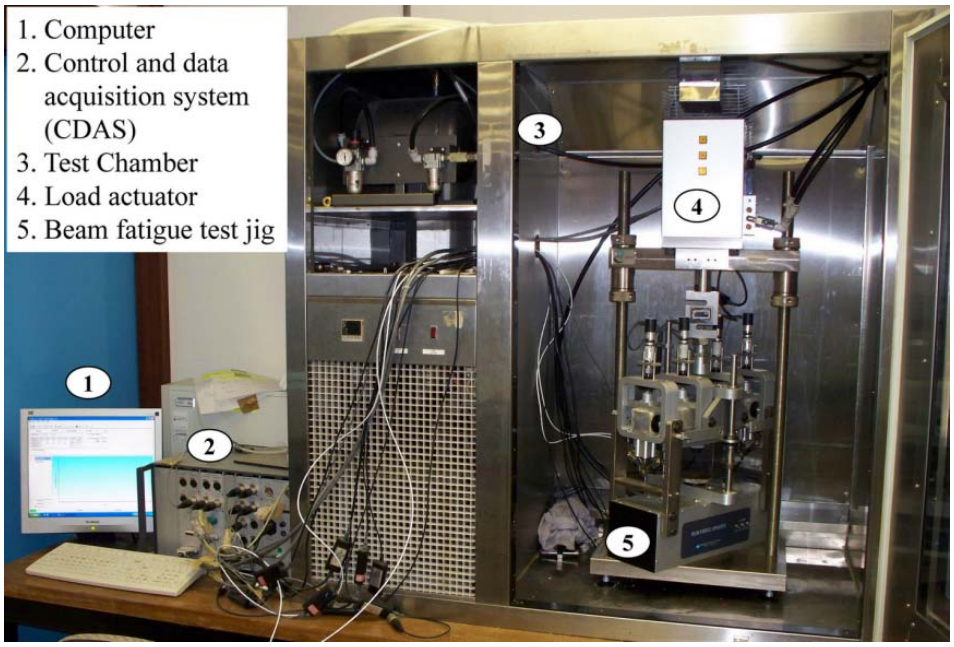

Figure 3.14: Beam fatigue apparatus

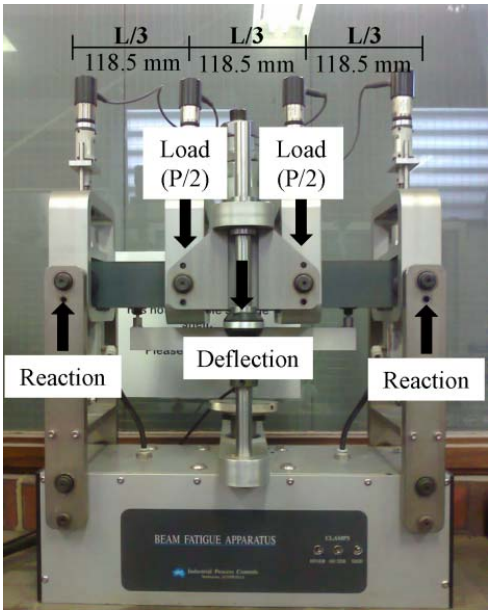

Figure 3.15: Beam fatigue test jig

In this study, two different forms of testing were undertaken in order to gain a better understanding of the characteristics of CTB through strain-control fatigue testing which consists of the constant strain and the multi-strain test. A total of ten beam samples were used to evaluate the fatigue characteristics of CTB. There were five beams for each type of CTB (3% and 5% cement). Four beams underwent constant strain tests by being subjected to four different levels of strain. The last beam was tested using the multi-strain test.

3.8.1 Controlled constant strain test

This is a conventional standard test to obtain the fatigue life of the material at each strain level, in order to determine the fatigue relationship. The levels of strain used in this study were 50, 100, 150 and 200 microstrains (με). Each beam specimen was subjected to a single value of strain until the test was terminated due to fatigue failure, or until the one-million cycles point was reached.

Table 3.3 summarises the flexural stiffness and the number of test cycles at each level of applied strain for 3% and 5% cement CTB. Not all specimens experienced fatigue failure after completing one million cycles of loading. The values of the initial flexural stiffness of 5% cement samples were considerably higher than those for the 3% cement samples.

Table 3.3: Summary of fatigue test results for CTB

Microstrain	Flexural stiffness (MPa)			No. of cycles for crack initiation phase
	Initial	End of crack initiation phase	End of test	
Cement content 3%				
50	12,579	N/A	13,500	N/A
100	9,617	8,131	8,050	31,780
150	5,687	4,281	4,442	73,940
200	1,985	1,866	1,760	57,250
Cement content 5%				
50	20,500	N/A	21,966	N/A
100	20,407	20,203	20,733	71,340
150	14,721	12,463	12,155	130,810
200	22,510	13,311	11,797	175,790

As the tests were conducted using the strain-control mode, the test machine adjusted the load magnitude in order to keep a constant deflection of the beam. Figure 3.16 illustrates an example of the range of load intensities, which varied from 1.7 kN to 0.8 kN and were applied to a 5% cement CTB sample to maintain a constant deflection of 200 με.

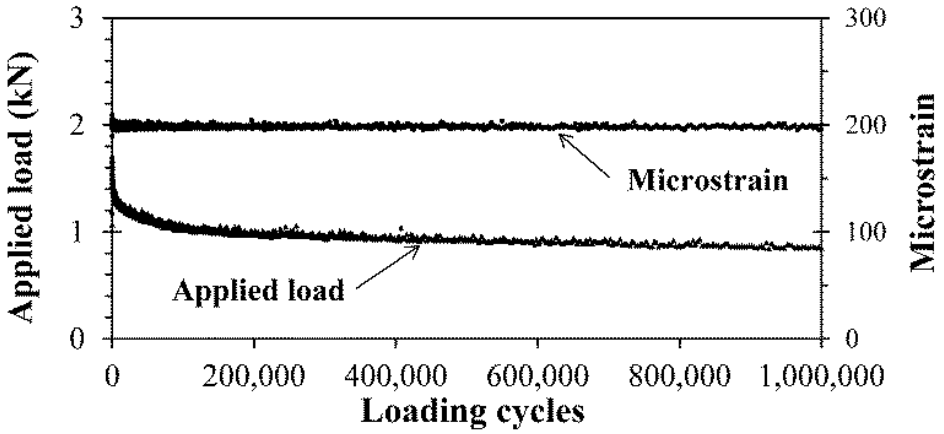

Figure 3.16: Load applied to 5% cement CTB to maintain a constant 200 με

3.8.1.1 Constant strain test result for 3% cement CTB

It can be seen from Figure 3.17 that all 3% cement CTB samples completed one million cycles of loading, and did not evidence fatigue failure from the applied strain ranging from 50 με - 200 με. Thus a fatigue relationship cannot be drawn. The initial stiffness decreased dramatically as the applied strain was increased in steps.

The beam sample performed well against fatigue under the strain condition of 50 με. The beam retained its stiffness of 12,579 MPa during the course of the one-million cycle test. At the end of the test, the stiffness was recorded at 13,500MPa. Due to the application of 100 με, the beam specimen lost stiffness after repetitive loading; although the loss in stiffness after one million cycles was minimal. During its crack initiation phase, the specimen lost stiffness, decreasing from 9,617 MPa to 8,131 MPa; a decrease of approximately 16% in the first 31,780 cycles. Following this, the stable crack growth phase lasted for approximately 97% of the test time, and its stiffness dropped to 8,050 MPa at the end of the test. With the application of 150 με, the beam lost around a quarter of its stiffness. It decreased from an initial stiffness of 5,687 MPa to 4,281 MPa during the crack initiation stage of the first 73,940 cycles. The sample then underwent the stable crack growth phase and retained its stiffness effectively throughout the duration of the test. For the 200 με test, the stiffness at the end of the test was 1,760 MPa with the initial stiffness being recorded at 1,985 MPa. Its stiffness dropped to 1,866 MPa during 57,250 cycles of the crack initial phase.

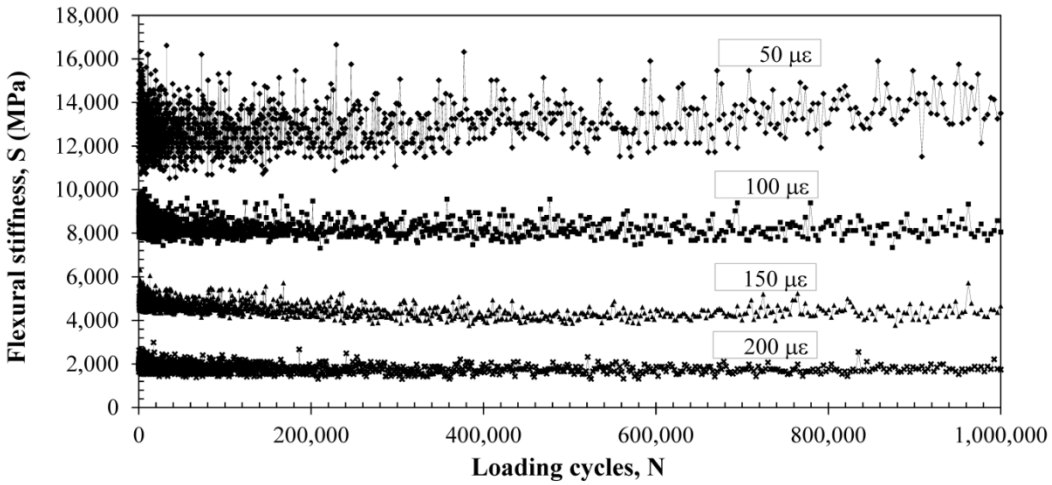

Figure 3.17: Test results for CTB (3% cement) under constant strain control

3.8.1.2 Constant strain test result for 5% cement CTB

Figure 3.18 illustrates the test results for 5% cement CTB samples subjected to an applied strain range of 50 με - 200 με. All samples completed one million cycles of loading, hence a fatigue relationship could not be developed. However, for the 5% cement samples, 200 με triggered fatigue failure, while the other samples did not undergo fatigue. The initial stiffness of the test samples was not substantially different (approximately 20,000 MPa) with the exception of the 150 με example.

At 50 με, two stages of cracking, i.e., the crack initiation phase and the stable crack growth phase, were unable to be determined. The stiffness of the beam subjected to 100 με dropped from 20,407 MPa to 20,203 MPa through the crack initiation stage in the first 71,340 cycles. The decrease in stiffness continued throughout the stable crack growth phase. However, after 600,000 cycles, beam stiffness increased as a result of a fault in the apparatus such that the applied microstrain was just below 100. The initial stiffness of the beam in the 150 με condition was much lower than that of the other beams. This sample lost around 15% of its stiffness during the initial crack phase and then became stable throughout the test. During its crack initiation stage at 130,810 cycles, the stiffness decreased from 14,721MPa to 12,463MPa. Stiffness then decreased slightly in the stable crack growth phase and terminated at 12,155 MPa.

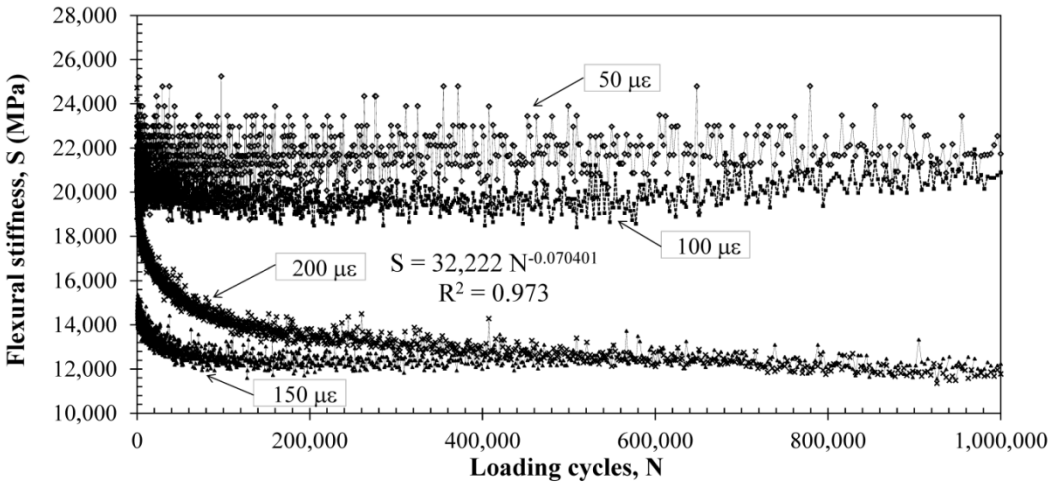

Figure 3.18: Relationship between stiffness (S) and loading cycles (N) for CTB (5% cement) under constant strain-control mode varied from 50 με - 200 με

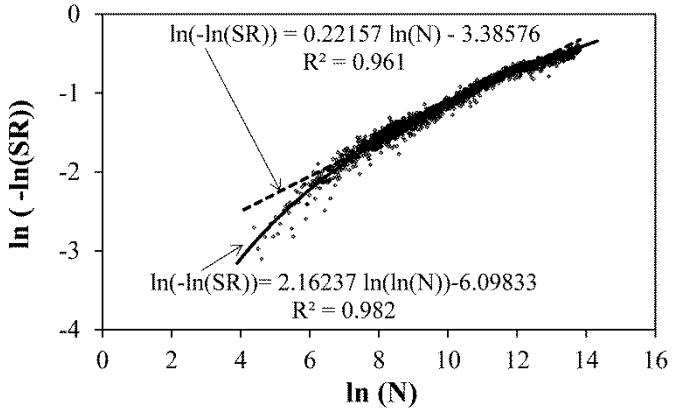

Figure 3.19: Relationship between stiffness ratio (SR) and loading cycles (N) for CTB (5% cement) subjected to 200 με

It is evident that a 5% cement sample can trigger fatigue failure at 200 με when stiffness is reduced to almost 50%. Stiffness decreased critically by around 41%, from 22,510 MPa to 13,311 MPa in the crack initiation phase covering the first 175,790 cycles. After one million cycles, stiffness reduced to 11,797 MPa, which is close to 50% of the initial stiffness, i.e., 11,255 MPa.

The fatigue life of the beam was then evaluated by making projections based on the test data. The power relationship of the number of loading cycles (N) and the flexural stiffness (S) provided a fatigue life of approximately three million cycles. ASTM D7460-10 (American Soeciety of Testing and Materials 2010) suggests a linear relationship between ln(ln(-SR)) and ln(N) for the projection of the failure point which, in the tests, resulted in a fatigue life of 827,775 cycles. The term SR

represents the stiffness ratio between beam stiffness at any cycle and its initial stiffness. It was found that the relationship between ln(ln(-SR)) and ln(ln(N)) provided an extrapolated fatigue failure point at around 1.42 million cycles. The relationship between the stiffness ratio (SR) and the loading cycles (N) for the 5% cement samples subjected to 200 με is shown in Figure 3.19.

All three aforementioned relationships provided a high degree of determination (R^2). The three equations and the corresponding fatigue life measures are summarised in Table 3.4. The power law in Eq. 3.3 (see Table 3.4) has previously been adopted to predict the fatigue life of CTB samples in Western Australia (Yeo 2011). However, based on these experimental results, the extrapolated value of fatigue life was unreasonably high despite providing a high R^2. Unexpectedly, the relationship in Eq. 3.4 (see Table 3.4) specified by ASTM D7460-10, predicted a lower fatigue life than that which actually occurred (an example of fatigue life estimation is shown in ASTM D7460-10. Figure 3.19 demonstrates that the relationship is not linear at low values of ln (N). Accordingly, the relationship of ln(ln(-SR)) and ln(ln(N)) was initiated as shown in Eq. 3.5 (see Table 3.4) and this led to the optimum R^2 and the most reasonable fatigue failure measure. However, other experimental results may vary due to the possible use of diverse materials and material sources. Thus, the ln(ln(-SR)) and ln(ln(N)) relationship is proposed as an additional option for the calculation of the extrapolated fatigue life.

Table 3.4: Projection of the fatigue life for 5% cement CTB subjected to 200 microstrains

Eq.	S-N relationship*	Fatigue life (cycles)	R^2	Projection method
(3.3)	$S = 32{,}222\ N^{(-0.070401)}$	3,080,658	0.97	Power law
(3.4)	$\ln(\ln(-SR)) = 0.2216 \ln(N) - 3.3858$	827,775	0.96	ASTM D7460-10
(3.5)	$\ln(\ln(-SR)) = 2.1624 \ln(\ln(N)) - 6.0983$	1,417,114	0.98	Modified ASTM D7460-10

** S = stiffness, N = number of loading cycles, and SR = stiffness ratio, i.e., the ratio of the stiffness in any cycle to the initial stiffness*

The experimental results reveal that the fatigue phenomenon does not occur if the strains in CTB induced by repetitive loading are lower than 200 με, or less than one million cycles, under controlled laboratory conditions. Ultimately, a fatigue relationship cannot be drawn from this experimental data. The fatigue behaviour of CTB subjected to higher levels of strain requires further investigation.

3.8.2 Controlled multi-strain test

The standard fatigue test (Austroads 2006a) outlined in the previous section is time-consuming and requires a large number of specimens. This test was undertaken in order to examine the stiffness degradation and recovery of a sample under multi-levels of strain. The test was also employed as a precursor to the development of a new testing protocol which aims to reduce both the testing time and the number of test specimens. In the multi-strain fatigue test (Austroads 2006a), each beam was subjected to multiple values of strain. A με of 50 was first applied, and then increased in increments of 50, up to a maximum of 200 and stepping down to 50 at the same incremental rate. A total of 19-strain magnitude was applied to each beam. Each loading lasted for 3,000 cycles (5 minutes). Thus a total of 57,000 cycles was completed. Figure 3.20 illustrates the loading pattern applied to each beam in the test.

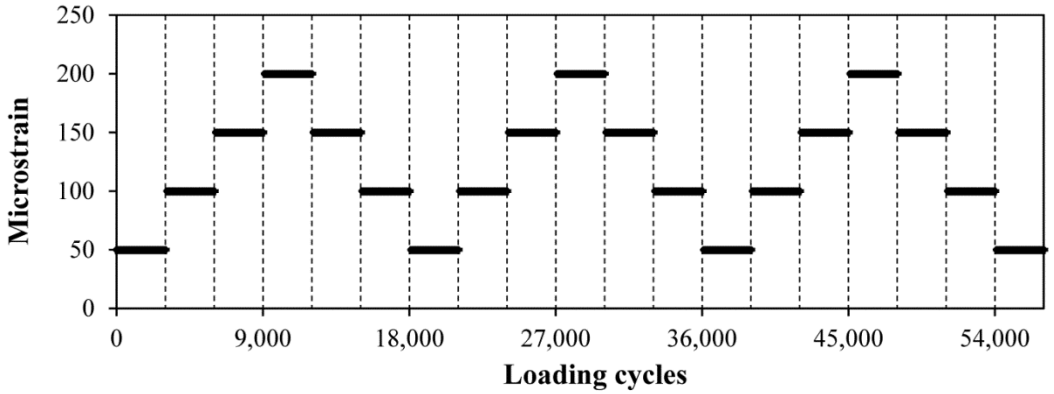

Figure 3.20: Levels of microstrain applied for controlled multi-strain test

The results of the multi-strain test from the 3% and 5% cement samples are illustrated in Figure 3.21. A rapid decrease in stiffness is evident at various stages in

the test. For the 3% cement sample, the stiffness reduced sharply to about 50% of the initial stiffness when subjected to 100 με in the second stage. The stiffness of the 5% cement sample reduced dramatically to almost 40% of the initial stiffness when subjected to 150 με in the third stage. From rapid decrease in stiffness, it is assumed that the cracking in the specimens occurs rapidly, with the samples then reaching the stable crack growth phase for the remainder of testing. In general, the stiffness of the beam decreases as the applied strain increases and vice versa. However, the stiffness never returns to its previous stiffness level (at the same με level), while the strain diminishes step by step. The correlations between loading cycles and the stiffness for each strain level for the 3% and 5% cement samples are presented in Figure 3.21c and Figure 3.21d respectively. The stiffness degradation corresponded to the number of loading cycles as per the power law and provided an R^2 of more than 70%.

The multi-strain fatigue test effectively expressed the degradation and recovery of the stiffness of a CTB specimen through a stepwise increase and decrease in applied strain. This test has the potential for development, and through this, a new approach may be found to reduce the length of testing time and the number of specimens required. More extensive analysis based on these test results is required for greater accuracy. If successful, this analysis should enable effective predictions regarding the stiffness of beams subjected to a certain number of cycles.

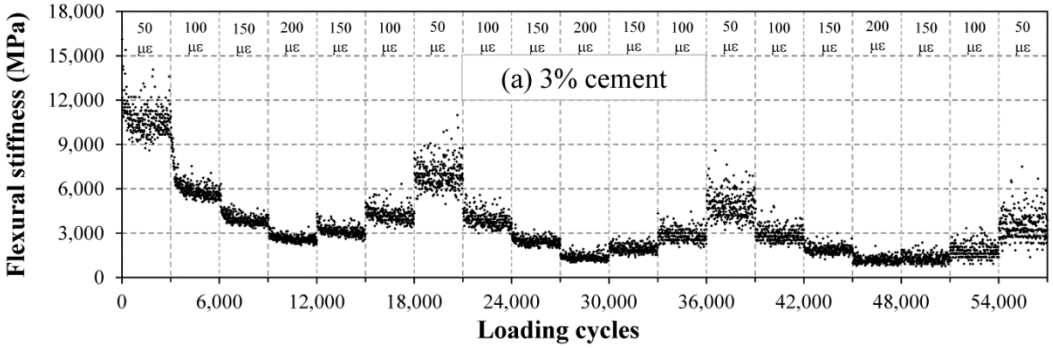

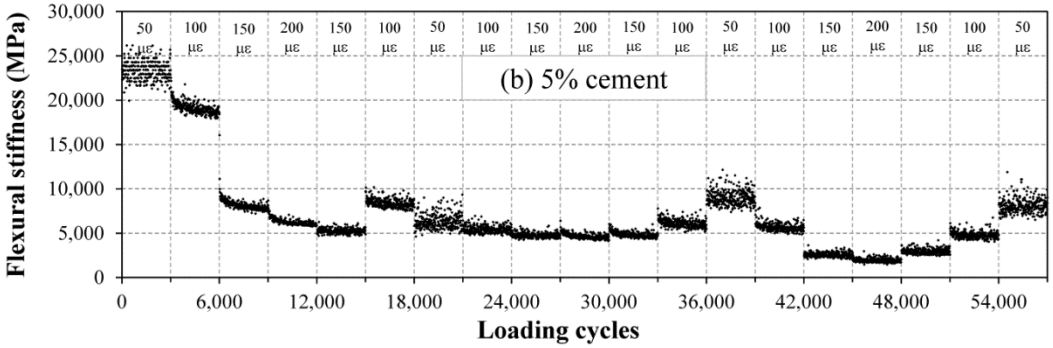

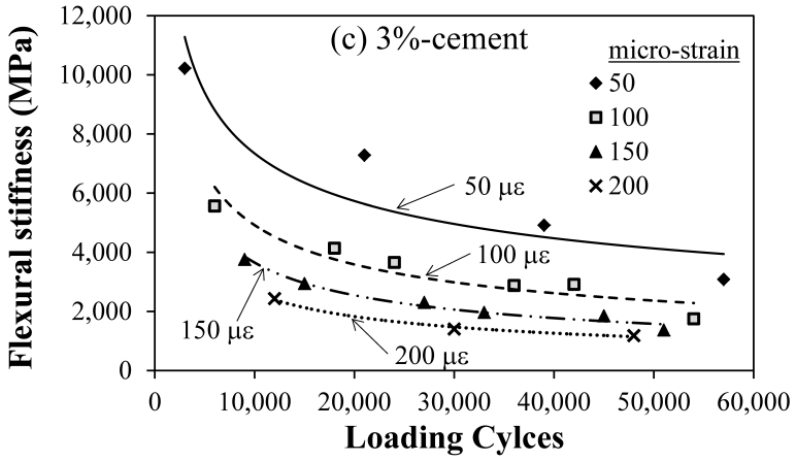

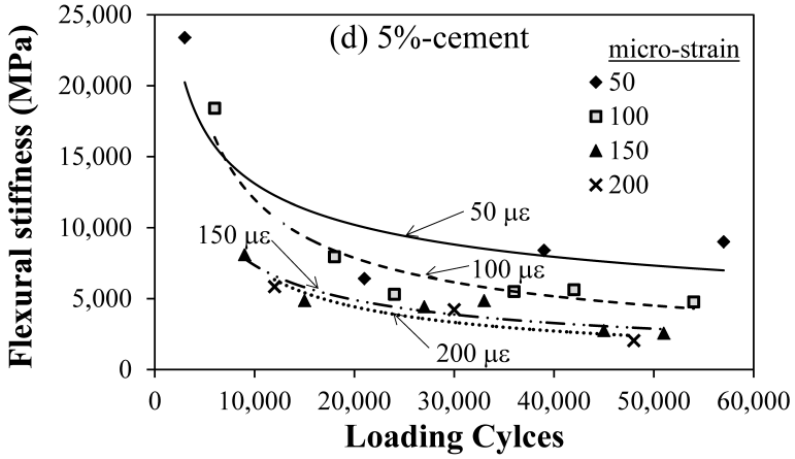

Figure 3.21: Test results for 3% and 5% cement samples subjected to multi-strain

3.9 Summary

The investigation into the characteristics of CTB in terms of UCS, shrinkage and flexural fatigue was performed using variations in the amount of cement content. The gradation of all samples was controlled to ensure that they were identical. Based on the modified compaction tests, the differences in the density and moisture content of all mixtures were found to be insignificant.

The UCS and the elastic modulus of the test samples improved as the cement content was increased from 2% to 6%. However, shrinkage in the CTB did not increase with the addition of cement. The least shrinkage value was found in the 4% cement sample. The shrinkage of CTB decreased as the cement content was increased from 2% to 4% and then further increased to a cement content of up to 6%. The shrinkage of all test samples reached at least 80% of the total possible shrinkage after 21 days of drying, and insignificantly increased after 90 days of drying. Shrinkage is mainly dependent on moisture loss from drying shrinkage and autogenous shrinkage (or self-desiccation). It was assumed that the high shrinkage in the higher cement content of CTB i.e., 5% and 6%, was dominated by self-desiccation. Conversely, the shrinkage in the low cement content, 2% - 3%, was predominantly caused by drying shrinkage.

The flexural fatigue tests were conducted under the strain-control mode of 50 με, 100 με, 150 με and 200 με for the 3% and 5% cement samples. Two different forms of strain-control testing were carried out; constant strain and multi-strain. For the constant strain test, all 3% and 5% cement samples underwent one million cycles of loading. Only the 5% cement sample, subjected to 200 με, could trigger fatigue failure. Thus the fatigue life of this sample was projected based on the experimental data. The results revealed that the fatigue phenomenon does not occur if the strain in CTB induced by repetitive loading is lower than 200 με, and as such a fatigue relationship could not be drawn from the experimental data. Therefore the fatigue behaviour of CTB subjected to higher levels of strain requires further investigation. The multi-strain test was then initiated to examine the degradation and recovery of the stiffness of a specimen. This was carried out in increased steps with decreases in applied strain, with a view to developing a test protocol to reduce the testing time and the number of test specimens.

CHAPTER 4
BASIC PROPERTIES OF HCTCRB

This chapter initially describes the constituent materials and production process of HCTCRB as well as the preparation of test specimens under laboratory conditions. The relevant variables in each procedure that influence the HCTCRB properties are also detailed. The subsequent section reports on experimental works regarding the mechanical and non-mechanical properties of the material. All test methods were mainly in accordance with Austroads and Main Roads Western Australia (MRWA) standards. The basic non-mechanical properties include particle-size distribution (PSD), and the moisture-density relationship. A micro-scale study using scanning electron microscopy (SEM) is also detailed. The strength of the material in terms of shear strength parameters, taken from static triaxial and unconfined compressive strength (UCS) tests, is then reported upon.

4.1 Materials

Standard CRB samples were collected from a local quarry in Perth, and stored in a number of 20 kg plastic containers (see Figure 4.1). The fresh, damp CRB samples were placed in an oven to dry at a temperature of between 105 °C and 110 °C for 24 hours (Main Roads Western Australia 2011b). Dry CRB samples from each of four buckets were then mixed thoroughly, and split using a material divider until the required quantity was obtained, in order to minimise any variation between the samples. The maximum particle size of CRB is 19 mm; the usual requirement for basecourse. The significant properties of CRB were examined in accordance with MRWA specification (Main Roads Western Australia 2010b).

The stabilising agent used in this study is General Purpose Portland Cement (GP cement), conforming to the standard AS 3972-1997 (Standards Australia 1997).

(a)

(b)

(c)

(d)

Figure 4.1: CRB samples, and preparation (a) fresh and damp samples (b) ovens for material drying (c) dry CRB (d) a material divider

4.2 HCTCRB

Figure 4.2 demonstrates the manufacturing process of HCTCRB in the research laboratory which represents actual factory practices and construction sites. The HCTCRB in this research was made by blending standard CRB with 2% cement (by mass of dry CRB); the typical cement content used in the general manufacturing process in WA. Dry CRB and cement were put into a mixer and blended for 5 minutes to allow consistent distribution of cement throughout the CRB. The prescribed amount of water was then added to the mixture for a period of 10 minutes until the mixture was uniform in colour and texture. The amount of water used was in accordance with MRWA specifications (Main Roads Western Australia 2008, 2009, 2010b, 2011a, 2012a); that is the minimum moisture content of the mix at 90% optimum moisture content (OMC) of CRB. Accordingly, the fresh mixture was

stored in closed containers, and cured in a temperature-controlled room (25 °C) to maintain constant curing conditions for specified hydration periods. Once the desired hydration time was completed, the hydrated mixture was returned to the mixer (without additional water) to break the cementitious bonds generated during the hydration reaction. This procedure, called a re-treating process, aimed to produce a cement-modified material whilst maintaining unbound basecourse characteristics in order to provide effective material engineering properties. Eventually, HCTCRB was obtained; its appearance, as shown in Figure 4.3 is similar to CRB coated with cement. Subsequently, a number of HCTCRB specimens were compacted to simulate the compaction of the basecourse layer in the field. Finally, the specimens were subjected to a series of several tests in order to evaluate their material properties.

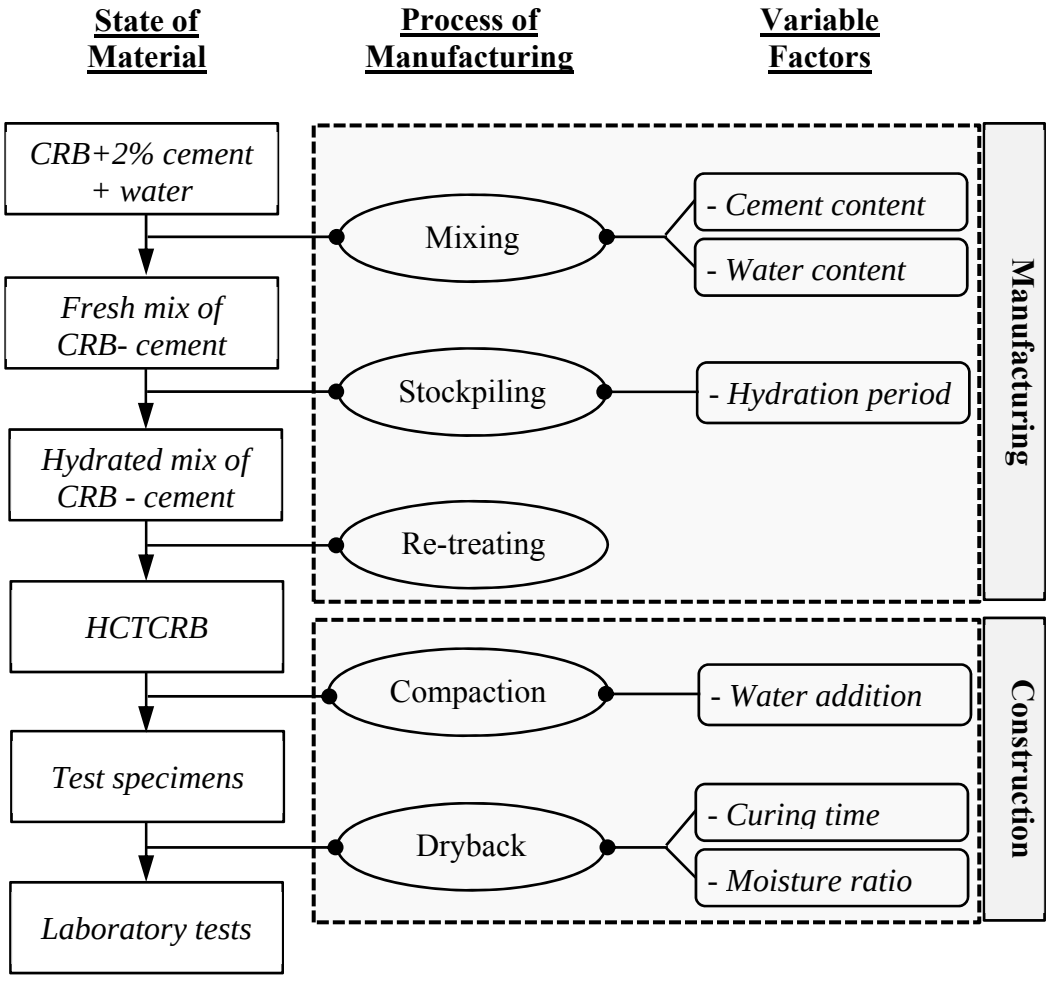

Figure 4.2: Diagram of procedure and factors during manufacturing of HCTCRB

(a)

(b)

(c)

(d)

Figure 4.3: Photographs showing the manufacturing of HCTCRB (a) mixing constituent materials (b) fresh mixture sealed in plastic bag (c) re-treating the hydrated mixture (d) HCTCRB

In the manufacturing and construction procedures there are considerable variables that may affect the material properties of the HCTCRB. These factors are:

- Cement content

  For normal CTB, higher cement content provides greater strength. It may also cause a material to stiffen and undergo fatigue and shrinkage cracking. The effect of the amount of cement content on the properties of HCTCRB may be different from that on common CTB as HCTCRB's cementitious bonds are broken after hydration. Even though only 2% cement is commonly specified for HCTCRB stabilisation by MRWA, examination of HCTCRB properties,

after being subjected to a wide range of cement content, should deliver more accurate results as to how the amount of cement content affects the material.

- Mixing water content

  Moisture content is a major factor affecting the performance of pavement materials. Main Roads Western Australia (2008) specified a range of water content of 90% - 120% of the optimum moisture content (OMC) of CRB for preparation of HCTCRB. The specified OMC was later amended to be no less than 90% of OMC of CRB (Main Roads Western Australia 2010b).

- Hydration period

  The MRWA specifications for pavements have changed periodically. For example, in 2010, the minimum hydration period was extended from 7 days to 21 days (Main Roads Western Australia 2010b). With regard to the manufacturer's perspective on the range of hydration periods for HCTCRB, a shorter period is preferred in order to minimise the problem of demand for greater stockpile areas, which take up more space for longer periods. In practice, contractors produce enormous amount of the mixture which cannot be used up in such a short time. Some manufacturers have stored the HCTCRB in the factory for up to 90 days. Thus the effect of various hydration periods on the performance of HCTCRB should be evaluated.

- Water addition during compaction

  With longer hydration periods, the moisture content of the hydrated mixes becomes lower. As a result, HCTCRB samples may be too dry to compact after a lengthy hydration period. Therefore, additional water may be required for compaction in order to achieve a target density. Therefore the influence of this additional water on material performance after compaction must also be critically examined.

- Dryback

  All pavement specifications throughout Australia require pavement materials to be dried back prior to construction of the upper layer (Midgley 2009).

MRWA's specifications (Main Roads Western Australia 2008, 2009, 2010b, 2011a, 2012a) are given as to moisture ratio and moisture content of the material with respect to its OMC, which depends on the type of basecourse materials used. As a result, it is important to observe the performance of HCTCRB in the dryback process in relation to HCTCRB's different moisture ratios.

4.3 Basic properties of HCTCRB

4.3.1 Moisture - density relationship

Modified compaction tests according to WA 133.1 (Main Roads Western Australia 2012b) were conducted initially to determine the appropriate amount of water for CRB-cement mixture. The sample was compacted in 5 equal layers in a mould of 105 mm diameter and 115.5 mm height. Compaction was achieved with 25 blows of a 4.9 kg rammer at a 450 mm drop, which provided a compaction energy of 21.62 J per blow, and 2703 kJ/m^3.

Figure 4.4: Demonstration of the modified compaction equipment and compacted sample

The maximum dry density (MDD) achieved for CRB was 2.3 ton/m^3 at an optimum moisture content (OMC) of 5.8 %. The MDD and OMC of the CRB-cement mixture were measured at 2.33 ton/m^3, and 6.3 % respectively. HCTCRB samples were then prepared by blending crushed rock with 2% cement (by dry mass of CRB) and 6.3 % water (by dry mass of CRB and cement blend). The fresh CRB and cement mixtures were placed in sealed plastic bags and stored in a temperature-controlled room

(25˚C) at 7, 14, 28 and 45 day hydration periods to produce HCTCRB. Once the hydration periods ended, each mix was then put back into the same mixer to break the cementitious bonds. Modified compaction tests were then performed on each HCTCRB sample. The moisture–density relationships i.e., the OMC and MDD of the materials are presented in Figure 4.5, and summarised in Table 4.1.

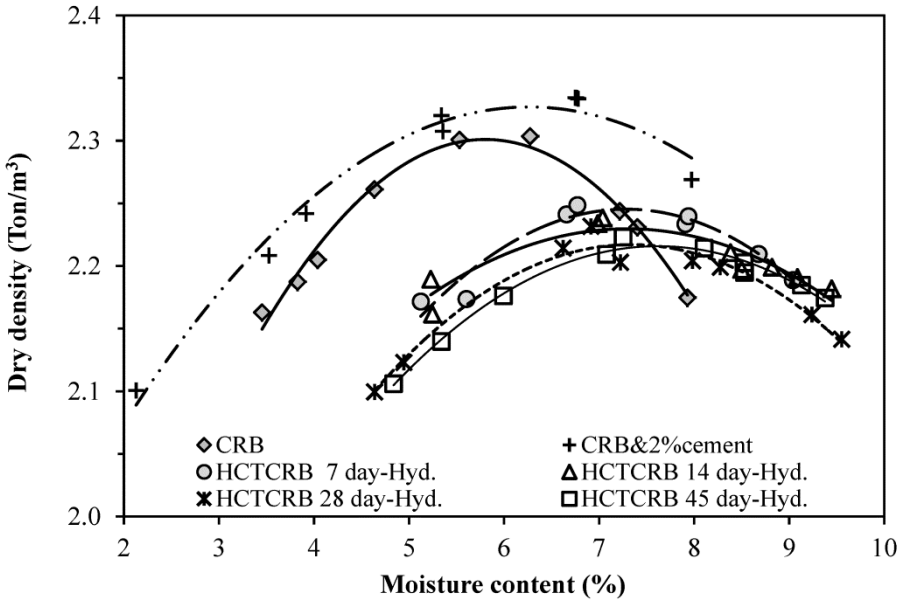

Figure 4.5: Moisture-density relationship of CRB, CRB-cement, and HCTCRB over various hydration periods, derived from modified compaction

Table 4.1: OMC and MDD of CRB, CRB-cement mixture, and HCTCRB

Material	OMC (%)	MDD (ton/m^3)
CRB	5.80	2.301
CRB + cement2%	6.26	2.327
HCTCRB		
7 day hydration	7.28	2.245
14 day hydration	7.30	2.230
28 day hydration	7.34	2.217
45 day hydration	7.62	2.216

Compared to the CRB, the OMC of HCTCRB increased considerably by approximately 25%, while the corresponding MDD decreased marginally by 3%.

The differences in the OMC and MDD of HCTCRB samples at various hydration periods were found to be insignificant. For longer hydration periods, varying from 7 to 45 days, there was an approximate 5% increase in OMC with a 1% decrease in MDD. It is the substandard gradation of HCTCRB which induces an increase in OMC and a reduction in the MDD. This is due to the lack of fine grains, and an additional amount of water which would be required to lubricate the material particles during compaction.

4.3.2 Particle size distribution (PSD)

A series of sieve analyses, conforming to test method WA115.1 (Main Roads Western Australia 2011c), was used to examine the particle size distribution (PSD) or gradation of HCTCRB and CRB samples. PSD after compaction was also examined in terms of how the modified compaction process affected the gradation characteristics of the materials. The PSD of HCTCRB samples was measured (although the MRWA specification does not apply for HCTCRB), in order to investigate changes in the material gradation characteristics after the manufacturing process. The effects of the hydration period on the PSD of HCTCRB were also investigated over hydration periods of 7, 14, 28, and 45 days.

The gradation curves of CRB before and after compacting conditions are presented in Figure 4.6. Compaction energy broke down individual particles of CRB to smaller particles, but its gradation still conformed to the specifications. The dust ratio (the ratio of the percentage passing by mass through the 0.075mm sieve to the 0.425mm sieve) of CRB was 0.45 which is in the range of the 0.35 to 0.60 specified in the standard (Main Roads Western Australia 2010b). The uniformity coefficient (Cu) and coefficient of curvature (Cc) of CRB were 12.5 and 2.0 respectively.

Figure 4.7 and Figure 4.8 demonstrate the gradation curves of HCTCRB after varying hydration periods before and after compaction respectively. It can be seen that the hydration period does not significantly affect the gradation characteristics of different HCTCRB samples. The gradation curves of all HCTCRB samples before and after compaction did not comply with MRWA specification (Main Roads Western Australia 2010b). The gradation curves of HCTCRB shifted to the right of

the CRB curve due to a cementitious reaction of the cement, with the fine particles of CRB forming the larger grains, while the coarse grains were unable to maintain cement bonding after the re-treating process. This resulted in a slight change in the gradation of the coarse grain (i.e., larger than 4.75 mm). The dust ratio of HCTCRB samples was in the range of 0.05 to 0.23. Cu values were in between 6.1 and 7.4, and Cc values varied from 0.8 to 1.2 for HCTCRB samples. The compaction energy broke the HCTCRB particles, resulting in fine particles (with a grain-size smaller than 4.75 mm) which were within the specifications. However, the particles larger than 4.75 mm shifted beyond the upper limit of the specification.

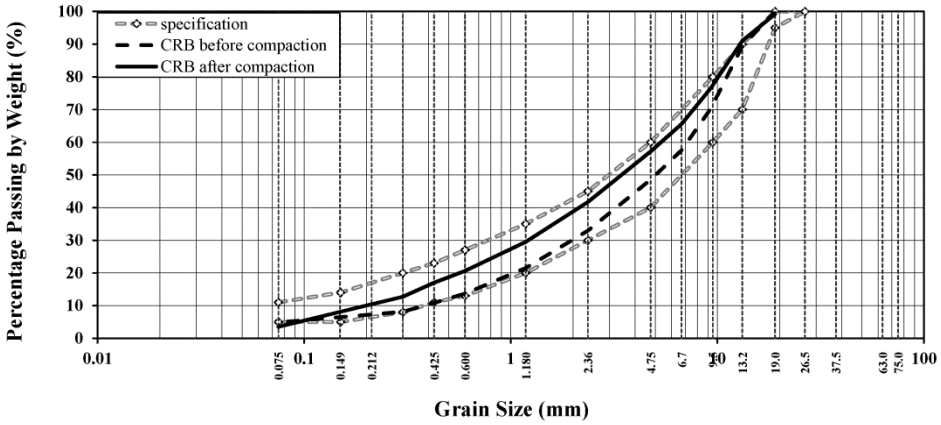

Figure 4.6: Gradation of CRB before and after compaction

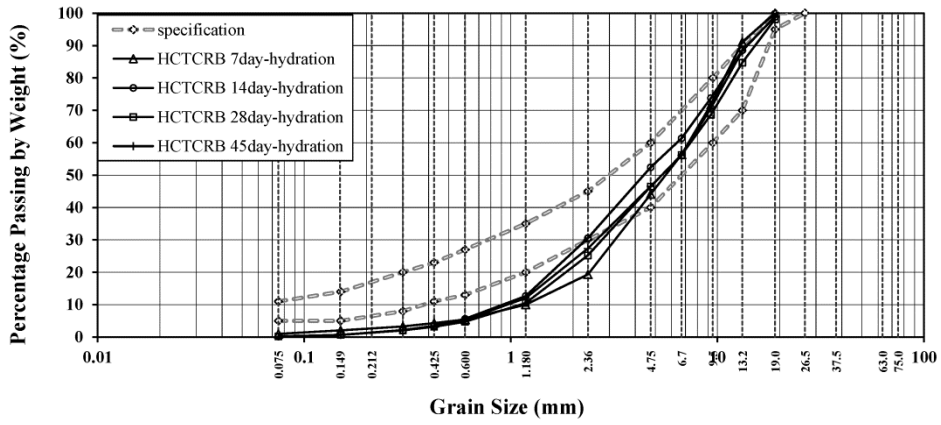

Figure 4.7: Gradation of HCTCRB before compaction for various hydration periods

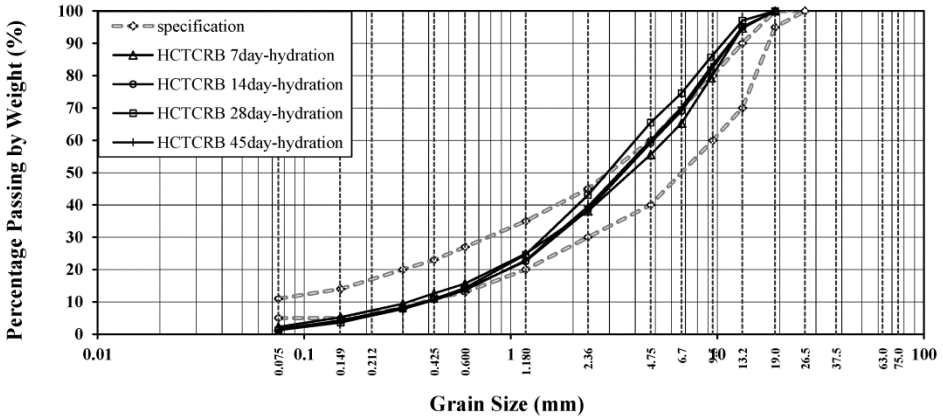

Figure 4.8: Gradation of HCTCRB after compaction for various hydration periods

Table 4.2: PSD parameters of CRB and HCTCRB samples

Material	Dust Ratio	C_u	C_c
CRB	0.45	12.5	2.0
HCTCRB			
7 day hydration	0.23	6.1	1.2
14 day hydration	0.08	7.0	0.9
28 day hydration	0.06	6.2	0.8
45 day hydration	0.05	7.4	0.9

4.3.3 Particle shape and surface

A scanning electron microscope (SEM) with a digital camera was used to document the particle surfaces of CRB and HCTCRB at 7 and 14 day of the hydration periods. Each material was prepared with its individual appropriate OMC. Backscatter electron, and secondary electron images were collected. Backscatter images are useful for finding areas of different composition, with the heavier elements showing up more brightly. Secondary electron images are useful for imaging the surface of the material, as the electrons are reflected closer to the surface of the material.

SEM images of HCTCRB showed indistinguishable differences between various hydration period samples, therefore only representative pictures of HCTCRB were used for comparison with those of the CRB. Backscatter electron images (Figure 4.9) show that the CRB sample is a more consistent grey, indicating the almost

homogeneous nature of the material. The HCTCRB sample has more shades of light and dark, resulting from the cement added to the particle surfaces.

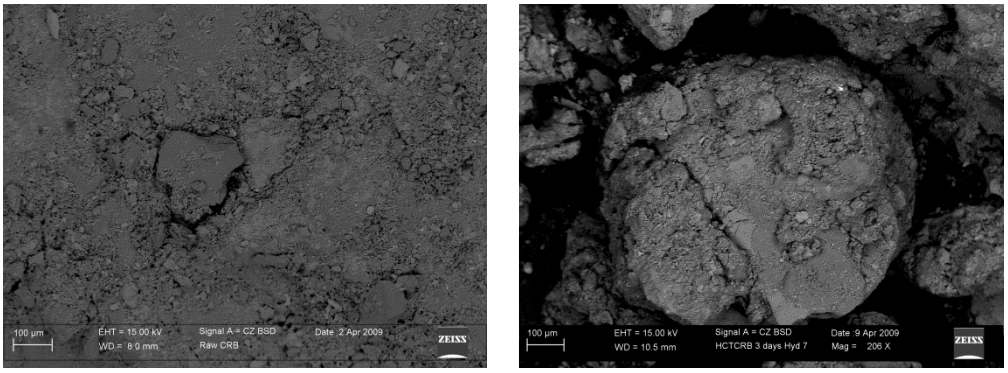

Figure 4.9: Backscatter electron images of CRB (Left), and HCTCRB (Right)

The secondary electron images of CRB and HCTCRB in Figure 4.10 present individual surfaces, shapes, and particle appearance. The HCTCRB sample has a smoother, more rounded surface compared to that of the CRB, which was formed by crushing large mineral portions which had sharp edges and corners. This is indicative of the increased cohesion, and the decreased surface friction of the HCTCRB, which is consistent with the addition of cement to the original material. To quantify these expected characteristics based on the material's appearance, it was deemed necessary to perform further static triaxial shear tests.

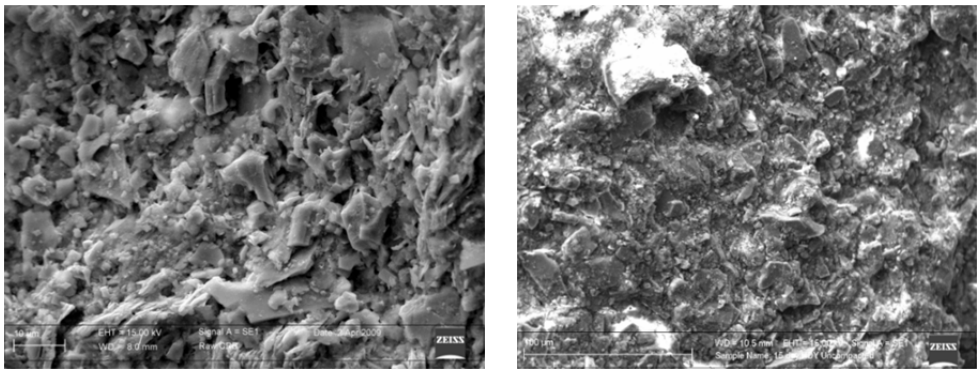

Figure 4.10: Secondary electron images of CRB (Left), and HCTCRB (Right)

The elemental spectra of CRB and HCTCRB are shown in Figure 4.11. The CRB spectrum indicates that the significant major compound is SiO_2, whilst the HCTCRB

spectrum displays the base elements from the CRB with supplementary elements from the added cement.

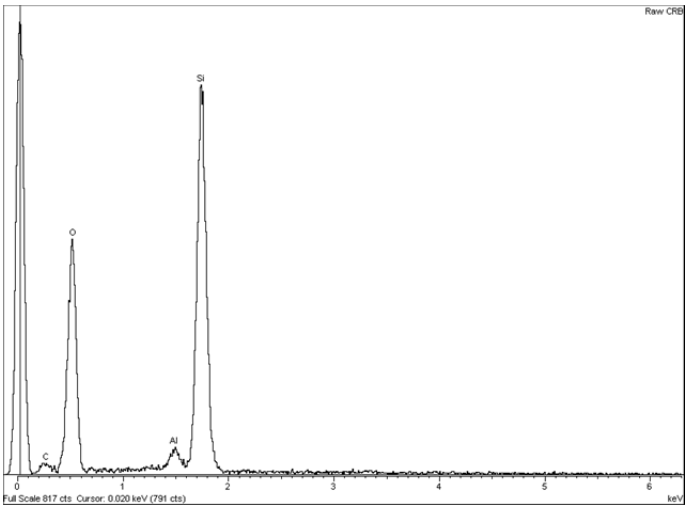

(a)

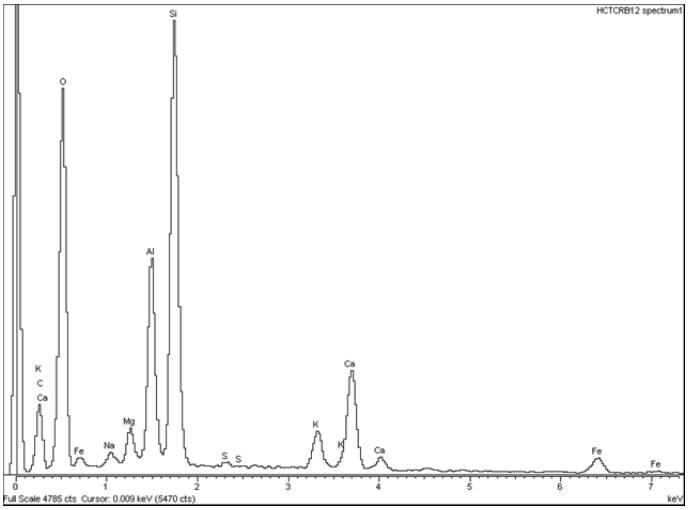

(b)

Figure 4.11: The elemental spectra of materials (a) CRB, and (b) HCTCRB

4.3.4 Unconfined compressive strength (UCS) tests

Unconfined compressive strength is a common and simple parameter for use in the mix design and the structural design of cement stabilised materials. Most specifications for cement stabilised materials require a minimum UCS for the design and construction of stabilised pavements. Examples may be found in the USA (Goerge 2002; United States Department of Transport 2003), the UK, China, South

Africa (Molenaar et al. 2011), and South Korea (Cho et al. 2006). Even though the minimum UCS is specified for CTB, the maximum UCS should be limited in order that the material be neither too weak nor too stiff; thus minimising the propensity to failure. For instance, the Portland Cement Association (PCA) suggested that to limit the crack-width in CTB, the maximum 7-day UCS be 2.07 MPa (300 psi) for fine-grained soils, and 3.1 MPa (450 psi) for coarse-grained soils (Goerge 2002). These guidelines are based on a number of studies in the field and the laboratory in the USA.

There are also strength criteria in WA for UCS. Main Roads Western Australia (2010b) limits the maximum UCS values of HCTCRB samples prepared by the modified compaction to 1.0 MPa and 1.5 MPa at 7-day and 28-day curing times. However, the minimum limits for UCS are not indicated in the specification. Austroads (2006b) categorises the stabilised materials (using cement, lime or chemical binders) in terms of UCS, as modified materials (0.7 MPa < UCS < 1.5 MPa) or bound materials (UCS > 1.5 MPa). These criteria were quantified for samples prepared using standard compaction efforts, 28 day curing periods, and 4-hour soak conditions.

In this investigation, the UCS test method, WA 143.1 and WA143.2 (Main Roads Western Australia 2012c, d), were followed. The tests were conducted for the HCTCRB specimens that were hydrated for 7 days. UCS tests were assessed for eight sets of specimens compacted by two compaction efforts i.e., standard compaction and modified compaction; followed by 7 and 28 day curing periods. The samples were then subjected to two different soaking conditions; that of unsoaked, and that of a 4-hour soak prior to the tests. The modified compaction method used was as previously described in 4.3.1. A standard compaction method uses the same compaction mould as in the modified method and applies 25 blows per layer. However, the standard method compacts a material in 3 equal layers with a 2.7 kg rammer at a 300 mm drop. After extrusion from a mould, all samples were wrapped and cured in a controlled environment of 25 °C at a minimum of 90% relative humidity.

During the tests, a UCS test machine applied a monotonic compression load on the specimens with a displacement rate of 1 mm/minute until the tests were completed. Figure 4.12 depicts the UCS results for all samples. UCS values for all types of samples improved as the curing time increased from 7 days to 28 days. The modified compacted and unsoaked specimens delivered the highest strength; 0.7 MPa at 7 days, increasing to 0.84 MPa at 28 days. These UCS values were also lower than the MRWA limits (7-day UCS of 1.0 MPa). The samples prepared by standard compaction and soaked for 4 hours resulted in the lowest UCS at 0.03 MPa at 7 days, increasing to 0.14 MPa at 28 days. These sample strengths were much lower than the Austroads criteria for modified materials and bound materials, as mentioned earlier. Thus HCTCRB still do not incorporate the modified material (based on the UCS-criteria of MRWA and Austroads) which is specified for pavement materials in WA.

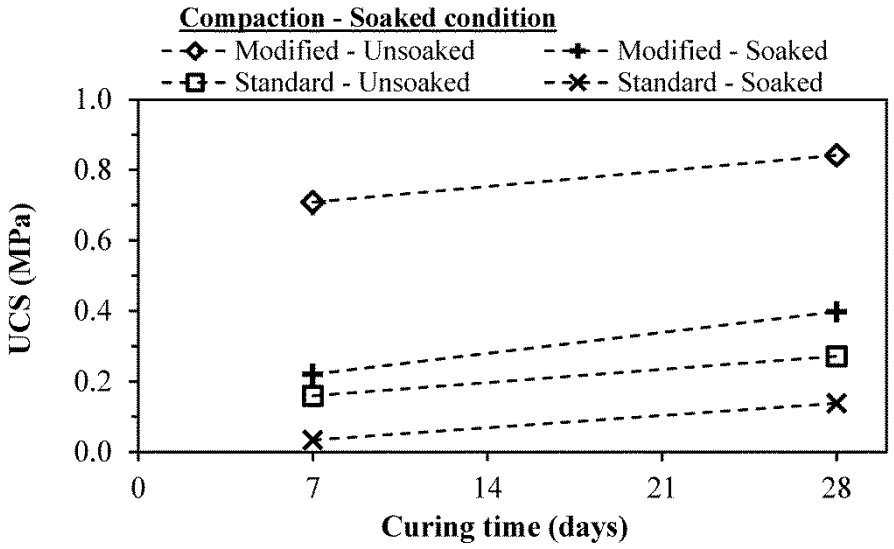

Figure 4.12: UCS test results for HCTCRB samples at 7-day hydration period

4.3.5 Static triaxial tests

Static triaxial tests (see Figure 4.13) were performed under drained conditions with no suction measurement during tests, to obtain the cohesion (c), and the internal friction angle (ϕ) values of HCTCRB after a 7-day hydration period. Tests were also undertaken on the CRB. Using a modified compaction method, the samples were prepared in a standard mould of 100 mm in diameter and 200 mm in height. Compaction was carried out with 25 blows of a 4.9 kg hammer at a 450 mm drop

(height) in eight even layers. HCTCRB and CRB specimens at a 7-day hydration period were compacted at 100% OMC to achieve the density of 100% MDD of the individual material. In these tests, the responses of the materials were collected from a set of three shearing processes with constant confining pressures of 50 kPa, 100 kPa and 150 kPa for HCTCRB, and 40 kPa, 60 kPa and 80 kPa for CRB.

Figure 4.13: The static triaxial test

Figure 4.14 and Figure 4.15 exhibit the set of stress-strain relationships, and the corresponding peak deviator stress of CRB and HCTCRB respectively. It can be seen that the higher the confining pressure, the higher the peak strength and corresponding strain. All three curves in Figure 4.14 and Figure 4.15 demonstrate strain-softening after the peak strength was reached. This means that HCTCRB behaves as an unbound granular material, even with the addition of 2% cement. It differs to the conventional cement-stabilised materials which generally display a more brittle nature such as have high elastic modulus, lower strain at the peak stress and the steeper stress-strain curve after reaching peak stress.

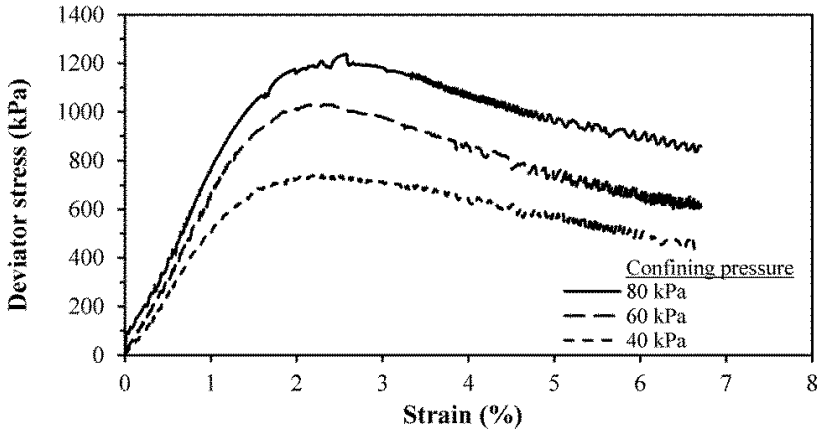

Figure 4.14: Stress-strain relationships of CRB from static triaxial tests

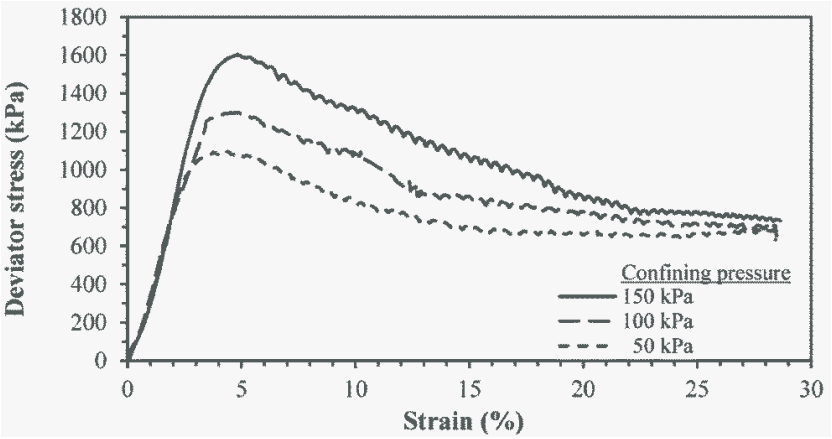

Figure 4.15: Stress-strain relationships of HCTCRB (7-day hydration period) from static triaxial tests

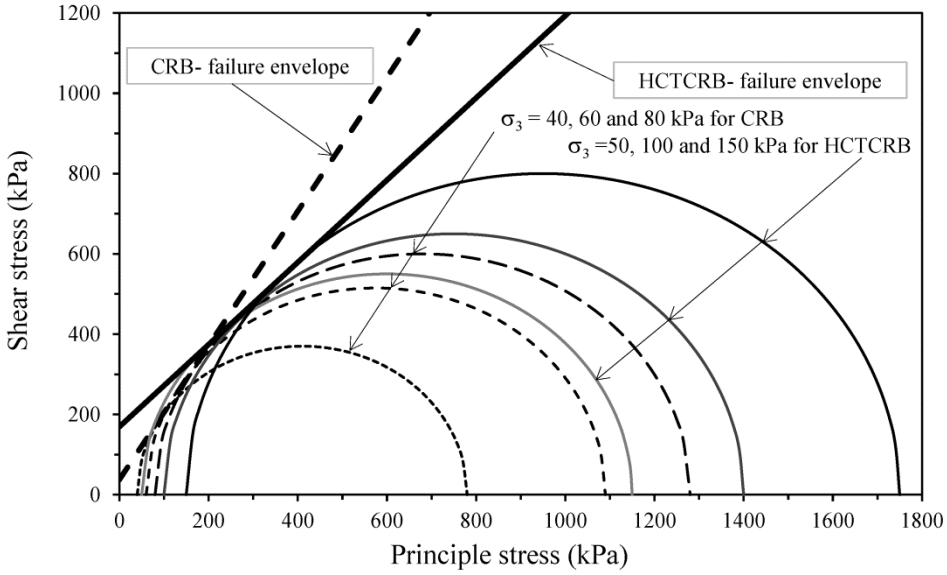

Figure 4.16: Mohr's circles and the Mohr-Coulomb failure envelopes for CRB and HCTCRB

Figure 4.16 shows Mohr's circles, and the Mohr-Coulomb failure envelope for these static triaxial tests. A straight line was drawn through the data to form a Mohr-Coulomb failure envelope to obtain the shear strength parameters (c and ϕ). The results show that the envelope corresponding to the peak stresses is linear for the stress range tested, and within the conventional Mohr-Coulomb stress space. Thus the proper envelopes correspond to an internal friction angle (ϕ), and an apparent cohesion (c) of 59° and 38 kPa for CRB, and 46° and 169 kPa for HCTCRB. These results support the interpretation of the SEM study, in that the cement content of HCTCRB has modified the shear strength characteristics of CRB to increase its cohesive strength but the internal friction has decreased.

4.4 Summary

This chapter presented the physical and performance characteristics of HCTCRB in comparison with those of standard CRB. Experiments were conducted under various conditions (such as hydration periods, and degrees of compaction), to examine physical properties such as gradation and surface properties, and strength characteristics such as UCS and shear strength parameters.

The particle size characteristics of CRB before and after compaction conform to MRWA specifications for basecourse materials, whereas the gradation of HCTCRB before and after compaction does not meet the specification requirements. However, these specifications do not apply for HCTCRB. It was also found that the hydration periods did not significantly affect the gradation characteristics of the HCTCRB

SEM analyses and static triaxial tests proved that CRB has higher internal friction angles but less cohesion than HCTCRB. SEM images of CRB and HCTCRB revealed that the CRB was well crushed with sharp edges and a rough surface. The particles of HCTCRB were covered by cement paste and had smooth surfaces. Static triaxial tests were performed to identify the shear strength parameters of both materials. The cohesion and angle of internal friction parameters for CRB were 38 kPa and 59° respectively; and for HCTCRB, 169 kPa and 46° respectively.

The UCS values for modified compacted and unsoaked specimens were lower than the MRWA limits. The samples prepared by standard compaction and soaked for 4 hours resulted in a much lower UCS than the Austroads criteria for modified materials and bound materials.

More sophisticated tests are reported on in Chapter 5, which presents the mechanical properties of HCTCRB under cyclic loading, thus simulating in-service conditions.

CHAPTER 5
MECHANICAL CHARACTERISATION OF HCTCRB

Static triaxial tests are usually employed to determine the angle of internal friction and the cohesion of soils. Test samples of soil are subjected to static-axial stress until failure at a range of constant confining pressures. In pavement engineering, a set of cyclic axial stresses (loading and unloading), and lateral confining stresses are applied to a single test specimen. This test, known as the repeated load triaxial (RLT) test, simulates the stress conditions in pavement materials under repetitive wheel loadings. RLT tests produce measures of accumulated unrecoverable strain during the course of cyclic stresses (so called permanent deformation), resilient strain due to unloading, and a resilient modulus. The resilient modulus is defined as the ratio of the cyclic axial stress to the resilient axial strain. All these results are essential inputs for the mechanistic-empirical pavement analysis and design. This chapter explains the laboratory investigation undertaken for the repeated load triaxial (RLT) test and sample preparation. The performance evaluation in terms of permanent deformation (PD) and resilient modulus (M_R) was carried out for HCTCRB, with variations in factors during manufacturing and construction.

5.1 Repeated load triaxial (RLT) test

5.1.1 Test method

In this study, the mechanical properties of materials such as the resilient modulus (M_R) and permanent deformation (PD) were measured, using a repeated load triaxial (RLT) test in accordance with Austroads standard test method AG:PT/T053 (Austroads 2007a). In this study, all test samples were compacted at their OMCs which were below the saturated moisture content. The tests were conducted under drained conditions, samples were not saturated and suction measurement was not performed.

The RLT test apparatus comprises a computer with software, a control and data acquisition system (CDAS), a triaxial cell connected with a load actuator, and a confining pressure and linear variable differential transducer (LVDT), as shown in Figure 5.1. The applied stresses and sample information are defined through the

interfacing of the computer with the testing software. The cyclic axial stresses and confining stresses are produced from a pneumatic control system capable of accurately applying a defined stress. Two external linear variable differential transducers (LVDTs) are attached to the top of the triaxial cell to measure the axial deformations of the specimens. The repeated vertical force waveform, lasting for a period of 3 s, comprises a load pulse width of 1 s with rise and fall times of up to 0.3 s, as shown in Figure 5.2. During the test, the actual values of deviator stresses, confining stresses, and sample deformations were measured and acquired by CDAS and then transferred to a computer. These values enabled the determination of the resultant stresses and strains in the samples.

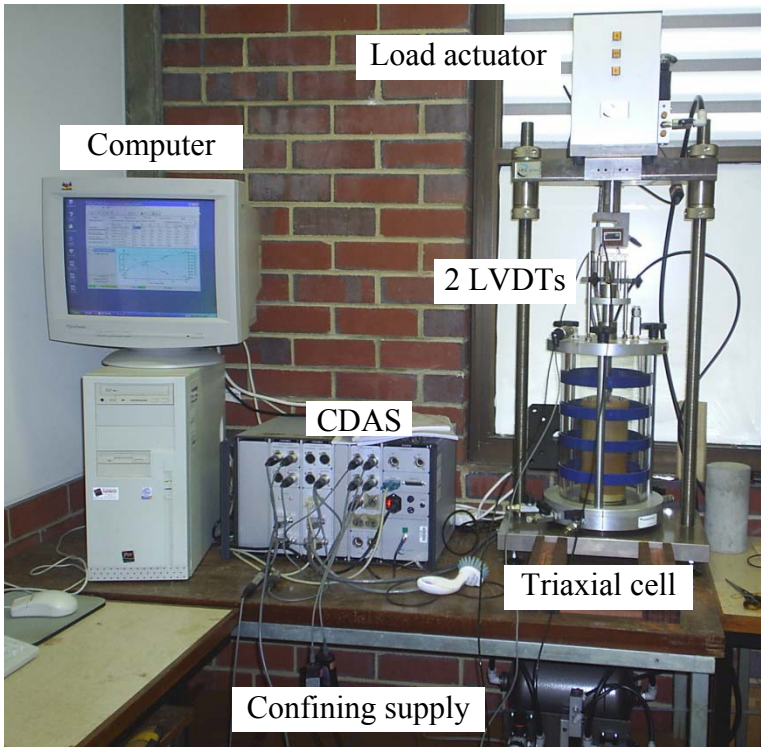

Figure 5.1: Repeated load triaxial (RLT) test apparatus

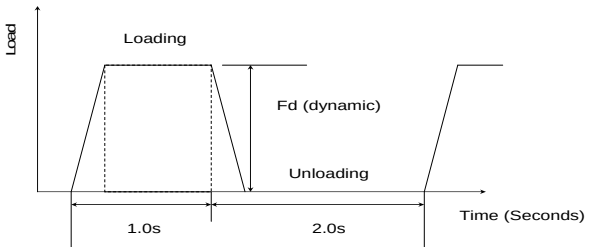

Figure 5.2: The vertical force waveform for RLT test (Austroads 2007a)

Permanent deformation tests were performed at a constant confining pressure (σ_3) of 50 kPa throughout the tests. Each sample was subjected to three stages of deviator stress (σ_d) i.e., 350 kPa, 450 kPa and 550 kPa. At each stress stage, the machine applied 10,000 cycles of vertical force to a sample.

The resilient modulus tests were performed under applied stress conditions in 66 stress stages with different deviator and confining stresses, in order to simulate sophisticated traffic loadings (see Figure 5.3). The stress ratio between the deviator stress and the confining stress (σ_d/σ_3) varied from 2 at the first stage to 25 at the final stage. The deviator stresses varied from 100 kPa to 600 kPa, while the confining stresses ranged from 20 kPa to 50 kPa. One thousand loading cycles of pre-conditioning was carried out prior to the tests. The aim of the process was to allow the end caps to bed-in to the specimen and to ensure that the applied stresses and resilient strains became stable under the imposed stress conditions. Subsequently, 66 stresses were applied to each specimen in stages (stage no's. 0 – 65) to conduct the resilient modulus test. At each stress stage, a minimum of fifty loading cycles was applied to the specimen. Each stage terminated when the standard deviations of the last six values of the resilient moduli were less than 5%, or until two hundred loading cycles were reached. The stages then continued in order until all given stress stages were completed.

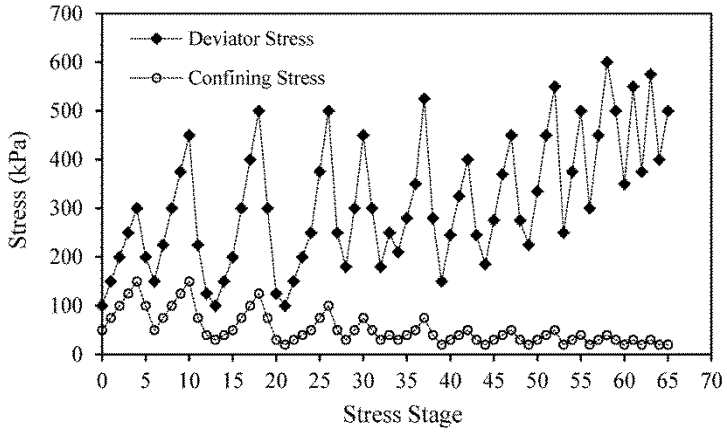

Figure 5.3: Applied stresses and stress stages of the resilient modulus tests (Austroads 2007a)

In Figure 5.4, the failure envelopes for both CRB and HCTCRB, from the static triaxial tests, were plotted against the applied stresses of a resilient modulus test

according to the test method AG:PT/T053. All applied stresses were lower than the failure envelopes of both materials which indicates that both materials were able to sustain all 66 stress stages in the RLT test.

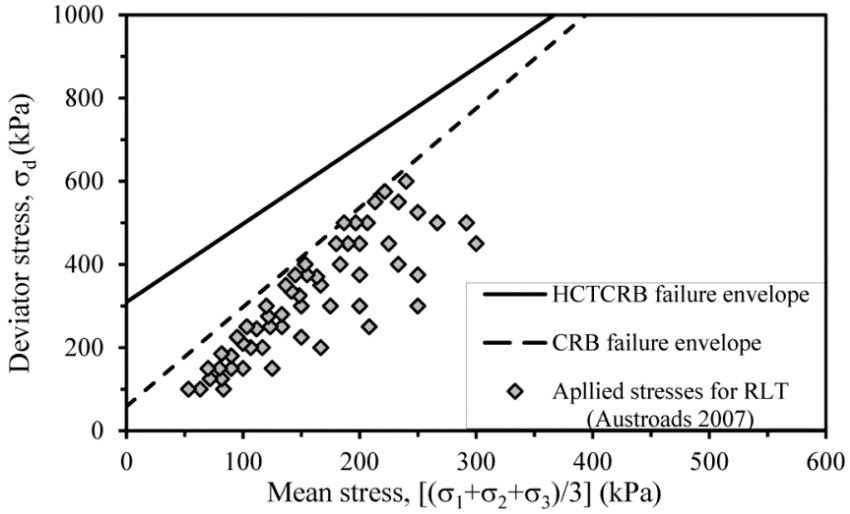

Figure 5.4: Comparison of failure lines for CRB and HCTCRB

MRWA specified a range of MR for HCTCRB as a minimum of 800 MPa and a maximum of 1,500 MPa (Main Roads Western Australia 2011a). Afterward, Main Roads Western Australia (2012a) has increased the minimum MR to 1,000 MPa while still limited maximum value at 1,500 MPa.

For permanent deformation, Vuong and Arnold (2006) proposed requirement for PD characteristic of basecourse materials in term of strain rate during the 3 stages of the test for use in different design traffic as shown in Table 5.1. The terms “stable”, “unstable” and “failure” in this table are defined in relation to an increasing loading cycles as follow.

- Stable - permanent strain rates decrease, and/or resilient strain rates decrease or remain constant while a number of loading cycle increases.
- Unstable - permanent strain rates decrease or remain constant, and/or resilient strain rates remain constant or increase while a number of loading cycle increases.
- Failure - permanent strain rates remain constant or increase, and resilient strain rates increase while a number of loading cycle increases. If the total

permanent strain undergoes 1.5% to 2.0% strain, it is also considered as failure.

Table 5.1: Requirements for characteristic of basecousre materials from PD tests (Vuong and Arnold 2006)

Stage No.	Confining pressure (kPa)	Deviator stress (kPa)	Design traffic (ESA)		
			Light $< 10^6$	Medium 10^6-10^7	Heavy $>10^7$
1	50	350	Stable	Stable	Stable
2	50	450	Unstable	Unstable	Stable
3	50	550	Failure	Unstable to failure	Stable to unstable

5.1.2 Specimen preparation

Using a modified compaction method, the test specimens were produced in a standard 100 mm diameter, 200 mm high mould. Compaction was achieved with 25 blows of a 4.9 kg rammer at a 450 mm drop, in 8 layers. Each layer was scarified to a depth of 6 mm prior to compaction of the next layer, to assure an effective bond between the layers. After compaction, the specimens were cured in wrapped moulds for 28 days to prevent moisture loss, and then removed from the moulds. The specimens were set up successively upon the RLT apparatus. The top platen was placed on the specimen and a rubber membrane placed over the specimen and both platens. Finally, the sample was sealed in the system with o-rings at the top and bottom.

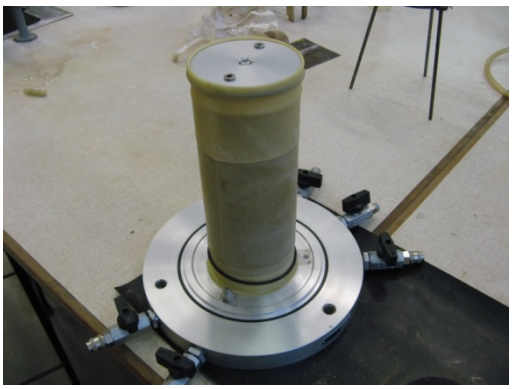

Figure 5.5: Specimen preparation for RLT test

5.2 Stress dependency of HCTCRB

The resilient modulus test for CRB and HCTCRB samples was preliminarily performed to evaluate the stress dependency behaviour of the materials. The HCTCRB at 7-day hydration period and CRB specimens were compacted at 100% OMC to achieve 100% MDD in the individual material. The test results for both materials are displayed in Figure 5.6. Figure 5.7 demonstrates the M_R plotted against the deviator stress at different confining pressures for the CRB and HCTCRB 7-day hydration samples. Figure 5.8 presents the relationship of the M_R and the confining stress at different deviator stress levels for the CRB and HCTCRB 7-day hydration samples. It was found that the deviator and confining stresses significantly affected the resilient responses of materials as the M_R values rose with increases in applied stress. At a constant confining pressure, the M_R increased with increasing deviator stresses. However, the incremental rates decreased at higher levels of confinement. Similarly, at a constant deviator stress, the M_R climbed with higher confining stresses, and the incremental rates were less pronounced at higher deviator stresses.

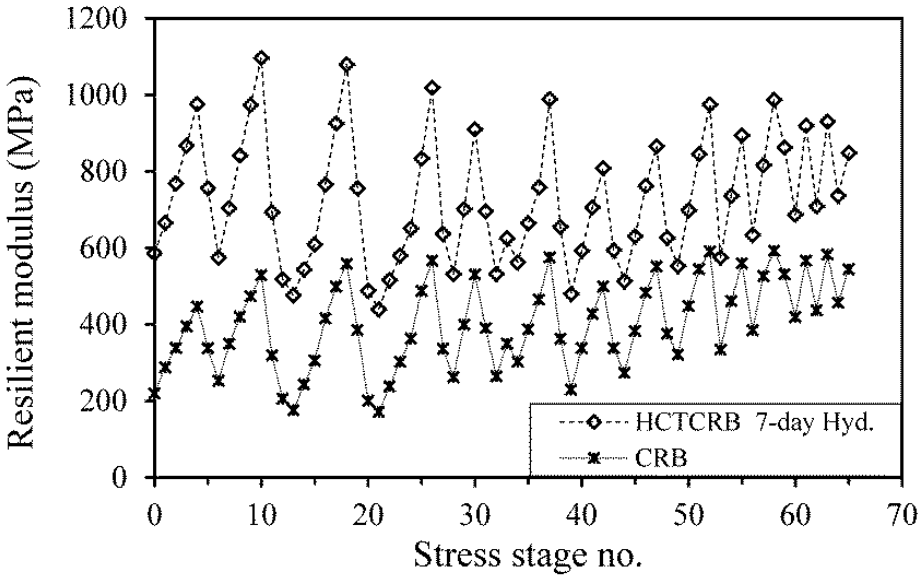

Figure 5.6: M_R test results for CRB and HCTCRB at the 7-day hydration period

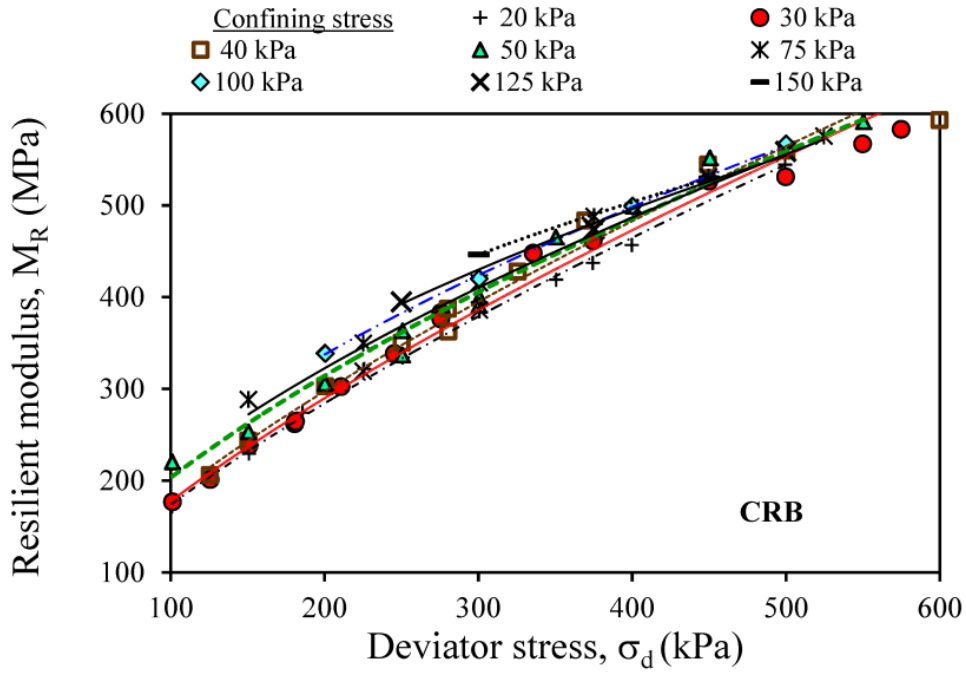

(a)

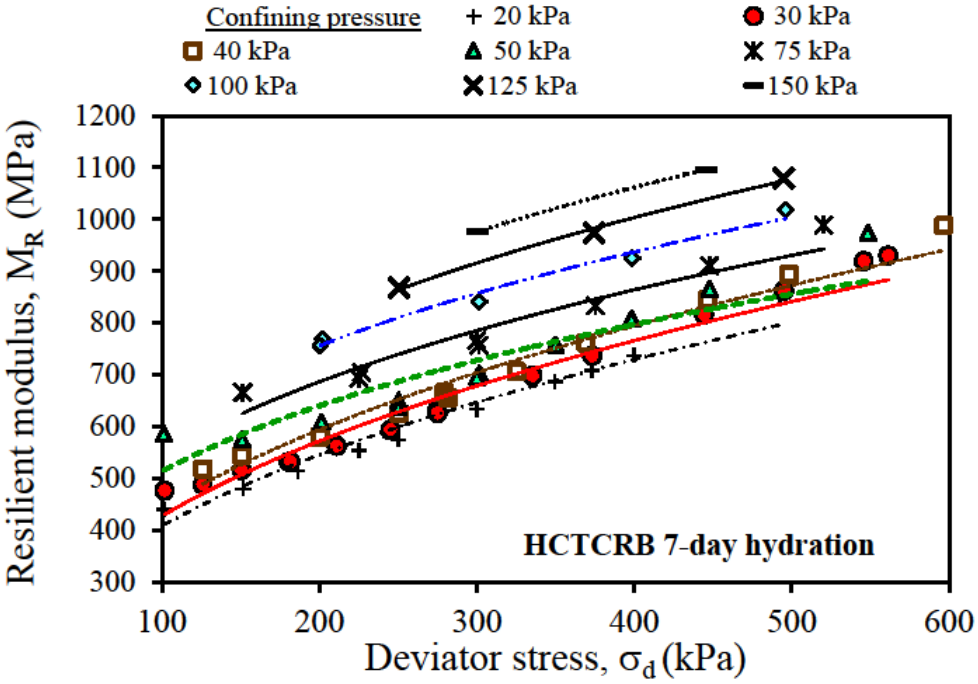

(b)

Figure 5.7: M_R - σ_d relationships at different levels of σ_3

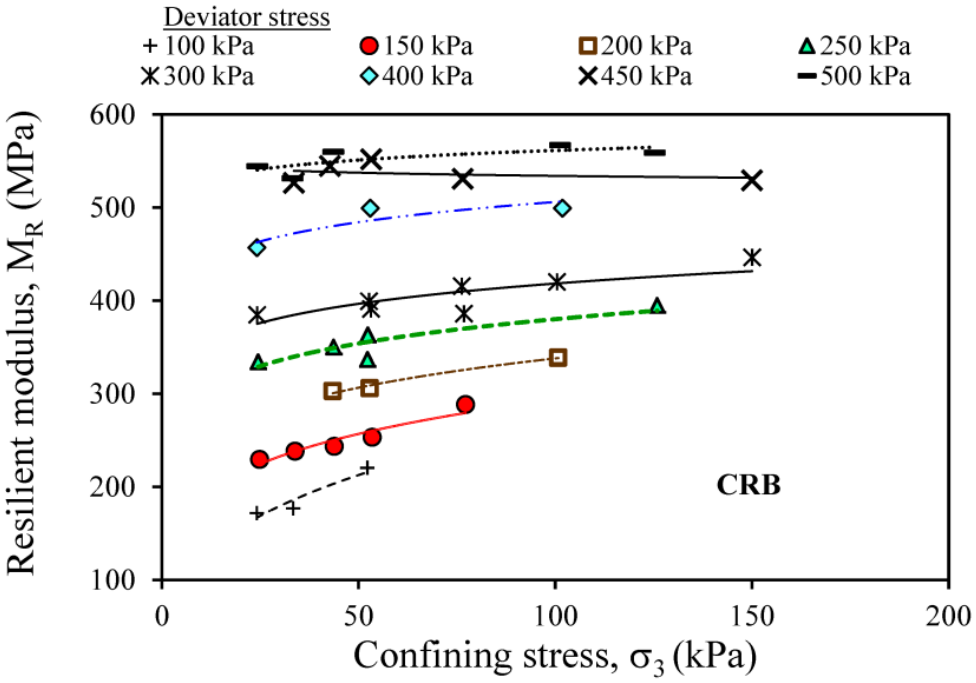

(a)

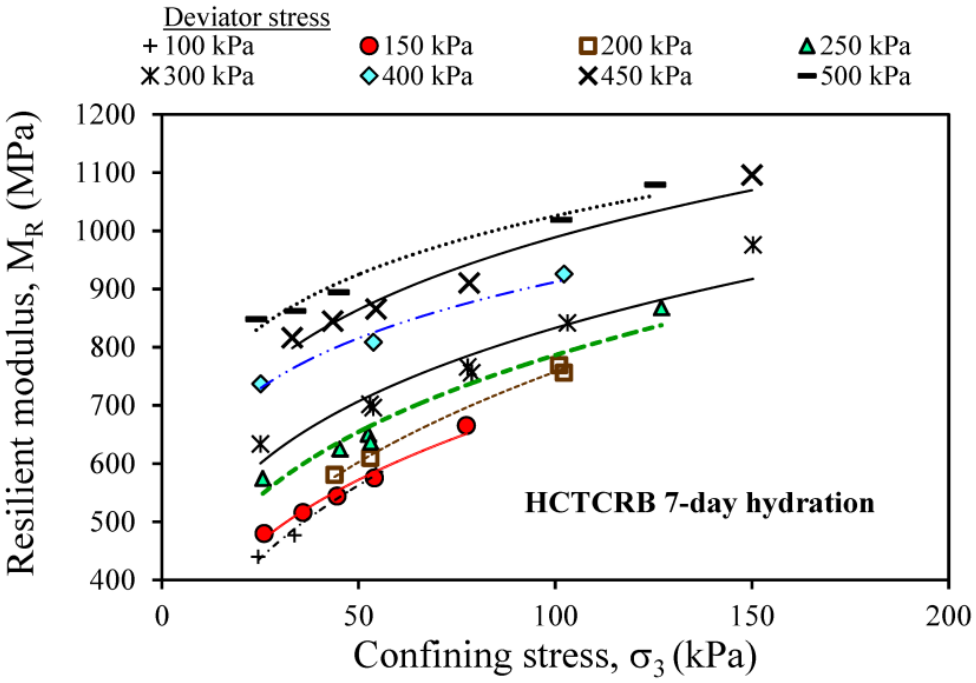

(b)

Figure 5.8: M_R - σ_3 relationships at different levels of σ_d

The relationships of M_R-σ_d at different levels of σ_3 and M_R-σ_3 at various levels of σ_d were assessed using the power law as follows:

$$M_R = a(\sigma_d)^b \quad (5.1)$$

$$M_R = m(\sigma_3)^n \quad (5.2)$$

where a, b, m and n are the relationship coefficients.

The parameters a and m reflect the magnitude of M_R, while b and n represent the incremental rates of M_R. The tested data in Figure 5.7 and Figure 5.8 were evaluated using Eq. 5.1 and 5.2, and following this, all coefficients (a, b, m and n) were obtained. These coefficients were plotted against various levels of σ_3 and σ_d, and are presented in Figure 5.9. The relationships in Figure 5.9 clearly indicate that increasing the applied stresses (σ_3 and σ_d) results in higher magnitudes of M_R, although the incremental rates of M_R are reduced at higher levels of applied stresses.

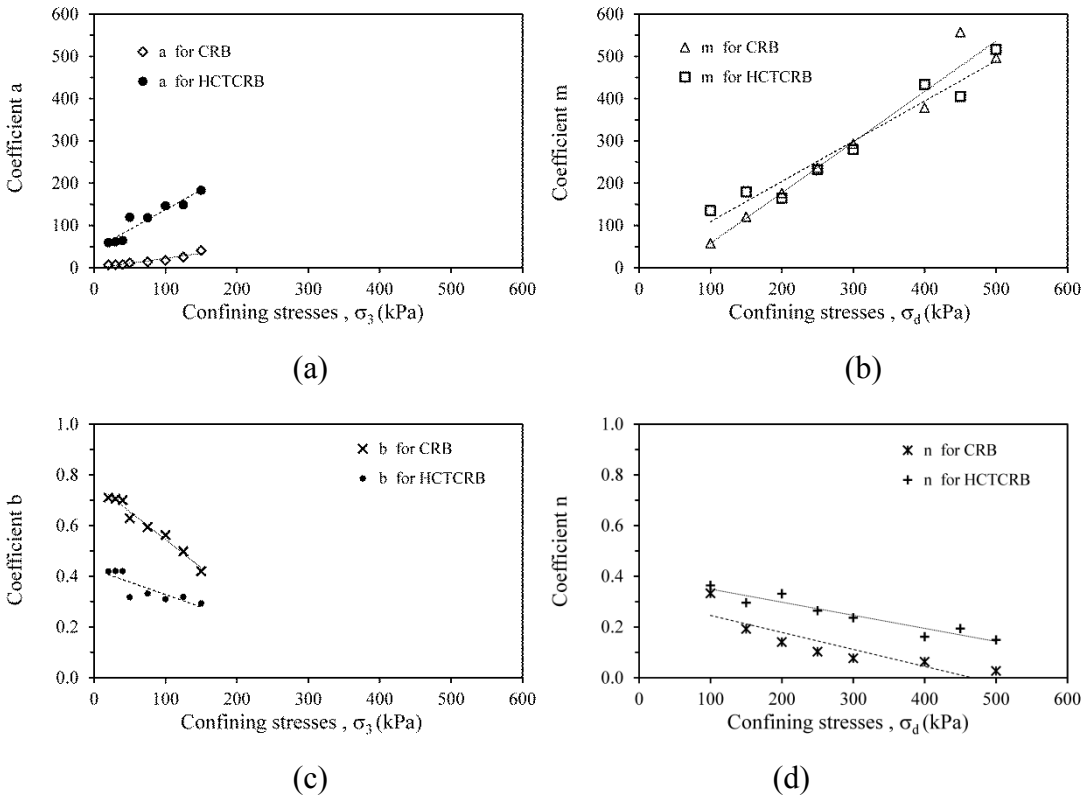

Figure 5.9: The relationships amongst the coefficients (in Eq. 5.1and 5.2) and the applied stresses for CRB and HCTCRB

5.3 Performance of HCTCRB

This section details the performance characteristics of HCTCRB in terms of permanent deformation and resilient modulus. Factors affecting the material's performance, such as constituent material proportion, hydration periods, and moisture content were explored. The amount of mixing water for CRB and cement was kept constant at the OMC of CRB-cement throughout the study. The impact of the cement content of 1%, 2% and 3% by dry mass of CRB was examined, as explained in section 5.3.1. In sections 5.3.2 and 5.3.3, HCTCRB samples made with 2% cement were investigated with regard to hydration periods and moisture contents (during compaction and after dryback). Figure 5.10 summarises the variation in the studied factors.

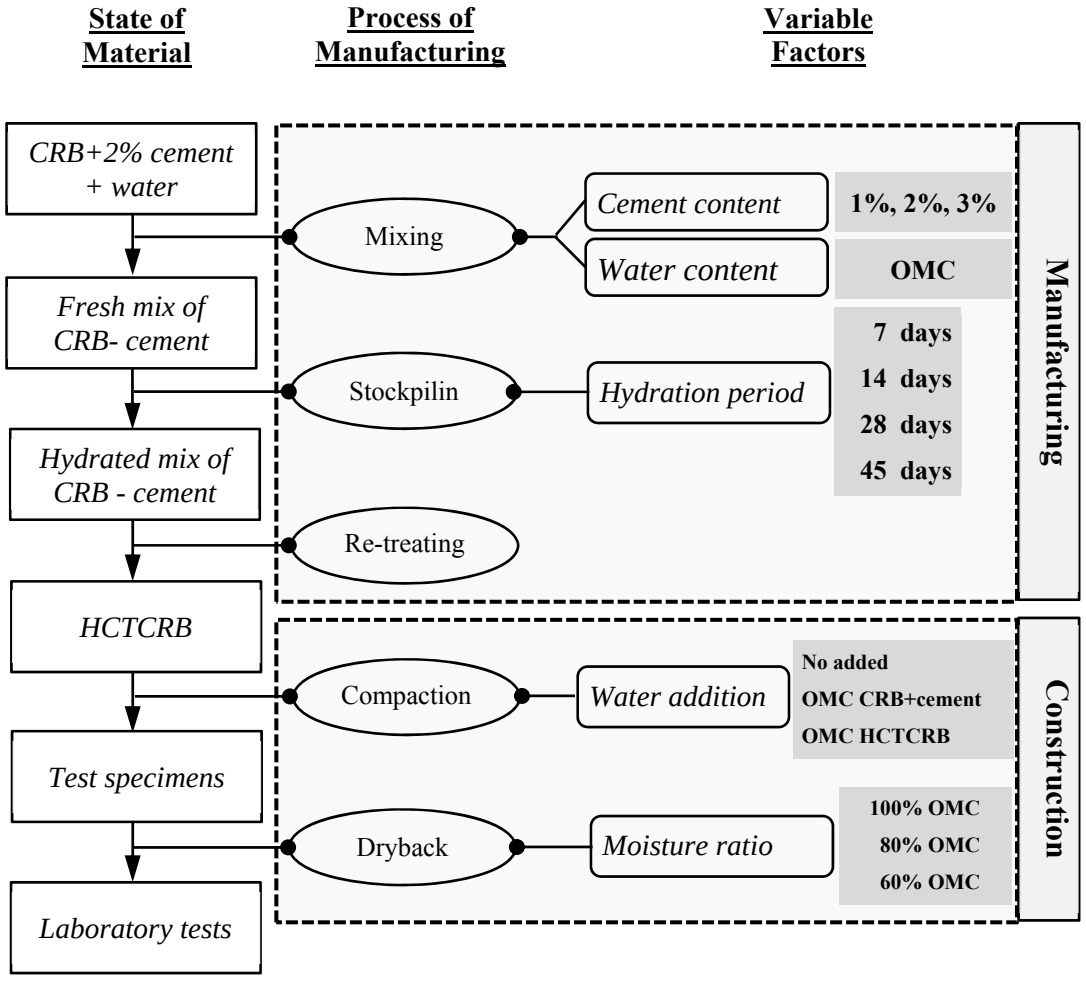

Figure 5.10: The variation in the studied factors

5.3.1 Effect of cement content

HCTCRB samples at the 7-day hydration period were prepared with cement contents of 1%, 2% and 3% by mass of dry crushed rock base. In increasing the cement content from 1% to 3%, insignificant increases in the MDD (less than 1% difference) were noticed, with slight reductions in the OMC (less than 4%). Optimum amounts of water were adopted for the blending of crushed rock base and cement in order to produce HCTCRB.

The UCS tests were evaluated for the HCTCRB specimens at 7 day and 28 day curing times. UCS tests were also conducted for the specimens that had completed the resilient modulus tests, the results are shown in Figure 5.11. The HCTCRB samples with 2% cement proved to be the strongest of the three samples, while the 3% cement sample was the weakest. The 28-day UCS results were 250 kPa, 280 kPa and 180 kPa for 1%, 2% and 3% cement content respectively.

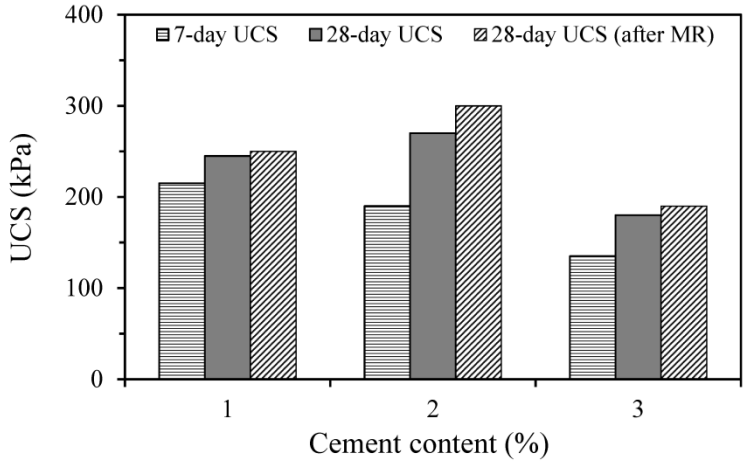

Figure 5.11: UCS for HCTCRB with variations in cement content

Permanent deformation (PD) in terms of percentage of strain for samples made with 1%, 2% and 3% cement were 0.42, 0.46 and 0.70 respectively (Figure 5.12). The resilient modulus test results plotted against 66 stress stages are shown in Figure 5.13. The resilient modulus (M_R) value of HCTCRB samples were between 400 MPa and 1200 MPa for the 1% cement sample, 600 MPa to 1500 MPa for the 2% cement sample, and 350 MPa to 1150 MPa for the 3% cement sample.

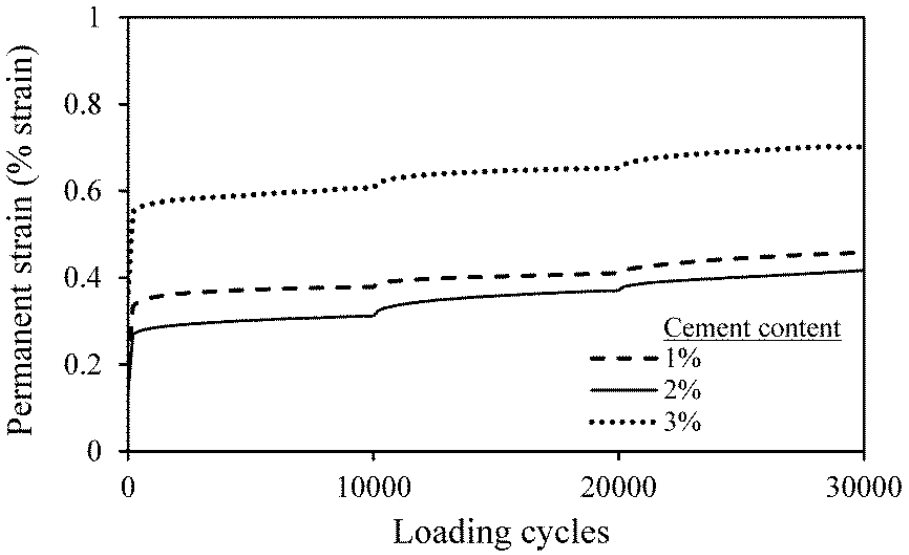

Figure 5.12: PD of HCTCRB samples with variations in cement content

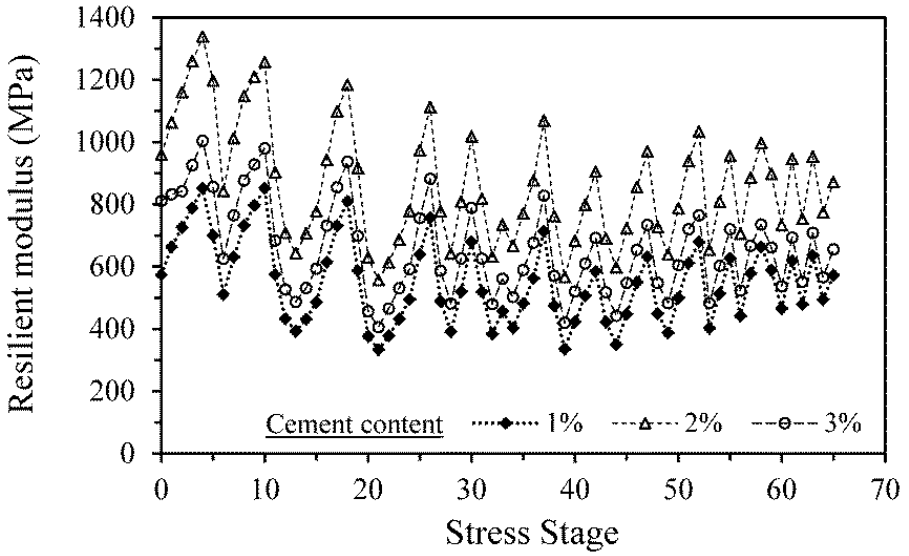

Figure 5.13: M_R of HCTCRB samples with variations in cement content

Similar trends in UCS, PD and M_R test results show that the HCTCRB samples with 3% cement performed the least well, even though they contained the greatest cement content of the three samples. This was a consequence of water consumption during the hydration reaction. At the end of the hydration time, and prior to making the specimen, its moisture content dropped to approximately 83% of the OMC. Thus, the material was quite dry from lack of water, and the specimen could not be compacted properly due to insufficient lubrication of the grains during compaction.

Figure 5.14: The HCTCRB specimens with 1%, 2% and 3% cement content

The moisture content after the completion of the hydration of the 1% and 2% cement samples were approximately 91% and 89 % respectively. These two samples were able to be compacted and were more qualified than the 3% cement content samples. It appeared that the 1% and 2% cement content samples still contained a suitable amount of water to compact the specimens, as shown in Figure 5.14. It can be clearly seen that the surfaces of the 1% and 2% cement samples were smoother than the 3% cement sample. The 3% cement sample also had a greater number of pores which resulted in its more defective performance.

5.3.2 Effect of hydration period and amount of water added during compaction

This section examines the effects of hydration periods and water added during compaction on the performance of HCTCRB. Section 5.3.3 then evaluates the effect of the samples' moisture ratios after the dryback process.

The effect of the hydration period was studied at 7, 14, 28 and 45 day periods. Once each mix had completed the desired hydration period, it was returned to the mixer to break the bonds; and then compacted with variations in the added water content. There were three different levels of water added during compaction, namely type A, B and C. Figure 5.15 presents a schematic diagram for the moisture conditions of the three types of samples. For type A, each mix was compacted without additional water (i.e., in its state of moisture at the end of the hydration period). The moisture contents of the HCTCRB samples after the re-treating process were: 5.7%, 5.6%, 5.3% and 5.0% for the 7, 14, 28 and 45 day hydration periods respectively. Type B

represents the amount of water that was added to the HCTCRB samples during compaction, up to the OMC of the CRB–cement mixture (6.26%). Lastly, type C samples were the samples to which water was added to reach the OMC of the individual hydration period (see Table 4.1).

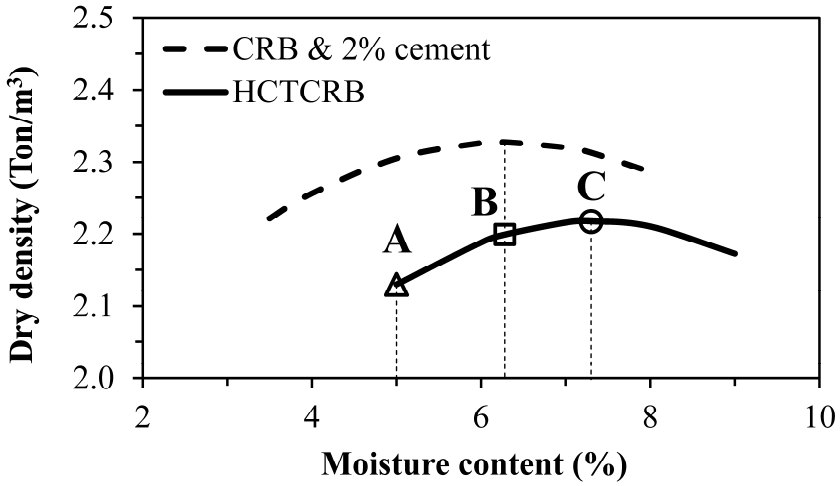

Figure 5.15: Schematic compaction curves for showing moisture conditions of the test samples in this study

The dry density of type A and B samples was generally lower than that of type C, due to type A and B samples being compacted at a moisture content lower than their OMC. The dry density of all tested samples with respect to their individual MDD (see Figure 4.5 and Table 4.1) is summarised in Table 5.2. All samples were tested immediately at the end of the 28-day curing time without the dryback process.

Table 5.2: Dry density of HCTCRB samples with respect to their individual MDD.

Hydration Period	Type A	Type B	Type C
7 days	93.7% MDD	95.8% MDD	98.4% MDD
14 days	94.1% MDD	99.6% MDD	98.3% MDD
28 days	93.4% MDD	97.6% MDD	98.7% MDD
45 days	93.2% MDD	95.2% MDD	99.3% MDD

Figure 5.16 presents the RLT test results of HCTCRB at various hydration periods (7, 14, 28 and 45 days) and with different amounts of water (type A, B and C). The abbreviations in this figure stand for hydration periods and the amounts of added water during compaction for each specimen;

- number 7, 14, 28 and 45 represent hydration periods in days, and

- A, B and C stand for the type of added water during compaction
- For example, 7A represents the sample of 7 day-hydration period and type A (no added water during compaction).

The results for type A samples indicate that sample 14A showed the best performance in terms of the PD of the four hydration periods while 7A was the weakest sample. The % strains for 7A, 14A, 28A and 45A were 0.48, 0.42, 0.45 and 0.49 respectively. In contrast, the 45A sample provided the highest M_R values, which ranged from 550MPa –1350 MPa, followed by 7, 14 and 28 day hydration samples which varied from 700MPa –1200MPa, 300MPa –1000 and 300MPa –850MPa respectively.

For type B, sample 7B showed the best PD performance while 14B was the weakest sample, despite being the densest. The % strains were 0.46 for 7B, 1.06 for 14B, 0.66 for 28B and 0.50 for 45B. The 7B sample also provided the highest M_R values which ranged from 300MPa–1000 MPa. The M_R results for 14B, 28B and 45B were 300MPa–740MPa, 200MPa–650MPa and 330MPa–870 MPa respectively.

Lastly, for type C samples, sample 28C showed the best performance in terms of PD, while sample 14C was the weakest sample. The % strains of 1.01, 1.69, 0.78 and 1.46 were observed for 7C, 14C, 28C and 45C respectively. However, 45C provided the highest M_R values which ranged from 300–800 MPa. There were minor differences in M_R results between 7C, 14C and 28C, which ranged from 200MPa–650MPa, 200MPa–700MPa and 200MPa–600 MPa, respectively.

Figure 5.17 and Figure 5.18 summarise the RLT test results of HCTCRB with variations in hydration periods (7, 14, 28 and 45 days) and water addition (types A, B and C). The effect of hydration periods on HCTCRB performance could not be determined due to the related consistent trends between PD and M_R versus the hydration periods. However, the moisture content of the test samples had a significant impact on the RLT results regardless of the dry density. The higher water addition up to the OMC of HCTCRB (i.e., type C samples) resulted in a decrease in M_R and an increase in the PD of the material, even though it induced a higher dry density, which indicates that HCTCRB is still susceptible to a range of moisture

contents. These results due to the influence of increasing moisture content dominated the dry density development. The moisture content of type C samples were approximately 15 % and 35 % higher than those of type B and A, respectively. Whereas, the improvement in dry density of type C samples was only about 2 % and 5 % in comparison with those of type B and A samples, respectively.

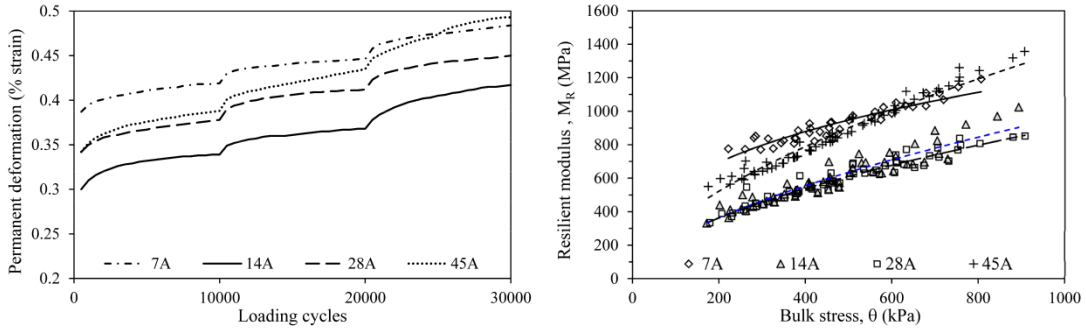

(a)

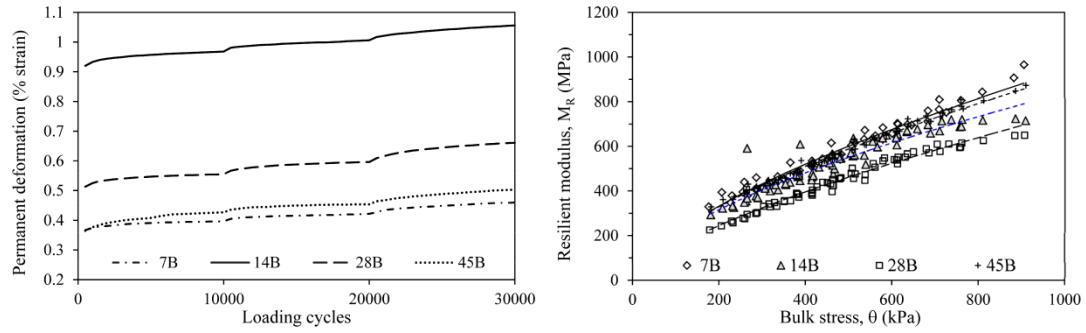

(b)

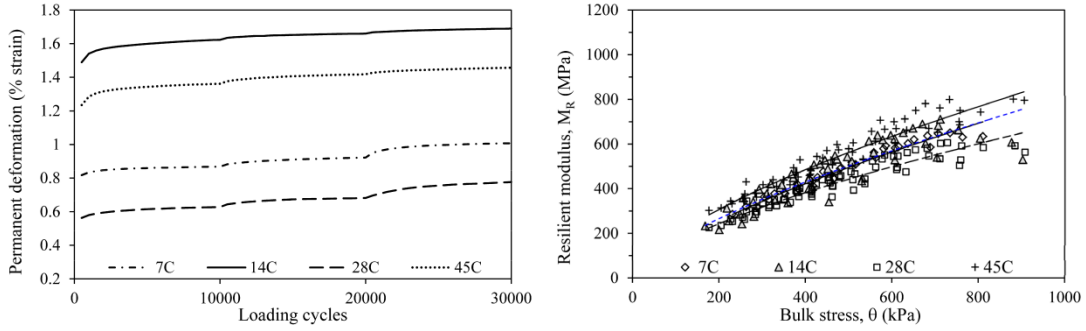

(c)

Note: For abbreviations in the graphs;

- *7, 14, 28 and 45 represent hydration periods in days, and*
- *A, B and C stand for the type of added water during compaction*

Figure 5.16: RLT test results of HCTCRB with variations in hydration periods and levels of water without dryback (a) Type A (b) Type B (c) Type C

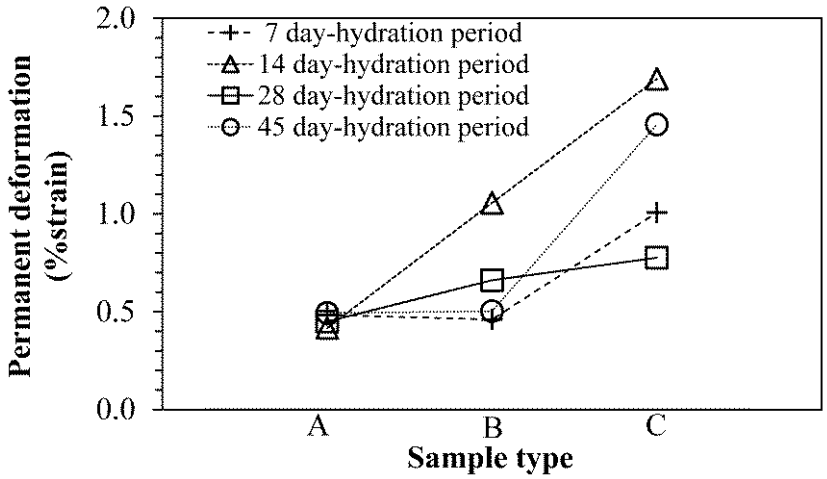

Figure 5.17: PD of HCTCRB with variations in hydration periods and added water (no dryback)

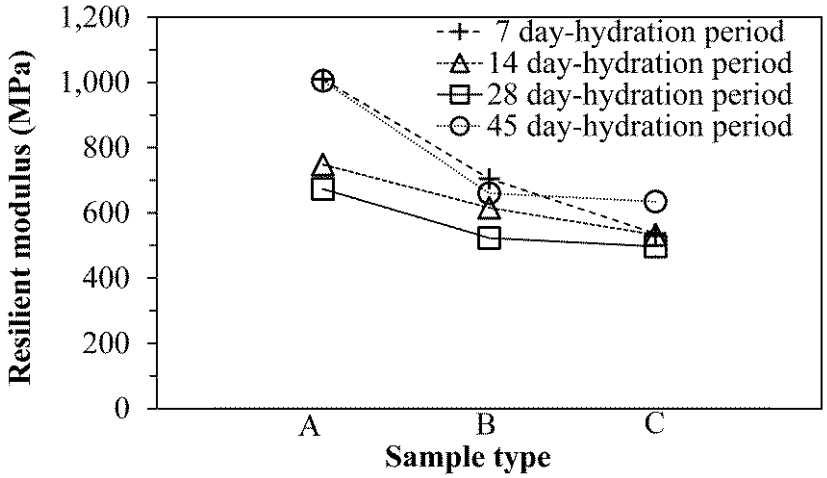

Figure 5.18*:* M_R of HCTCRB with variations in hydration periods and added water (no dryback)

5.3.3 Effect of moisture content after dryback

After compaction, but prior to the tests, the samples were dried using the dryback process. Three categories of dryback were used i.e., no dryback, dryback to 80% of OMC, and dryback to 60% of OMC. The 28-day and 45-day hydration samples with three levels of added water (A, B and C) were tested after the dryback process, as categorised above. It was found that the moisture content of the HCTCRB at 28-day and 45-day hydration periods decreased to about 80% of the OMC of CRB–cement mixture as a consequence of water consumption through the hydration reaction and curing process. Table 5.3 shows the moisture content after curing, and the dry density of the samples used in this study.

Table 5.3: Moisture content and dry density of HCTCRB samples

Sample	Moisture Content[1]		Dry Density[2]
	% OMC_m	% OMC of HCTCRB	
28A	80.5%	68.9% OMC_{28}	93.4% MDD_{28}
28B	97.9%	83.8% OMC_{28}	97.6% MDD_{28}
28C	113.6%	97.2% OMC_{28}	98.7% MDD_{28}
45A	77.3%	63.7% OMC_{45}	93.2% MDD_{45}
45B	98.0%	80.8% OMC_{45}	95.2% MDD_{45}
45C	117.8%	97.1% OMC_{45}	99.3% MDD_{45}

Notes:

1. OMC_m, OMC_{28} and OMC_{45} denote the OMC of CRB-cement mix, HCTCRB of 28 days and 45 days of hydration period, respectively.
2. MDD_{28} and MDD_{45} denote the MDD of HCTCRB at 28 and 45-day hydration periods.

The series of PD and M_R results are presented in Figure 5.19 and Figure 5.20 respectively. Symbols in these figures, such as 28B–80DB represent the sample with a 28-day hydration period, prepared by type B water addition and dried to 80% of its OMC.

5.3.3.1 Permanent deformation

The PD of samples of type 28A reduced from 0.45% to 0.38% strain, as the moisture content decreased from 80% to 60% of OMC_m. For the type 28B samples, the results showed a small difference between the PD of samples which were dried to 80% and 60% of OMC_m. The % strains were 0.66, 0.51 and 0.50 for samples with no dryback, and 80% OMC_m and 60% OMC_m, respectively. The PD of samples of type C decreased from 0.78% to 0.60% strain as a result of the moisture content decreasing from 97.2% to 80% of OMC_{28}. However, the driest sample (60% OMC_{28}) deformed uncharacteristically to a 0.66 % strain, which was greater than that of the 80% OMC_{28}.

The PD of samples of type 45A reduced from 0.49% to 0.42% strain, as the moisture content decreased from 80% to 60% of OMC_m. For samples of type 45B, the %

strains were 0.50, 0.47 and 0.39 for samples with no dryback, 80% OMC_m and 60% OMC_m, respectively. Finally, the PD of samples of type 45C were 1.46%, 1.25% and 0.90% strain for samples with no dryback, 80% OMC_{45} and 60% OMC_{45}, respectively.

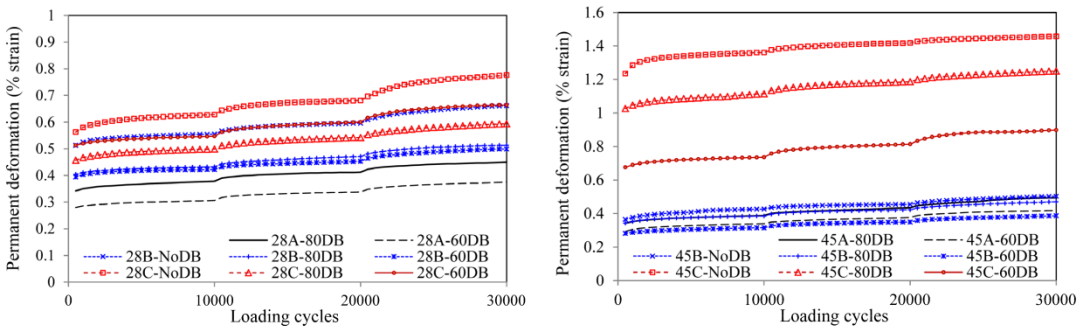

Figure 5.19*:* PD of HCTCRB samples at 28-day and 45-day hydration periods, with variations in water addition and degree of dryback

5.3.3.2 Resilient modulus

Two samples of type 28A provided a similar M_R, varying from 300MPa to 900 MPa. A sample of type 28B, increased its M_R from a range of 200MPa–700 MPa to 350MPa–1000 MPa and 400MPa–1200 MPa as the moisture decreased from 97.9% to 80% and 60% of OMC_m. The M_R values of samples of type 28C were 200MPa–650 MPa for the no dryback sample, 380MPa–900 MPa for the sample with dryback to 80% OMC_{28}, and 800MPa–1300 MPa for the sample with dryback to 60% OMC_{28}.

The M_R values of samples of type 45A were 550MPa–1360 MPa and 580MPa–1490 MPa for the samples at 80% and 60% of OMC_m. For type 45B samples, the M_R increased from a range of 330MPa–870 MPa to 520MPa–1240 MPa and 600MPa–1500 MPa as a result of moisture decreasing from 98.0% to 80% and 60% of OMC_m. The M_R values of type 45C were 200MPa–650 MPa for the no dryback sample, 350MPa–1080 MPa for the sample with dryback to 80% OMC_{45} and 430MPa–1170 MPa for the sample with dryback to 60% OMC_{45}.

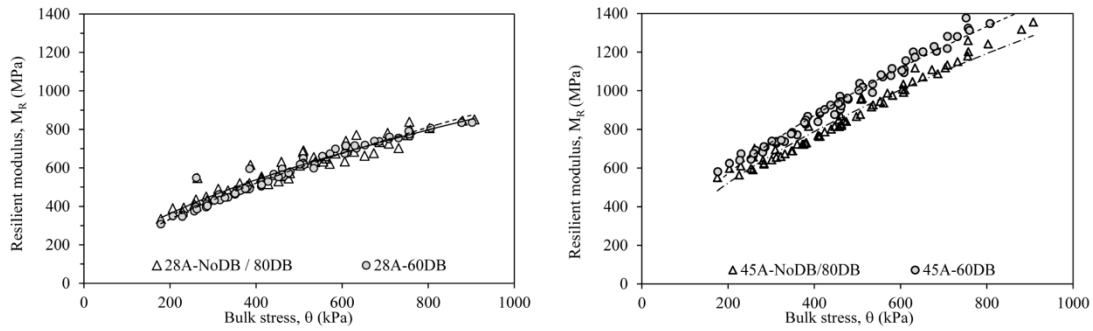

(a)

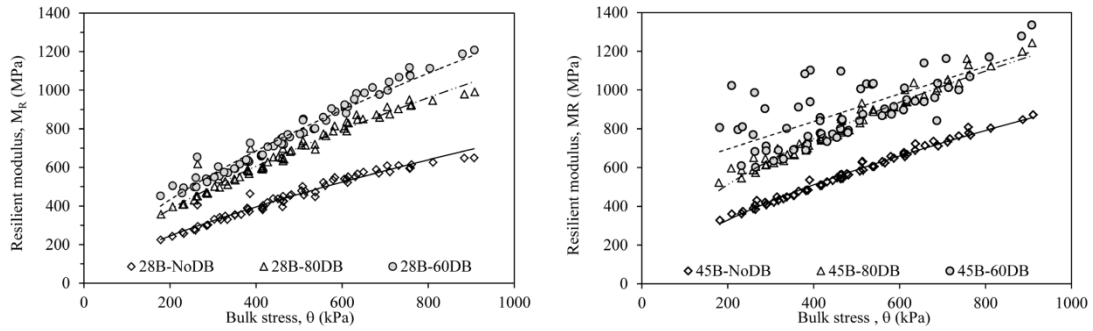

(b)

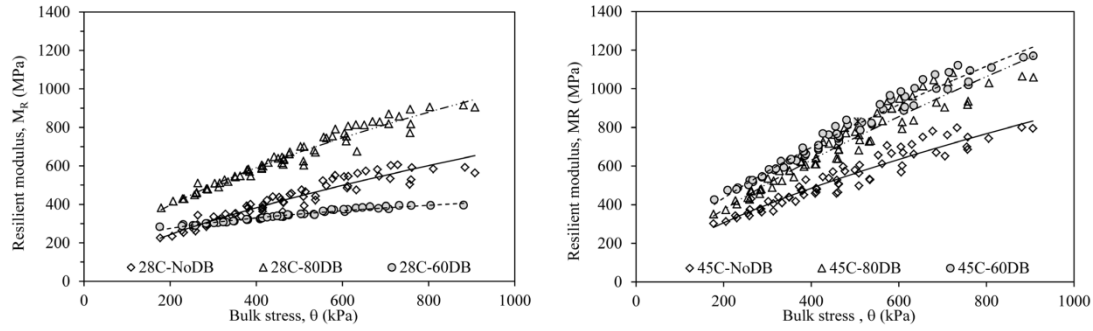

(c)

Figure 5.20: M_R of HCTCRB samples at 28-day and 45-day hydration periods, with variations in water added, and degree of dryback, for (a) Type A, (b) Type B and (c) Type C

The changes in PD and M_R results due to moisture content are summarised in Figure 5.21 and Figure 5.22 respectively. Both figures clearly show that adding water during compaction and dryback (generally performed in the field) significantly affects the performance of HCTCRB in terms of PD and M_R. In general, a higher amount of water added during compaction causes a decrease in PD and M_R performance (compared to samples without added water). Although the samples have higher dry densities, they do not show improved performance after curing. This indicates that

without dryback, HCTCRB tends to show moisture sensitivity. The dryback process, which aims to achieve a drier condition in order to maximise pavement life, can also lead to the improvement of HCTCRB performance, depending on the amount of additional water. After all test samples had undergone the dryback process, an evaluation of the material performance was made in comparison to that with no dryback and with the same water content. It was found that the M_R of type B and C samples were almost equivalent to those of type A, while the PD values of type B and C samples were higher than or equivalent to those of type A. It is noted that based on the results of this study, HCTCRB still has some degree of moisture sensitivity, and this must be considered in order to use this material effectively.

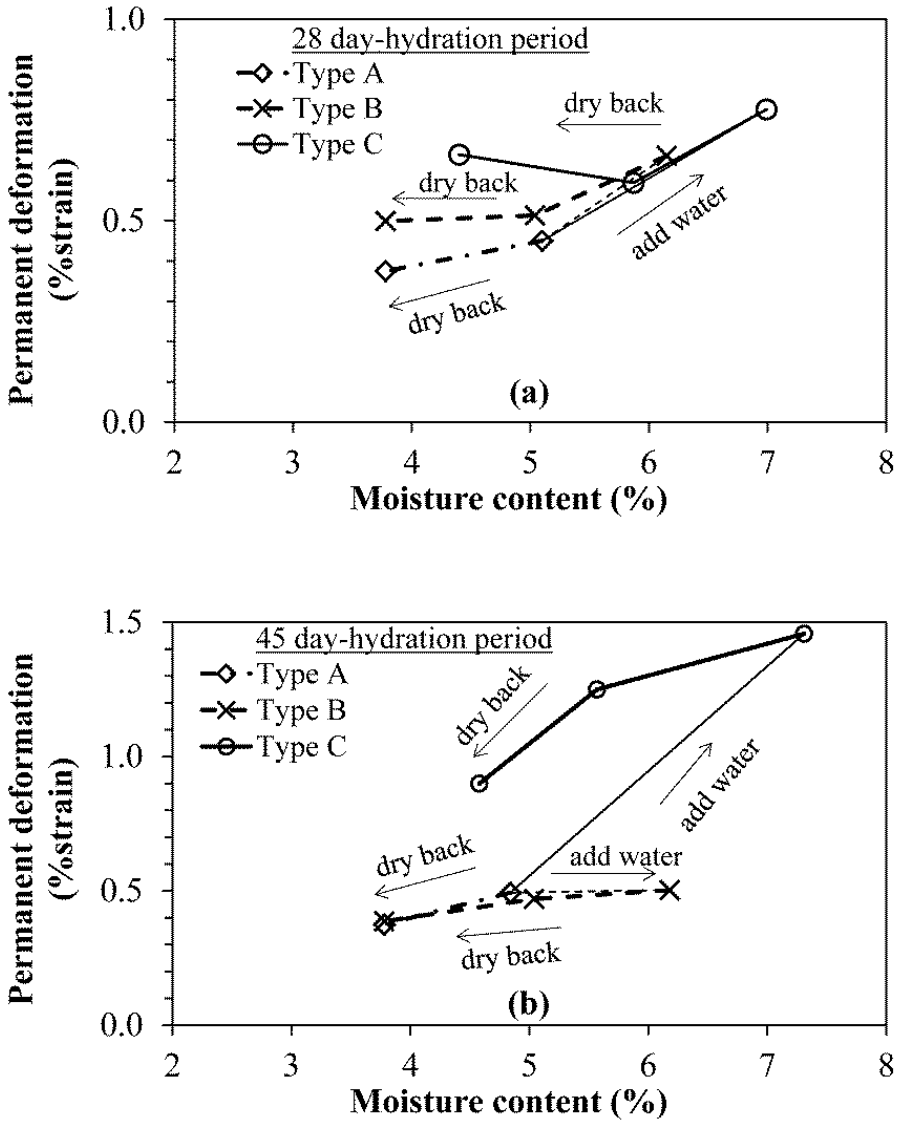

Figure 5.21: PD of HCTCRB samples with variations in the addition of water and degree of dryback, for (a) 28-day hydration period, and (b) 45-day hydration period

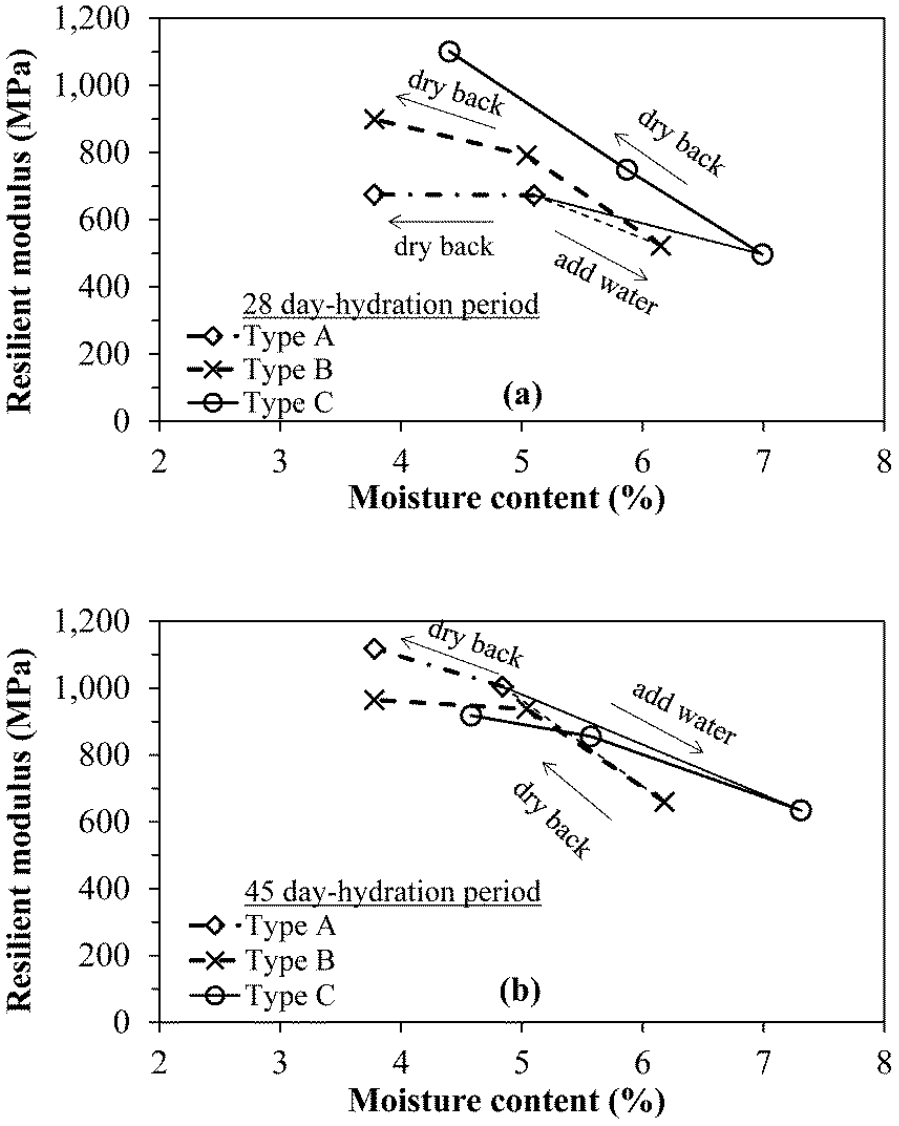

Figure 5.22: M_R of HCTCRB samples with variations in water added, and degree of dryback, for (a) 28-day hydration period, and (b) 45-day hydration period

5.3.4 Implications of the experimental results

The PD and M_R test results for all HCTCRB samples (at 7, 14, 28 and 45-day hydration periods) with variations in moisture content during compaction and dryback are presented in Figure 5.23 and Figure 5.24. A higher amount of water added during the compaction (type B and C) of test samples tends to deteriorate the PD and M_R performance (compared to samples without additional water) of test samples. This is despite the fact that all these samples have higher dry density conditions. Although samples of type B and C were dried to the same point as type A samples, PD values were reduced but were still higher or equivalent to those of type

A. The M_R of type B and C samples might be improved in order to be comparable to that of type A at the same moisture content. Hence the dryback process shows the potential for improving material performance, depending on the amount of additional water. Adding higher amounts of water, even up to the OMC of HCTCRB, resulted in a more defective performance, although this can induce a higher dry density. This effect indicates that HCTCRB is still affected by a range of moisture contents. Based on the findings of this study, it should be noted that in the field, adding water to the material in order to increase workability in compaction may result in an adverse performance of the HCTCRB.

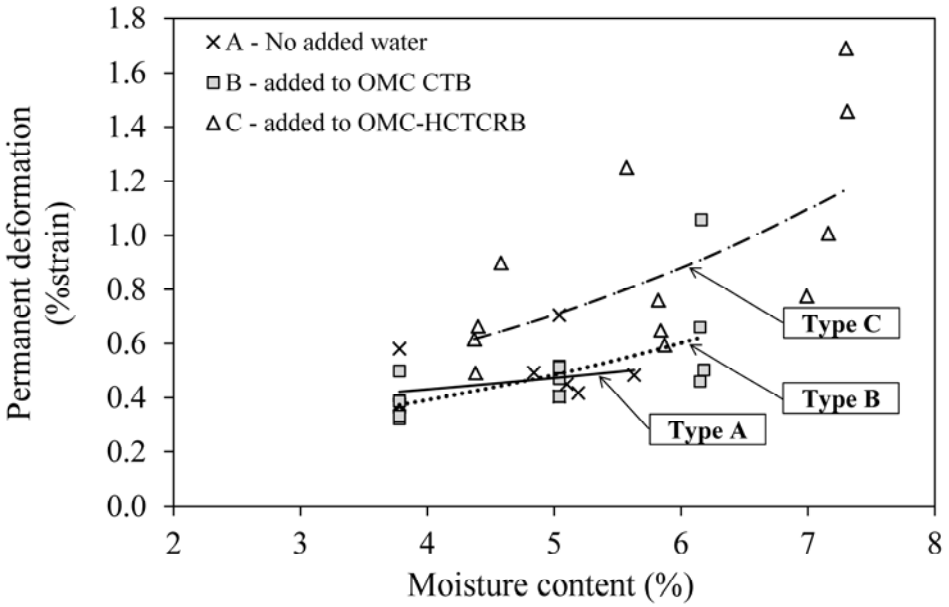

Figure 5.23: PD of HCTCRB samples at 7, 14, 28 and 45-day hydration periods with variations in moisture content

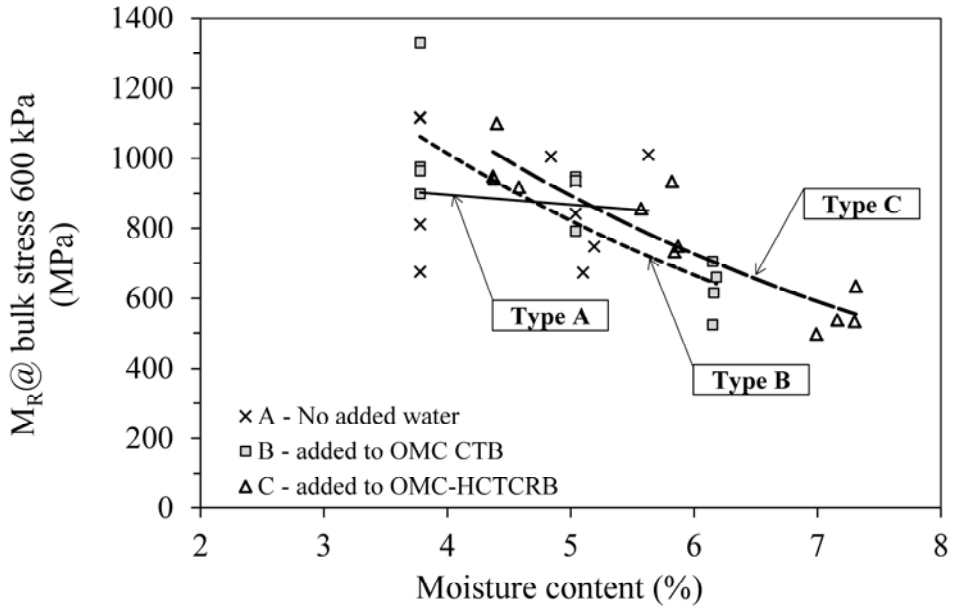

Figure 5.24: M_R of HCTCRB samples at 7, 14, 28 and 45-day hydration periods with variations in moisture content

5.4 Summary

HCTCRB exhibited stress-dependency behaviour under the RLT tests. In general, the deviator and confining stresses considerably affected the resilient responses of the materials, as increases in the applied stresses resulted in higher M_R values but lower incremental rates of M_R. At a constant confining pressure, the M_R increased with an increase in deviator stress. However, the incremental rates decreased at higher levels of confinements. Similarly, at a constant deviator stress, the M_R climbed with higher confining stresses but the rates of increase were less pronounced at higher deviator stresses.

UCS, PD and M_R results for HCTCRB made with 1%, 2% and 3% cement indicates that the 2% cement samples were the strongest. The 3% cement samples performed the least well, despite possessing the greatest cement content of the three samples. This occurrence was a consequence of higher water consumption during the hydration reaction which resulted in a drier material. Thus the material could not be compacted effectively due to insufficient water which is required to lubricate the material grains during compaction. The other two samples (1% and 2% cement

content) contained a suitable amount of water and were able to be compacted, which made them more effective specimens than those with 3% cement content.

Performance evaluation of HCTCRB in terms of M_R and PD was carried out under various conditions including hydration periods, water addition during compaction, and dryback. All these factors significantly affected HCTCRB performance. However, a consistent performance trend with regard to the hydration period could not be found. Higher amounts of water added during compaction generally caused a decrease in PD and M_R performance (compared to samples without the addition of water). Even though the samples had higher dry densities they did not show effective performance after curing. After all test samples were subjected to the dryback process, performance assessments were made and compared to sample performance with no dryback and with the same water content. It was found that the M_R of type B and C samples was almost equivalent to those found in type A, while the PD values of type B and C samples were higher than or equivalent to those of type A. It should be noted, that based on the results of this study, HCTCRB still has some degree of moisture sensitivity, and this must be taken into account for effective use of this material.

CHAPTER 6
UNSATURATED SOILS AND MATRIC SUCTION FOR UNBOUND GRANULAR MATERIALS

The repeated load triaxial test (RLT test), when performed in accordance with Austroads standard test method AG: PT/T053 does not incorporate the unsaturated soil concept or suction measurement. However, in today's pavement engineering environment, the evaluation of the resilient response of pavement materials under traffic loading, in combination with the effects of suction, has become an important research area. Despite this, suction measurements taken in laboratories or in the field require additional sophisticated tests and equipment. The motivation for this chapter is to overcome the difficulties with the suction measurement of Crushed Rock Base (CRB), being the main material of HCTCRB which has been used throughout this study. It has been found that suction plays a significant role in the overall performance of CRB as a basecourse material. This chapter demonstrates a new mechanistic framework which combines the unsaturated characteristics of unbound granular materials into the cyclic response. The proposed method still performs the typical standard tests, such as the static triaxial tests, as well as the RLT tests, although the RLT test is performed without matric suction measurement. The inclusion of suction measurement into the resilient response of materials is obtained by integrating the relationships derived from unsaturated soil theory into the analysis of both static traixial test and RLT test results. The framework was validated using laboratory test data from CRB, a typical basecourse material conforming to the specification of Main Roads Western Australia (2010b).

6.1 General background

Unbound granular materials (UGMs), as basecourse layers in multi-layered pavement structures, tend to be in an unsaturated condition. At the construction stage, particles of UGMs are lubricated with water, under compaction conditions. The aim is to achieve the desired material density believed to provide durability in pavements. The amount of water added in the compaction process cannot practically elevate compacted UGMs up to a fully saturated condition, which is the condition familiar to most geotechnical engineers. The behaviour of soils under completely dry

or completely saturated conditions is fairly well studied and understood. However, the understanding of unsaturated soils, particularly unsaturated unbound granular materials (UUGMs), is not as advanced in comparison to that of saturated soils and unsaturated cohesive soils. With pore fluid in granular pavement materials; usually seen in terms of a two-phase system containing both water and air, (although other geotechnical engineering applications could include other gases or liquids), water and air contents have been shown to have a major effect on granular pavement material response. However, the attempts to quantify this effect have mainly been made through empirical methods (Theyse 2000), and more advanced works based on unsaturated soil concepts (Heath et al. 2004; Khoury and Zaman 2004; Ekblad and Isacsson 2007; Theyse et al. 2007; Sawangsuriya et al. 2009; Cary and Zapata 2011).

In modern unsaturated soil mechanics, the suction in a soil pore matrix is significant to the overall performance of soils under unsaturated conditions. Modern unsaturated soil mechanics only emphasises the seeking of an explanation of unsaturated soils under natural conditions. However, there is no single theory or body of knowledge which comprehensively explains the complex behaviour of pavement base materials (i.e., materials in the base and subbase layers) which are all under compacted *and* unsaturated conditions. (Kodikara 2006) presented a new framework for modelling the volumetric response of unsaturated soils, with an emphasis on compacted and unsaturated soils. However, it is still an ongoing study requiring more practical refinements for use in the geotechnical engineering field, and as yet it cannot be implemented into the authoritative literature on unsaturated conditions in pavements. With regard to existing knowledge of modern unsaturated soil mechanics, when characterising material it is essential to consider the unsaturated behaviour of pavement base materials. This is particularly the case in Australia, where no unsaturated soil concept is used in pavement design and analysis.

In Australia, ever-increasing levels of road freight, and the demand for increased payloads are not only impacting upon axle loads and tyre pressures but they are also having a detrimental effect upon road networks. The performance of granular pavements with thin asphalt surfaces (i.e., the normal pavement type used Australia-wide) has declined dramatically, as evidenced by an increased incidence of rutting, roughness, and flushing (Harris and Lockwood 2009). This puts into question the

reliability of many of Australia's ageing flexible granular pavements (Austroads 2007b). Consequently, Austroads (2007a) has introduced more sophisticated material characterisation methods through the RLT test. The test assists in identifying granular pavement materials (i.e., materials for base and subbase) of suitable engineering and mechanical parameters for effective performance and workability as granular pavements. Information from the RLT test may also be used by manufacturers of unbound granular materials to design a product to meet Austroads' requirements (Austroads 2007b). Despite the above measures, the unsaturated condition of pavement material is still not considered in pavement material analysis and design in Australia. A new pavement analysis method (Austroads 2012a) was recently introduced which relies on more sophisticated procedures of finite element analysis. However, it is still not included in the effects of unsaturated soil phenomena when considering the cyclic behaviour of aggregate base and subbase materials. Cyclic behaviour analysis is undertaken to determine suitable values of input parameters (i.e., resilient moduli of pavement base and subbase materials) for pavement analysis (Austroads 2010c).

This study aims to present a new mechanistic framework which includes the response of UUGMs in RLT test procedures with no suction measurement. The proposed framework can be applied in conjunction with an effective stress concept and a resilient response model of unsaturated soils to determine the cyclic response of UUGMs with a range of water contents under typical field loading conditions. The framework was validated using laboratory test data from standard CRB conformed to Main Roads Western Australia (2010b).

6.2 Water conditions in pavements

Water conditions in pavements can be ideally modelled as shown in Figure 6.1 (Kodikara 2006). There is usually a variation in the amount of water in pavements due to the compaction process. At the compaction stage, the initial water content (w_i), which is usually close to the optimum moisture content (OMC) (e.g., 95% or 98% of OMC), is derived from standard or modified compaction tests. In Australia, the practical construction standards of road and highway pavements usually require the drying back of the basecourse layer prior to the asphalt sealing process. The

dryback process aims to provide a more effective pavement performance. Due to environmental conditions, variable water content will be lost over time until reaching equilibrium (w_{eq}). In addition, there is the major influence of seasonal changes together with the side effects resulting from various pavement characteristics and configurations. This produces surface water infiltration, vapour movement, water intrusion, and an elevated pavement through the wetting and drying processes after w_{eq} is reached.

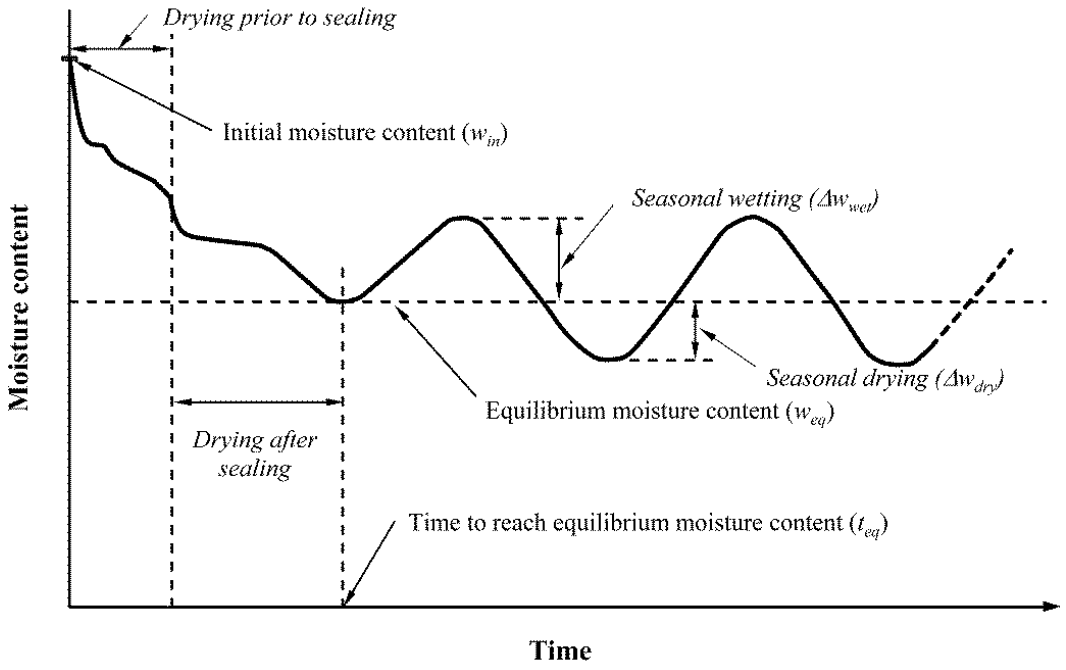

Figure 6.1: Idealised visualisation of water fluctuation in pavements (Kodikara 2006)

Most testing protocols for pavement materials generally evaluate the material properties at the construction condition stage (i.e., after the compaction process). However, they do not allow for the adjustment of pavement materials in service or after construction, when their properties can alter from their initial state, due mainly to changes in the water content of the pavement. When characterising pavement material responses in pavement design and analysis, water fluctuation phenomena in pavements has no standard or laboratory testing protocol which takes this into account. The proposed framework in this paper aims to overcome this shortcoming.

The amount of water in soils and pavement materials can be defined by the degree of saturation (S_w) which can be expressed as;

$$S_w = \frac{wG_s}{e} : 0 \ll S_w \ll 1 \quad (6.1)$$

where w = the gravimetric water content; e = the void ratio, and Gs = the specific gravity of the soil.

Usually, the gravimetric water contents of UUGMs are less than 10% by mass of the dry unit weight (γd) of UUGMs, typically between 2.0 - 2.4 times that of water (Heath et al. 2004). The compaction characteristics of UUGMs can be represented in a series of compaction tests as compaction curves, with a maximum dry density and an optimum water content, of which the saturation curves based on the G_s of a material, can be included.

6.3 The stress concept for unsaturated soils

Total suction in soils is a combination of matric suction and osmotic suction. Matric suction is the attracting force which is the product of capillary force and surface tension in soil pores. Osmotic suction is generated by the presence of soluble salt in pore water (Liang et al. 2008). Osmotic suction is negligible in terms of impact, as changes across a range of moisture contents are slight. Hence, it is reasonable to omit the osmotic component and present only the matric suction measurements of the soil (Fredlund 1979).

$$\psi = (u_a - u_w) + \pi \quad (6.2)$$

where ψ = total suction, u_a - u_w = matric suction, u_a = pore air pressure, u_w = pore water pressure, and π = osmotic suction.

The shear strength in soils is generally defined using the Mohr-Coulomb failure criteria, as shown in Eq. 6.3. For saturated soils, the total normal stress is a summation of the effective stress and pore water pressure. The effective stress of saturated soils is presented as Eq. 6.4.

$$\tau = c' + \sigma' \tan \emptyset' \quad (6.3)$$

$$\sigma' = \sigma - u_a \quad (6.4)$$

where τ = the shear stress, c'= the effective cohesion, σ = the total normal stress, σ' = the effective stress, ϕ'= the effective internal friction angle.

Matric suction is incorporated in order to determine the shear strength of unsaturated soils. Two main approaches are now widely accepted and used by geotechnical engineers i.e., the effective stress approach (Bishop 1959), and the independent state variable approach (Fredlund 1979).

The originally proposed effective stress approach, in which the shear strength is evaluated on both the basic effective shear strength parameters of c' and ϕ' is defined as:

$$\sigma' = (\sigma - u_a) + \chi(u_a - u_w) \quad (6.5)$$

$$\tau = c' + [(\sigma - u_a) + \chi(u_a - u_w)] \tan \emptyset' \quad (6.6)$$

where χ is the effective stress parameter (i.e., the Bishop parameter) which has values ranging from 0 for dry soils to 1 for fully saturated soils.

The independent state variable approach is described in a mathematical equation in which the shear strength of unsaturated soil can be evaluated as follows:

$$\tau = c' + (\sigma - u_a) \tan \emptyset' + (u_a - u_w) \, tan \, \emptyset^b \quad (6.7)$$

where $\emptyset^b$ = the internal friction angle with respect to the matric suction, $(u_a - u_w)$.

The framework development in this study is presented as an effective solution to determining the stress of unsaturated soils (i.e., UUGMs) with the added

consideration of soil suction. Based on the literature reviews, the independent state variable approach (see Eq. 6.7), requires extensive and time consuming laboratory testing to determine all material parameters. The equipment needed for this purpose is generally sophisticated and is virtually unavailable in general geotechnical engineering laboratories. In addition, the level of expertise required for determining $\emptyset^b$ is not usually found in most laboratories (Khalili and Khabbaz 1998). Furthermore, the unsaturated soil theory has only recently been introduced into the field of pavement engineering. Therefore, the lack of expertise for dealing with sophisticated testing and analysing of test results is a significant barrier to bringing the unsaturated soil concept into the characterisation of pavement materials. For the original effective stress approach (see Eq. 6.5), there are some concepts for developing the framework in this study. The advantage of the effective stress approach is that changes in shear strength, along with changes in total stress, pore water pressure, and pore air pressure relate to a single stress variable (σ'). This variable matches with a single stress history of the normal characterisation of the soil strength, unlike the independent state variable approach which requires more than one variable (Khalili and Khabbaz 1998). Above all, the effective stress approach requires quite limited testing of soils in unsaturated states. The main difficulty of the effective stress approach is the determination of χ, as there is no generally reliable method to determine the values of χ, particularly at very low saturation. However, this is of little consequence to the modelling of UUGMs as these low saturation levels are unlikely to be encountered in real pavement conditions (Heath et al. 2004). Furthermore, it should be noted that the effective stress concept is a macroscopic concept and cannot be proven or disproven by using a theoretical model expressed at a microscopic level (Khalili and Khabbaz 1998). Consequently, this study relies upon the effective stress approach (Eq. 6.5) used in the framework development.

6.4 Soil suction of UUGMs in pavements

In unsaturated soil mechanics, matric suction, which is the difference between air and water pressure in soil pores, plays a main role in the overall performance of unsaturated soils. The relationship between the matric suction and the degree of saturation in soils is often referred to as the soil water characteristic curve (SWCC). The SWCC has become pivotal to the implementation of unsaturated soil mechanics

into geotechnical engineering practice (Fredlund et al. 2011). An example of the SWCC as it occurs in varied soil types is illustrated in Figure 6.2. It can be clearly seen that the SWCC is highly dependent on soil types as well as their states. Furthermore, fine-grained soils (e.g., clays) can generally sustain a higher matric suction than coarser-grained soils with the same moisture content (see Figure 6.2); and loose clays can undergo large volumetric changes as a result of changes in soil suction (i.e., changes in water content) and net stresses. The SWCC can thus be represented as being dependent on void ratio or stress states (e.g. Jotisankasa et al. 2009). This wide variation can be problematic for geotechnical engineering practice in the field.

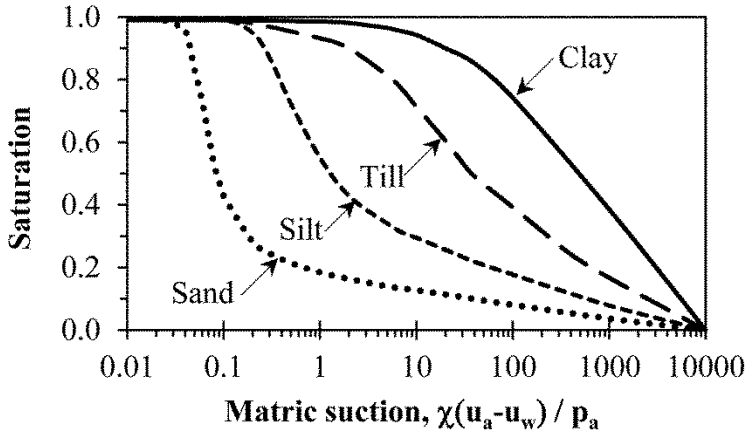

Figure 6.2: Soil-Water Characteristic Curve (SWCC) of different soil types (Vanapalli et al. 1999)

Practically, most geotechnical engineers have generally been of the opinion that coarse-grained soils or UUGMs have quite low soil suction (i.e., matric suction) and that the suction is not significant enough to affect the overall performance of unsaturated coarse-grained soils. In addition, in the case of UUGMs, they are generally well-compacted and do not have a large fines content, and this would therefore result in very small volumetric strains from changes in the water contents. This is why the suction in coarse-grained soils is often ignored in geotechnical engineering and in practical road and highway design and analysis in particular.

The performance of pavement materials is largely dependent on their moisture content. Moisture ingress to the pavement caused by infiltration through the road surface and shoulders, seepage from side slopes and high ground back slopes to the

road pavement, and fluctuations in the water table level. Changes in moisture or temperature within pavement or environment cause the moisture transfer within pavement by suction, and evaporate or absorb water between pavement and environment (Austroads 2010c). Movement of moisture in pavements and environment are illustrated in Figure 6.3. Pavement materials are usually constructed at the optimum moisture content which is below the saturation state. Then it is attempted to retain the unsaturated condition in order to maintain the strength and stiffness of materials throughout the services life. Thus pavement structures are normally constructed above the water table and drainage system is assigned to avoid excessive water infill to the pavement. Harris and Lockwood (2009) reported that the moisture content of various basecourse materials during rainy season (June) ranged from about 40 % to 90 of their OMC which are still below the saturated condition. Walker (1997) found significant suctions developed in compacted base materials.

Therefore, from a modern pavement engineering viewpoint, one cannot ignore soil suction in conventional pavement engineering practice, particularly with regard to the near-pavement surface where confining stresses are low, and a high degree of hysteresis is present in the SWCC between the wetting and drying cycles. This is particularly true of the thin asphalt surface pavement network in Australia. The statement "soil suction still influences the behaviour of coarse-grained pavement material" can be very easily supported by Figure 6.4 showing a compacted CRB sample (i.e., the basecourse material used in this study) after extrusion from the compaction mould. In Figure 6.4, the compacted CRB sample, without any confining pressure, can stand and does not disintegrate from the compaction condition at its OMC with the applied suction of 65 kPa, determined from the filter paper water content method (Cameron et al. 2011). Figure 6.4 also easily proves that the suction element in compacted pavement materials is still significant to UUGMs and it cannot be neglected.

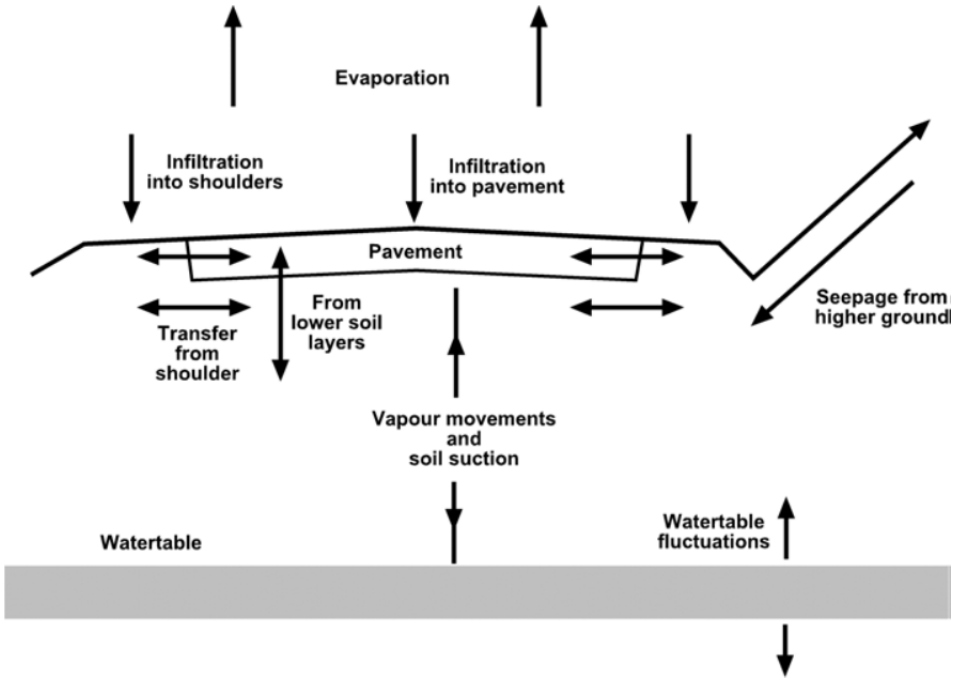

Figure 6.3: Moisture movements in road pavements (Austroads 2010c)

Figure 6.4: The compacted CRB sample after extrusion from a compaction mould

6.5 Normalisation of cyclic response of UUGMs and matric suction

6.5.1 Cyclic response of UUGMs

The cyclic response of pavement materials (e.g., unbound granular basecourse and UUGMs) is usually characterised through the resilient modulus, M_R (see Eq. 6.8) which is also a fundamental parameter in flexible pavement design (Cary and Zapata 2011). Resilient modulus characteristics are inherently complex and depend on different factors such as stress conditions, moisture content, densities, the number of loading repetitions, compaction energy inputs, and soil thixotropy (Seed et al. 1962). During the development of modern pavement engineering over the last few decades, several predictive models of M_R have been developed in an attempt to incorporate the effects of the aforementioned factors into the M_R estimation.

$$M_R = \frac{\sigma_d}{\varepsilon_r} \tag{6.8}$$

where M_R is the resilient modulus, σ_d is the repeated deviator stress (cyclic stress in excess of confining pressure), and ε_r is the resilient (recoverable) strain in a vertical direction.

To date, most modern pavement design and analysis methods have emphasised and demonstrated the importance of the effects of moisture content (i.e., one environmental factor). These effects can lead to a significant change in the resilient modulus of an unbound granular base material where there is a fluctuation in material moisture contents resulting from the environment during the pavement's design life. Most resilient modulus predictive models that have been proposed only account for variations in stress conditions (Austroads 2012a). However, these models rely on an overall stress analysis, i.e., there is no consideration of the effective stress concept and no accounting for the resilient modulus response from the perspective of unsaturated soil mechanics. This is despite the fact that pavement base materials are in an unsaturated condition in nature. As for the unsaturated condition of normal pavement bases, it has been recognised that the variation in stress state conditions in pavement due to seasonal changes can be related to changes in matric suction; a fundamental variable of the stress state in unsaturated soils. Based on this reason,

there have been several studies demonstrating the strong relationship between the resilient modulus and matric suction (Khoury and Zaman 2004; Theyse et al. 2007; Sawangsuriya et al. 2009; Cary and Zapata 2011). Consequently, over the last few decades, resilient modulus predictive models which consider soil suction as part of the predictive parameters have been proposed (Fredlund et al. 1977; Parreira and Goncalves 2000; Yang et al. 2005; Liang et al. 2008). However, all of them require suction parameters (e.g., matric suction measures) which are generally obtained from the suction measurements taken in laboratories or in the field. Due to the inherent difficulties of suction measurement, resilient modulus predictive models with these suction parameters are not very practical and have as yet, not led to any implementation in Australia.

In 2012, Austroads; the association of Australian and New Zealand road transport and traffic, released new models demonstrating developments in pavement design; the aim being to obtain a more effective representation of granular behaviour in pavement response. A finite element program, namely APADS, was developed, which integrates the nonlinear behaviour of granular materials (Austroads 2012a). The predictive resilient modulus model, or so-called "universal model" (Witczak and Uzan 1988) presented in Eq. 6.9, adopted among the classical resilient modulus predictive modulus models (Dunlap 1963; Brown and Pell 1967; Monismith et al. 1967; Hicks 1970; Boyce 1980; Johnson et al. 1986; Nataatmadja and Parkin 1989; Nataatmadja 1992), has been investigated by (Austroads 2010c, 2012a). This was done in order to take into account the effect of both confining and shear stresses on the unbound granular material resilient modulus, as (Austroads 2012a) believed that the application of the universal model would be the most compatible with regard to Australian pavement base materials. These developments have led to this study, which also uses the universal model for the resilient modulus estimation.

$$M_R = k_1 \left[\frac{\theta}{p_a}\right]^{k_2} \left[\frac{\tau_{oct}}{p_a}\right]^{k_3} \tag{6.9}$$

where θ = the mean normal stress $\frac{\sigma_1+\sigma_2+\sigma_3}{3}$; τ_{oct} = the octahedral shear stress = $\frac{\sqrt{2}}{3}\sigma_d$ for standard triaxial compression loading; where σ_d is the deviator stress); p_a = atmospheric pressure, and k_1, k_2, k_3 = the regression model (material) parameters.

However, Eq. 6.9 does not consider the unsaturated condition of base and subbase materials with regard to Austroads pavement design and analysis (Austroads 2010c). As mentioned previously, for Australian pavement design, the matric suction (u_a-u_w) should be incorporated into a more rational resilient modulus predictive model. There is a significant need to modify the universal model (Eq. 6.9) so that it includes matric suction as one of the predictive variables. The effective stress approach (Bishop 1959), as presented in Eq. 6.5, was used to incorporate the matric suction into the universal model. Consequently, Eq. 6.9 can be rearranged to take matric suction into account in the resilient modulus estimation as follows:

$$M_R = k_1 \left[\frac{\theta + \chi(u_a - u_w)}{p_a}\right]^{k_2} \left[\frac{\tau_{oct}}{p_a}\right]^{k_3} \quad (6.10)$$

6.5.2 SWCC and $\chi(u_a\text{-}u_w)$ model for UUGMs

The soil water characteristic curve (SWCC) which is used extensively for unsaturated soil property function estimation is proposed for virtually every physical process where soils become unsaturated (Fredlund et al. 1977; van-Genuchten 1980; Fredlund 1995, 2000; Fredlund and Pham 2006). Furthermore, the SWCC is also widely used for the estimation of in-situ soil suction. To overcome the difficulty of soil suction measurement as found in common geotechnical and pavement laboratories, the development of the framework in this study used selected SWCCs for UUGMs from the proposed empirical equations used to describe the SWCCs of soils (Sillers et al. 2001). Some of the commonly used SWCC equations, along with more recent SWCC equations developed within the geotechnical engineering discipline have been presented in various literatures (Gardner 1958; Brooks and Corey 1964; Brutsaert 1966; McKee and Bumb 1987; Fredlund and Xing 1994; Pereira and Fredlund 2000; Fredlund and Pham 2006; Fredlund et al. 2011).

Based on previous studies into SWCC- related unbound granular materials (Fredlund 2002; Gitirana and Fredlund 2004; Heath et al. 2004; Ekblad and Isacsson 2007), the van Genuchten equation (van-Genuchten 1980), one of the most commonly used SWCC equations, was selected for this study as the SWCC empirical equation to

initially determine the matric suction of UUGMs with a given amount of water content. The van Genuchten equation can be rearranged to solve the issue of soil matric suction in terms of the gravimetric water content as follows:

$$u_a - u_w = \frac{1}{a}\left[\left(\frac{w_s}{w}\right)^{\frac{1}{m}} - 1\right]^{\frac{1}{n}} \quad (6.11)$$

If the three fitting parameters, a, m, and n for the van Genuchten equation are known, along with the saturated gravimetric water content, w_s, the soil matric suction (u_a - u_w) can be calculated. The use of this equation is limited to the range between the air-entry value and the residual suction of a soil because of the asymptotic nature of the equation (Fredlund et al. 2011) and the over-prediction of suction as a drying condition (i.e., the saturation approaches zero (Heath et al. 2004)). However, the van Genuchten equation is still practical with regard to the mechanical behaviour of UUGMs usually being within a range of quite narrow suction values. It is also able to account for a small gap in the change in water content due to pavement field conditions.

However, there has been debate about the SWCC of coarse granular materials used extensively in road construction, in terms of whether the SWCC can be effectively used to describe such unsaturated coarse granular media. Among the relatively rare studies on the unsaturated behaviour of coarse granular materials, Ekblad and Isacsson (2007) proposed the work described in this study, and determined the SWCC for coarse (maximum particle size 90 mm) granular materials having various gradations, by using the relationship of the relative apparent permittivity measured through time-domain reflectomery (TDR) and volumetric water content, along with the concurrent matric suction which was measured with a tensiometer. Based on the Ekblad and Isacsson (2007) study, a series of SWCCs was constructed from the measurements which were taken simultaneously with the TDR calibrations. Matric suction was monitored until a stable condition was reached. The water content was increased in steps, each increase resulting in a reduction in matric suction. The test results were then fitted to the SWCC models of Brooks and Corey (1964) and van-Genuchten (1980), the van Genuchten model showed a closer correlation to all

measured values. A unified predictive equation (Ekblad and Isacsson 2007) was then formulated, following the highest correlation for each parameter of the van Genuchten model, with soil parameters as follows:

$$\theta_v = \left(\frac{1}{1+[a(lnP_f)\psi]^{n(D_{10})}}\right)^{(1-\frac{1}{n(D_{10})})} \times [\theta_s - \theta_r(P_f)] + \theta_r(P_f) \quad (6.12)$$

where θ_v = the volumetric water content; a and n = two out of the three fitting parameters of a, m, and n for the van Genuchten equation, whereas (m=1-1/n); ψ = the matric suction = u_a - u_w; θ_s = the volumetric water content at saturation; θ_r = the residual volumetric moisture content; P_f = the amount of fines for the van Genuchten model; and D_{10} = the nominal sieve size through which 10% of the material is passing.

To overcome the difficulty in dealing with the complexity of Eq. 6.12, and the unfamiliarity of the volumetric water content terms, a unified predictive equation of SWCC expressed in Eq. 6.12 was rearranged to solve the matric suction issue in terms of water content:

$$u_a - u_w = \frac{1}{a(lnP_f)} \times \left[\left(\frac{w_s-1}{w-1}\right)^{\frac{1}{m}} - 1\right]^{\frac{1}{n(D_{10})}} \quad (6.13)$$

where w = the gravimetric water content; w_s = the water content in the saturation condition; and a, m, n, P_f and D_{10} are the same as the definitions given in Eq. 6.12.

From Eq. 6.13, the terms of $\chi(u_a - u_w)$ can be obtained by multiplying χ with Eq. 6.13 and applying the assumption that $\chi = S = \frac{w\, G_s}{e}$; where χ = Bishop's parameter, G_s = soil-specific gravity and e = the void ratio at a particular density. Eq. 6.13 becomes:

$$\chi(u_a - u_w) = \left(\frac{w\, G_s}{e}\right) \times \frac{1}{a(\ln P_f)} \times \left[\left(\frac{w_s-1}{w-1}\right)^{\frac{1}{m}} - 1\right]^{\frac{1}{n(D_{10})}} \quad (6.14)$$

Based on Eq. 6.14, it can be clearly seen that $\chi(u_a - u_w)$ is the effective suction confinement, which is required to determine the effective stress in an unsaturated soil (see Eq. 6.5). $\chi(u_a - u_w)$ can be obtained through the inputs taken from the soil's physical properties (e.g., w, w_s, e, G_s, P_f, and D_{10}) and the three fitting parameters of the van Genuchten model (e.g., a, m, and n). The real matric suction measurements, required for constructing the real SWCC of unsaturated soils, are not needed. Note that there is no requirement for a back calculation to determine the χ values, which would require complex and sophisticated laboratory tests (e.g., triaxial tests and direct shear tests with suction measurements).

The modified predictive resilient modulus model with $\chi(u_a - u_w)$, is presented in Eq. 6.10. The newly proposed model of $\chi(u_a - u_w)$, or the effective suction confinement, derived from the classical SWCC empirical equation of the modified van Genuchten model (Ekblad and Isacsson 2007), is presented in Eq. 6.14. These equations were used as a basis for the development of the mechanical framework. Through this, the resilient modulus of the unsaturated coarse granular pavement base material without suction measurement may be determined.

6.6 Experimental works

In this study, laboratory works were required to carry out investigations into the normalisation of the unsaturated response of UUGMs under cyclic loading condition. The repeated load triaxial tests, in conjunction with the static drained (i.e., air and water) triaxial compression tests, were performed to characterise the cyclic behaviour of UUGMs without suction measurement. In order to overcome the involvement of suction measurement, test samples of a particular target density (i.e., 98% MDD based on normal specifications for compaction tests for road and highway construction) were prepared, with variations in the moisture content. A targeted range of test sample moisture contents can be determined from the characteristics of water in pavements (see Figure 6.1). This ensures that the moisture contents of the test samples are in-between the initial water content (w_i), which is usually close to the optimum moisture content for compaction, and an equilibrium water content (w_{eq}), point, at which the condition of the moisture in the pavement is relatively constant. In this study, the information from a pavement trial investigation by Main

Roads Western Australia (Harris and Lockwood 2009) was used to target such a range of test sample moisture contents. As the results of this pavement trial show, the moisture range in the pavement trial was approximately 95% OMC for w_i and 60% OMC for w_{eq} in a basecourse layer. Consequently, within this study, test samples were compacted at 95% OMC to achieve a target density of 98% MDD, followed by two drier conditions of 80% OMC and 60% OMC, which were set up and performed using the dryback process. The dryback process is used to dry out the samples after compaction, up to a certain amount of moisture content, with the main purpose of maximising pavement service life. The intention is also to improve the performance of asphalt surfacing by allowing satisfactory penetration of a primer binder into the pavement surface (Australian Road Research Board 2003). The test sample preparation, with three different levels of moisture content of the same target densities as those of the dryback process, was deemed an appropriate sample preparation procedure. The aim was to avoid uncertainties during the compaction process, and to replicate the drying-out phenomena of a pavement base material in pavements, which is generally drier up to the point of equilibrium in moisture content, with one compaction at construction stage.

Figure 6.5 shows a modified compaction curve of CRB in accordance with the standard test method (Main Roads Western Australia 2012b). Figure 6.5 also illustrates the water content of 5.8% OMC with 2.4 ton/m^3 of the MDD with 2.87 of the G_s of CRB.

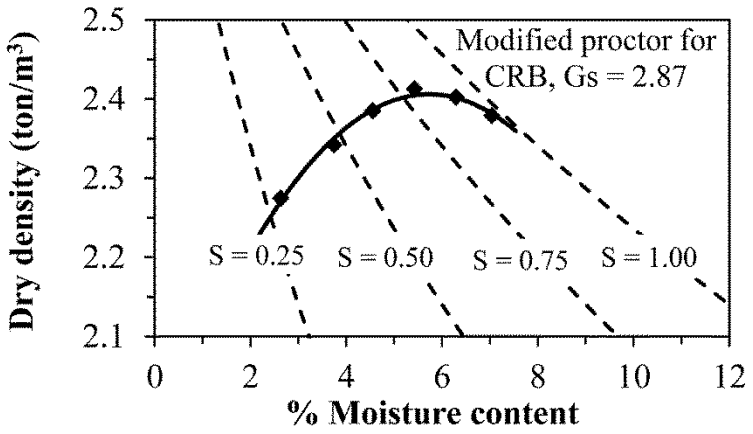

Figure 6.5: Modified compaction curve of CRB with saturation curves

6.6.1 Static triaxial tests

Static drained triaxial compression tests were conducted in conjunction with RLT tests in order to normalise the unsaturated response of the UUGM (i.e., CRB) to its cyclic behaviour. It can be seen from Eq. 6.10 that $\chi(u_a - u_w)$, or the effective suction confinement, is required as a key variable to determine the resilient modulus model. The results from a series of static drained triaxial compression tests can lead to the determination of an $\chi(u_a - u_w)$ value for the water content of a given soil with no real suction measurement. Heath et al. (2004) proposed a method to determine $\chi(u_a - u_w)$ from the results of a series of static triaxial tests. This method is based on the effective friction angle (ϕ') determined from the Mohr-Coulomb failure envelope and the corresponding values of the deviator stresses at failure (q_{max}) associated with the effective stress in an unsaturated soil concept (Bishop 1959). By assuming $\phi = \phi'$, the value of $\chi(u_a - u_w)$ at a given amount of moisture content can be determined by using Eqs. 6.15, 6.16 and 6.17 as follows:

$$\emptyset' = \emptyset \tag{6.15}$$

$$\sin \emptyset' = \frac{q_{max}}{2\sigma_3' + q_{max}} \tag{6.16}$$

$$\sigma_3' = \sigma_3 + \chi(u_a - u_w) \tag{6.17}$$

Figure 6.6, taken from Heath et al. (2004), illustrates an example of the results from static drained triaxial compression tests in terms of the Mohr-Coulomb failure envelope and the constant friction angle (ϕ). It can be seen from Figure 6.6, that the Mohr-Coulomb failure envelopes depend upon the test sample densities (i.e., the void ratios of 0.241 and 0.179). It can also be observed that the differing moisture content (i.e., 3% and 5%) of the test samples that have the same density does not affect the Mohr-Coulomb failure envelopes (i.e., all test results are in line with each other in the same failure envelope). This shows why, in this study, test samples were prepared with three moisture content levels at one given density to obtain the Mohr-Coulomb failure envelope with a friction angle (ϕ).

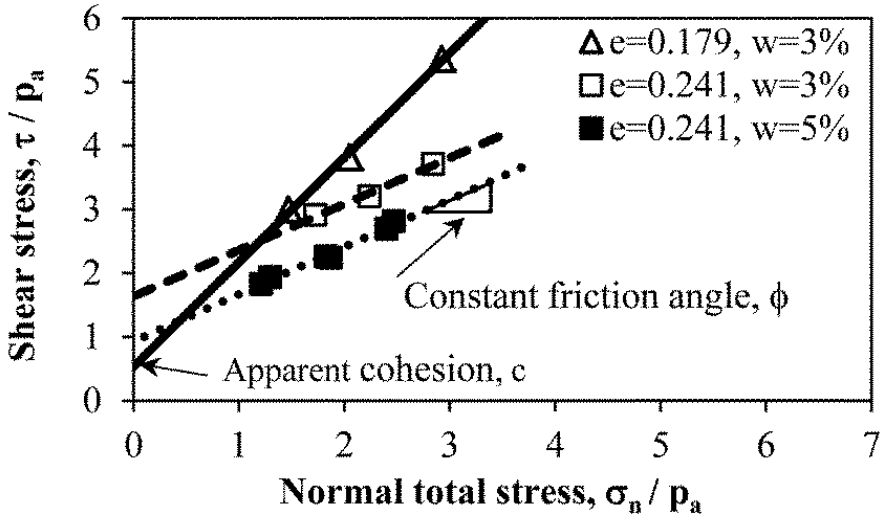

Figure 6.6: Mohr-Coulomb failure envelopes from drained triaxial compression tests (Heath et al. 2004)

In the study, the drained triaxial compression tests, with no suction measurement taken during the tests, were performed for test samples at the target dry density of 98% MDD, with moisture content varying from 95% down to 80% and 60% of OMCs. All CRB samples were compacted at 95% OMC and 98% MDD. For each test sample, the material was compacted in a standard mould, of 100 mm in diameter and 200 mm in height, with eight even layers. Modified compaction was achieved with 25 blows of a 4.9 kg rammer from a drop (height) of 450 mm onto each layer. The test samples for 80% and 60% OMC were achieved by using the drying process (i.e., dryback) for the compacted samples in a controlled chamber of 50% relative humidity at 23°C until the required moisture of 80% and 60% OMC was reached. The material responses were determined from the corresponding deviator stresses at failure through a set of three constant confining pressures at 35 kPa, 70 kPa and 100 kPa.

Figure 6.7 and Figure 6.8 show the stress-strain relationships in the test samples at 60%, 80%, and 95% of OMC and at 35 kPa, 70 kPa, and 100 kPa confining pressure levels. Mohr's circles and the Mohr–Coulomb failure envelope for these static triaxial tests are illustrated in Figure 6.9. The results show that the envelope corresponding to the peak stresses at failure is linear for the given confining pressure range (i.e., from 35 kPa to 100 kPa). Thus the appropriate envelopes correspond to the shear strength parameters of the friction angle (ϕ) of 55˚ and the cohesion (c) of 99 kPa.

From the static triaxial test results, if it is assumed that the matric suction of UUGMs is relatively low in comparison with that of clayey soils, then the assumption can be made that the total friction angle (ϕ)does not differ greatly from the effective friction angle (ϕ′), or approximately Ø=Ø' for the analysis of this framework. When Ø=Ø'=55° and the corresponding values of the deviator stresses are at failure (q_{max}) and the confining pressures (σ3) of 35 kPa, 70 kPa and 100 kPa (see Figure 6.8) are substituted in Eqs. 6.15 – 6.17, a set of static triaxial test results may be obtained as shown in Table 6.1.

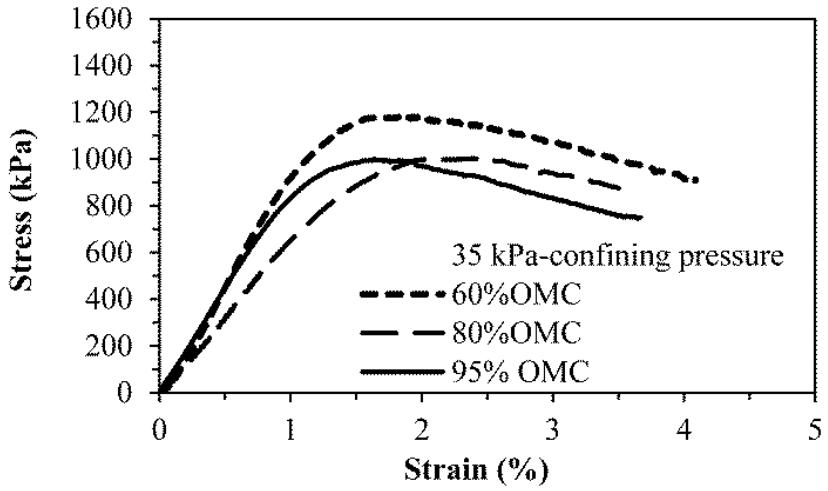

Figure 6.7: Stress-strain curves for CRB with moisture content varying from 60%-95% OMC at confining pressure 35 kPa

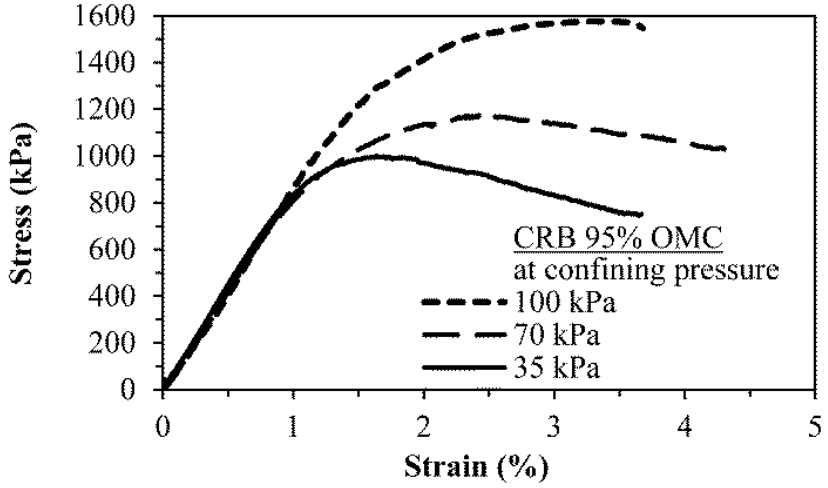

Figure 6.8: Stress-strain curves for CRB at 95% OMC and confining pressure range of 35-100 kPa

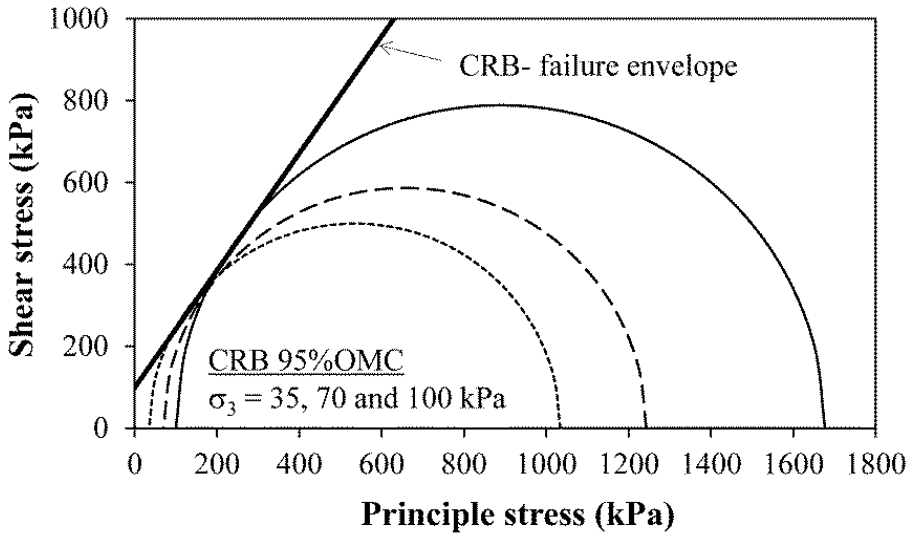

Figure 6.9: Mohr's circles and the Mohr–Coulomb failure envelope for CRB at 95% OMC moisture content and 98% MDD

6.6.2 Repeated load triaxial tests

The resilient modulus was investigated through repeated load triaxial tests (RLTT), in accordance with Austroads standard test method AG:PT/T053 (Austroads 2007a), as detailed in section 5.1. The tests were performed under drained conditions and suction measurement was not taken.

The test specimen sizes of 100 mm in diameter and 200 mm in height were also prepared in a similar manner to the samples for the static triaxial test. The test was performed on specimens at the target dry density of 98% MDD with moisture contents varying from 95% down to 80% and 60% of the OMC. The resilient modulus test results are presented in Figure 6.10 in which they illustrate the normal form of the relationship between the resilient moduli found in the CRB with 66 stress stages. It is evident that the resilient modulus increases as the moisture content decreases. It may be remarked that the resilient modulus value is stress and moisture dependent. There were minor differences in the resilient modulus results for CRB samples at 95% OMC and 80% OMC. The resilient modulus for a sample at 60% OMC improved by approximately 25% over the initial condition (95% OMC).

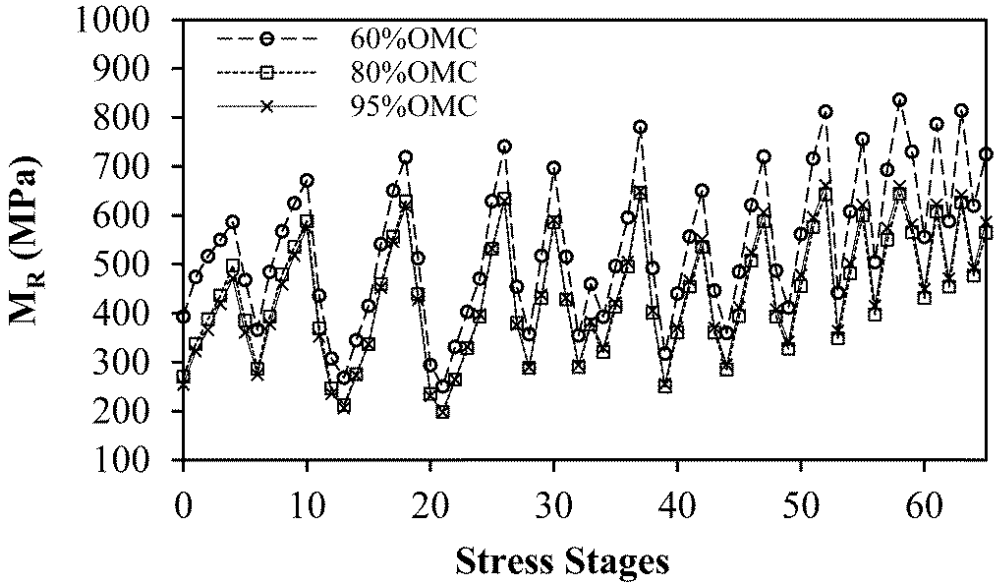

Figure 6.10: Resilient moduli of CRB with various moisture content

6.7 Validation of experimental results

The validation of the framework to estimate the resilient moduli of a pavement base material under different cyclic loading conditions, in accordance with Austroads standard test method AG:PT/T053, can be performed by the comparison of the estimated values from Eqs. 6.9 and 6.10, as shown in Figure 6.11. For the first data set, a total stress concept was used (i.e., no consideration of soil suction), following Eq. 6.9. The total stress regression parameters, or the material parameters (i.e., k_1, k_2, and k_3) of the model were determined using a least-squared regression approach to all the test data at 80% OMC after dryback. This is usually the preference when representing construction conditions in the field, based on Western Australian experience.

For the second data set, $\chi(u_a - u_w)$ was included (see Eq. 6.10), using the suction model parameters calculated from the static triaxial test data (see Table 6.1). In addition, a new least-squared analysis was performed to obtain the effective stress model parameters of the regression analysis from all test data at 60%, 80%, and 95% OMC which represents moisture conditions in the field (i.e., after construction and up to an equilibrium state). Table 6.2 illustrates the regression (material) parameters of both M_R predictive models with matric suction and no matric suction (i.e., Eqs. 6.9 and 6.10 respectively).

Table 6.1: The results from static triaxial tests and analysis

Moisture ratio (% OMC)	σ_3 (kPa)	q_{max} (kPa)	ϕ	ϕ'	σ'_3 (kPa)	$\chi(u_a - u_w)$ (kPa)
95% OMC	35	999	55.03	55.03	110.05	75
80% OMC	35	1003	55.03	55.03	110.49	76
60% OMC	35	1183	55.03	55.03	130.32	95

It can be seen in Figure 6.11 that the inclusion of matric suction towards $\chi(u_a - u_w)$ produces an improved estimation of the resilient response. Figure 6.11 also shows that the predicted resilient modulus values from the total stress concept of Eq. 6.10 are mostly underestimated. This is not reliable in terms of pavement design and analysis as it would definitely lead to an uneconomical pavement structure. It should also be noted that based on the regression model parameters shown in Table 6.2, there are great differences between the regression parameter values of the M_R predictive models from both approaches. This would raise concerns with regard to any pavement design and analysis methods which relied on the regression parameters from the M_R predictive model. For example, the total stress approach may not still be reliable, particularly with regard to the universal model (Witczak and Uzan 1988), as represented in Eq. 6.9.

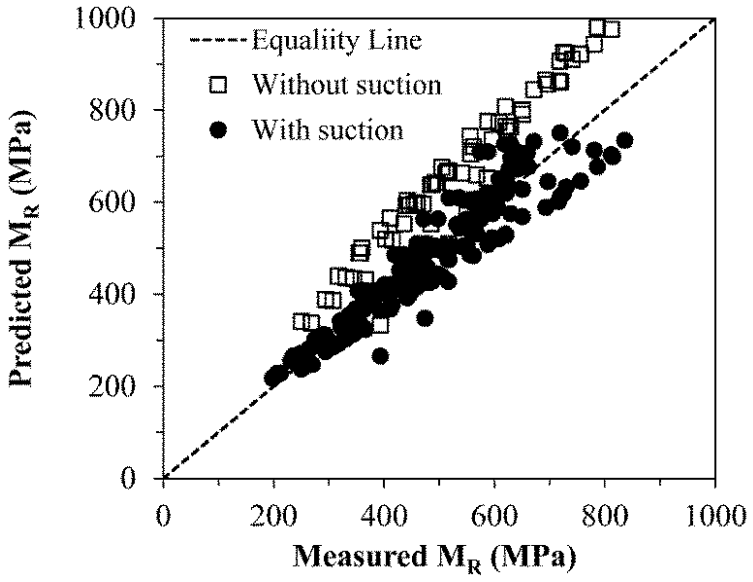

Figure 6.11: Comparison of measured and predicted resilient moduli

Table 6.2: The regression parameters of M_R predictive models from the validation

Resilient modulus model for:	Regression parameters		
	k_1	k_2	k_3
No matric suction (80% of OMC)	415.2	0.284	0.393
With matric suction (60%, 80% and 95% of OMC)	244.9	0.602	0.356

Figure 6.12 shows a graph of the $\chi(u_a - u_w)$ model, demonstrating the effective suction confinement $\chi(u_a - u_w)$ across a range of moisture contents derived from Eq. 6.14. From this graph, the effective suction confinement $\chi(u_a - u_w)$ which is required for the M_R predictive model with suction (i.e., Eq. 6.10) can easily be determined graphically when the moisture contents are known for CRB with different void ratios (i.e., different densities). The three fitting parameters of the van Genuchten model (e.g., a, m, and n) can be obtained from the regression analysis through Eq. 6.14 by using three effective suction confinement measures $\chi(u_a - u_w)$ from Table 6.1, along with the CRB's physical properties (e.g., w, w_s, e, G_s, P_f, and D_{10}).

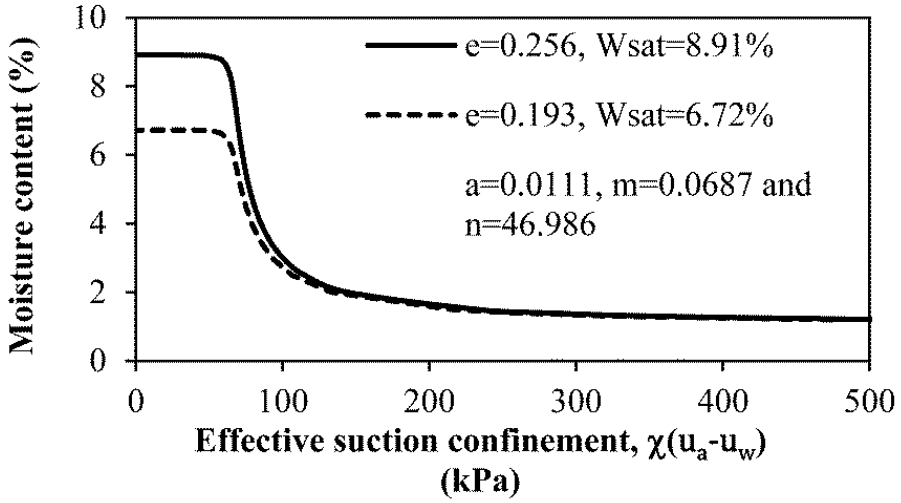

Figure 6.12: Effective suction confinement of CRB at different void ratios

6.8 Proposed framework

The procedure for incorporating the unsaturated characteristics of an unbound granular pavement base material into its cyclic behaviour, in order to obtain a more reliable estimation of M_R from the resilient modulus predictive model, is summarised as follows:

1) Perform a series of static drained triaxial compression tests on at least three test samples having a given (target) density (i.e., a representative density in the field). These three tests should be performed on samples with a range of water contents at a suggested 60%, 80% 95% OMC, prepared by using the dryback process.

2) Use the Mohr-Coulomb failure criteria determined from the results of a static drained triaxial compression test series to obtain the friction angle (ϕ).

3) Determine the matric suction confinement $\chi(u_a - u_w)$ for each moisture content measure using Eqs. 6.15 – 6.17 with a corresponding confining pressure (σ_3) and the deviator stress at failure (q_{max}), based on the assumption of $\phi = \phi'$. An example set of results from this step can be seen in Table 6.1.

4) Perform a series of repeated load triaxial tests on at least three test samples having the same water content conditions as the static drained triaxial compression tests, to determine the resilient moduli (M_R) over a range of stress conditions. (In this study, the stress condition regime from Austroads (2007a) was used and water contents of 60%, 80% 95% OMC are suggested).

5) Perform the regression analysis based on Eq. 6.10. Using the M_R test results from the repeated load triaxial test series (i.e., over a moisture range of 60%, 80% and 95% OMC), and a set of the calculated matric suction confinement measures $\chi(u_a - u_w)$, obtain the M_R model (material) parameters (i.e., k_1, k_2, and k_3).

6) The resilient modulus model, with the inclusion of matric suction confinement $\chi(u_a - u_w)$, can be finally obtained for pavement analysis and design.

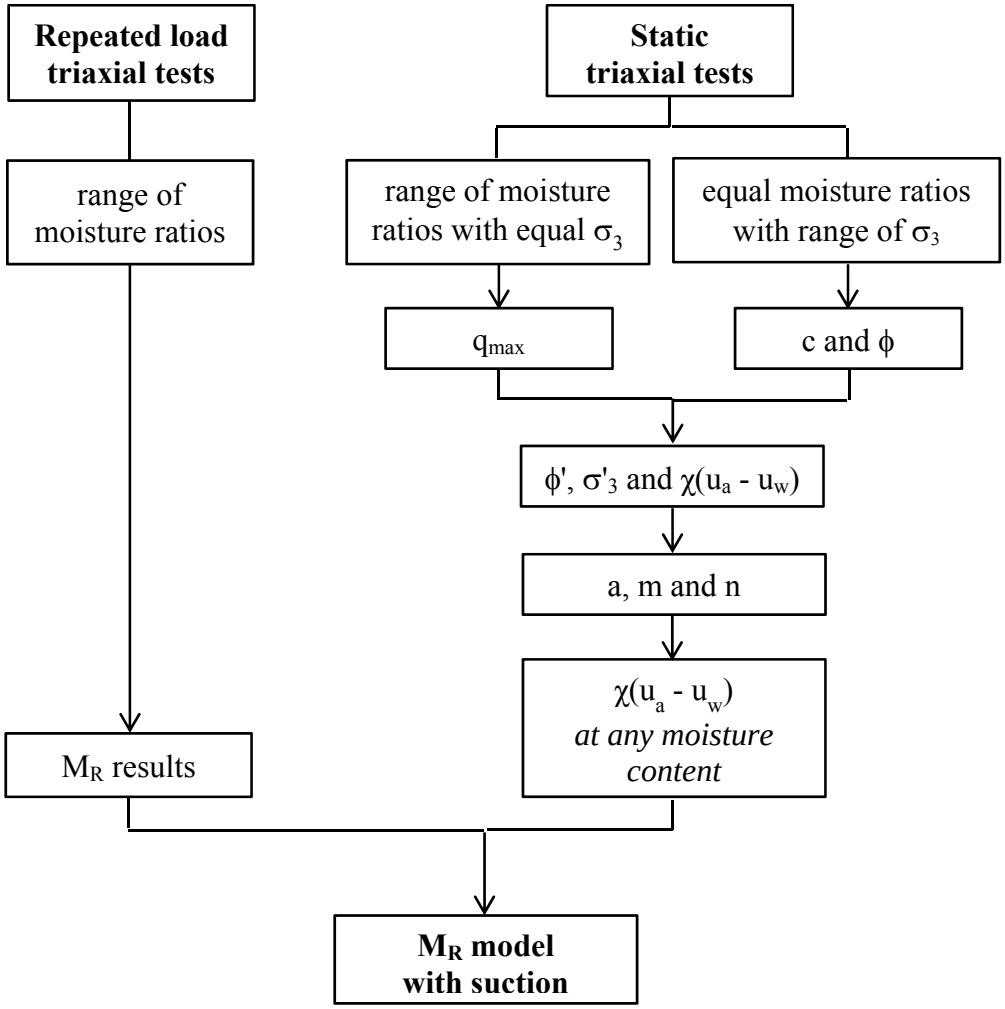

Figure 6.13: Diagram summarising the procedures for proposed framework

6.9 Summary

This chapter has presented a new mechanistic framework for determining the cyclic behaviour of unsaturated unbound granular materials (UUGMs), which are generally pavement base materials. The framework adopted the effective stress concept (Bishop 1959) and a modified form of the van-Genuchten (1980) SWCC equation proposed by Ekblad and Isacsson (2007), to determine the effective stress of UUGMs

without real suction measurement. The resilient modulus model (i.e., the modified universal model) with the inclusion of matric suction was also introduced, based on the procedure to obtain the matric suction confinement $\chi(u_a - u_w)$ and the regression model parameters (i.e., k_1, k_2, and k_3).

From the study, the following conclusions may be drawn:

1. Soil suction is still influential with regard to the performance of coarse-grained pavement material and it cannot be neglected. This is contrary to the usual practice of most geotechnical and pavement engineers which assumes that there is quite low soil suction (i.e., matric suction) with regard to coarse-grained soils, and that this is not significant enough to affect the overall performance of unsaturated coarse-grained soils. The effects of soil suction can be clearly demonstrated in the near-pavement surface of a thin asphalt surface pavement network in Australia, where confining stresses are low, with a high degree of hysteresis in the SWCC between the wetting and drying cycles in particular. Moreover, In Figure 6.4, without using confining pressure, the compacted CRB sample can stand and not disintegrate which might occur if using suction in the sample. Figure 6.4 also simply proves that the suction in compacted pavement materials is still significant to UUGMs and it should be considered as a highly relevant factor in pavement design and analysis.

2. Matric suction can be included into the consideration of the cyclic response of UUGMs through the resilient modulus (M_R) model (see Eq. 6.10). The M_R predictive model with the inclusion of suction confinement, $\chi(u_a - u_w)$, can be performed without real matric suction measurements by using normalising procedures associated with an application of the (Bishop 1959) effective stress concept and the principle of the van-Genuchten (1980) SWCC equation.

3. The predicted resilient modulus values from Eq. 6.9 of the universal model (Witczak and Uzan 1988) tend to be under-estimated, and this would lead to uneconomical results for pavement design and analysis.

4. The M_R predictive model which includes $\chi(u_a - u_w)$, gives a more reliable estimation than that of the universal model (Witczak and Uzan 1988), which can be clearly seen in Figure 6.11.

5. The $\chi(u_a - u_w)$ model (see Figure 6.12) can be constructed based on Eq. 6.14, along with the inputs from the normalising processes and the material's physical properties.

6. There was a great difference between the regression parameter values of the M_R predictive models from both approaches (i.e., without suction and with suction, as shown in Eqs. 6.9 and 6.10). This would therefore raise concerns with regard to any pavement design and analysis methods which relied on the regression model parameters from the traditional M_R predictive model, such as whether the total stress approach is still reliable, in particular the universal model (Witczak and Uzan 1988) shown in Eq. 6.9.

7. A new mechanical framework was introduced to incorporate the unsaturated characteristics of UUGMs into the cyclic response without matric suction measurement, and to obtain a more reliable resilient modulus (M_R) prediction model with the inclusion of matric suction.

CHAPTER 7
STRUCTURAL ANALYSIS FOR HCTCRB PAVEMENTS

In this chapter, the resilient modulus test results for all HCTCRB samples were implemented into the analysis and design of a typical multi-layered pavement structure for WA. Pavement design aims to assess the capacity of any given pavement configuration e.g., pavement layer thicknesses, in terms of allowable number of equivalent standard axles (ESAs) or number of standard axle repetitions (SAR). In general, the structural analysis of pavement is carried out prior to pavement design. This allows assessment of the pavement's behaviour and properties, for example whether it displays linearity or non-linearity, or whether it is isotropic or anisotropic. From the analyses, the responses of pavement materials i.e., the critical strains at the bottom of an asphalt layer and at the top of subgrade can then be converted into allowable ESAs for the given pavement thickness.

7.1 Resilient modulus of HCTCRB for pavement analysis and design

The resilient modulus (M_R) is an important input into the structural analysis and design of pavement. In this study, HCTCRB samples were used in resilient modulus tests bound by particular conditions. These included: hydration periods (7, 14, 28 and 45 days), amount of added water during compaction (no added water, OMC of CRB-cement and OMC of HCTCRB) and degree of dryback (60%, 80% and no dryback). The test results for all samples are shown in Figure 7.1.

The scatter pattern of the test data is visible due to the different test sample conditions which produced differing HCTCRB resilient moduli. This data provided a relatively low degree of determination (R^2) of about 40%, when evaluated with the bulk stress model (Eq. 7.1) and the universal model (Eq. 7.2). To normalise the critical conditions appropriate to the resilient moduli of HCTCRB, the moisture and density conditions of HCTCRB were integrated with the bulk stress model and the universal model to improve the R^2, as expressed in Eq. 7.3 and 7.4 respectively. The moisture content ratio (WCR) is the ratio of moisture content in any sample to the average optimum moisture content of HCTCRB. The dry density ratio (DDR) is the ratio of the dry density of any sample to the average maximum dry density of

HCTCRB. The experimental results were then evaluated once more and yielded Eq. 7.5 and 7.6 respectively, and provided R^2 values which were improved to approximately 70% (see Figure 7.2 and Figure 7.3). The values of the DDR being 0.98 and the WCR being 0.70, which were in keeping with the requirements of Main Roads Western Australia (2012a), were substituted into Eq. 7.5 and 7.6 and eventually resulted in Eq. 7.7 and 7.8. These two equations were then used in the resilient modulus models of HCTCRB in the pavement analysis.

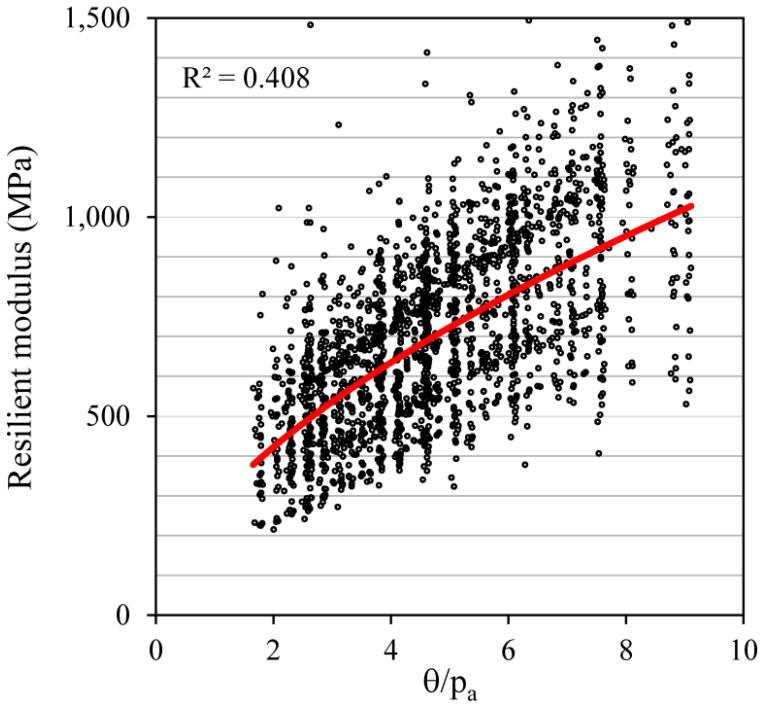

Figure 7.1: Resilient modulus test results for all HCTCRB samples

$$M_R = k_1\left(\frac{\theta}{p_a}\right)^{k_2} \tag{7.1}$$

$$M_R = k_1\left(\frac{\theta}{p_a}\right)^{k_2}\left(\frac{\tau_{oct}}{p_a}\right)^{k_3} \tag{7.2}$$

$$M_R = k_1(DDR)^a(WCR)^b\left(\frac{\theta}{p_a}\right)^{k_2} \tag{7.3}$$

$$M_R = k_1(DDR)^a(WCR)^b\left(\frac{\theta}{p_a}\right)^{k_2}\left(\frac{\tau_{oct}}{p_a}\right)^{k_3} \tag{7.4}$$

$$M_R = 206(DDR)^{1.187}(WCR)^{-0.932}\left(\frac{\theta}{p_a}\right)^{0.588} \quad (7.5)$$

$$M_R = 191(DDR)^{1.179}(WCR)^{-0.930}\left(\frac{\theta}{p_a}\right)^{0.651}\left(\frac{\tau_{oct}}{p_a}\right)^{-0.060} \quad (7.6)$$

where M_R = resilient modulus; pa = atmospheric pressure (100 kPa); θ = bulk stress; τ_{oct} = octahedral shear stress; DDR = dry density ratio; WCR = moisture content ratio; and a, b, k_1, k_2 and k_3= regression constant

For DDR=0.98 and WCR=0.70, the resilient modulus models for HCTCRB become;

$$M_R = 280\left(\frac{\theta}{p_a}\right)^{0.588} \quad (7.7)$$

$$M_R = 260\left(\frac{\theta}{p_a}\right)^{0.651}\left(\frac{\tau_{oct}}{p_a}\right)^{-0.060} \quad (7.8)$$

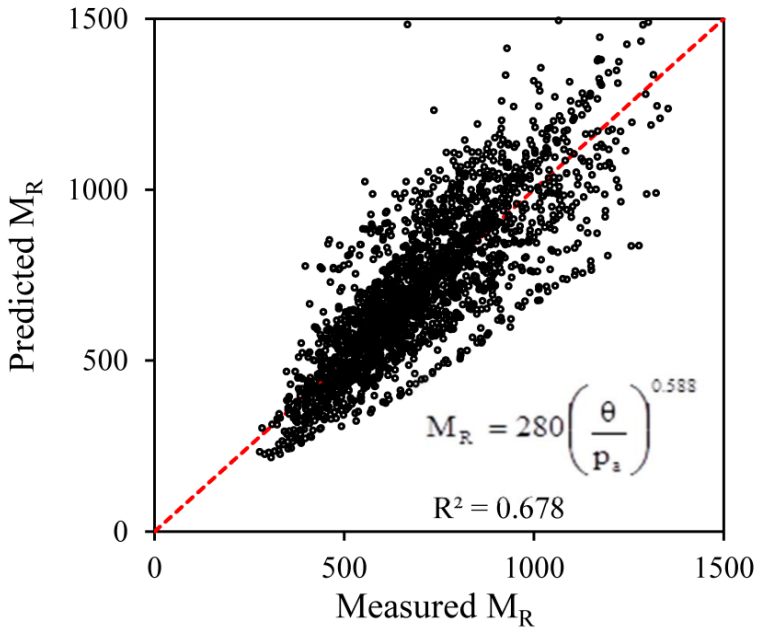

Figure 7.2: The specific bulk stress model for HCTCRB

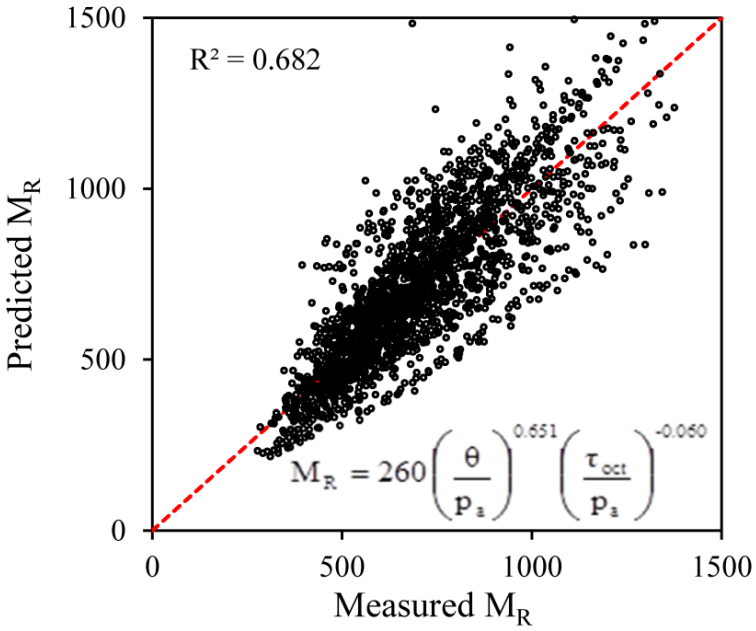

Figure 7.3: The specific universal model for HCTCRB

7.2 Structural analysis for a typical HCTCRB pavement

Pavement analyses in this study covered various states of materials i.e., linearity or non-linearity, and isotropy or anisotropy of pavement materials, using three types of available software. The analyses that accounted for the anisotropy and quasi-non-linearity of materials were performed using Circly 5.0 (Mincad Systems 2009), this being a popular and commonly used software for pavement analysis and design in Australia. Everstress 5.0 (Washington State Department of Transportation (WSDOT) 2005) was used for the analysis of linearity and non-linearity of isotropic materials. A three- dimensional finite element analysis (3D FEA) of pavement structure was also carried out using Abaqus 6.10 (Dassault Systèmes 2010). The analysis of the pavement structure provided the responses of pavement materials in terms of stress and strain behaviour. Based on (Austroads 2010c) criteria, the allowable ESA of a certain pavement is usually converted from the strain values occurring in pavement layers (such as asphalt and subgrade) by applying transfer functions. Finally, allowable ESAs or SARs for specific pavement configurations were obtained and then evaluated as to whether such pavement would be capable of carrying the designed ESA (DESA) or designed SAR (DSAR).

7.2.1 Design criteria and transfer functions

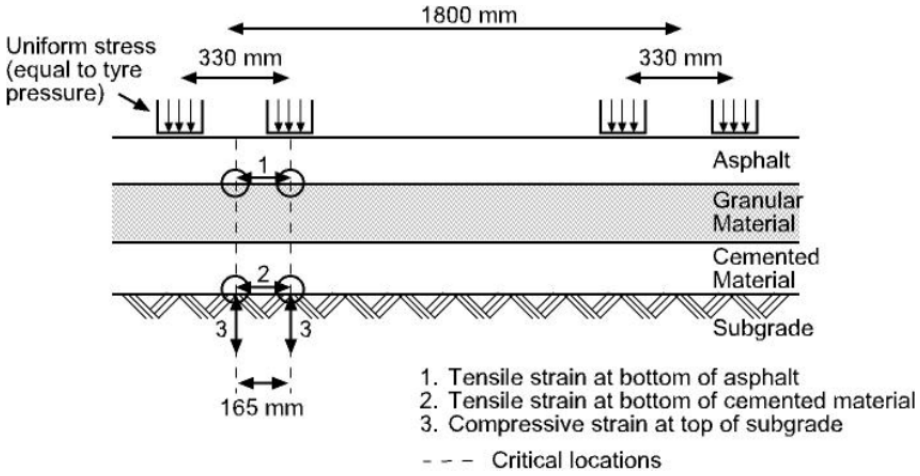

Figure 7.4: Design criteria for flexible pavements (Austroads 2010c)

Austroads (2010c) established applied loading and critical responses for flexible pavement analysis and design, as shown in Figure 7.4. Standard loading is represented by a single axle with dual tyres with a total load of 80 kN. The total load is allocated equally; 20 kN to each tyre, and distributed uniformly with a tyre pressure of 750 kPa over a circular area (radius of 92.1 mm) on the contact surface. Circular loading is normally applied with regard to analysis by Circly and Everstress. For 3D FEA, loading contact is transformed from a circle into a rectangle of equivalent area (Huang 2004). The shapes and dimensions of the load contact used for analysis are shown in Figure 7.5.

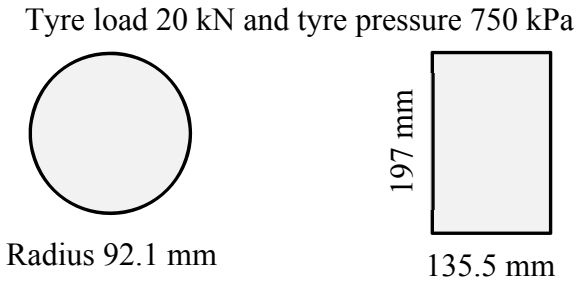

Figure 7.5: Loading shapes for pavement analysis

The critical responses in pavement consist of the horizontal tensile strain (ε_t) at the bottom of an asphalt layer, the horizontal tensile strain (ε_t) at the bottom of the

cemented materials and the vertical compressive strain (ε_c) at the top of the subgrade. However, this study did not use cemented material in the pavement. The values of strain from the analysis results are usually converted to allowable SARs by associated transfer functions, i.e., Eq. 7.9 for asphalt and Eq. 7.10 for subgrade (Austroads 2010c).

$$N = RF\left(\frac{6918(0.856V_b + 1.08)}{S^{0.36}\mu\varepsilon}\right)^5 \quad (7.9)$$

$$N = \left(\frac{9300}{\mu\varepsilon}\right)^7 \quad (7.10)$$

where N = the allowable number of standard axle repetitions; με = critical microstrain in the considered material; RF = reliability factor for asphalt fatigue; V_b = % of binder volume; S = elastic modulus of asphalt in MPa

A typical pavement structure used in the analysis throughout this study comprised four layers of asphalt surface in addition to an HCTCRB basecourse, and a crushed limestone subbase on a subgrade of Perth sand, as detailed in Table 7.1.

Table 7.1: A typical pavement configuration

Layer	Material	Thickness (mm)	Vertical modulus (MPa)	Poisson's ratio
Surface	Asphalt	50	2,500	0.40
Basecourse	HCTCRB	200	varied	0.35
Subbase	Crushed limestone	200	300	0.35
Subgrade	Perth sand (CBR 10)	infinite	100	0.35

7.2.2 Pavement analysis by Circly

Circly has program features which comply with the Austroads (2010c) approach to mechanistic empirical pavement analysis and design. Asphalt is assumed to be homogeneous, elastic and isotropic. Unbound granular materials and subgrade are assumed to be anisotropic and from this the ratio of vertical modulus to horizontal modulus is assigned, in this case being 2. However, Poisson's ratio for both directions is equal. Unbound granular layers (such as basecourse and subbase) are divided into 5 equal sub-layers. The modulus for each layer is then reduced by a reduction factor (R), as stated in Eq. 7.11. This reduction demonstrates the quasi-non-linearity of the materials (Saleh et al. 2009) as the modulus decreases with depth. However, each sub-layer still acts as a linear elastic material with a constant modulus throughout the depth of each sub-layer. There is also another condition for the modulus of the overlying layer, as shown in Eq. 7.12, which depends on its thickness and the modulus of the adjacent underlying layer. The two conditions for modulus calculation indicate that the modulus of the overlying layer is also greatly dependent on the proximity of the underlying layer, rather than solely on itself.

$$R = \left(\frac{E_{v1}}{E_{v2}} \right)^{\left(\frac{1}{5}\right)} \tag{7.11}$$

$$E_{v1} = E_{v2} * 2^{\left(\frac{t_1}{125}\right)} \tag{7.12}$$

where R = the reduction factor for the modulus of the overlying layer; E_{v1} = modulus of the overlying layer; E_{v2} = modulus of the adjacent underlying layer; t_1 = thickness of the overlying layer.

Although Circly is routinely used in investigations of anisotropy and sub-layering cases, it is still capable of analysing fully elastic and isotropic cases. Thus this study performed pavement analyses using Circly to cover the three cases summarised in Table 7.2.

Table 7.2: Three cases for analysis using Circly

Case	Basecourse and Subbase	Subgrade
C1	Sub-layering (quasi-non-linear) and anisotropy	Anisotropy
C2	Sub-layering (quasi-non-linear) and isotropy	Isotropy
C3	Fully elastic (no sub-layering) and isotropy	Isotropy

From Figure 7.1, the average M_R for all HCTCRB samples was 700 MPa. At the average applied bulk stress of 470 kPa from the standard tests, the M_R of HCTCRB varied from 300 MPa to 1,000 MPa. Thus, analyses were conducted over this range of M_R. The analysis results, as illustrated in Figure 7.6, revealed that isotropic and fully elastic cases produced lower strain values (i.e., with higher allowable ESAs) than anisotropic and sub-layering cases. The maximum vertical compressive strain on the top of the subgrade, when loaded, commonly occurred midway between two tyres. The maximum tensile strain at the bottom of an asphalt layer is usually located directly beneath the tyre. In using the Circly analysis, this study found that the tensile strain at the bottom of asphalt was less sensitive to the different analysis approaches. However it was more sensitive to the basecourse modulus in comparison with the compressive strain at the top of the subgrade. For both sub-layering cases (C1 and C2), the inputs of M_R 900 MPa and higher produced indistinguishable responses due to the condition in Eq. 7.12 that limited the M_R of HCTCRB to approximately 900 MPa.

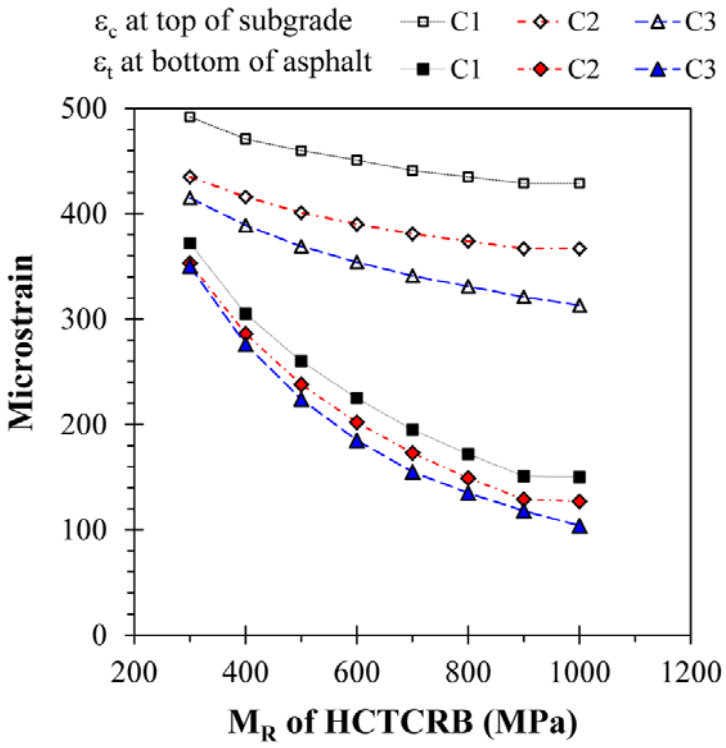

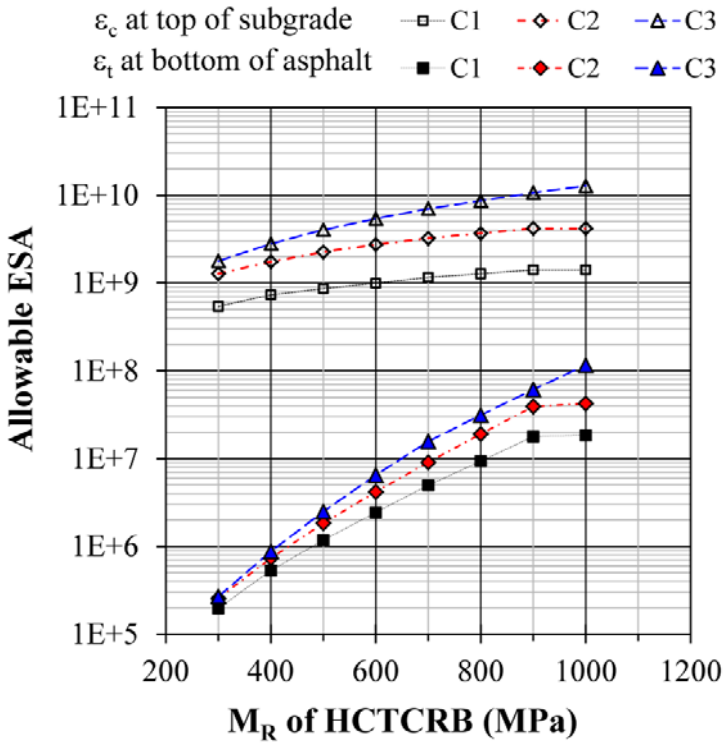

Figure 7.6: Analysis results from Circly

7.2.3 Pavement analysis by Everstress

This study also utilised Everstress in its analysis. Although Everstress was unable to make a determination regarding the anisotropic case, it was able to account for the linearity and non-linearity of the unbound granular materials. The results from the fully elastic and isotropic analyses are presented in Figure 7.7.

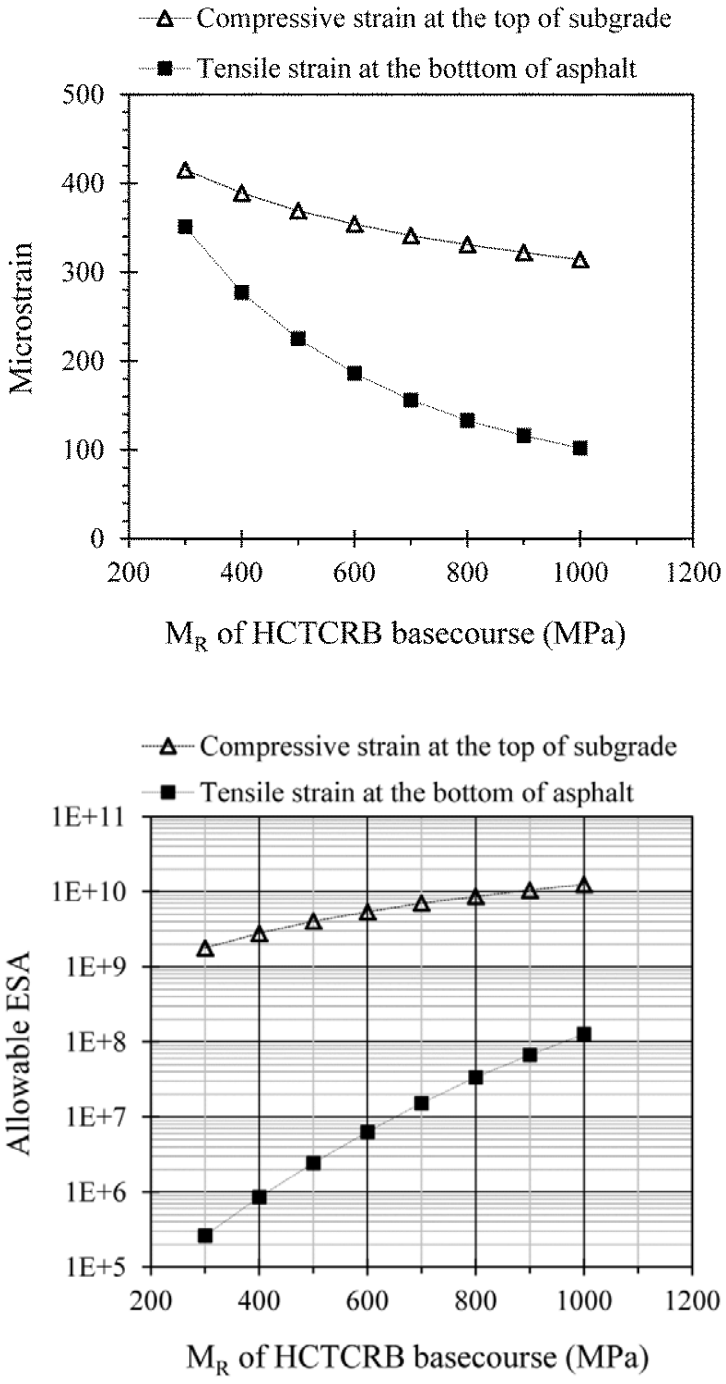

Figure 7.7: Analysis results from Everstress for isotropic and fully elastic materials

For non-linear analysis cases, Everstress uses the bulk stress model for coarse-grained unbound granular materials and the deviator stress model for fine-grained subgrade. However, this study only accounted for the non-linearity of the HCTCRB basecourse using the resilient modulus model in Eq. 7.7. Everstress also requires the initial modulus as the input, together with the bulk stress model parameters (k_1 and k_2). It then uses an iterative procedure to adjust the modulus according to the induced stress throughout the layer depth. It was found that at a given thickness of HCTCRB, the variation in the initial modulus (300 MPa – 1,000 MPa in this study) yielded the identical M_R value for HCTCRB. The resilient modulus values of HCTCRB, which varied with its thickness, are illustrated in Figure 7.8.

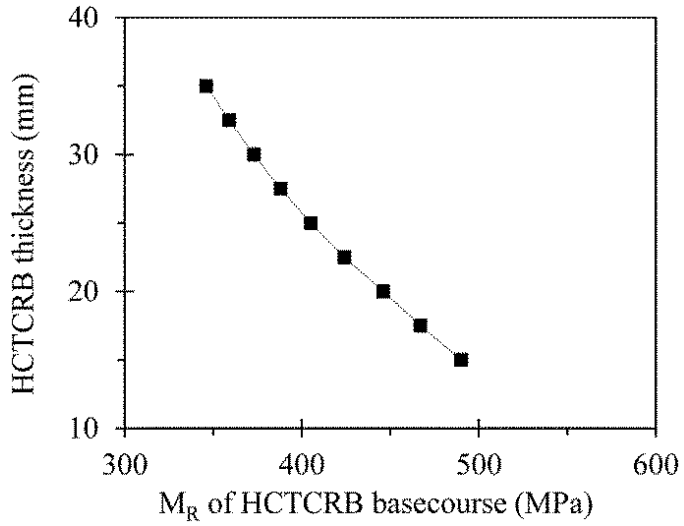

Figure 7.8: Variation of M_R with thickness for HCTCRB from non-linear analysis

Saleh et al. (2009) conducted the resilient modulus test for unbound granular materials and used the average values from the tests as inputs into Circly. They found that the responses from anisotropic and quasi-non-linear cases produced by Circly were much lower than those from the non-linear isotropic analysis produced by Everstress for a particular pavement. This may be due to the M_R input for Circly being higher than it should have been.

An average M_R of 700 MPa for HCTCRB obtained from the tests seems too high as an input for Circly and linear cases. Figure 7.8 shows that the M_R of HCTCRB over a

typical range of its thickness would not be as high as 700 MPa. Based on the average values from Figure 7.8, the M_R for HCTCRB should be 400 MPa for Circly and linear analysis.

7.2.4 Finite element modelling for pavement analysis

This study employed Abaqus software for the three dimensional finite element model (3D FEM) of pavement with isotropic and linear elastic pavement materials. A sub-layering technique was also used for the isotropic basecourse and subbase layers in addition to the simple isotropic and linear elastic analyses. A pavement model size of 5 m long (in the direction of the traffic) by 6 m in a transverse direction and 2.5 m in depth was used for modelling. This was subjected to a load of four rectangular tyres of 20 kN and 750 kPa each (see Figure 7.4 and Figure 7.5). Due to the two symmetrical planes (as shown in Figure 7.9), only a quarter portion was necessary for the carrying out of the analysis. The final model is shown in
Figure 7.10.

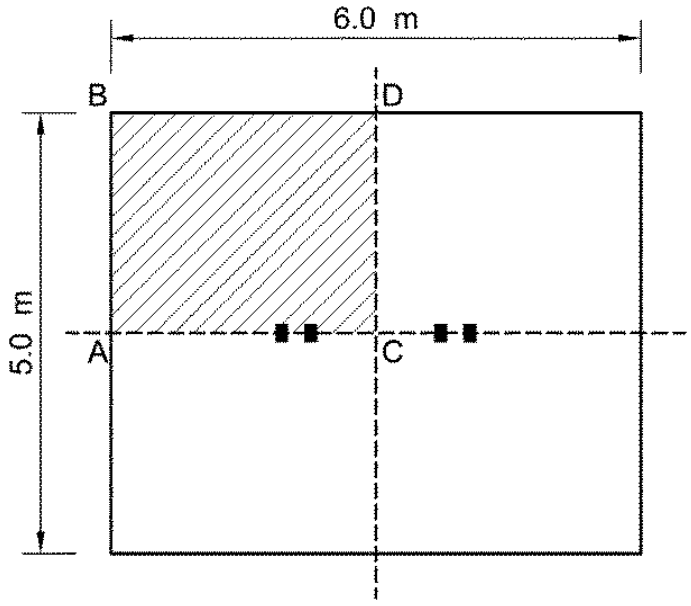

Figure 7.9: Top view of pavement model with standard axle load

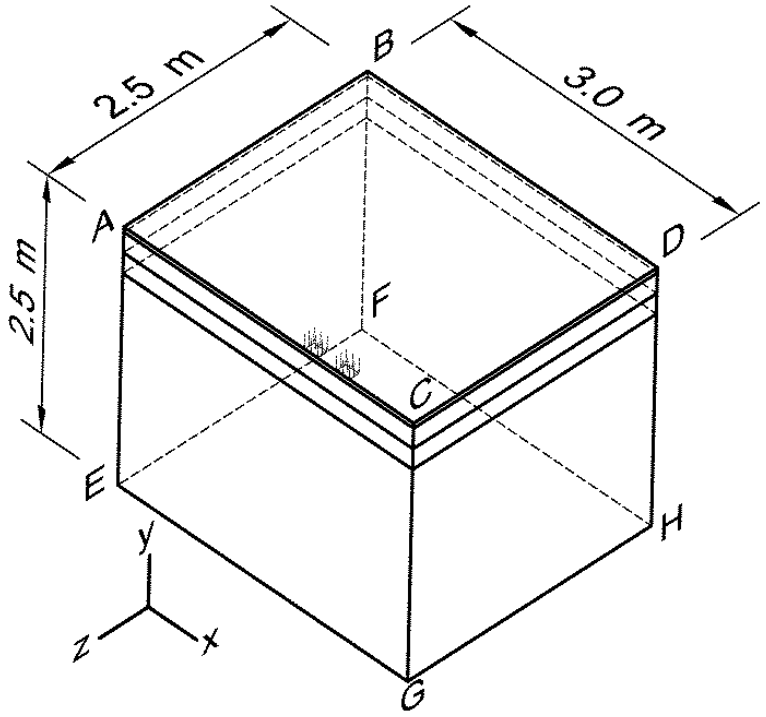

Figure 7.10: 3D FEM for one quarter of the pavement

The pavement was modelled with C3D20R (Continuum 3-Dimensional 20-node element with reduced integration) brick elements. The boundary conditions of the model consisted of:

- symmetry along the z-axis on the EACG plane;
- symmetry along the x-axis on the GCDH plane;
- restraint of horizontal movement along the z-axis on plane HDBF;
- restraint of horizontal movement along the x-axis on plane EABF; and
- restraint of movement along the x, y and z-axes on bottom plane EFHG.

Examples of the analysis results chosen from the isotropic and linear cases for the M_R of HCTCRB 400 MPa are demonstrated in Figure 7.11 to Figure 7.14. The critical strain responses resulting from two analysis cases with variations in the M_R of the HCTCRB of 300 MPa – 1,000 MPa were compared, as seen in Figure 7.15. It was found that the critical strains from the sub-layering case were higher than in the conventional analysis. The difference in magnitudes of strain due to the different analysis approaches were more pronounced for the subgrade compressive strain than for the asphalt tensile strain.

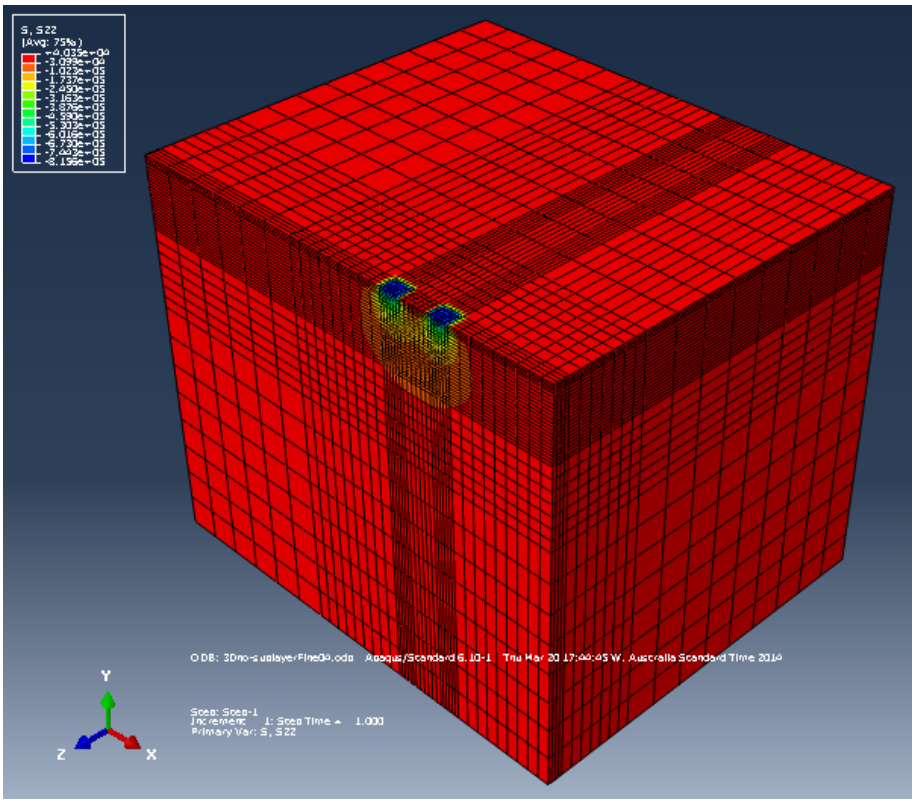

Figure 7.11: An example of vertical stress in a pavement model

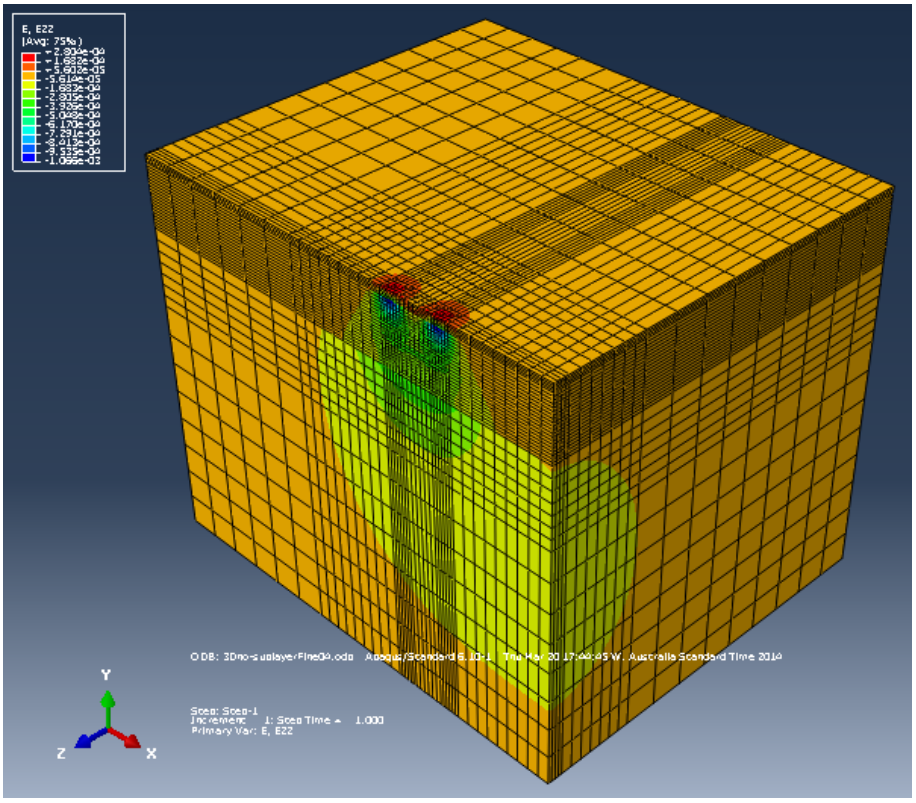

Figure 7.12: An example of vertical strain in a pavement model

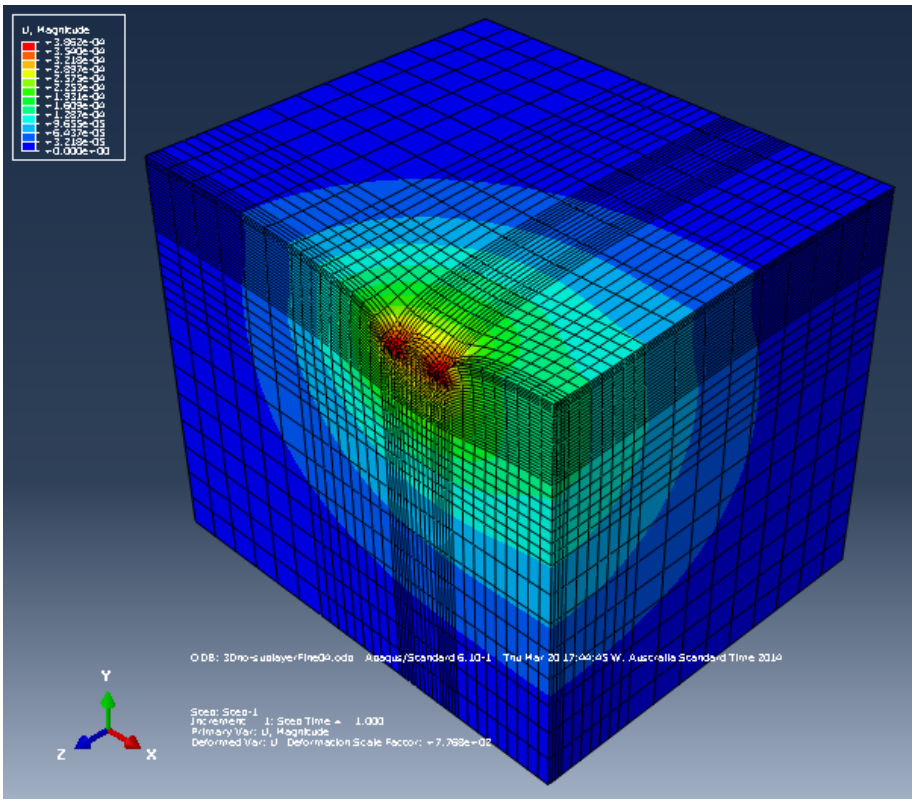

Figure 7.13: An example of deflection in a pavement model

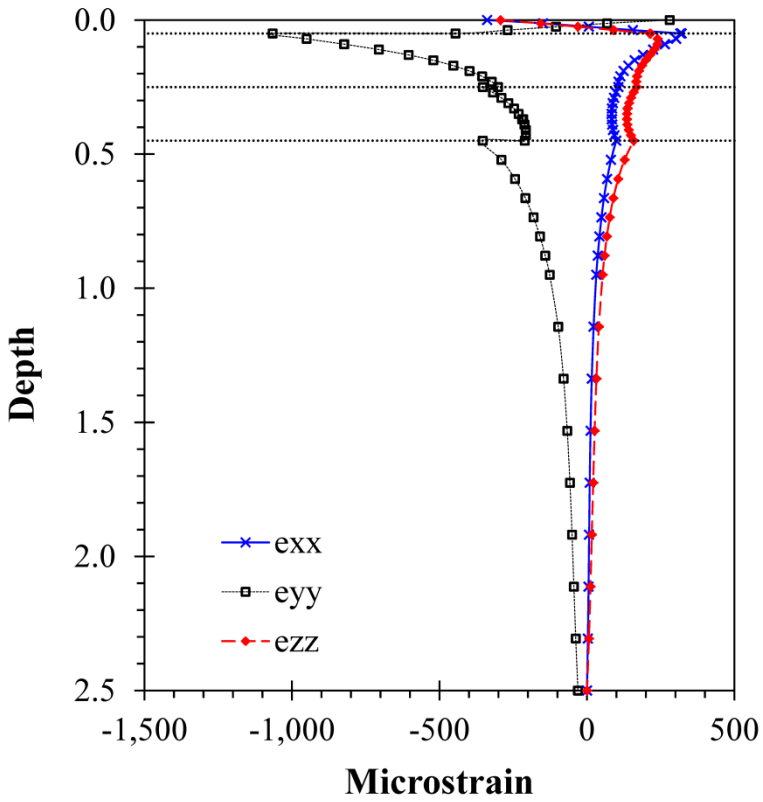

Figure 7.14: An example of strain under an outer wheel over the entire depth of pavement

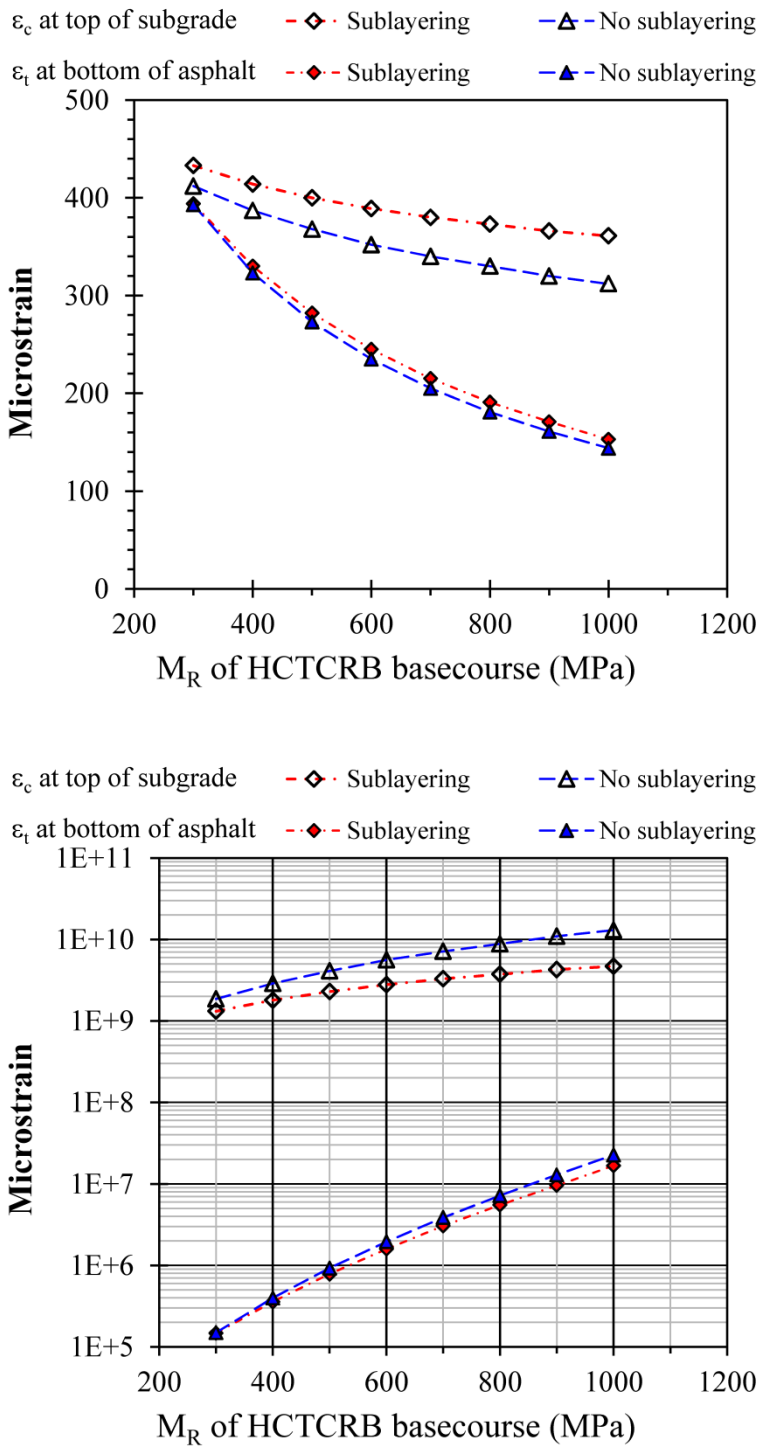

Figure 7.15: Critical strain in pavement using FEM in Abaqus

7.2.5 Comparison of various analysis methods

This section compares the results of the various approaches which were carried out using the three types of software. In all cases, the allowable ESAs were governed by

the tensile strain at the bottom of the asphalt. It was also found that the tensile strain at the bottom of the asphalt did not differ greatly in the values resulting from the three different methods of analysis. However, the tensile strain appeared to be highly dependent on the basecourse moduli, unlike the compressive strain at the top of the subgrade which exhibited values not greatly different to those of the basecourse moduli.

The approach involving the isotropic and fully elastic case was the simplest, and is therefore presented first, below (see Figure 7.16). For both cases of strain at the bottom of the asphalt layer and the bottom of the subgrade layer, all critical responses differed insignificantly, with the exception of the tensile strain in the asphalt analysed by 3D FEA which was deemed the most accurate method. There were significant differences in the results of the strains at the bottom of the asphalt layer. It is possible that the Circly and Everstress analyses, which provided almost identical results, may have under-estimated the critical responses, leading to an overestimation of the allowable ESAs.

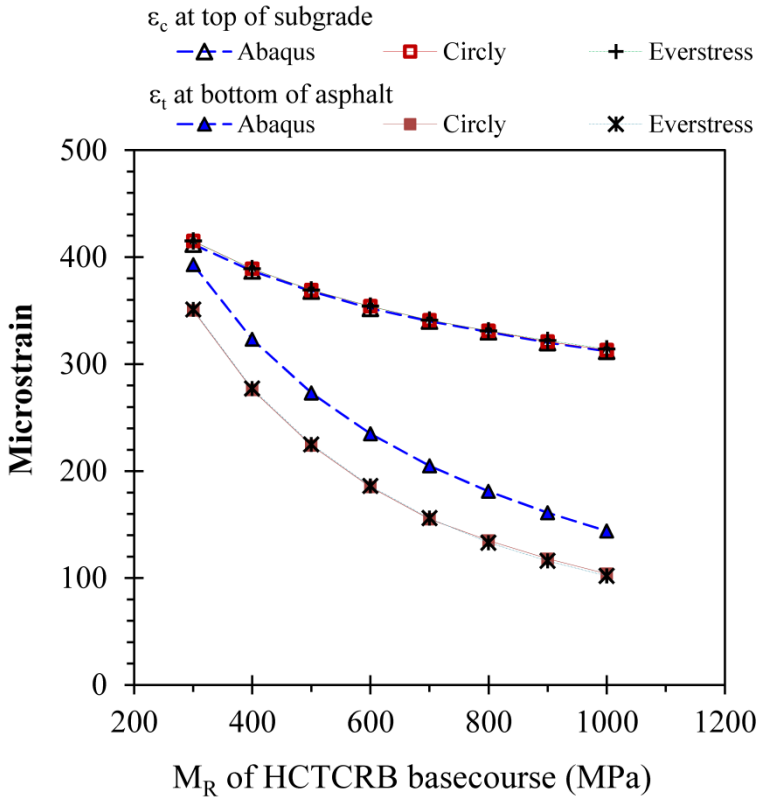

Figure 7.16: Comparison of isotropic and fully elastic case from the three types of software

The comparison of routine analyses using each of the three types of software (i.e., fully elastic and isotropic analyses by Everstress and Abaqus, and anisotropic with sub-layering by Circly) is shown in Figure 7.17. The critical tensile strain in the asphalt used for Circly and Abaqus showed minor differences (approximately 5%). However, the critical compressive strains on the subgrade determined by Circly were significantly higher than those from Abaqus (approximately 25%). This does not affect the allowable ESAs for thick asphalt pavement design which is governed by the tensile strain of asphalt. Nevertheless, for thin asphalt pavements (less than 40 mm) or unbound granular pavements, Circly provides the more conservative allowable ESAs due to the higher strain on the subgrade. Thus, with pavement analysed by Circly, the anisotropic and sub-layering techniques are still reliable for use in pavement analysis and design. However, care are must be taken with the M_R inputs derived from the resilient modulus tests. Based on this study, and that of Saleh et al. (2009), the average M_R from the test results seemed too high for use as an input into the linear and quasi-non-linear analyses. An appropriate M_R input must be carefully determined through the induced stress conditions over the range of typical pavement configurations.

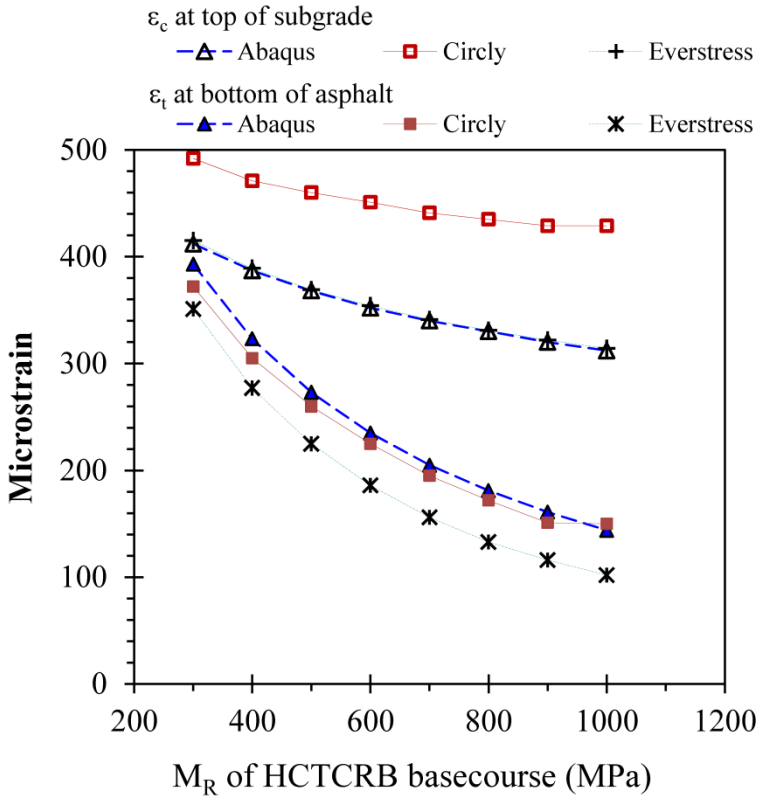

Figure 7.17: Comparison of the results from three conventional analysis methods

7.3 Summary

The resilient modulus test results were implemented into the pavement analysis and design. A typical pavement structure was set up and analysed using various approaches depending on the different degrees of material isotropy and linearity. The main conclusions from this evaluation can be presented as follows:

1. The resilient modulus models representing the stress dependency of HCTCRB at specific moisture and density conditions (Main Roads Western Australia 2010) based on the bulk stress model and the universal model are:

$$M_R = 280\left(\frac{\theta}{p_a}\right)^{0.588}$$

$$M_R = 260\left(\frac{\theta}{p_a}\right)^{0.651}\left(\frac{\tau_{oct}}{p_a}\right)^{-0.060}$$

2. The average resilient modulus from all experimental data was quite high for linear and quasi-non-linear analyses, which produced an overestimation of the allowable amount of traffic loading. Based on the stress-dependent analyses conducted and concerned with the thickness range of the basecourse layer, a typical value for the M_R of HCTCRB may be determined as being approximately 400 MPa.

3. The Circly pavement analysis, using the anisotropic and sub-layering technique, is still deemed reliable in comparison with the various approaches examined in this study. However, there remains a concern regarding the reliability of the value of the M_R input derived from the resilient modulus tests. The average M_R from the test results appeared to be too high for an effective analysis to be undertaken.

4. Changes in the tensile strain in the asphalt with the modulus of the basecourse material are more pronounced than those in the subgrade compressive strain.

However, the compressive strain at the top of the subgrade is more sensitive to analysis methods.

5. Pavement analysis and design is governed by the tensile strain of asphalt which is greatly dependent on the basecourse modulus. This indicates the importance of understanding the properties of basecourse materials in order for them to be used effectively.

CHAPTER 8
CONCLUSIONS AND RECOMMENDATIONS

8.1 Conclusions

An evaluation of HCTCRB in terms of basic soil properties and mechanical performance was conducted, with variations in the properties of the material during manufacturing and construction. Following this, HCTCRB performance factors such as the resilient modulus and permanent strain were assessed using a model that was able to account for the dependency of stress, along with the intrinsic material properties. In the final stage of this study, the test results were implemented for use in the mechanistic-empirical pavement analysis and design.

Along with the characterisation of HCTCRB, parallel work was also performed on other pavement materials related to HCTCRB. This included ascertaining the performance of a standard crushed rock base (CRB) sample with suction effect and investigating the significant characteristics of common cement-treated base (CTB).

8.1.1 Material characterisation for HCTCRB

The major findings resulting from the investigation into and the tests on HCTCRB are presented below.

1. The HCTCRB samples were prepared by standard compaction and soaked for 4 hours; this produced a much lower UCS than the Austroads criteria for modified materials and bound materials. The UCS values for modified compacted and unsoaked specimens were also lower than those given by MRWA limits. This may indicate that HCTCRB does not behave in the manner that Austroads specifies as modified or bound materials.

2. SEM analyses and static triaxial tests proved that CRB has higher internal friction angles but less cohesion than HCTCRB. This is due to the sharp edges and rough surfaces of CRB particles as compared to the smooth surfaces of HCTCRB particles. The cohesion and angles of internal friction

derived from the static triaxial tests for CRB were 38 kPa and 59° respectively; and for HCTCRB, 169 kPa and 46° respectively.

3. UCS, PD and M_R results for HCTCRB made with 1%, 2% and 3% cement indicate that 2% cement is the optimum amount of content when manufacturing HCTCRB. The 3% cement samples performed the least well as a consequence of higher water consumption during the hydration reaction period, which resulted in a drier material and lower workability.

4. The hydration periods, amount of added water for compaction, and degree of dryback significantly affected HCTCRB performance. However, a related trend of material performance in relation to the hydration periods was inconclusive.

5. The moisture content of the samples played an important role in the performance of HCTCRB. Higher amounts of water added during compaction generally caused a decrease in PD and M_R performance (compared to samples without the addition of water) even after dryback. This indicates that HCTCRB still has some degree of moisture sensitivity and thus the amount of added water for compaction must be carefully controlled for effective HCTCRB performance.

6. HCTCRB exhibited stress-dependency behaviour under repeated load triaxial tests. All resilient modulus test results covering the range of hydration periods, the amount of added water for compaction and the degree of dryback were evaluated using the bulk stress model and the universal model. The resilient modulus models of HCTCRB at the dry density ratio of 98% and degree of dryback of 70% are expressed as follows:

$$M_R = 280\left(\frac{\theta}{p_a}\right)^{0.588}$$

$$M_R = 260\left(\frac{\theta}{p_a}\right)^{0.651}\left(\frac{\tau_{oct}}{p_a}\right)^{-0.060}$$

7. Based on stress-dependent analyses of a range of HCTCRB thicknesses, a typical value for the M_R of HCTCRB should be about 400 MPa for linear and quasi-non-linear analyses. The use of the average resilient modulus computed from all the test results tended to underestimate the critical responses in pavement, i.e., it overestimated the allowable amount of traffic loading.

8. Using Circly, Everstress and Abaqus, a typical pavement structure with varying degrees of isotropy and linearity was analysed. The pavement analysed by Circly, using anisotropic and sub-layering techniques, was still reliable in comparison with the other approaches detailed in this study. A major concern with the use of Circly is the reliability of the M_R value input.

8.1.2 Characterisation of unbound granular material with suction effect

9. This study also proposed a framework incorporate the soil suction effect into the cyclic response of unbound granular materials without the need for real matric suction tests. The M_R predictive model, with the inclusion of suction confinement $\chi(ua - uw)$, can be performed by using normalising procedures associated with the application of the Bishop (1959) effective stress concept and the principles of the van van-Genuchten (1980) SWCC equation. The framework was validated after testing the shear strength and resilient modulus of standard CRB. These tests delivered a promising result in terms of greater accuracy and a higher degree of determination compared with conventional analysis.

8.1.3 Characteristics of a cement-treated base (CTB) sample

10. The shrinkage test results from this study revealed that the amount of shrinkage in CTB did not necessarily increase with higher cement content. The shrinkage of CTB reduced with an increase in cement content from 2% to 4%. However, shrinkage actually increased as a cement content of up to 6% was added. It was assumed that the higher shrinkage with the greater cement content of 5% and 6% was mainly due to self-desiccation. By

contrast, the shrinkage in the low cement content of 2% - 3%, was predominantly caused by drying shrinkage due to excess water in the mix.

11. Flexural fatigue tests were conducted by following a standard test method under the strain-control mode of 50 με - 200 με for the 3% and 5% cement samples. Only the 5% cement sample triggered fatigue failure when subjected to 200 με. Thus a fatigue relationship could not be drawn from the experimental data. This revealed that the fatigue phenomenon does not occur if the strain in 3% and 5% cement CTB induced by repetitive loading is lower than 200 με.

12. An additional multi-strain fatigue test was initiated to examine the stiffness degradation and recovery of CTB from a stepwise increase and decrease in applied strain. The aim of this was to develop a testing protocol to reduce the testing time and the number of test specimens entailed in a conventional fatigue test.

8.2 Recommendations for further work

1. Current MRWA specifications require the minimum amount of water to be of 90% OMC of CRB for mixing with cement and CRB at the initial stage of HCTCRB production. This amount of water may be insufficient due to the fact that after hydration some moisture is lost. Water is then sometimes added during construction which may then cause inferior performance of the HCTCRB in the field. Thus HCTCRB should be further characterised for determining the appropriate amount of mixing water.

2. The long-term performance of HCTCRB and re-cementing in HCTCRB requires further study in order to assess the probability of HCTCRB becoming stiffer over time and becoming prone to fatigue cracking in a similar manner to that of bound materials.

3. The finite element modelling account of nonlinear and anisotropic properties for all pavement materials requires further work. This is necessary in order to obtain more accurate details of the responses of materials in pavement analysis and design.

4. The proposed framework that incorporates the suction effect into the resilient responses of pavement materials, without undertaking real suction tests, should be further validated to encompass a wider range of unbound granular materials.

5. Based on this study, fatigue failure was not evidenced in the applied strain up to 200 με. Thus, additional series of tests are recommended for CTB samples in terms of applying higher levels of applied strain in order to trigger fatigue and eventually produce a fatigue relationship.

6. Further multi-strain fatigue tests are recommended to investigate various durations of applied loading, levels of strain and patterns of loading steps. The test results would then require extensive analysis. For example, using the dissipated energy approach or stiffness degradation approach would further contextualise an appropriate scenario for the test setup.

REFERENCES

AASHTO. (2003). AASHTO Designation: T 307-99 Standard Method of Test for Determining the Resilient Modulus of Soils and Aggregate Materials.

Abojaradeh, M. A., Witczak, M. W., Mamlouk, M. S. and Kaloush, K. E. (2003). Validation of Initial and Failure Stiffness Definitions in Flexure Fatigue Test for Hot Mix Asphalt. *Journal of Testing and Evaluation, 35*(1), 1 - 8.

Adamson, L. (2012). *An Investigation into the Cement Content of Stabilised Pavement.* (Master of Philosophy), Curtin University, Western Australia.

Adaska, W. S. and Luhr, D. R. (2004). *Control of reflective Cracking in Cement Stabilized Pavements.* Paper presented at the Fifth International RILEM Conference on Reflective Cracking in Pavements, Limoges, France.

Adu-Osei, A. (2000). Characterization of Unbound Granular Layers in Flexible Pavements *Report ICAR 502-3*: Texas Transportation Institute, The Texas A&M University System, College Station, Texas.

Allen, J. (1973). *The effect of non-constant lateral pressures of the resilient response of granular materials.* (Doctor of Philosophy), University of Illinois at Urbana-Champaign, Urbana, Illinois.

American Soeciety of Testing and Materials. (2010). ASTM D4760-10 Standard test method for determining fatigue failure of compacted asphalt concrete subjected to repeated flexural bending.

Andrei, D., Witczak, M. W., Schwartz, C. W. and Uzan, J. (2004). Harmonized Resilient Modulus Test Method for Unbound Pavement Materials. *Transportation Research Record: Journal of the Transportation Research Board, 1874*, 29 - 37.

Anochie-Boateng, J., Paige-Green, P. and Mgangira, M. (2009). *Evaluation of Test Methods for Estimating Resilient Modulus of Pavement Geomaterials.* Paper

presented at the The 28th Southern African Transport Conference, Pretoria, South Africa.

Arnold, G. K. (2004). *Rutting of Granular Pavements.* (Doctor of Philosophy), University of Nottingham, Nottingham, England.

Artamendi, I. and Khalid, H. (2004). *Different approaches to depict fatigue of bituminous materials*. Paper presented at the The 15th European Conference of Fracture, Stockholm, Sweden.

Arulrajah, A., Piratheepan, J., Bo, M. W. and Sivakugan, N. (2012). Geotechnical characteristics of recycled crushed brick blends for pavement sub-base applications. *Canadian Geotechnical Journal 49*, 796 – 811.

Attia, M. and Abdelrahman, M. (2010). Modeling the Effect of Moisture on Resilient Modulus of Untreated Reclaimed Asphalt Pavement. *Transportation Research Record: Journal of the Transportation Research Board, No. 2167*, 30 – 40.

Australian Road Research Board. (1991). National workshop on elastic characterisation of unbound pavement materials and subgrades *APRG report No. 3* (pp. 134). Vermont South, Victoria.

Australian Road Research Board. (2003). APRG Technical Note 13 Control of Moisture in Pavements during Construction. Australia.

Austroads. (1992). Pavement design: a guide to the structural design of road pavements *Austroads Publication No. AP-17/92*. Sydney, NSW: Austroads.

Austroads. (2002). Mix Design For Stabilised Pavement Materials. In G. Foley (Ed.), *Austroads Publication No. AP-T16/02*. Sydney, NSW: Austroads.

Austroads. (2003). Development of Performance-Based Specifications for Unbound Granular Materials - Part A: Issues and Recommendations. In B. T. Vuong (Ed.), *Austroads Publication No. AP-T29/03*. Sydney, NSW: Austroads.

Austroads. (2005). Guide to Pavement Technology: Part 1: Introduction to Pavement Technology. In K. Sharp (Ed.), *Austroads Publication No. AGPT01/05*. Sydney, NSW: Austroads.

Austroads. (2006a). AG: PT/T233 Fatigue life of compacted bituminous mixes subject to repeated flexural bending.

Austroads. (2006b). Guide to Pavement Technology Part 4D: Stabilised Materials. In B. Andrews (Ed.), *Austroads Publication No. AGPT04D/06*. Sydney, NSW: Austroads.

Austroads. (2007a). AG: PT/T053 Determination of Permanent Deformation and Resilient Modulus Characteristics of Unbound Granular Materials Under Drained Conditions.

Austroads. (2007b). Optimum Use of Granular Bases: Material Selection for Detailed Performance Evaluation. In B. Vuong, G. Jameson & L. Choummanivong (Eds.), *Austroads Publication No. AP–T85/07*. Sydney, NSW: Austroads.

Austroads. (2008a). Construction Report for Cemented Test Pavements – Influence of Vertical Loading on the Performance of Unbound and Cemented Materials. In R. Yeo (Ed.), *Austroads Publication No. AP–T103/08*. Sydney, NSW: Austroads.

Austroads. (2008b). The Development and Evaluation of Protocols for the Laboratory Characterisation of Cemented Materials. In R. Yeo (Ed.), *Austroads Publication No. AP–T101/08*. Sydney, NSW: Austroads.

Austroads. (2008c). Fatigue Performance of Cemented Materials under Accelerated Loading – Influence of Vertical Loading on the Performance of Unbound and

Cemented Materials. In R. Yeo (Ed.), *Austroads Publication No. AP–T102/08*. Sydney, NSW: Austroads.

Austroads. (2008d). Technical Basis of Austroads Guide to Pavement Technology Part 2: Pavement Structural Design. In G. Jameson (Ed.), *Austroads Publication No. AP–T98/08*. Sydney, NSW: Austroads.

Austroads. (2010a). Assessment of Rut-resistance of Granular Bases using the Repeated Load Triaxial Test. In G. Jameson, B. Vuong, M. Moffatt, A. Martin & S. Lourensz (Eds.), *Austroads Publication No. AP–R360/10*. Sydney, NSW: Austroads.

Austroads. (2010b). Cost effective structural treatments for rural highways: cemented materials. In A. Gonzalez, A. Howard & R. d. Carteret (Eds.), *Austroads Publication No. AP-T168/10*. Sydney, NSW: Austroads.

Austroads. (2010c). Guide to Pavement Technology Part 2: Pavement Structural Design. In G. Jameson (Ed.), *Austroads Publication No. AGPT02/10*. Sydney, NSW: Austroads.

Austroads. (2012a). Development of a Nonlinear Finite Element Pavement Response to Load Model. In A. Gonzalez, D. Bodin, G. Jameson, M. Oeser & B. Vuong (Eds.), *Austroads Publication No. AP–T199-12*. Sydney, NSW: Austroads.

Austroads. (2012b). Preliminary Investigation of the Influence of Micro-cracking on Fatigue Life of Cemented Materials. In G. Jameson & A. Howard (Eds.), *Austroads Publication No. AP–T198-12*. Sydney, NSW: Austroads.

Austroads. (2013a). Feasibility Study of using Wheel-tracking Tests and Finite Element Modelling for Pavement Permanent Deformation Prediction. In D. Bodin, M. Moffatt & A. Lim (Eds.), *Austroads Publication No. AP-T228-13*. Sydney, NSW: Austroads.

Austroads. (2013b). Review of Definition of Modified Granular Materials and Bound Materials. In G. Jameson (Ed.), *Austroads Publication No. AP-R434-13*. Sydney, NSW: Austroads.

Azam, A. M. and Cameron, D. A. (2013). Geotechnical Properties of Blends of Recycled Clay Masonry and Recycled Concrete Aggregates in Unbound Pavement Construction. *Journal of Material in Civil Engineering, 25*(6), 788 - 798.

Baburamani, P. (1999). Research Report ARR 334 Aspahlt fatigue life prediction models- A literature review. Vermont South, Victoria: ARRB Transport Research Ltd.

Barksdale, R. D., Alba, J., Khosla, N. P., Kim, R., Lambe, P. C. and Rahman, M. S. (1997). Laboratory determination of resilient modulus for flexible pavement design *NCHRP Web Document 14 (Project 1-28)*: Transportation Research Board, National Research Council.

Bishop, A. W. (1959). The principle of effective stress. *Tecknish Ukeblad, 109*(39), 859-863.

Boyce, J. R. (1976). *The Behaviour of Granular Materials Under Repeated Loading.* (Doctor of Philosophy), University of Nottingham, England.

Boyce, J. R. (1980). *A nonlinear model for the elastic behaviour of granular materials under repeated loading.* Paper presented at the International symposium on soils under cyclic and transient loading, Swansea, Wales.

Boyce, J. R., Brown, S. F. and Pell, P. S. (1976). *The resilient behaviour of a granular material under repeated loading.* Paper presented at the The 8th ARRB Conference.

Brooks, R. H. and Corey, A. T. (1964) Hydraulic properties of porous media. *Colorado Hydrology Paper No. 3 (March)*: Colorado State University, Fort Collins.

Brown, S. F. (1996). Soil Mechanics in Pavement Engineering. *Geotechnique, 46*(3), 383 - 426.

Brown, S. F. and Pell, P. S. (1967). *An experimental investigation of the stresses, strains and deflections in a layered pavement structure subjected to dynamic loads.* Paper presented at the 2nd International Conference on the Structural Design of Asphalt Pavements, University of Michigan, Ann Arbor, USA.

Brutsaert, W. (1966). Some methods of calculating unsaturated permeability. *Transactions of the ASAE (American Society of Agricultural Engineers), 10*, 400-404.

Butkus, F. (2004). *Pavement Engineering Report No. 2004/14 M*. Main Roads Western Australia, Western Australia.

Cameron, D. A., Azam, A. and Rahman, M. M. (2011). *Properties of recycled demolition waste for pavement construction.* Paper presented at the International Conference on Advances in Geotechnical Engineering 2011, Perth, Australia.

Cary, C. E. and Zapata, C. E. (2011). Resilient modulus for unsaturated unbound materials. *Road Materials and Pavement Design, 12*(3), 615-638.

Cauley, R. F. and Kennedy, T. W. (1972). Improved Tensile Strength for Cement-Treated Base and Subbase *Report No. 98-11*: Center for Highway Research, The University of Texas at Austin, Texas.

Cerni, G., Cardone, F., Virgili, A. and Camilli, S. (2012). Characterisation of permanent deformation behaviour of unbound granular materials under repeated triaxial loading. *Construction and Building Materials, 28*, 79-87.

Chakrabarti, S. and Kodikara, J. (2005). Shrinkage Behaviour of Crushed Basaltic Rock and Residual Clay Mixture Stabilised with Cementitious Binders. *International Journal of Pavement Engineering, 6*(1), 27-37.

Chan, F. W. K. (1990). *Permanent deformation resistance of granular layers in pavements.* (Doctor of Philosophy), University of Nottingham, Nottingham, England.

Chazallon, C., Hornych, P. and Mouhoubi, S. (2006). Elastoplastic Model for the Long-Term Behavior Modeling of Unbound Granular Materials in Flexible Pavements. *International Journal of Geomechanics, 6*(4), 279 – 289.

Chen, D. H., Chang, G. and Fu, H. (2011). Limiting Base Moduli to Prevent Premature Pavement Failure. *Journal of Performance of Constructed Facilities, 25*(6), 587-597.

Chen, D. H., Hong, F. and Zhou, F. (2011). Premature Cracking from Cement-Treated Base and Treatment to Mitigate Its Effect. *Journal of Performance of Constructed Facilities, 25*(2), 113 - 120.

Chen, D. H., Scullion, T., Lee, T. C. and Bilyeu, J. (2008). Results from a Forensic Investigation of a Failed Cement Treated Base. *Journal of Performance of Constructed Facilities, 22*(3), 143 - 153.

Cho, Y. H., Lee, K. W. and Ryu, S. W. (2006). Development of Cement-Treated Base Material for Reducing Shrinkage Cracks. *Transportation Research Record, Journal of the Transportation Research Board, 1952* 134–143.

Christopher, B. R., Schwartz, C. and Boudreau, R. (2006). *FHWA NHI-05-037 Geotechnical Aspects of Pavements*. National Highway Institute, Federal Highway Administration, U.S. Department of Transportation, Washington, D.C.

Dassault Systèmes. (2010). *Abaqus/CAE User's Manual*. Providence, RI, USA.

Department of Planning Transport and Infrastructure. (2011). Specification, Part 215 Supply of Pavement Materials. South Australia.

Department of Transport and Mainroads. (2012). MRTS08 Plant-Mixed Stabilised Pavements using Cement or Cementitious Blends. Queeensland.

Dunlap, W. A. (1963). A report on mathematical model describing the deformation characteristics of granular materials *Technical Report no. 1, Project 2-8-62-27*: Transportation Institute, Texas, USA.

Dunlop, R. J., Moss, P. J. and Dodd, T. A. H. (1975). *Prediction of Cracking in Soil-cement.* Paper presented at the 2nd Australia-New Zealand Conference on Geomechanics Brisbane, Queensland, Australia.

Duske, G. C. and Pender, M. J. (1998). *Measurement of Resilient Modulus and Permanent Strain Behaviour of Roading Materials.* Paper presented at the Roading Geotechnics 98 : New Zealand Geotechnical Society Symposium 1998, Auckland.

Dynatest. CSIR Licensed Products. Retrieved January 2014 www.dynatest.com/download.ashx?m=1561

Edwards, J. P. (2007). *Laboratory Characterisation of Pavement Foundation Materials.* (Doctor of Engineering), Loughborough University.

Ekblad, J. and Isacsson, U. (2007). Time-domain reflectometry measurements and soil-water characteristic curves of coarse granular materials used in road pavements. *Canadian Geotechnical Journal,, 44*(7), 858-872.

Feliberti, M., Nazarian, S. and Srinivasan, T. (1992). *Critical evaluation of parameters affecting resilient modulus tests on subgrades*. Center for Geotechnical and Highway Materials Research, The University of Texas at El Paso.

Fredlund, D. G. (1979). Second Canadian Geotechnical Colloquium: Appropriate concepts and technology for unsaturated soils. *Canndian Geotechnical Journal, 16*, 121 - 139.

Fredlund, D. G. (1995). *The scope of unsaturated soil mechanics: an overview. Invited keynote address.* Paper presented at the Proceeding of the First International Conference on Unsaturated Soils, Paris, France, 6-8 September 1995.

Fredlund, D. G. (2000). The 1999 R. M. Hardy Lecture: The implementation of unsaturated soil mechanics into geotechnical engineering. *Canadian Geotechnical Journal, 37*(5), 963-986.

Fredlund, D. G. (2002). *Use of the soil-water characteristic curve in the implementation of unsaturated soil mechanics.* Paper presented at the Proceeding of the 3rd International Conference on Unsaturated Soils, Recife, Brazil, 10-13 March 2002.

Fredlund, D. G., Began, A. T. and Wong, P. K. (1977). Relation between resilient modulus and stress conditions for cohesive subgrade soils. *Transportation Research Record, 642*, 73-81.

Fredlund, D. G. and Pham, H. Q. (2006). *A volume-mass constitutive model for unsaturated soils in terms of two independent stress state variables.* Paper presented at the Proceeding of the Fourth International Conference on Unsaturated Soils, ASCE, Carefree, Arizona.

Fredlund, D. G., Sheng, D. C. and Zhao, J. D. (2011). Estimation of soil suction from the soil-water characteristic curve. *Canadian Geotechnical Journal,, 48*(2), 186-198.

Fredlund, D. G. and Xing, A. (1994). Equations for the soil-water characteristic curve. *Canadian Geotechnical Journal,, 31*(4), 521-532.

Gabr, A. R. and Cameron, D. A. (2012). Properties of Recycled Concrete Aggregate for Unbound Pavement Construction. *Journal Of Material in Civil Engineering, 24*(6), 754 – 764.

Garber, S., Rasmussen, R. O. and Harrington, D. (2011). Cement-Treated Base, *Guide to Cement-Based Intregrated Pavement Solutions* (pp. 6-1 – 6-5): Portland Cement Association, Skokie, Illinois

Gardner, W. R. (1958). Some steady state solutions of the unsaturated moisture flow equation with application to evaporation from a water table. *Soil Science, 85*(4), 228-232.

Gidel, G., Hornych, P., Chauvin, J.-J., Breysse, D. and Denis, A. (2001). Anew approach for investigating the permanent deformation behaviour of unbound granular material using the repeated load triaxial apparatus. *Bulletin des Laboratoires des Ponts et Chaussees, 223*(4359), 5 - 21.

Gitirana, G. F. N. and Fredlund, D. G. (2004). Soil-water characteristic curve equation with independent properties. *Journal of Geotechnical and Geoenvironmental Engineering, 130*(2), 209-212.

Goerge, K. P. (1968). Shrinkage Characteristic of Soil-Cement Mixtures. *Highway Research Record, No. 255*, 42-58.

Goerge, K. P. (2002). Minimizing Cracking in Cement-Treated materials for Improved Performance *Research and Development Bulletin RD123*: Portland Cement Association, Skokie, Illinois.

Guo, P. and Emery, J. (2011). Importance of strain level in evaluating resilient modulus of granular materials. *International Journal of Pavement Engineering, 12*(2), 187 – 199.

Halsted, G. E. (2010). *Minimizing Reflective Cracking in Cement-Stabilised Pavement Bases.* Paper presented at the Annual Conference of the Transportation Association of Canada, Halifax, Nova Scotia.

Harris, D. and Lockwood, N. (2009). *Pavement Engineering Report No. 2009/5 M*. Main Roads Western Australia, Western Australia.

Heath, A., Pestana, J., Harvey, J. and Bejerano, M. (2004). Normalizing Behavior of Unsaturated Granular Pavement Materials. *Journal of Geotechnical and Geoenvironmental Engineering, 130*(9), 896-904.

Hicks, R. G. (1970). *Factors influencing the resilient properties of granular materials.* (Doctor of Philosophy), University of California, Berkeley, Berkeley, California.

Hicks, R. G. and Monismith, C. L. (1971). Factors influencing the resilient response of granular materials. *Highway Research Record, No.345*, 15 - 31.

Huang, Y. H. (2004). *Pavement Analysis and Design* (2 ed.). Upper Saddle River, NJ: Pearson Prentice Hall.

Huurman, M. (1997). *Permanent deformation in concrete block pavements.* (Doctor of Philosophy), Delft University of Technology, Netherlands.

Jin, M. S., Lee, K. W. and Kovacs, W. D. (1994). Seasonal Variation of Resilient Modulus of Subgrade Soils. *Journal of Transportation Engineering, 120*(4), 603 – 616.

Johnson, T. C., Berg, R. L. and Dimillo, A. (1986). Frost action predictive techniques: an overview of research results. *Transportation Research Record, Jounal of Transportation Research Board, 1089*, 147-161.

Jotisankasa, A., Coop, M. and Ridley, A. (2009). The mechanical behaviour of an unsaturated compacted silty clay. *Géotechnique, 59*(5), 415 - 428.

Kalcheff, I. V. and Hicks, R. G. (1973). A Test Procedure for Determining the Resilient Properties of Granular Materials. *Journal of Testing and Evaluation, 6*(1), 472 - 479.

Keeley, R. (2004). *Stabilisation of pavement materials in Western Australia.* Paper presented at the Seminar on Austroads and Industry Developments in Road Stabilisation, Perth, Western Australia.

Khalili, N. and Khabbaz, M. H. (1998). A unique relationship for χ for the determination of the shear strength of unsaturated soils. *Géotechnique, 48*(5), 681-687.

Khoury, N., Brooks, R., Zaman, M. M. and Khoury, C. N. (2009). Variations of Resilient Modulus of Subgrade Soils with Postcompaction Moisture Contents. *Transportation Research Record, Jounal of Transportation Research Board, 2101*, 72 - 81.

Khoury, N. N. and Zaman, M. (2004). Correlation among resilient modulus, moisture variation and soil suction for subgrade soil. *Transportation Research Record, Jounal of Transportation Research Board, 1874*, 99-107.

Kodikara, J. (2006). *Cenceptual Approaches for Considering Shrinkage Cracking in the Cement Stabilised Pavement Mix Design.* Paper presented at the The 22nd ARRB Conference, Canberra, ACT.

Kolisoja, P. (1997). *Resilient deformation characteristics of granular materials.* (Doctor of Philosophy), Tampere University of Technology, Tampere, Finland.

Lekarp, F., Isacsson, U. and Dawson, A. (2000a). State of the Art I: Resilient Response of Unbound Aggregates. *Journal of Transportation Engineering, 26*(1), 66 - 75.

Lekarp, F., Isacsson, U. and Dawson, A. (2000b). State of the Art II: Permanent Strain Response of Unbound Aggregates. *Journal of Transportation Engineering, 26*(1), 76 - 83.

Liang, R., Rabab'ah, S. and Khasawneh, M. (2008). Predicting moisture-dependent resilient modulus of cohesive soils using soil suction concept. *Journal of Transportation Engineering, 134*(1), 34-40.

Little, N. D., Scullion, T., Kota, P. B. V. S. and Bhumiyan, J. (1995). Guidelines for Mixture Design and Thickness Design for Stabilised Bases and Subgrades

Report No. FHWA/TX-95/1287-3F: Texas Transportation Institute, The Texas A&M University System College Station, Texas.

Main Roads Western Australia. (2008). Specification 501 Pavements. Western Australia: Main Roads Western Australia.

Main Roads Western Australia. (2009). Specification 501 Pavements. Western Australia: Main Roads Western Australia.

Main Roads Western Australia. (2010a). Engineering Road Note 9. Western Australia: Main Roads Western Australia.

Main Roads Western Australia. (2010b). Specification 501 Pavements. Western Australia: Main Roads Western Australia.

Main Roads Western Australia. (2011a). Specification 501 Pavements. Western Australia: Main Roads Western Australia.

Main Roads Western Australia. (2011b). Test Method WA 110.1 Soil and Granular Pavement Material Moisture Content: Convection Method. Western Australia: Main Roads Western Australia.

Main Roads Western Australia. (2011c). Test Method WA 115.1 Particle Size Distribution: Sieving and Decantation Method. Western Australia: Main Roads Western Australia.

Main Roads Western Australia. (2011d). Western Australian Road Hierarchy.

Main Roads Western Australia. (2012a). Specification 501 Pavements. Western Australia: Main Roads Western Australia.

Main Roads Western Australia. (2012b). Test Method WA 133.1 Dry Density/Moisture Content Relationship: Modified Compaction Fine and Medium Grained Soils. Western Australia: Main Roads Western Australia.

Main Roads Western Australia. (2012c). Test Method WA 143.1 Determination of the Unconfined Compressive Strength of Laboratory Compacted Specimens. Western Australia: Main Roads Western Australia.

Main Roads Western Australia. (2012d). Test Method WA 143.2 Determination of the Unconfined Compressive Strength of Hydrated Cement Treated Crushed Rock Base. Western Australia: Main Roads Western Australia.

McKee, C. R. and Bumb, A. C. (1987). Flow-testing coalbed methane production wells in the presence of water and gas. *Society of Petroleum Engineering (SPE) Formation Evaluation, Richardson, Texas*, 599-608.

Midgley, L. (2009). *Best Practice for the Preparation of New Granular Pavements for Thin Bituminous Surfacing.* Paper presented at the The 13rd International Flexible Pavements Conference, Queensland, Australia.

Mincad Systems. (2009). *Circly 5 User Manual*.

Molenaar, A. A. A., Xuan, D., Houben, L. J. M. and Shui, Z. (2011). *Prediction of the Mechanical Characteristics of Cement Treated Demolition Waste for Road Bases and Subbase.* Paper presented at the The 10th Conference on Asphalt Pavements for Southern Africa, KwaZulu-Natal, South Africa.

Monismith, C. L., Seed, H. B., Mitry, F. G. and Chan, C. K. (1967). *Prediction of pavement deflections from laboratory tests.* Paper presented at the 2nd International Conference on the Structural Design of Asphalt Pavements, University of Michigan, Ann Arbor, MI, USA.

Morgan, J. R. (1966). *The response of granular materials to repeated loading.* Paper presented at the The 3rd ARRB Conference.

Nataatmadja, A. (1992). *Resilient modulus of granular materials under repeated loading.* Paper presented at the 7th International Conference on Asphalt Pavements, Nottingham, UK.

Nataatmadja, A. and Parkin, A. K. (1989). Characterization of granular material for pavement analysis. *Canadian Geotechnical Journal,, 26*(4), 725-730.

National Cooperative Highway Research Program. (2000). Appendix DD-2: Resilient Modulus as Function of Soil Moisture-A Study of the Expected Changes in Resilient Modulus of the Unbound Layers with Changes in Moisture for 10 LTPP sites. In I. ARA, ERES Division (Ed.), *NCHRP Project 1-37A: Guide for Mechanistic–Empirical Design of New and Rehabilitated Pavement Structures.* Washington, D.C.: Transportation Research Board, National Research Council.

National Cooperative Highway Research Program. (2004a). Laboratory Determination of Resilient Modulus for Flexible Pavement Design *Research Results Digest No. 285*: Transportation Research Board of the National Academies.

National Cooperative Highway Research Program. (2004b). NCHRP Project 1-37A Guide for Mechanistic -Empirical Design of New and Rehabilitated Pavement Structures. In I. ARA, ERES Consultants Division (Ed.): Transportation Research Board, National Research Council.

National Cooperative Highway Research Program. (2008). NCHRP Synthesis 382 Estimating Stiffness of Subgrade and Unbound Materials for Pavement Design. In A. J. Puppala (Ed.), *A Synthesis of Highway Practice*. Washington, D.C.: Transportation Research Board of the National Academies.

Parreira, A. B. and Goncalves, R. F. (2000). *The influence of moisture content and soil suction on the Resilent modulus of a lateritic subgrade soil.* Paper presented at the International Conference on Geotechnical and Geological Engineering, Melbourne, Australia.

Payne, G. (2012). Arteries of Life: The Complete Process for Building and Upgrading Roads in Western Australia and; Roads in the Southern River Electorate *Internship Report*. Murdoch University.

Pereira, J. and Fredlund, D. G. (2000). Volume change behavior of collapsible compacted gneiss soil. *Journal of Geotechnical and Geoenvironmental Engineering, 126*(10), 907-916.

Puppala, A. J., Mohammad, L. N. and Allen, A. (1999). Permanent deformation characterization of subgrade soils from RLT test. *Journal of Materials in Civil Engineering, 11*(4), 274 - 282.

Puppala, A. J., Saride, S. and Chomtid, S. (2009). Experimental and Modeling Studies of Permanent Strains of Subgrade Soils. *Journal of Geotechnical and Geoenvironmental Engineering, 135*(10), 1379 - 1389.

Rada, G. and Witczak, M. W. (1981). Comprehensive Evaluation of Laboratory Resilient Moduli Results for Granular Material. *Transportation Research Record: Journal of the Transportation Research Board, 810*, 23 - 33.

Rehman, S. (2012). *Materials Engineering Report No. 2010-13M*. Main Roads Western Australia, Western Australia.

Roads and Maritime Services. (2013). QA Specification R73 Construction of Plant Mixed Heavily Bound Pavement Course. New South Wales.

Roads Corporation. (2011). Standard Documents, Section 815 Cementitious Treated Crushed Rock for Pavement Subbase. Victoria.

Saleh, M., Dixit, V. and Radwan, E. (2009). Validation of the Austroads quasi nonlinear sublayering approach for the design of flexible pavements. *Road and Transport Research, 18*(2), 27 - 38.

Sawangsuriya, A., Edil, T. and Benson, C. (2009). Effect of suction on resilient modulus of compacted fine-grained subgrade soils. *Transportation Research Record: Journal of the Transportation Research Board, 2101*, 82-87.

Scullion, T. (2002). Field Investigation: Pre-Cracking of Soil-Cement Bases to Reduce Reflection Cracking. *Transportation Research Record, Jounal of Transportation Research Board, 1787*, 22 - 30.

Scullion, T., Sebesta, S., Harris, J. P. and Syed, I. (2005). Evaluating the Performance of Soil-Cement and Cement-Modified Soil for Pavements: A Laboratory Investigation *Research and Development Bulletin RD 120*: Portland Cement Association, Skokie, Illinois.

Seed, H. B., Chan, C. K. and Lee, C. E. (1962). *Resilience characteristics of subgrade soils and their relation to fatigue failures in asphalt pavements.* Paper presented at the Proceeding Conference on the Structural Design of Asphalt Pavements, University of Michigan, Ann Arbor, Michigan.

Seed, H. B., Mitry, F. G., Monismith, C. L. and Chan, C. K. (1965). Predictions of pavement deflection from laboratory repeated load tests *Report No. TE-65-6*: Soil Mechanics and Bituminous Material Research Laboratory, University of California, Berkeley.

Semmelink, C. J. (1991). *The Use of the DRTT K-Mould to Determine the Elastic and Shear Properties of Pavement Materials*. Pretoria, South Africa: Division of Roads and Transport Technology, CSIR.

Seyhan, U. and Tutumluer, E. (1998). *Characteristic of Unbound Aggregates Using the New Fastcell.* Paper presented at the The 1999 Federal Aviation Administration Technology Transfer Conference.

Sillers, W. S., Fredlund, D. G. and Zakerzaheh, N. (2001). Mathematical attributes of some soil–water characteristic curve models. *Geotechnical and Geological Engineering, 19*(3-4), 243-283.

Smith, R. E. (1974). A Laboratory Study of Factors Affecting the Shrinkage Characteristics of Cement Treated Base *Contract No. D3-3-34*: FHWA.

Souliman, M., Zeiada, W. A., Kaloush, K. E. and Mamlouk, M. S. (2012). *Assessment of different flexure fatigue failure analysis methods to estimate the number of cycles to failure of asphalt mixtures.* Paper presented at the 3rd Conference on Four-Point Bending, DAVIS, CA, USA.

Standards Australia. (1992). AS 1012.13-1992 Determination of Drying Shrinkage of Concrete for Samples Prepared in the Field or in the Laboratory. Sydney, New South Wales.

Standards Australia. (1995). AS 1289.6.8.1 Methods of Testing Soils for Engineering Purposes. Sydney, New South Wales.

Standards Australia. (1997). AS 3972-1997 Portland and Blended Cements. Sydney, New South Wales.

Steven, B. D. (2005). *The Development and Verification of a Pavement Response and Performance Model for Unbound Granular Pavements.* (Doctor of Philosophy), University of Canterbury, New Zealand.

Theyse, H. L. (2000). *The development of mechanistic-empirical permanent deformation design models for unbound pavement materials from laboratory and accelerated pavement test data.* Paper presented at the 5th International Symposium on Unbound Aggregate in Roads.

Theyse, H. L., Legge, T. F. H., Pretorious, P. C. and Wolff, H. (2007). A yield strength model for partially saturated unbound granular material. *International Journal of Road Materials and Pavement Design, 8*(3), 423-448.

Thom, N. H. and Brown, S. F. (1987). Effect of moisture on the structural performance of a crushed-limestone road base. *Transportation Research Record, 1121*, 50 – 56.

Tseng, K.-H. and Lytton, R. L. (1989) Prediction of Permanent Deformation in Flexible Pavement Materials. *ASTM STP 1016 Implication of Aggregates in the Design, Construction,and Performance of Flexible Pavements*: ASTM.

United States Department of Transport. (2003). Standard Specifications for Construction of Roads and Bridges on Federal Highway Projects. Washington, DC.: Federal Highway Administration, U.S. Department of Transport.

Uthus, L. (2007). *Deformation Properties of Unbound Granular Aggregates.* (Philosophiae Doctor), Norwegian University of Science and Technology, Trondheim, Norway.

Uzan, J. (1985). Characterization of granular material. *Transportation Research Record, No.1022*, 52 - 59.

van-Blerk, P. G. and Scullion, T. (1995). Evaluation of Stabilzed Base Durability Using a Modified South African Wheel Tracking Device *Research Report No. TX-96/2919-1*: Texas Transportation Institute, The Texas A&M University System College Station, Texas.

van-Genuchten, M. T. (1980). A closed-form equation for predicting the hydraulic conductivity of unsaturated soil. *Soil Science Society of America Journal,, 44*, 892-898.

Vanapalli, S. K., Fredlund, D. G. and Pufahl, D. E. (1999). The influence of soil structure and stress history on the soil structure and stress history on the soil-water characteristics of a compacted till. *Géotechnique, 49*(2), 143-159.

Veverka, V. (1979). Raming van de spoordiepte bij wegen met een bitumineuze verharding. *De Wegentechniek, 24*(3), 25–45 (in Dutch).

Vuong, B. T. and Arnold, G. (2006). Predicting in-service performance of alternative pavement materials for New Zealand conditions *Land Transport New*

Zealand Research Report 304. Wellington, New Zealand: Land Transport New Zealand.

Vuong, B. T. and Brimble, R. (2000). APRG 00/33 (MA) – Determination of Permanent Deformation and Resilient Modulus Characteristics of Unbound Granular Materials Under Drained Conditions.

Walker, P. J. (1997). Measurement of total suction and matric suction in pavement materials at Dandenong ALF site. *Road and Transport Research, 6*(4), 48 - 58.

Washington State Department of Transportation (WSDOT). (2005). *Everseries User's Guide*.

Witczak, M. W. and Uzan, J. (1988). The universal airport pavement design system *Report I of V: Granular material characterization*: University of Maryland, USA.

Wu, P. (2011). Cement-Bound Road Base Materials *Report 7-11-218-1*: Delft University of Technology, Netherlands.

Yang, R. R., Huang, W. H. and Tai, Y. T. (2005). Variation of resilient modulus with soil suction for compacted subgrade soils. *Transportation Research Record, Jounal of Transportation Research Board, 1913*, 99-106.

Yeo, Y. S. (2011). *Characterization of Cement Treated Crushed Rock Basecourse for Western Australian Roads.* (Doctor of Philosophy), Curtin University, Western Australia.

Yeo, Y. S. and Nikraz, H. (2011). Cement Stabilisation of Road Base Course: A chonological Development in Western Australia. *Australian Geomechanics, 46*(3), 53-62.

Zhang, J., Hou, D. W. and Han, Y. D. (2012). Micromechanical Modeling on Autogenous and Drying Shrinkages of Concrete. *Construction and Building Materials, 29*, 230-240.

APPENDIX :

RLT TEST RESULTS

Table A1: Properties of test samples used for the resilient modulus tests

Sample ID	Hydration period (days)	Water addition for compaction *	Target dryback	Dry density (t/m^3)	% moisture after dryback
M7A-NoDB			No dryback	2.103	5.60
M7A-80%DB	7	A	80%	2.091	5.04
M7A-60%DB			60%	2.099	3.78
M7B-NoDB			No dryback	2.151	6.23
M7B-80%DB	7	B	80%	2.140	5.04
M7B-60%DB			60%	2.159	3.78
M7C-NoDB			No dryback	2.208	7.05
M7C-80%DB	7	C	80%	2.217	5.82
M7C-60%DB			60%	2.223	4.37
M14A-NoDB			No dryback	2.098	5.19
M14A-80%DB	14	A	80%	2.119	5.04
M14A-60%DB			60%	2.113	3.78
M14B-NoDB			No dryback	2.221	6.19
M14B-80%DB	14	B	80%	2.215	5.04
M14B-60%DB			60%	2.193	3.78
M14C-NoDB			No dryback	2.193	7.30
M14C-80%DB	14	C	80%	2.201	5.84
M14C-60%DB			60%	2.196	4.38
M28A-NoDB			No dryback	2.087	5.10
M28A-80%DB	28	A	80%	2.087	5.10
M28A-60%DB			60%	2.057	3.78
M28B-NoDB			No dryback	2.160	6.15
M28B-80%DB	28	B	80%	2.157	5.04
M28B-60%DB			60%	2.127	3.78
M28C-NoDB			No dryback	2.185	7.14
M28C-80%DB	28	C	80%	2.171	5.86
M28C-60%DB			60%	2.194	4.39
M45A-NoDB			No dryback	2.058	4.84
M45A-80%DB	45	A	80%	2.058	4.84
M45A-60%DB			60%	2.088	3.78
M45B-NoDB			No dryback	2.111	6.17
M45B-80%DB	45	B	80%	2.114	5.04
M45B-60%DB			60%	2.103	3.78
M45C-NoDB			No dryback	2.182	7.31
M45C-80%DB	45	C	80%	2.203	5.56
M45C-60%DB			60%	2.211	4.57

* For type A, each mix was compacted without additional water (i.e., in its state of moisture at the end of the hydration period). Type B represents the amount of water that was added to the HCTCRB samples during compaction, up to the OMC of the CRB–cement mixture (6.26%). Lastly, type C samples were the samples to which water was added to reach the OMC of the individual hydration period.

Table A2: Properties of test samples used for the permanent deformation tests

Sample ID	Hydration period (days)	Water addition for compaction *	Target dryback	Dry density (t/m^3)	% moisture after dryback
P7A-NoDB			No dryback	2.117	5.63
P7A-80%DB	7	A	80%	2.107	5.04
P7A-60%DB			60%	2.099	3.78
P7B-NoDB			No dryback	2.162	6.15
P7B-80%DB	7	B	80%	2.165	5.04
P7B-60%DB			60%	2.175	3.78
P7C-NoDB			No dryback	2.216	7.16
P7C-80%DB	7	C	80%	2.222	5.82
P7C-60%DB			60%	2.207	4.37
P14A-NoDB			No dryback	2.110	5.19
P14A-80%DB	14	A	80%	2.060	5.04
P14A-60%DB			60%	2.124	3.78
P14B-NoDB			No dryback	2.200	6.16
P14B-80%DB	14	B	80%	2.221	5.04
P14B-60%DB			60%	2.194	3.78
P14C-NoDB			No dryback	2.187	7.30
P14C-80%DB	14	C	80%	2.192	5.84
P14C-60%DB			60%	2.186	4.38
P28A-NoDB			No dryback	2.081	5.10
P28A-80%DB	28	A	80%	2.081	5.10
P28A-60%DB			60%	2.062	3.78
P28B-NoDB			No dryback	2.208	6.15
P28B-80%DB	28	B	80%	2.154	5.04
P28B-60%DB			60%	2.127	3.78
P28C-NoDB			No dryback	2.191	6.98
P28C-80%DB	28	C	80%	2.197	5.86
P28C-60%DB			60%	2.194	4.40
P45A-NoDB			No dryback	2.050	4.87
P45A-80%DB	45	A	80%	2.050	4.87
P45A-60%DB			60%	2.088	3.78
P45B-NoDB			No dryback	2.111	6.17
P45B-80%DB	45	B	80%	2.114	5.04
P45B-60%DB			60%	2.103	3.78
P45C-NoDB			No dryback	2.182	7.31
P45C-80%DB	45	C	80%	2.203	5.56
P45C-60%DB			60%	2.211	4.57

* For type A, each mix was compacted without additional water (i.e., in its state of moisture at the end of the hydration period). Type B represents the amount of water that was added to the HCTCRB samples during compaction, up to the OMC of the CRB–cement mixture (6.26%). Lastly, type C samples were the samples to which water was added to reach the OMC of the individual hydration period.

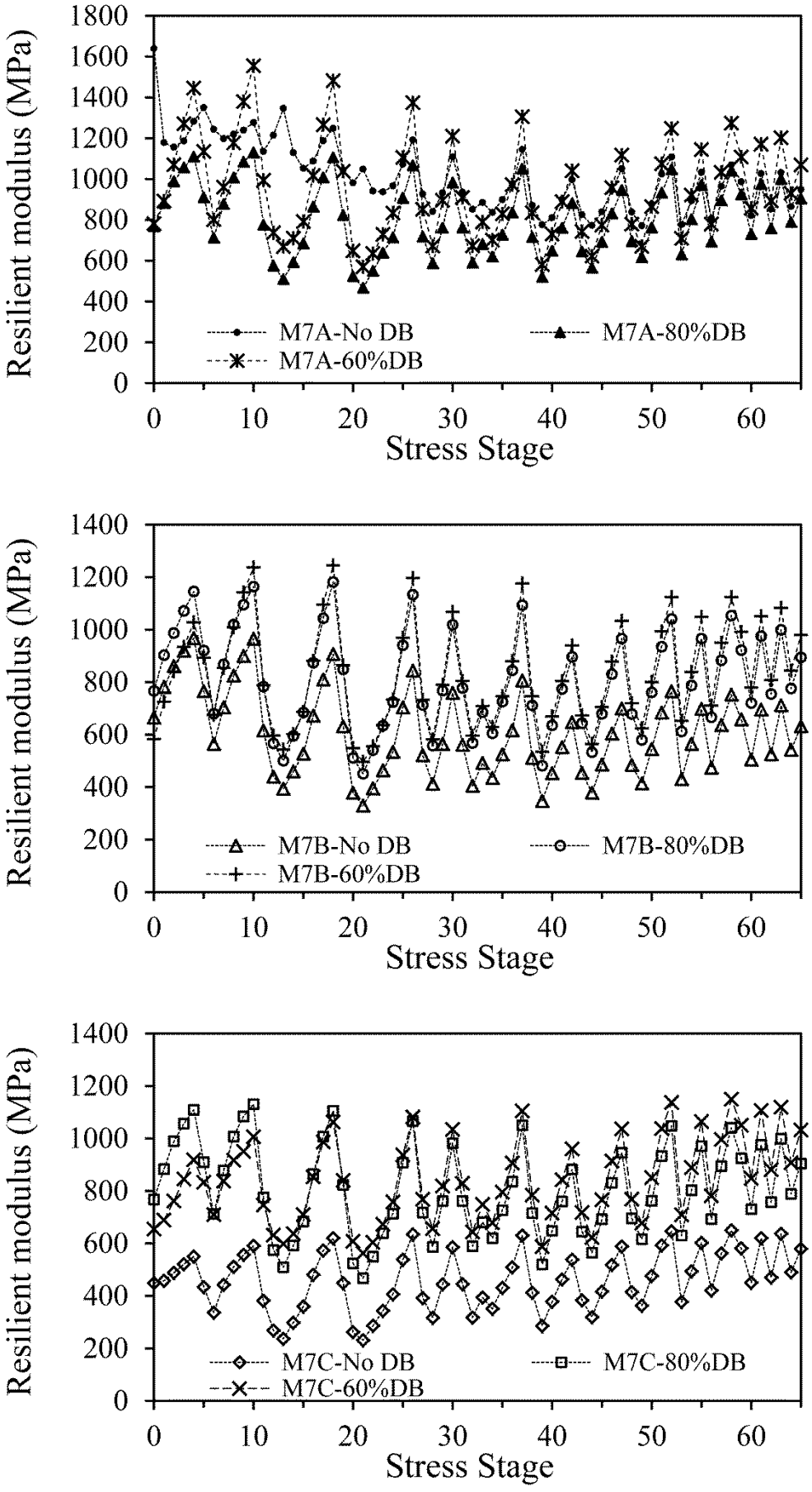

Figure A1: Resilient modulus test results for 7-day hydration period

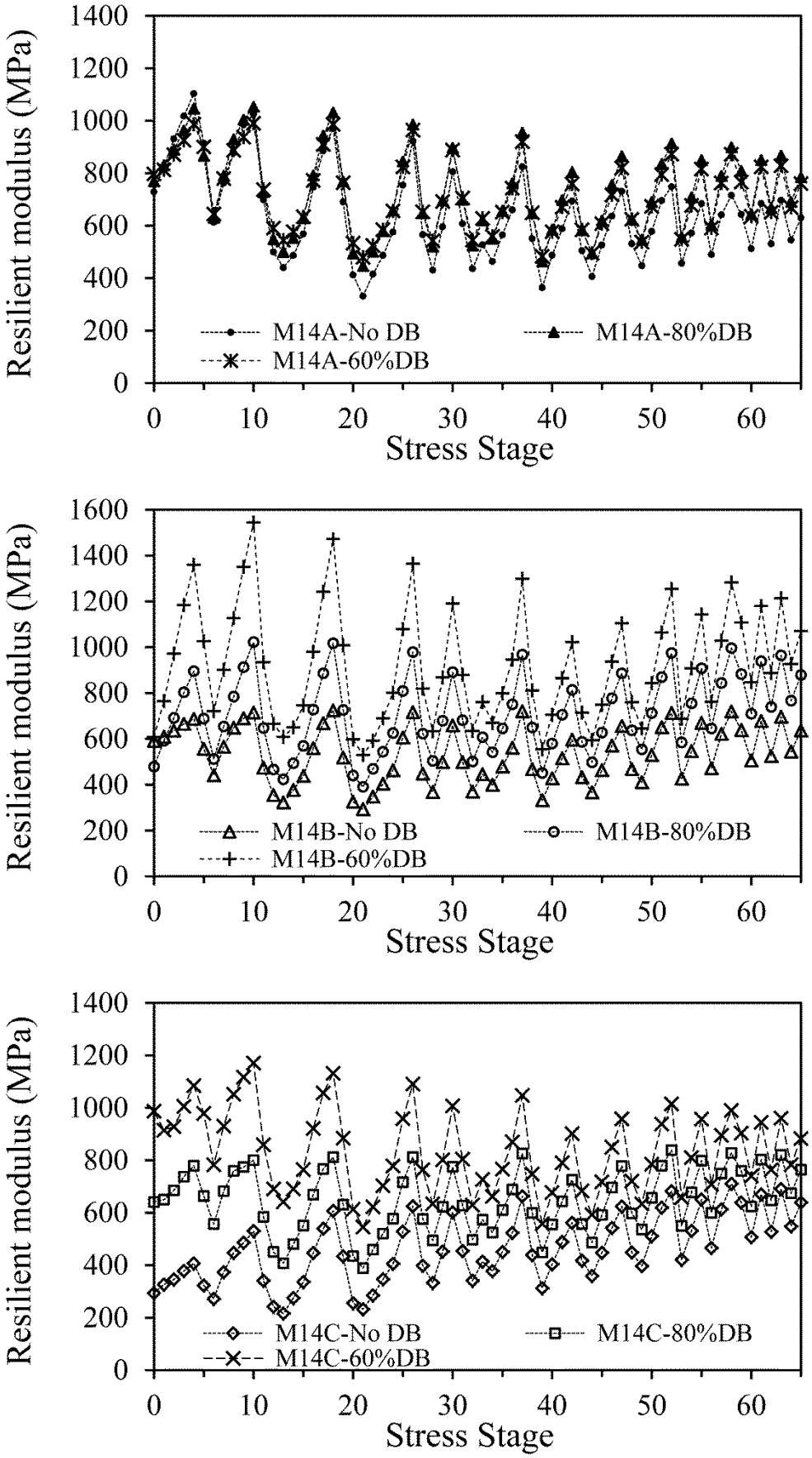

Figure A2: Resilient modulus test results for 14-day hydration period

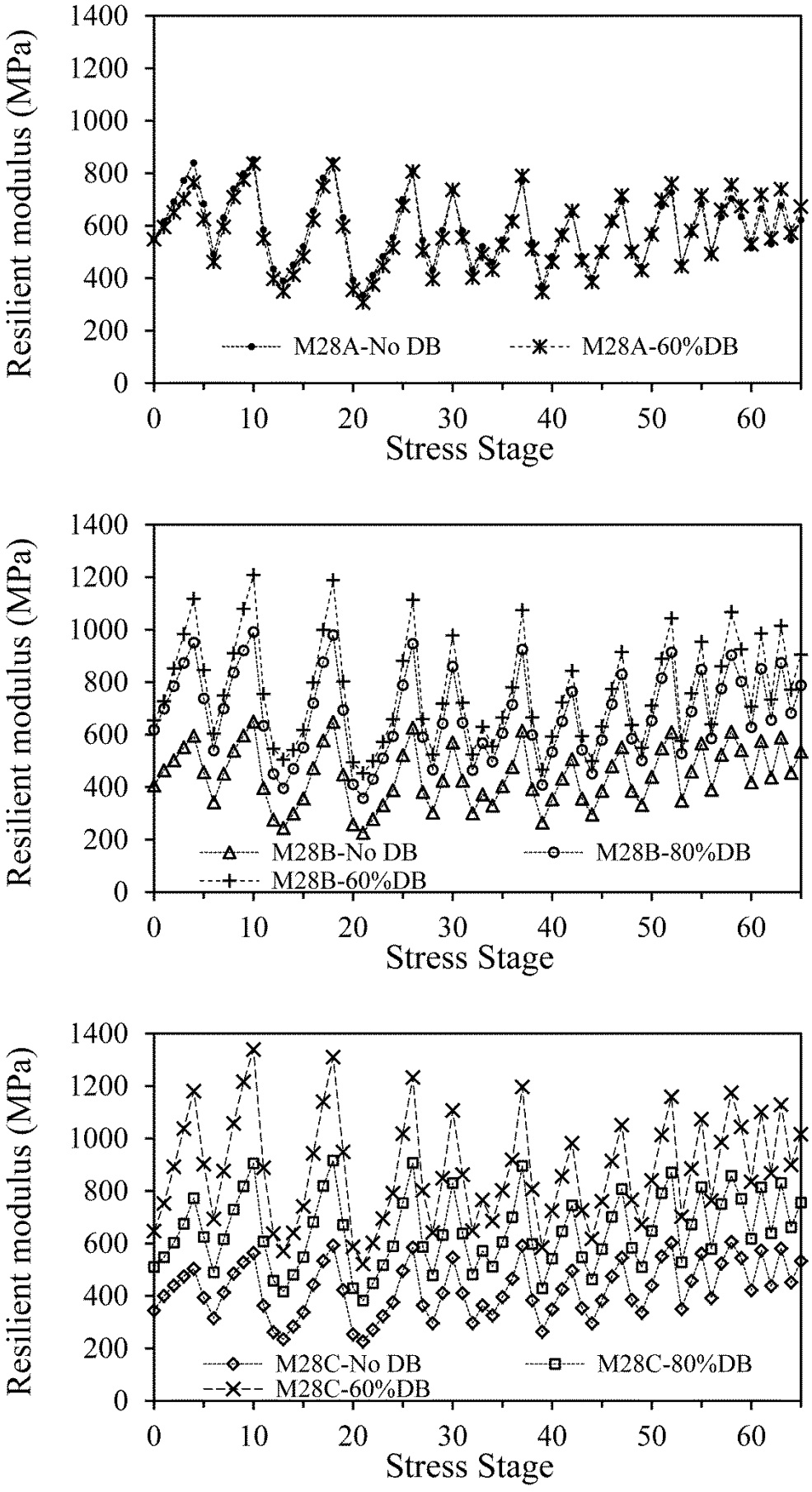

Figure A3: Resilient modulus test results for 28-day hydration period

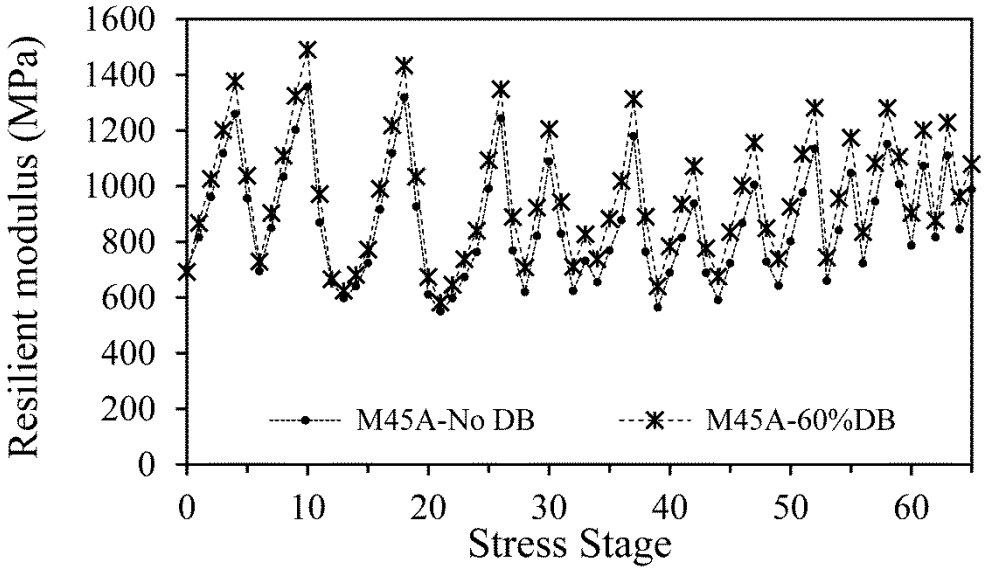

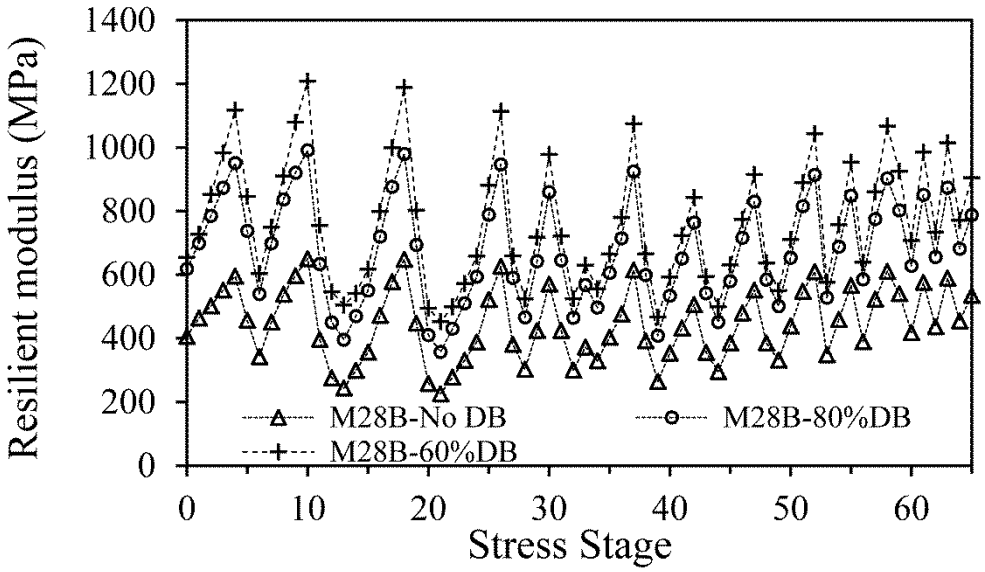

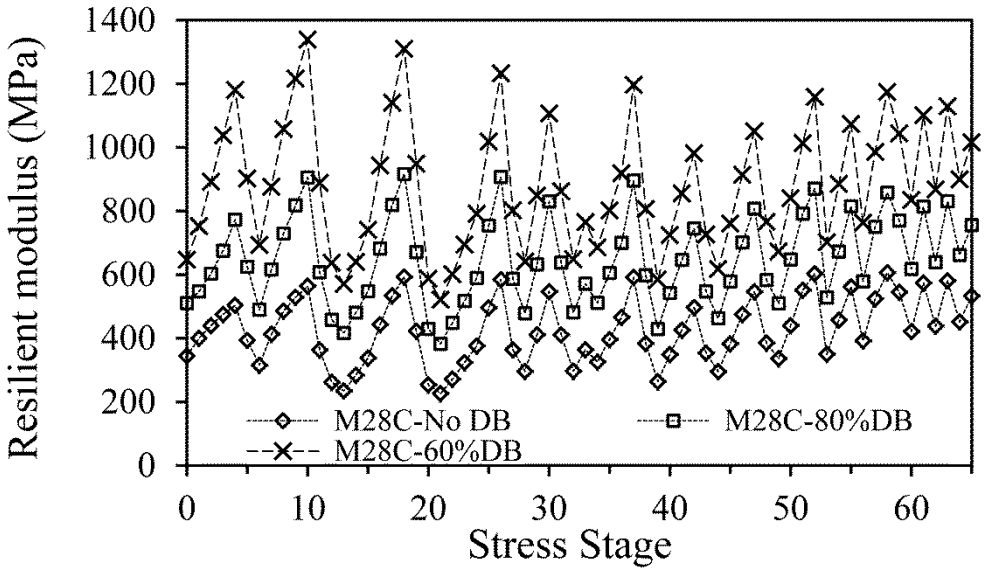

Figure A4: Resilient modulus test results for 45-day hydration period

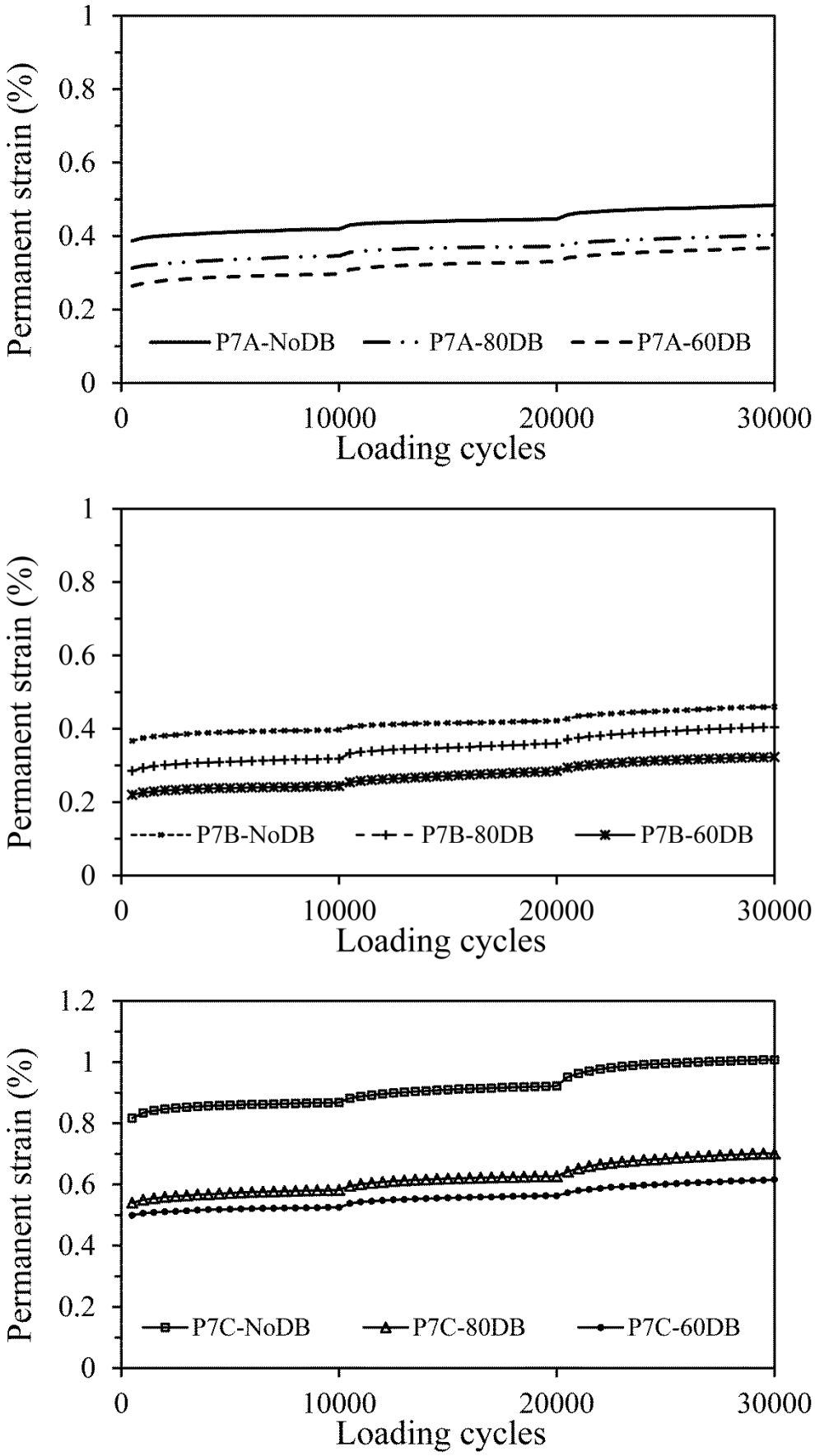

Figure A5: Permanent deformation test results for 7-day hydration period

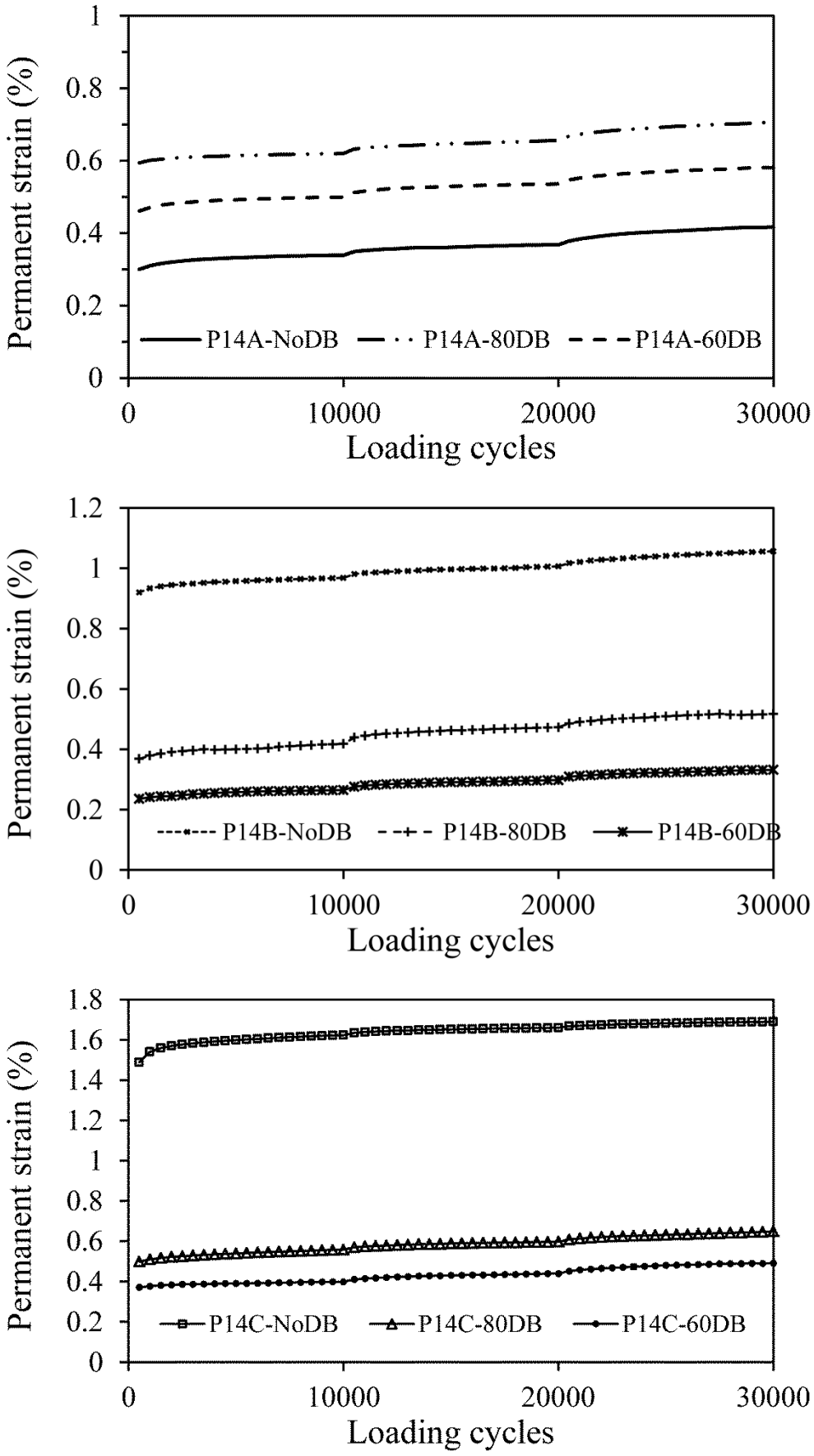

Figure A6: Permanent deformation test results for 14-day hydration period

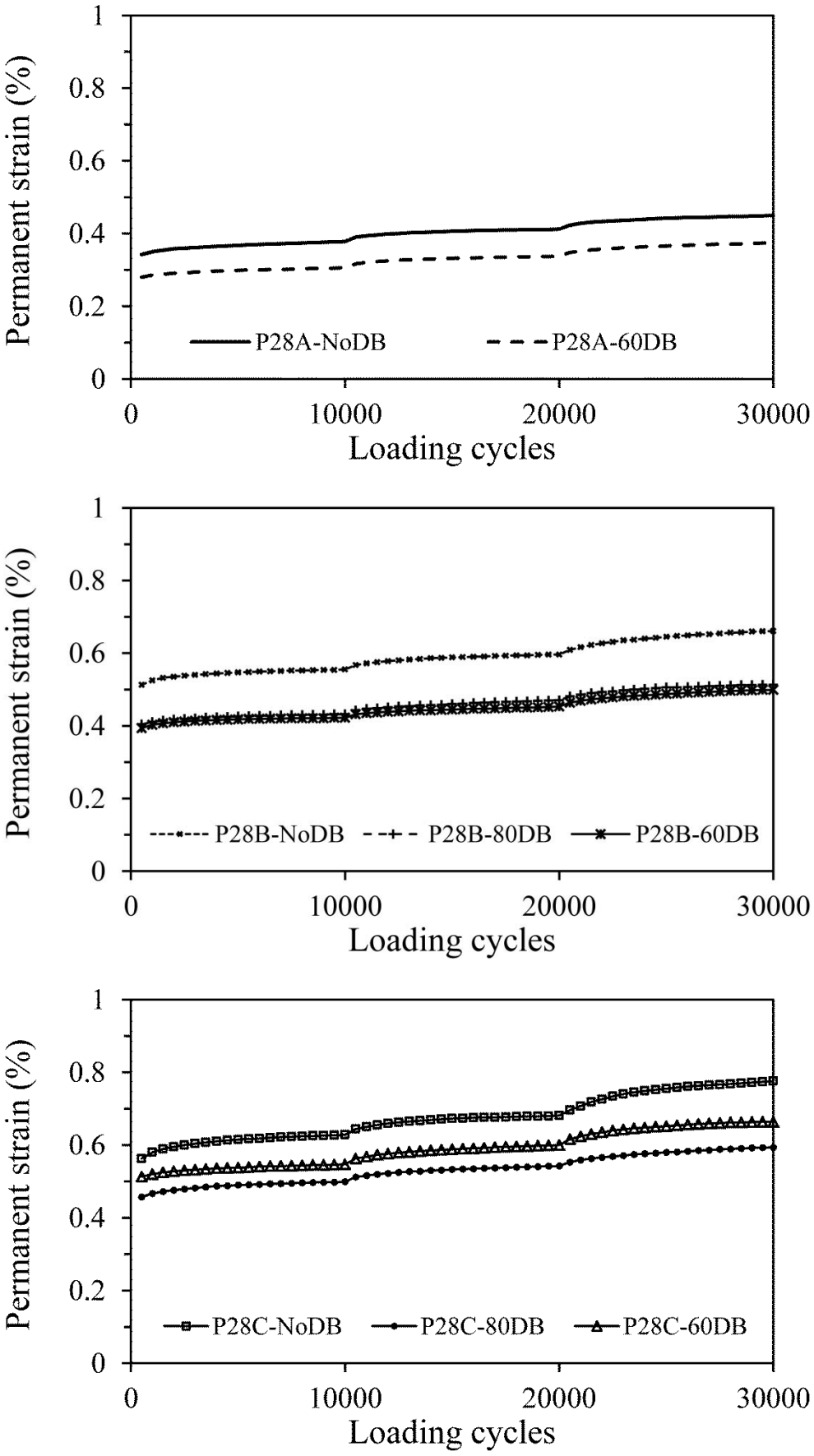

Figure A7: Permanent deformation test results for 28-day hydration period

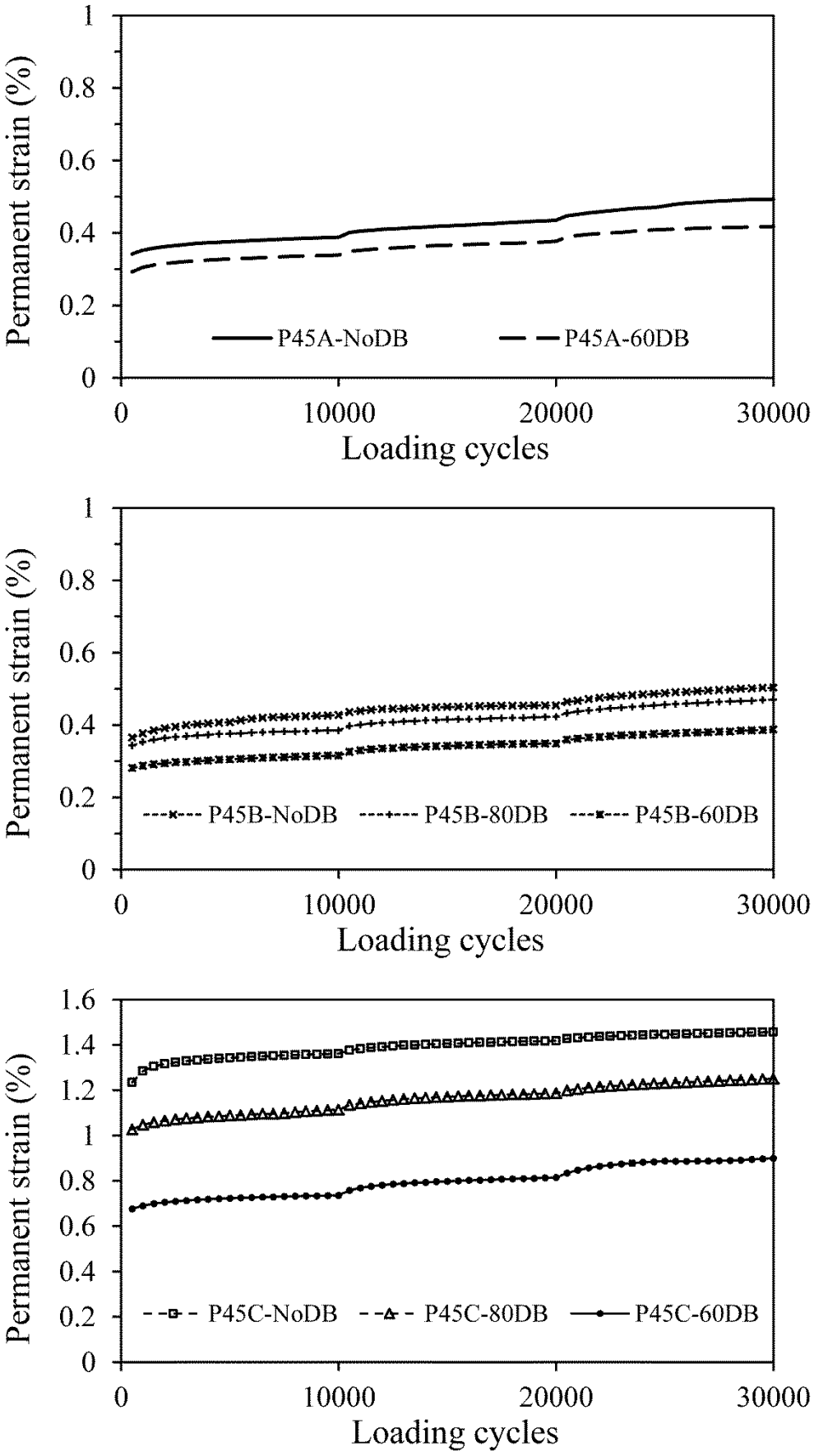

Figure A8: Permanent deformation test results for 45-day hydration period